Planning, Operation, and Management of Automated Transportation Systems: A Control-Theoretic Approach

A DISSERTATION
SUBMITTED TO THE FACULTY OF THE GRADUATE SCHOOL
OF THE UNIVERSITY OF MINNESOTA
BY

Shian Wang

IN PARTIAL FULFILLMENT OF THE REQUIREMENTS
FOR THE DEGREE OF
Doctor of Philosophy

Advisor: Michael W. Levin

December, 2022

Acknowledgements

It has been quite a journey spending the past few years at the University of Minnesota for my PhD studies. While winter in Minnesota is characterized by cold temperatures, the people I have worked and interacted with along the journey are among the most warmhearted. This dissertation would not have been possible without the tremendous support that I have received along the way.

I would like to take this opportunity to first thank my doctoral advisor, Dr. Michael Levin, who has given me the greatest amount of academic freedom that I could imagine to follow my own research interests throughout my PhD studies. While Dr. Levin likes to challenge me on difficult research questions, he is always available for discussion and has been encouraging me to keep moving forward no matter what challenges lie ahead. Dr. Levin knows exactly how much technical support he should provide to students at different stages of their graduate study in order to cultivate independent researchers. In addition to advising students on research, Dr. Levin is also a brilliant educator. His passion and enthusiasm for effective teaching will continue to motivate me to be an excellent teacher; it is what students really learn from the class that matters most. I have always looked upon Dr. Levin as a great mentor, who not only provides me with critical guidance in conducting interesting research but also nurtures me to be a brilliant educator to inspire the next generation of engineers. This dissertation would not have been possible without his tremendous support that I received over the past years.

I would also like to sincerely thank Dr. Alireza Khani, Dr. Raphael Stern, and Dr. Ryan Caverly for taking the time to read my dissertation and serving on the dissertation committee. I first got to know Dr. Khani when taking the course CEGE 5180 in Fall 2019. As a student without much background in conventional transportation engineering, Dr. Khani's course deepened my understanding of transportation planning,

operations, and management. It is from this course that I gained a better understanding of the logit model which I later successfully applied to the work presented in Chapter 2 of this dissertation. One thing I learnt from Dr. Khani, which I think is particularly important, is that one needs to consider transportation systems as a whole when aiming to develop effective solutions for some of the most pressing problems facing the society. This reinforces my pursuing of systematic and holistic approaches in future research endeavors.

I still recall the time when I was taking the course CEGE 8490 taught by Dr. Stern in Fall 2019. This special topic course was so interesting that it really motivated me to look deeper into vehicle automation and control and their impacts on traffic flow. I started to have discussion with him both in and outside the classroom while I took his class, which really helped me to get to know him better. Benefiting from our numerous conversations, we have been collaborating on some interesting and exciting research projects over the past years, resulting in multiple journal articles and conference proceedings. I am thankful to Dr. Stern for sharing his vision towards automated transportation systems over the next decade, which has motivated me to work on emerging research areas where I can contribute to making a long-lasting impact. Additionally, I really appreciate all of the support that I received from Dr. Stern over the period of my academic job search, without which I would not have survived the exhausting process.

I first met Dr. Caverly when taking his course AEM 8423 in Spring 2020. I was truly amazed by how much Dr. Caverly cares for his students, including those from other departments. I took the opportunity to carry out a course project with Dr. Caverly leading to a publication in American Control Conference, with its extension published by Transportation Research Part C. It is the collaboration with Dr. Caverly that has inspired me to be as rigorous as possible in conducting research, even when it comes to a punctuation in writing scientific papers. Moreover, I am particularly grateful to Dr. Caverly for sharing the document "Reflections on My Academic Job Search", which significantly benefited me in preparing for faculty interviews and in negotiating an offer afterwards. I would not have been able to successfully land a faculty position without the continued support of Dr. Caverly.

I would also like to acknowledge the support that I have received, both academically and personally, from Dr. Zongxuan Sun. As a professor in Mechanical Engineering at

the University, Dr. Sun has tremendous experience in automotive propulsion systems. Working with Dr. Sun has considerably expanded my domain knowledge to gain a much deeper understanding of the mechanism of vehicle motion, which I believe would be very beneficial for my future research on automated vehicles. I also had the opportunity to have several conversations with Dr. Sun regarding research, teaching, and personal pursuits. It is the discussions with him that reinforce my goal of becoming a professor to inspire the next generation of STEM leaders.

In addition to the faculty mentioned above, I also would like to extend a special thanks to my former advisor, Dr. N. U. Ahmed. It is Dr. Ahmed who first exposed me to scientific research when I was doing my Master's study at the University of Ottawa in Canada. As a mathematician working on control theory, Dr. Ahmed has been continuously encouraging me to develop rigorous approaches for solving challenging real-world problems in engineering sciences. He taught me step by step how to conduct solid research in my early academic career, and has continued to offer me tremendous support both academically and personally thereafter. Dr. Ahmed cares about not only my academic achievements but also my personal development, my family and friends. It is his work ethic that reinforces my understanding of "nothing comes easy." I am deeply indebted to Dr. Ahmed for all of his guidance and support along the way.

I am also fortunate to have met so many wonderful colleagues and friends during my stay at the University of Minnesota. Rongsheng Chen and Zhexian Li made me feel at home when I first moved from Ottawa to Minneapolis in the Summer of 2019. Having the road trip with both of you to Duluth is one of the best memories I have had in Minnesota. Rongsheng, I wish you all the best with the next chapter of your career at Beijing Jiaotong University; Zhexian, I hope you will have a joyful and productive journey of your PhD study at the University of Southern California. I would also like to thank Mingfeng Shang and Tianyi Li for their accompany, support, and encouragement. I am lucky to have close friends like you and will miss the moments we shared, we laughed, we spent together – staying up for conference deadlines, running at RecWell, playing at the Baseline Tennis Center, and so much more! Over the past three years, I have made good friends from Civil Engineering and other disciplines, to whom I would like to extend many thanks, including Christopher Cheong, Yufeng Zhang, Pramesh Kumar, Jingru Gao, Tianhao Yan, Chen Hu, Jacob Margolis, Joshua Klavins, Aidan

Mahlberg, Jilong Jia, Arian Zare, Te Xu, Simanta Barman, Maziar Zamanpour, Di Kang, Rui Li, Mohammad Charara (CEGE Graduate Student Board), Wenbo Sun (HKU), Suiyi He (Mechanical Engineering), Haoyu Yang (Computer Science), Yunli Shao (ORNL). I am sorry for anyone that I missed, but I sincerely appreciate everyone that has been supportive along the way.

I would not have achieved what I had accomplished without the financial support of the Department of Civil, Environmental, and Geo- Engineering (Departmental Fellowship and a teaching assistantship), the Center for Transportation Studies (Matthew J. Huber Award, TRB Student Travel Awards), the University of Minnesota China Center (Hsiao Shaw-Lundquist Fellowship), the University of Minnesota (Doctoral Dissertation Fellowship), and the Minnesota Department of Transportation (including the 2020 ITS Minnesota Graduate Student Scholarship Award). I would also like to acknowledge the tremendous support that I have received from faculty and staff in the Department of Civil, Environmental, and Geo- Engineering at the University of Minnesota. Special thanks go to Dr. Vaughan Voller, former Director of Graduate Studies in our department, for writing me a strong recommendation letter along with polishing my application for the Doctoral Dissertation Fellowship, and Ms. Tiffany Ralston for assisting with transferring course credits from my Master's study to the PhD program and for coordinating everything in regard to my PhD exams.

Last but not least, I would like to greatly appreciate the unconditional love, support, comfort, guidance, and encouragement that I have received from my parents Mrs. Guihua Xu and Mr. Shiwu Wang, my sister Mrs. Man Wang, and my brother-in-law Mr. Jianli Li, every step of the way. My parents have nurtured me, guided me and comforted me; they have given me the most freedom that I can ever imagine in my personal development. I am forever grateful to my parents for cultivating me to be a person as much independent as I can be. My sister and brother-in-law have always been there for me, no matter the situation. They have taught me so much in life. Their invaluable experiences have helped me avoid many detours on the journey of life; their continuous encouragement has inspired me to keep moving no matter what lies ahead. Thank you, mom and dad, my sister and brother, I truly appreciate you for all that you have done for me.

Dedication

Dedicated to my parents Guihua Xu and Shiwu Wang, and my sister Man Wang.

Abstract

With the advent of emerging technologies like 5G network and wireless communication, automated vehicles (AVs) are expected to become increasingly available to travelers, offering a vast amount of benefits, such as enhanced traffic stability, reduced energy consumption, and optimized parking space allocation, among many others. It is highly anticipated that there will be a transitional period of the the auto market as human-driven vehicles (HVs) are gradually replaced by AVs. Many opportunities and challenges are expected to emerge during this transitioning process. To better prepare a nation for the arrival of AVs, in this dissertation we aim to address interesting yet pressing problems arising from vehicle automation in the context of planning, operation, and management of future transportation systems from a control-theoretic perspective.

In view of the inevitable coexistence of HVs and AVs during the transitioning period, we develop a continuous-time dynamical model to capture the interactive temporal evolution of the market share of these two types of vehicles. A discrete choice model is constructed and incorporated into the dynamical model for describing the likelihood of customers choosing HVs or AVs. To achieve a desired temporal integration of AVs into the auto market, monetary subsidies and investment in AV-specific infrastructure are considered as decision variables to promote the adoption of AVs. Further, an optimal control problem is formulated with the objective of achieving a desired market penetration rate (MPR) at the end of any given finite planning horizon, while minimizing the cost of AV subsidies and infrastructure investment. The time-dependent optimal AV integration policy is determined by solving the formulated optimization problem, allowing a government agency to subsidize AV purchases and invest in future transportation infrastructure in an adaptive manner. The proposed approach is observed to be effective and robust under various demand patterns, such as increasing, decreasing, and stochastic demands. A systematic cost-benefit analysis with sensitivity analysis is conducted to evaluate the desirability of AV integration. The promising results provide significant managerial insights for government agencies into developing long-term strategic planning policies for the integration of AVs.

Although appropriate incentive policies could accelerate the adoption of AVs, the MPR is expected to remain relatively low in the next thirty years or so, resulting in a predominantly human-driven mixed traffic flow consisting of HVs and AVs. Uniform traffic flow has been shown to be unstable in certain flow regimes due to collective behavior of human drivers, causing the well-observed stop-and-go waves. These traffic waves can arise even in the absence of merges, bottlenecks, or lane changing, and likely result in more energy consumption and emissions. Taking advantage of vehicle automation, we develop an approach to smoothing unstable traffic flow via optimal control of a small proportion of AVs in a predominantly human-driven traffic flow. These controlled AVs act as mobile actuators in mixed-autonomy traffic without changing the way HVs normally operate. We develop a general framework to describe mixed traffic flow with its dynamics abiding by car-following principles. Based on this framework, we synthesize optimal feedback controllers for AVs with the objective of minimizing speed disturbance, thereby resulting in smoother traffic. Following the necessary conditions of optimality prescribed by the Pontryagin's minimum principle, we present a computational algorithm for determining the optimal AV control strategy. The general framework is further illustrated using the intelligent driver model (IDM) and optimal velocity with relative velocity (OVRV) model for HVs and AVs, respectively, to show the effectiveness of the proposed approach on traffic smoothing, as well as the improvement on vehicle fuel economy and emissions.

While the optimal AV controller synthesized above is shown to be effective in smoothing unstable mixed traffic, its performance on improving traffic stability is yet to be proven analytically and car-following safety is ensured in a fairly conservative manner. To address these challenging issues, we synthesize appropriate feedback controllers for AVs leveraging nonlinear stability theory. Specifically, we are interested to analytically synthesize appropriate feedback controllers of AVs for smoothing nonlinear mixed traffic in its general functional forms, covering a broad class of deterministic car-following models commonly seen in the literature. Essentially, AVs are controlled to operate in such a way that they closely track a virtual speed profile, i.e., a subtler version of the disturbance resulting from the immediately preceding vehicle. Thus, traffic waves are reduced when propagating backward across controlled AVs. Based on the general functional form of car-following dynamics, we derive a class of effective additive AV

controllers that are proven to be able to ensure convergence in speed tracking, leading to smoother traffic. In addition, a set of sufficient conditions is devised for guaranteeing car-following safety. Notably, unlike many existing studies the feedback controllers synthesized require only local traffic information without having to rely on high degrees of vehicle connectivity, and the rate of traffic smoothing is readily tunable, which is useful for practical implementation. The proposed approach is further illustrated with a theoretical IDM and commercially available adaptive cruise control (ACC) vehicles represented by a well-calibrated IDM.

In spite of the benefits promised by AVs like enhancing traffic stability shown above, emerging AV technologies open a door for cyberattacks, where a select number of AVs are compromised to drive in an adversarial manner. This could result in a network-wide increase in traffic congestion and vehicle fuel consumption, degrading the performance of transportation systems. Hence, developing effective attack mitigation strategies for AVs is critically important as AVs gradually become a reality. To this end, we derive optimal feedback control law for AVs in the presence of cyberattacks. Notably, attacks are only assumed to have a bounded magnitude (for remaining stealthy) without being subject to any specific probability distribution, which is not only of theoretical interest but also relaxes the assumptions of prior studies. More importantly, to deal with lack of knowledge of malicious attacks, we, for the first time, formulate a min-max control problem to minimize the worst-case potential disturbance to traffic flow. Specifically, under the framework of mixed-autonomy traffic presented before we consider two types of cyberattacks on AVs, namely false data injection attack on sensor measurements and malicious attack on AV control commands. Further, we derive a set of necessary conditions of optimality for the min-max control problem, based on which an iterative computational algorithm is developed for determining the optimal control (driving) strategy of AVs in a decentralized manner. The effectiveness of the proposed approach is demonstrated via numerical simulation considering different levels of attack severity.

Contents

List of Tables

List of Figures

Chapter 1

Introduction

1.1 Automated Transportation Systems

Over the past few decades, tremendous progress has been made in the development of intelligent transportation systems (ITS). The pace of advancement of ITS has grown even faster in recent years due to the advent of emerging technologies, such as connected vehicles (CVs), automated vehicles (AVs), and connected automated vehicles (CAVs), among others, making the highly anticipated automated transportation system increasingly achievable. The future transportation system is expected to be significantly reshaped thanks to these technological innovations, promising various types of potential benefits to the society. For example, using vehicle connectivity, CVs are shown to be able to drastically reduce travel delays at signalized intersections, with their impact on delay reduction increasing over the increase of CV penetration rate [1]. With more advanced AV technologies, traffic congestion is expected to be significantly reduced, resulting in $60 billion of annual savings for the US economy [2]. With the integration of CV and AV technologies, CAVs are able to take the potential benefits of these new technologies to the next level. For instance, using vehicle connectivity and Signal Phase and Timing information (CV technology), 9.1%–19.7% fuel benefits can be achieved for the most common internal combustion engine-based CAVs, with co-optimization of vehicle speed and powertrain operations (AV technology) [3]. Despite the many impressive potentials promised by these emerging technologies, a host of new challenges, particularly those related to vehicle automation, continue to arise in automated transportation systems,

such as safety and ethical concerns in regard to assigning responsibility when an AV crashes or causes a crash and how they should interact with human drivers in mixed-traffic environments [4, 5], spatial re-organization of cities including road infrastructure deployment [6], among many others. To be able to identify these critical challenges is the first step towards making full use of new technologies.

While emerging ITS technologies are rapidly evolving, in this dissertation we focus on the planning, operation, and management of automated transportation systems in the presence of AVs. It has been revealed in prior studies that AVs are likely to offer a vast amount of opportunities, ranging from enhancing traffic safety [7], to reducing fuel consumption and traffic congestion [8], to increasing city mobility and parking benefits [9, 10], among many others [2, 11–13]. It is easy to envision a fully automated traffic environment, i.e., 100% market penetration rate (MPR) of AVs, where AVs are likely to travel with a shorter headway leading to substantial improvements on traffic throughput [14, 15]. However, many of the benefits due to the advent of AVs are becoming increasingly visible even at a relatively low MPR. For example, it has been shown by, mathematical analysis, optimization studies and field experiments, that only a small fraction of well controlled AVs with specific requirements on vehicle connectivity can stabilize mixed traffic, resulting in smoother traffic flow [16–18] with promising improvements on vehicle energy consumption and greenhouse gas emissions [19, 20]. In fact, a relatively low MPR is highly anticipated for at least the next thirty years [8], when human-driven vehicles (HVs) are gradually replaced by AVs. Being able to assist the general public to properly navigate through the dynamic transitional period is the first step towards making full use of the benefits that emerging AV technologies have to offer.

1.2 Control-Theoretic Approaches in Traffic Control and Management

There are many prominent areas of dynamical systems and control theory, including systems governed by linear and nonlinear ordinary differential equations, stochastic differential equations, and partial differential equations, among others [21]. The remarkable advance of this field is due to the unprecedented interest, interaction and contribution

of pure and applied mathematics and physical and engineering sciences. As a matter of fact, a number of useful control techniques have been successfully applied to solving interesting and challenging research questions arising in transportation engineering.

In urban road networks traffic lights at intersections is the major control measure for regulating vehicular movements. There have been a significant amount of traffic signal control strategies proposed at various levels of applicability, such as stage-based strategies SIGSET [22] and SIGCAP [23] and dynamic programming approaches [24, 25] for isolated intersection control, MAXBAND [26] and TRANSYT [27] for fixed-time coordinated intersection control, SCOOT [28] and RHODES [29] for coordinated traffic-responsive intersection control, max-pressure signal controls [30, 31] for urban traffic networks with performance guarantees, and more recently optimal control of CAVs at autonomous (signal-free) intersections [32, 33].

In freeway networks ramp metering is one of the prominent control measures for regulating highway traffic [34], which includes a series of variations, such as fixed-time ramp metering strategies, reactive ramp metering strategies, nonlinear optimal ramp metering strategies, link control strategies like variable speed limit control and changeable message signs, among others [35]. Notably, the linear quadratic regulator (LQR) theory and linear/nonlinear feedback control theory are extensively employed in designing appropriate ramp metering control strategies [36–38]. An excellent review on traffic control strategies can be found in [35].

In light of the advent of AVs in the near future, an increasing amount of research effort has been put into mixed-autonomy traffic control and management from a wide range of research communities, such as transportation engineering, urban planning, electrical engineering, and computer science, among many others. Since AVs are envisioned to be capable of acting as mobile actuators in mixed traffic, they are able to significantly impact the properties of mixed traffic flow, which offers a new paradigm (Lagrangian traffic flow control [39, Chapter 5]) for traffic planning, operation and management in the era of AVs. As a result, control theory is gaining a considerable amount of research interest in addressing some of the pressing problems arising in automated transportation systems in the presence of AVs.

For example, game theory [40] and optimal control theory [41] have been applied to design proper incentive programs for accelerating the adoption of AVs at the planning

stage from the perspective of a government agency. Linear stability theory has been employed to synthesize appropriate AV controllers for stabilizing mixed traffic [42]. Specifically, LQR theory [43] and H-infinity approach [44] have been used to design control laws for CAVs to achieve head-to-tail string stability, meaning that the speed disturbances are attenuated when reaching the tail vehicle from the lead vehicle. With the assumption on vehicle connectivity lifted, optimal AV controllers are synthesized using the well-known Pontryagin minimum principle for traffic smoothing, leading to head-to-tail string stability given a sufficient MPR [45]. More recently, the power of control theory has been observed in developing intelligent driving strategies of AVs in the presence of cyberattacks. For example, a distributed neural network based adaptive control is proposed for AVs under denial-of-service (DoS) attacks to ensure platooning formation with a desired longitudinal spacing [46]. To correct tracking errors for CAVs, a flocking control strategy is developed in the event of false data injection and DoS attacks [47]. For the platooning of connected and automated trucks, an improved longitudinal control strategy is proposed to enhance platoon stability considering falsified wireless communication information [48].

1.3 Problem Statements and Contributions

As mentioned before, AVs are anticipated to bring fruitful benefits to the future automated transportation system, wherein various opportunities as well as challenges could arise due to vehicle automation. To this end, we are particularly interested to research the planning, operation, and management of automated transportation systems in the presence of AVs from a control-theoretic perspective. Specifically, we study the following four research questions: (1) optimal policy for integrating AVs into the auto market; (2) optimal control of AVs for traffic smoothing; (3) feedback smoothing of nonlinear mixed traffic via control of AVs with performance guarantees; and (4) optimal control of AVs in the presence of cyberattacks. These studies have led to a series of research papers [41, 45, 49–53].

1.3.1 Optimal Policy for Integrating AVs into the Auto Market

With the advent of emerging technologies, AVs are expected to become increasingly available to travelers, bringing in tremendous potentials to reshape the future transportation system. However, many of the benefits related to AVs rely on a fairly high MPR in the transportation system [2, 54]. Clearly, before becoming fully automated, the ground transportation system will inevitably experience a transitional period when HVs are gradually replaced by AVs before AVs take up a full penetration in the auto market. This is, in fact, optimistically projected to be the case for at least the next thirty years [8]. For a heterogeneous traffic environment in the presence of both HVs and AVs, it is fairly challenging to fully understand the explicit impact of introducing AVs to the existing traffic, particularly at various MPRs. It has been shown that the road capacity could drop due to undesired vehicle speed variations and traffic shockwaves in mixed traffic with a low MPR of AVs [55]. To ensure a gradual and smooth market transition from low to high MPRs of AVs, it would be beneficial to develop long-term strategic planning policies from the perspective of a government agency.

In view of the coexistence of HVs and AVs, there is expected to be an interactive temporal evolution in terms of their market shares. In this work, we aim to capture such temporal evolution by developing a dynamical model taking into account the market interactions between HVs and AVs. This mathematical model is time-variant by nature as the market shares of these two types of vehicles dynamically evolve over time. More importantly, we will focus on studying how incentive programs like monetary subsidies and infrastructure investment could impact the adoption of AVs since customer preferences are largely determined by these attributes of the alternatives (HVs and AVs). Hence, one needs to consider how those attributes would influence customer choices in opting HVs or AVs, and how customer decisions could in turn impact the evolution of the market share of each vehicle type. With this in mind, we aim to design optimal incentive policies for promoting the integration of AVs into the auto market. In addition, we are also interested to examine how such AV integration policies would perform in response to different vehicle demand patterns, planning horizons, etc.

Inspired by the classical Lotka-Volterra equations, we develop a continuous-time dynamical model to describe the temporal evolution of the market share of vehicles. A

discrete choice model is constructed and incorporated into the dynamical model to describe the likelihood of customers choosing HVs or AVs. To achieve a desired temporal integration of AVs, monetary subsidies and AV infrastructure investment are considered as decision variables to promote the adoption of AVs. Further, an optimal control problem is formulated with the objective of achieving a desired MPR of AVs at the end of the planning horizon, while minimizing the cost associated with AV subsidies and infrastructure investment. We prove the existence of an optimal AV integration policy. Moreover, we derive necessary conditions of optimality characterizing the mathematical properties of the optimal integration policy. Based on the optimality conditions derived, an iterative computational algorithm is developed to determine the time-dependent integration policy, which allows a government agency to appropriately subsidize AV purchases and invest in AV infrastructure in an adaptive manner. The proposed approach is shown to be effective and robust under different vehicle demand patterns via extensive numerical experiments. In addition, a systematic cost-benefit analysis is conducted, along with appropriate sensitivity analysis, to evaluate the desirability of AV integration. The results of this research topic are presented in Chapter 2 (also in [41, 49]), which are expected to provide useful managerial insights for government agencies to assist with the development of long-term strategic planning policies in the era of AVs.

1.3.2 Optimal Control of AVs for Traffic Smoothing

Traffic congestion is a long-standing problem that has gained a significant amount of interests from a broad range of research communities. Over the past few decades, a considerable amount of research has gone into understanding the cause of traffic congestion and developing effective strategies for its mitigation. It has been observed that traffic congestion is not only caused by some noticeable triggers, such as lane changing, bottlenecks and merging, but could also occur often in the absence of any of these aforementioned triggers. This is simply due to the nature of unstable traffic flow in which small perturbations amplify and grow into stop-and-go waves traveling upstream in the flow. As a consequence of the collective behavior of human drivers, unstable traffic flow could result in greater traffic congestion and higher energy consumption and emissions than smooth traffic flow.

Thanks to technological advancements of vehicular sensing and communication, AVs

are expected to offer a new paradigm for traffic control thanks to the potential of serving as mobile actuators in mixed traffic, thereby enabling Lagrangian traffic flow control. This opens a door for future traffic regulation and congestion mitigation. Prior studies have shown that, with a high degree of connectivity and automation connected automated vehicles are capable of stabilizing unstable mixed traffic flow, thereby smoothing traffic. However, the proposed approaches largely rely on high degrees of connectivity in the sense that the controlled AV has to be able to communicate with a number of vehicles, if not all other vehicles. Furthermore, most prior studies use car-following models linearized at the equilibrium state to design the control law for AVs, which may not guarantee reliable performance due to the nonlinear nature of mixed traffic flow. In addition, an optimal control policy of AVs is yet achieved in the context of smoothing traffic via control of AVs. In this work, we aim to address these issues by designing an optimal feedback control for AVs to smooth a predominantly human-driven nonlinear traffic flow, without requiring vehicle-to-vehicle communication.

Specifically, we develop an effective approach to smoothing unstable traffic flow via optimal control of AVs in a predominantly human-driven traffic flow, with controlled AVs acting as mobile actuators without changing the way HVs normally operate. We develop a general framework to describe mixed-autonomy traffic in the presence of HVs and AVs, whose dynamics abides by generic nonlinear car-following principles. Based on this framework, we formulate an optimal control problem with the objective of minimizing AV speed disturbances, and prove the existence of an optimal AV control policy. Following the necessary conditions of optimality prescribed by the Pontryagin minimum principle, we present a computational algorithm for determining the optimal AV driving strategy with analytical proof on its convergence. The mathematical model presented is further illustrated using the intelligent driver model (IDM) and the optimal velocity with relative velocity (OVRV) model for HVs and AVs, respectively. A series of numerical results of this topic is presented in Chapter 3 (also in [45]), showing the effectiveness of the proposed approach on traffic smoothing as well as the improvement on vehicle fuel economy and emissions.

1.3.3 Feedback Smoothing of Nonlinear Mixed Traffic via Control of AVs with Performance Guarantees

As introduced in the above Section 1.3.2, an optimal AV controller is synthesized for smoothing nonlinear mixed traffic without being limited to linearized car-following dynamics. While the approach developed is shown to be effective, analytical proofs on the stability of mixed traffic, in the presence of controlled AVs, are not derived. In addition, car-following safety is achieved only in a conservative manner. To tackle these issues, we aim to synthesize a class of additive AV feedback controllers useful for traffic smoothing, with analytical guarantees on system performance and car-following safety based on a novel idea of virtual speed tracking.

Specifically, we analytically synthesize a class of AV feedback controllers to effectively smooth nonlinear mixed traffic in its general functional form, covering a broad class of deterministic car-following models commonly seen in the literature. By leveraging feedback control theory, AVs are controlled to operate in such a way that they closely track a virtual speed profile, i.e., a subtler version of the disturbance resulting from the immediate preceding vehicle. Consequently, traffic waves are reduced when propagating backwards across controlled AVs. Based on the general functional form of car-following dynamics, we derive a class of effective additive AV controllers that are proven to be able to ensure convergence in speed tracking, leading to smoother traffic flow. In addition, a set of sufficient conditions is devised for guaranteeing car-following safety. Notably, unlike many existing studies the feedback controllers synthesized for AVs require only local traffic information without having to rely on high degrees of vehicle connectivity. In addition, the rate of traffic smoothing is readily tunable, which is useful for practical implementation. The proposed approach is demonstrated on a theoretical IDM and a well-calibrated IDM describing commercially available adaptive cruise control (ACC) vehicles. Extensive numerical results are presented in Chapter 4 (also in [50, 51]) to show the effectiveness and robustness of the feedback controllers synthesized for AVs on smoothing nonlinear mixed traffic.

1.3.4 Optimal Feedback Control Law for AVs in the Presence of Cyberattacks

In spite of the benefits promised by AVs, emerging AV technologies open a door for cyberattacks, where a select number of AVs are compromised to drive in an adversarial manner. This may not only cause a network-wide increase in traffic congestion and vehicle fuel consumption, but also result in unexpected disruption to normal traffic flow causing financial loss or even loss of human lives. Consequently, cyberattacks on AVs pose a significant risk to the safety, reliability, and efficiency of future transportation systems. Therefore, developing effective attack mitigation strategies for AVs is necessary and valuable as AVs gradually become a reality.

While developing effective attack mitigation strategies for AVs is greatly desired, it is rather challenging due to the lack of knowledge of adversaries. Limited prior studies have assumed deterministic attacks or stochastic attacks with a given probability distribution (e.g., a Gaussian distribution), which is far from realistic due to the malicious nature of stealthy attacks. In addition, most of these studies presume that all vehicles communicate with each other, which may not be readily achieved in the near future. While the impacts of cyberattacks on AVs and vehicular platoons have been revealed in recent studies, there is a lack of effort in developing effective control strategies for AVs in the presence of attacks.

To tackle the challenges mentioned above, we derive an optimal feedback control law (driving strategy) for AVs in the presence of cyberattacks, using only local traffic information. Unlike many prior works assuming constant attacks or stochastic attacks with a specific probability distribution, we only assume attacks to have a bounded magnitude (for remaining stealthy) without being subject to any given statistical distribution, which is not only of theoretical interest but also relaxes the assumptions seen in prior studies. From a modeling standpoint, this also appears to be more realistic considering lack of knowledge of malicious attacks. To deal with lack of knowledge of attacks on AVs, we, for the first time, formulate a min-max control problem to minimize the worst-case potential disturbance to traffic flow. Specifically, under the framework of mixed traffic we consider two common types of cyberattacks, namely false data injection attack on sensor measurements and malicious attack on AV control commands. Based on the

mathematical framework involving these attacks, we derive a set of necessary conditions of optimality for the min-max control problem, allowing for the development of an iterative computational algorithm to determine the optimal control (driving) strategy of AVs in a decentralized manner. Considering different levels of attack severity, the numerical results on this topic are presented in Chapter 5 (also in [52, 53]) showing effectiveness of the proposed approach.

1.4 Dissertation Organization

The remainder of the dissertation is organized as follows. Chapter 2 studies the problem of gradually integrating AVs into the auto market with optimal incentive programs, which is expected to be useful from a planning standpoint for accelerating the adoption of AVs. In Chapter 3, an optimal controller is synthesized for AVs to smooth nonlinear traffic flow, requiring only local traffic information without being subject to vehicle connectivity. To achieve analytical guarantees on system performance, a class of effective additive controllers is synthesized for AVs in Chapter 4 with provable convergence in tracking a designed speed and sufficient conditions for car-following safety. In Chapter 5, we devise optimal feedback control law for AVs in the presence of cyberattacks to better manage future automated transportation systems against malicious adversaries. We summarize the dissertation in Chapter 6 and briefly discuss some interesting research directions for future work.

Chapter 2

Optimal Policy for Integrating Automated Vehicles into the Auto Market

2.1 Introduction

The future transportation system is expected to be significantly reshaped with the advent of AVs. AVs are anticipated to offer a vast amount of opportunities, ranging from reducing vehicle fuel consumption and traffic congestion [8], to increasing city mobility and parking benefits [10], among many others [2, 11–13]. In a fully automated transportation system, i.e., 100% market penetration rate (MPR) of AVs, AVs are likely to travel with a shorter headway yielding substantial improvements on traffic throughput [14, 15]. Moreover, controlled AVs have been shown to be able to stabilize mixed traffic, resulting in smoother traffic flow [18, 44, 45]. In recent years, shared automated vehicles (SAVs) have gained a great deal of public interest as a possible less expensive and more efficient version of today's ridehailing companies and taxis [56]. With the introduction of electric vehicles (EVs), the many possible benefits of an SAV fleet could be expanded towards becoming more energy efficient, more reliable, and more environmentally friendly when coupled with renewable power [57].

However, many of the aforementioned benefits related to AVs rely on a fairly high

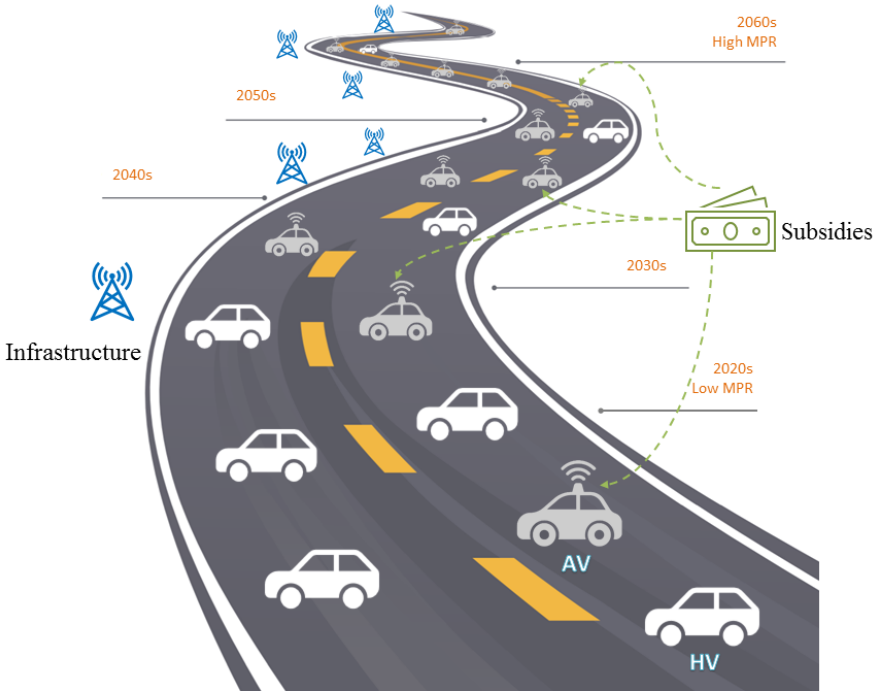

Figure 2.1: A conceptual illustration of strategic AV integration, with monetary subsidies for AV purchases and investment in AV-specific infrastructure; AV: automated vehicle, HV: human-driven vehicle [41].

MPR of AVs in the transportation system [2, 54]. Clearly, before becoming fully automated, the ground transportation system will witness the coexistence of HVs and AVs, which is in fact optimistically projected to be the case for at least the next thirty years [8]. For a heterogeneous traffic environment with both HVs and AVs, it remains challenging to fully understand the explicit impact of introducing AVs to the existing traffic, particularly at various MPRs. It has been shown that the road capacity is likely to drop due to undesired vehicle speed variations and traffic shockwaves in mixed traffic with a low MPR of AVs [55]. To ensure a gradual market transition from low to high MPRs, it would be crucial to develop long-term strategic planning policies from the perspective of government agencies. To this end, a conceptual illustration of this idea is shown in Fig. 2.1.

Recently, several studies have been conducted in an effort to promote the adoption of AVs, such as [40, 58–62]. In [58], exclusive AV lanes with reduced travel costs are

designed to promote the adoption of AVs with a fixed potential AV market size for each origin-destination pair. A profile-case best-worst scaling model is applied to model the adoption behavior of fully AVs, indicating that the purchase price, incentive policies, and infrastructure investment like exclusive lanes for AVs are the dominant factors when it comes to people choosing HVs or AVs [60]. In addition to deploying AV lanes, subsidizing the purchase of AVs by government agencies is also considered subject to a fixed budget [61]. To accelerate the adoption of AVs by subsidies, a dynamic games approach is proposed in an attempt to capture the information asymmetry between the government agency and the subsidized entities [40]. Since not all vehicles in mixed traffic have communication capabilities, the deployment of roadside units to overcome connectivity gap could be beneficial from a strategic planning perspective [62]. These studies have considered promoting the adoption of private AVs. By contrast, a cost of ownership analysis is conducted to inform early adoption of commercial AVs in the taxi and freight sectors in the UK, due to possible substantial reduction of driver costs in commercial operations through automation [59].

The early studies mentioned above indicate that it is of great significance to develop appropriate policies for integrating AVs into the auto market. Most of the existing work approach the problem with static optimization, without explicitly considering the continuous temporal dynamics of the auto market. This approach appears to be challenging for deriving AV integration policies that are adaptive to the time-variant MPR of AVs. The temporal evolution, however, is captured in [40] using a diffusion of innovations (DOI) model. Although it is capable of describing the evolution of the AV market share, the choice of customers purchasing HVs or AVs is yet incorporated explicitly. By contrast, we develop a continuous-time dynamical model capable of capturing the interactive temporal dynamics of the market share of HVs and AVs. The dynamical model developed is inspired by the well-known Lotka-Volterra equations [63, 64] with explicit consideration of customer preferences for opting HVs or AVs.

The dynamic market share of HVs and AVs is described by a pair of controlled nonlinear ordinary differential equations. Since it has been shown that customers are much more sensitive to the purchase price and provision of AV-specific infrastructure (e.g., exclusive AV lanes [58], roadside units [62], etc) in choosing between HVs and

AVs [60, 65–67], we consider adaptive monetary AV subsidies and investment in AV-specific infrastructure as decision variables for promoting the desired temporal integration of AVs. A discrete choice model is constructed and incorporated into the dynamical model to describe the likelihood of customers opting HVs or AVs. Further, an optimal control problem is formulated with the objective of achieving a desired MPR of AVs at the end of the planning horizon, while minimizing the cost associated with AV subsidies and infrastructure investment. We prove the existence of an optimal AV integration policy. By virtue of the classical minimum principle [68], a set of necessary conditions of optimality are tailored for mathematically characterizing the optimal integration policy, thanks to the favorable properties of the dynamical model developed. Based on the optimality conditions, an iterative computational algorithm is developed to determine the time-dependent AV integration policy applicable for both deterministic and stochastic demands, which allows the government agency to appropriately subsidize AV purchases and invest in AV-specific infrastructure in an adaptive manner. Further, a systematic cost-benefit analysis is conducted, along with appropriate sensitivity analysis, from a modeling prospective to evaluate the desirability of AV integration.

The dynamical model developed exhibits a high degree of generality in the sense that (1) it allows for easy inclusion of a wide range of vehicle types, e.g., HVs, AVs, EVs, etc. by introducing additional dimensions to the system state; (2) the decision constraint set can be readily modified in response to the change of funding availability; and (3) the optimal AV integration policy can be obtained for any finite planning horizon, leaving a lot of room for adjustment. Due to the generality of the dynamical model, the practicable implementability of the decision variables, and the efficiency of the computation based on the optimality conditions, the procedure presented in this chapter is expected to provide significant managerial insights for government agencies into developing long-term strategic planning policies in the era of AVs.

The main contributions of this chapter are briefly summarized as follows.

- We develop a continuous-time dynamical model capable of capturing the interactive temporal evolution of the market share of HVs and AVs. The mathematical model developed is general and can be easily extended to incorporate additional vehicle types, such as EVs.

- We construct a discrete choice model to describe the likelihood of customers opting HVs and AVs, with monetary AV subsidies and investment in AV-specific infrastructure employed as decision variables to promote the adoption of AVs. The discrete choice model is appropriately incorporated into the dynamical model for adaptive regulation of the temporal integration of AVs.

- We formulate an appropriate optimal control problem with the objective of achieving a desired MPR of AVs at the end of any given finite planning horizon, while minimizing the cost associated with AV subsidies and infrastructure investment. We prove the existence of an optimal AV integration policy and develop necessary conditions of optimality characterizing mathematical properties of the optimal policy.

- We develop an iterative computational algorithm for determining the time-dependent optimal AV integration policy, which allows the government agency to appropriately subsidize AV purchases and invest in AV infrastructure in an adaptive manner. Notably, this is not able to be achieved with agent-based simulations seen in prior studies.

- We conduct a systematic cost-benefit analysis, along with appropriate sensitivity analysis, to evaluate the desirability of AV integration. The results are informative and inspiring. For example, interesting correlations between vehicle demand patterns and the integration policy are revealed, which has yet gained much attention in the literature.

The remainder of this chapter is structured as follows. In Section 2.2, we develop a continuous-time dynamical model to describe the interactive temporal evolution of the auto market consisting of HVs and AVs. A discrete choice model is also constructed and incorporated into the mathematical model to represent the likelihood of customers choosing each type of vehicles. In Section 2.3, we formulate an appropriate optimal control problem with the objective of achieving a desired MPR of AVs at the end of the planning horizon, while minimizing the cost associated with AV subsidies and infrastructure investment. The existence of an optimal AV integration policy is proven also in Section 2.3. In Section 2.4, we derive the necessary conditions of optimality

tailored specifically for characterizing the optimal AV integration policy, by virtue of the mathematical properties exhibited by the dynamical model developed. Consequently, an iterative computational procedure is developed based on the optimality conditions for determining the time-dependent adaptive AV integration policy. In Section 2.5, a series of numerical experiments is conducted to show the effectiveness and robustness of the proposed approach under two distinct demand patterns. This chapter is concluded in Section 2.6 with reference to some interesting open research questions. The materials presented in this chapter are mostly taken from [41].

2.2 Mathematical Model

The well-known Lotka-Volterra model has been widely employed to characterize the interactive dynamics within a dynamical system consisting of a finite number of agents. For example, it has been used to describe the interdependent relationships among transportation, economic, and environmental systems for the planning of sustainable transportation systems [69, 70]. Inspired by the Lotka-Volterra equations capable of describing the dynamics of competing (and/or cooperating) agents in a given dynamical system, we extend its original form to characterize the temporal evolution of two competing vehicle types, namely HVs and AVs, in the auto market.

For a given market demand $d(t)$ at any time $t \geq 0$, customers are assumed to opt either HVs or AVs with a corresponding probability determined by a discrete choice model that shall be explicitly constructed later. Considering the number of HVs and AVs as the states of the dynamical system, it is noted that the rate of increase in the number of HVs and AVs is induced by vehicles being purchased. Moreover, with AVs becoming increasingly affordable and favorable for the general public more HV owners are likely to switch to AVs, which could result in a negative impact on HV ownership. By contrast, more customers are likely to remain committed to HVs if public perceptions of AVs are less favorable, which could result in a negative impact on AV adoption. This word-of-mouth effect is commonly observed within the social system of technology spreading [71] and can be well captured by the Lotka-Volterra model due to its capabilities of characterizing the competing dynamics among multiple agents.

To mathematically capture the unique dynamics arising in future auto market consisting of HVs and AVs, we extend the original Lotka-Volterra model and propose a pair of controlled first-order nonlinear ordinary differential equations to describe the temporal evolution of these two competing vehicle types in the market. To this end, the continuous-time dynamical model is given by

$$\dot{x}_{\mathrm{HV}}(t) = dx_{\mathrm{HV}}(t)/dt = P_1(t)d(t) - \gamma_1 x_{\mathrm{HV}}(t)x_{\mathrm{AV}}(t), \tag{2.1a}$$

$$\dot{x}_{\mathrm{AV}}(t) = dx_{\mathrm{AV}}(t)/dt = P_2(t)d(t) - \gamma_2 x_{\mathrm{HV}}(t)x_{\mathrm{AV}}(t), \tag{2.1b}$$

where $x_{\mathrm{HV}}(t)$ and $x_{\mathrm{AV}}(t)$ denote respectively the number of HVs and AVs at any time $t \in I \coloneqq [t_0, t_f]$, with I representing the planning horizon. The rate of change of the number of these two types of vehicles is denoted by $\dot{x}_{\mathrm{HV}}$ and $\dot{x}_{\mathrm{AV}}$, respectively. The function $d(t)$ represents the market demand for vehicles at time t. The functions, P_1 and P_2, describe respectively the probability of customers opting HVs and AVs, which shall be explicitly characterized afterwards. The positive parameters, γ_1 and γ_2, represent the interactive impact of one vehicle type on another, where the interaction is not necessarily symmetric. The dynamical model developed above considers two fundamental vehicle types, namely HVs and AVs. This is in line with the assumption made in many relevant studies [40, 58, 60, 66, 67]. However, the mathematical model exhibits a good level of generality in the sense that it can be easily extended to the case with n ($n = 3, 4, 5, \cdots$) vehicle types described correspondingly by a set of n coupled ordinary differential equations, with the second term of the above equations (2.1a) and (2.1b) replaced by the sum of the interactive impacts of other vehicle types due to their collective effect.

On the right-hand side of equations (2.1a) and (2.1b), the first terms describe the rate of increase in the number of HVs and AVs at time t, due to vehicles being purchased. The second terms characterize the rate of decrease of one vehicle type induced by the impact of the other. It is very similar to the mathematical characterization of interactive impacts of one agent on another observed in dynamic modeling for the planning of sustainable transportation systems [69]. Specifically, with AVs becoming increasingly affordable and favorable for the general public more HV owners are likely to switch to AVs, resulting in a negative impact on HV ownership, which is mathematically captured by the second term of equation (2.1a). By contrast, more customers

are likely to remain committed to HVs if public perceptions of AVs are less favorable, resulting in a negative effect on AV adoption, which is described by the second term of equation (2.1b). This word-of-mouth effect is commonly observed within the social system of technology spreading, including AV technology. In fact, from a mathematical perspective the interactive terms shown in equations (2.1a) and (2.1b) are similar to the diffusion process in DOI models describing new technology spreading in a social system [71].

A note on the classical Lotka-Volterra model: From a mathematical point of view, the classic Lotka-Volterra model is similar to the market penetration models [72–74]. More complex DOI models, such as [72–74], are particularly useful for agent-based simulation studies, without considering any optimization problem. By contrast, the dynamical model proposed in equations (2.1a) and (2.1b), as an extension of the classic Lotka-Volterra model, is capable of capturing the continuous temporal evolution of the market share, with explicit consideration of the choice of customers opting HVs or AVs. From a mathematical standpoint, the proposed dynamical model allows for in-depth analysis and appropriate formulation of optimization problems. In other words, the proposed model offers a deeper insight into the dynamically evolving market share of AVs and HVs. As a result, comprehensive managerial insights can be drawn for government agencies in developing long-term strategic planning policies. In addition, due to differentiability of the system dynamics with respect to the state variables (equations (2.1a) and (2.1b)), one can develop efficient computational procedures for determining the optimal decision policy, which shall be presented later.

As mentioned above, the variables $P_1(t)$ and $P_2(t)$ appearing in equations (2.1a) and (2.1b) denote the probability of choosing HVs and AVs, respectively. Since it has been shown that customers are much more sensitive to the purchase price and provision of AV-specific infrastructure in choosing between HVs and AVs [60, 65–67], we consider adaptive monetary AV subsidies and investment in AV-specific transportation infrastructure as decision variables for promoting the desired temporal integration of AVs. It is assumed that lower purchase prices and higher government investment in vehicle-specific infrastructure are preferred in terms of choosing HVs or AVs. In other words, the utility of choosing a certain type of vehicle dynamically increases with the decrease of the purchase price and with the increase of the amount of infrastructure

investment. Therefore, the utility function corresponding to choosing HVs over AVs at time t is given by

$$V_{\mathrm{HV}}(t) = \beta_1 + \beta_2 r(t) + \beta_3 z(t), \tag{2.2}$$

where β_1 is an alternative specific constant. The parameters $\beta_2 < 0$ and $\beta_3 > 0$ indicate that the utility of choosing HVs increases with the decrease of the average HV price $r(t)$ and with the increase of the government investment in HV-specific infrastructure $z(t)$. Clearly, the relative values of β_1, β_2 and β_3 can also scale the impact of $r(\cdot)$ and $z(\cdot)$ on the utility of choosing HVs. For example, a smaller value of β_2 indicates that customers are more sensitive to the price of HVs, while a larger value of β_3 implies a prevailing impact of infrastructure investment on the utility of opting HVs. Note that it is reasonable for AVs to utilize HV-specific infrastructure, i.e., AVs and HVs share the road. However, AV-specific infrastructure may not be easily accessible to HVs, such as exclusive AV lanes [58] and roadside units for AV communications [62]. The term "HV-specific" is adopted due to lack of proper wording. There is no control imposed on the variables associated with HVs. In other words, the average HV price $r(t)$ is not intentionally regulated and the amount of investment in HV-specific infrastructure $z(t)$ is considered as it has been planned for without any extra intervention. However, they can be easily considered as external control inputs if required. Similarly, the utility function for choosing AVs over HVs is given by

$$V_{\mathrm{AV}}(t) = \tilde{\beta}_1 + \tilde{\beta}_2 \left[h(t) - u_1(t)\right] + \tilde{\beta}_3 u_2(t), \tag{2.3}$$

where the alternative specific parameters $\tilde{\beta}_1$, $\tilde{\beta}_2 < 0$, and $\tilde{\beta}_3 > 0$ have similar interpretations as those appearing in equation (2.2). The function $h(t)$ represents the average price of AVs at time t and its value is likely to decrease with time due to increasing maturity of AV technologies and potential mass production of AVs [2]. In other words, the time-variant price $h(t)$ implicitly captures the innovation of AVs advancing over time and the economies of scale due to possible mass production. The variable $u_1(t)$ denotes the amount of average subsidy for purchasing AVs and is assumed to be less than $h(t)$, while $u_2(t)$ represents the amount of government investment in AV-specific infrastructure. Clearly, the utility function $V_{\mathrm{AV}}(t)$ is manageable since $u_1(t)$ and $u_2(t)$ are regulatable control inputs.

As commonly seen in discrete choice modeling, the error terms in the utility functions

introduced above are assumed to follow a Gumbel distribution [75]. Consequently, the estimated probability of choosing HVs over AVs is given by

$$P_1(t) = \frac{e^{V_{\mathrm{HV}}(t)}}{e^{V_{\mathrm{HV}}(t)} + e^{V_{\mathrm{AV}}(t)}}. \tag{2.4}$$

Similarly, the estimated probability of choosing AVs over HVs is given by

$$P_2(t) = \frac{e^{V_{\mathrm{AV}}(t)}}{e^{V_{\mathrm{HV}}(t)} + e^{V_{\mathrm{AV}}(t)}}. \tag{2.5}$$

Clearly, the decision variables u_1 and u_2 are bounded due to practicality, for example, $\underline{u}_1 \leq u_1 \leq \overline{u}_1$ and $\underline{u}_2 \leq u_2 \leq \overline{u}_2$, with $\overline{u}_1 \geq \underline{u}_1 \geq 0$ and $\overline{u}_2 \geq \underline{u}_2 \geq 0$. Let the vector of decision variables be defined as $u = (u_1, u_2)^T \in \mathbb{R}^2$. Hence, the associated constraint set can be written as

$$U \coloneqq \left\{ u = (u_1, u_2)^T \in \mathbb{R}^2 : \underline{u}_1 \leq u_1 \leq \overline{u}_1,\ \underline{u}_2 \leq u_2 \leq \overline{u}_2 \right\}. \tag{2.6}$$

Note that these variables are time-dependent, that is, they are functions of time. The argument t, for simplicity, has been omitted as seen also in the remainder of this chapter, whenever appropriate to do so.

Let $d_2(t) = d(t)P_2(t)$ denote the number of customers adopting AVs at time t. The mathematical correlation between $d_2(t)$ and the AV subsidy u_1 is summarized in the following lemmas.

Lemma 2.2.1. *Given a time-dependent total demand $d(t) > 0$, the demand for AVs, i.e., $d_2(t) = d(t)P_2(t)$, increases with the increase of the amount of subsidies $u_1(t)$.*

Proof. Taking the partial derivative of the AV demand $d_2(t)$ with respect to the decision variable $u_1(t)$, it follows that

$$\frac{\partial d_2(t)}{\partial u_1(t)} = \frac{\left[-\tilde{\beta}_2 e^{V_{\mathrm{AV}}(t)} \left(e^{V_{\mathrm{HV}}(t)} + e^{V_{\mathrm{AV}}(t)} \right) + \tilde{\beta}_2 e^{2V_{\mathrm{AV}}(t)} \right] d(t)}{\left(e^{V_{\mathrm{HV}}(t)} + e^{V_{\mathrm{AV}}(t)} \right)^2} = \frac{-\tilde{\beta}_2 d(t) e^{V_{\mathrm{HV}}(t) + V_{\mathrm{AV}}(t)}}{\left(e^{V_{\mathrm{HV}}(t)} + e^{V_{\mathrm{AV}}(t)} \right)^2} \tag{2.7}$$

Since $\tilde{\beta}_2 < 0$ and $d(t) > 0$, we have $\partial d_2(t)/\partial u_1(t) > 0$ for $t \in I$. That is, the demand for AVs, $d_2(t)$, increases with the increase of the amount of subsidies $u_1(t)$. This completes the proof. □

Similarly, the correlation between $d_2(t)$ and the amount of government investment in AV-specific infrastructure $u_2(t)$ is summarized as follows.

Lemma 2.2.2. *Given a time-dependent total demand $d(t) > 0$, the demand for AVs, i.e., $d_2(t) = d(t)P_2(t)$, increases with the increase of the amount of investment in AV-specific infrastructure u_2.*

Proof. Taking the partial derivative of the AV demand $d_2(t)$ with respect to the decision variable $u_2(t)$ yields

$$\frac{\partial d_2(t)}{\partial u_2(t)} = \frac{\left[\tilde{\beta}_3 e^{V_{\mathrm{AV}}(t)}\left(e^{V_{\mathrm{HV}}(t)} + e^{V_{\mathrm{AV}}(t)}\right) - \tilde{\beta}_3 e^{2V_{\mathrm{AV}}(t)}\right] d(t)}{\left(e^{V_{\mathrm{HV}}(t)} + e^{V_{\mathrm{AV}}(t)}\right)^2} = \frac{\tilde{\beta}_3 d(t) e^{V_{\mathrm{HV}}(t)+V_{\mathrm{AV}}(t)}}{\left(e^{V_{\mathrm{HV}}(t)} + e^{V_{\mathrm{AV}}(t)}\right)^2} \quad (2.8)$$

Since $\tilde{\beta}_3 > 0$ and $d(t) > 0$, we have $\partial d_2(t)/\partial u_2(t) > 0$ for $t \in I$. That is, the demand for AVs, $d_2(t)$, increases with the increase of the amount of investment in AV-specific infrastructure $u_2(t)$. This completes the proof. □

Remark 1. *Lemma 2.2.1 and Lemma 2.2.2 indicate that the total market demand $d(t)$ can be properly distributed among customers purchasing HVs and AVs by adjusting the amount of AV subsidies u_1 and that of the investment in AV-specific infrastructure u_2. This motivates us to consider u_1 and u_2 as the natural decision variables for promoting AV integration due to their ease of implementability, which is consistent with the observations revealed in [65–67].*

2.3 Problem Formulation

The objective is to determine the optimal policy for AV integration into the auto market over a given period of time I so that a desired MPR is achieved subject to practical constraints, while minimizing the cost associated with AV subsidies and infrastructure investment. As a result, the optimal integration policy will serve as a guideline for regulating AV subsidy and adjusting AV infrastructure investment.

For convenience of analysis, we shall write the system dynamics in a compact form. To this end, let $x = (x_{\mathrm{HV}}, x_{\mathrm{AV}})^T \in \mathbb{R}^2$ denote the state vector representing the number of HVs and AVs in the auto market. Hence, the system dynamics given by equation (2.1)

can be written in the following compact form

$$\dot{x} = f(t, x, u),\ t \in I \coloneqq [t_0, t_f]\,,\ x(t_0) = x_0, \tag{2.9}$$

where the nonlinear function $f : I \times \mathbb{R}^2 \times \mathbb{R}^2 \longrightarrow \mathbb{R}^2$ is measurable in t on I and continuous in x and u on $\mathbb{R}^2 \times \mathbb{R}^2$, representing the system dynamics identical to equation (2.1). As introduced before, $I \coloneqq [t_0, t_f]$ denotes the finite planning horizon readily adjustable for the government agency. The following property of the vector field f is easily verified.

Property 1. *The vector field f is continuously differentiable with respect to both the state x and the decision vector u.*

Definition 1. *The market penetration rate of AVs at any time $t \in I$ is defined as* $\phi(t) = \frac{x_{AV}(t)}{x_{HV}(t)+x_{AV}(t)}$.

Based on the goal mentioned above, we introduce the following objective functional

$$J(u) \coloneqq \int_{t_0}^{t_f} \ell(t, x(t), u(t))dt + \Phi(x(t_f)), \tag{2.10}$$

where, on the right-hand side, the first and second terms represent the running cost and terminal cost, respectively. We shall introduce the following assumptions on the functions ℓ and Φ.

Assumption 1. *The scalar-valued function ℓ is continuously differentiable with respect to both the state x and the decision vector u.*

Assumption 2. *The scalar-valued function Φ is continuously differentiable with respect to the state x.*

Note that the above Assumption 1 and Assumption 2 are fairly general in the sense that they are easily satisfied in a broad range of practical engineering applications, including the following general formulation for optimal AV integration. For instance, a desired MPR may be expected to be reached at the end of the planning horizon t_f, while minimizing the cost associated with AV subsidies and infrastructure investment. To this end, equation (2.10) is explicitly written as

$$J(u) = \underbrace{\int_{t_0}^{t_f} \left[u_1(t)d_2(t) + u_2(t)\right] dt}_{\text{running cost}} + \underbrace{(1/2)w\left(\phi(t_f) - \tilde{\phi}\right)^2}_{\text{terminal cost}}, \tag{2.11}$$

where the running cost denotes the sum of AV subsidies and investment in AV-specific infrastructure, and the terminal cost represents the penalty, with a positive weight w placed on the discrepancy between the desired MPR $\tilde{\phi}$ and the actual MPR $\phi(t_f)$ attained at the end of the planning period.

Remark 2. *The objective functional given by equation* (2.11) *is focused on reaching the desired MPR at the end of the planning horizon while minimizing the cost associated with the AV integration policy. This is reasonable from the perspective of policy design. However, one could also include the benefits obtained from AV adoption into equation* (2.11) *if necessary.*

In what follows, we show that minimizing the running cost of equation (2.11) can be equivalently written as a standard quadratic minimization form in terms of the decision vector u.

Proposition 2.3.1. *Let the integrand of the running cost of equation* (2.11) *be denoted by*

$$\ell(t, u(t)) = u_1(t)d_2(t) + u_2(t) \coloneqq \ell_1(t, u(t)) + \ell_2(t, u(t)), \tag{2.12}$$

with $\ell_1(t, u(t)) = u_1(t)d_2(t)$ *and* $\ell_2(t, u(t)) = u_2(t)$. *Given a time-dependent market demand* $d(t) > 0$, *the minimization of the running cost* $\int_{t_0}^{t_f} \ell(t, u(t))dt$ *is equivalent to minimizing the quadratic term* $\int_{t_0}^{t_f} (1/2)u^T Q u dt$, *where* $Q = diag(q_1, q_2) \in \mathbb{R}^{2\times 2}$ *is a positive semi-definite matrix representing the weight given to the cost associated with AV subsidies and infrastructure investment.*

Proof. It is easily observed that

$$\frac{\partial}{\partial u_1(t)}\ell_1(t, u(t)) = d_2(t) + u_1(t)\frac{\partial d_2(t)}{\partial u_1(t)} > 0, \tag{2.13}$$

due to the fact that $d_2(t) > 0$, $u_1(t) \geq 0$, and $\partial d_2(t)/\partial u_1(t) > 0$ for $t \in I$ as shown in Lemma 2.2.1. Hence, ℓ_1 is a monotonically increasing function with respect to the decision variable u_1. Thus, it is easy to verify that

$$\min \int_{t_0}^{t_f} \ell_1(t, u(t))dt \Longleftrightarrow \min \int_{t_0}^{t_f} (1/2)q_1 u_1(t)^2 dt,$$

subject to the system dynamics given by equation (2.1) and the compact constraint set U, with q_1 being a scalar-valued positive weight associated with the cost of AV subsidies. Similarly, we have

$$\min \int_{t_0}^{t_f} \ell_2(t, u(t))dt \Longleftrightarrow \min \int_{t_0}^{t_f} (1/2)q_2 u_2(t)^2 dt,$$

due to the fact that $u_2(t) \geq 0$ and $\ell_2(t, u(t)) = u_2(t)$ is an increasing affine function in u_2, with q_2 being a scalar-valued positive weight associated with the investment in AV-specific infrastructure. Therefore, it follows that

$$\begin{aligned}\min \int_{t_0}^{t_f} \ell(t, u(t))dt &= \min \int_{t_0}^{t_f} \left[\ell_1(t, u(t)) + \ell_2(t, u(t))\right] dt \\ &\Longleftrightarrow \min \int_{t_0}^{t_f} \left[(1/2)q_1 u_1(t)^2 + (1/2)q_2 u_2(t)^2\right] dt = \min \int_{t_0}^{t_f} (1/2)u^T Q u dt,\end{aligned}$$

where $Q = \text{diag}(q_1, q_2) \in \mathbb{R}^{2\times 2}$ is a positive semi-definite matrix representing the weight given to the cost associated with AV subsidies and infrastructure investment. This completes the proof. □

By virtue of Proposition 2.3.1, the objective functional given by equation (2.11) can be equivalently written as

$$J(u) = \int_{t_0}^{t_f} (1/2)u^T Q u dt + (1/2)w \left(\phi(t_f) - \tilde{\phi}\right)^2, \tag{2.14}$$

To achieve our objective the above equation (2.14) is to be minimized. Note that equation (2.14) with a standard quadratic form is one possible illustration of the general objective functional given by equation (2.10). Various explicit expressions of equation (2.10) can be appropriately defined depending on the specific goal to be achieved by the government agency. The weights, Q and w, are introduced to balance each term in the objective functional, depending on the preference of the decision maker. For example. the parameter w may be chosen significantly larger if much more emphasis is given to achieving the desired MPR. The equivalence transformation carried out above is to arrive at a quadratic objective functional, which is convex and smooth, making evaluation of derivatives easy to handle. This is commonly seen in dealing with optimal control of nonlinear dynamical systems [76].

Proposition 2.3.2. *The nonlinear function f in equation* (2.9) *is Lipschitz continuous with a Lipschitz constant $K \geq 0$, with respect to the state vector x.*

It is clear that the Proposition 2.3.2 comes from the fact that f has bounded first derivatives. In other words, the time derivative of each element on the right-hand side of equation (2.1) is bounded.

Now we shall present the well-known Grönwall's inequality that will be used later in the proof of existence of an optimal AV integration policy.

Lemma 2.3.3. *(Grönwall's inequality) Let ν, φ and g be real-valued functions defined on $I = [t_0, t_f]$. If g satisfies the integral inequality*

$$g(t) \leq \nu(t) + \int_{t_0}^{t} \varphi(s)g(s)ds, \ \forall\ t \in I,$$

where the function ν is non-decreasing and φ is non-negative, then

$$g(t) \leq \nu(t) \exp\left(\int_{t_0}^{t} \varphi(s)ds\right), \ \forall\ t \in I.$$

Let $\mathcal{U}_{ad}$ and $B_\infty(I, \mathbb{R}^2)$ denote the set of admissible AV integration policies and the space of bounded and real-valued functions from I to $\mathbb{R}^2$, respectively. Before addressing the optimal control problem formulated above, we shall first consider the question of existence of an optimal AV integration policy. This is presented in the following theorem.

Theorem 2.3.4. *Consider the dynamical system described by equation* (2.9) *with the objective functional given by equation* (2.10). *Let $x(t) = x(u)(t)$, $t \in I$, be the solution to equation* (2.9) *corresponding to the integration policy $u(t) \in \mathcal{U}_{ad}$. Then, there exists an optimal AV integration policy u^o at which J attains its minimum.*

Proof. First of all, we show that the control to solution map $u \longrightarrow x(u)$ from $\mathcal{U}_{ad}$ to $B_\infty(I, \mathbb{R}^2)$ is continuous. Let $u^k \in \mathcal{U}_{ad}$ be any admissible AV integration policy. Let $x^k = x(u^k)$ and $x^o = x(u^o)$ denote the solutions of equation (2.9) corresponding to the integration policies u^k and u^o, respectively. Clearly, x^k and x^o satisfy the following integral equations

$$x^k(t) = x_0 + \int_0^t f(s, x^k(s), u^k(s))ds, \ t \in I, \tag{2.15}$$

$$x^o(t) = x_0 + \int_0^t f(s, x^o(s), u^o(s))ds, \ t \in I, \tag{2.16}$$

where $x^k(t) = x(u^k)(t)$, and $x^o(t) = x(u^o)(t)$, $t \in I$. Subtracting equation (2.16) from equation (2.15) term by term, we obtain

$$x^k(t) - x^o(t) = \int_0^t \Big[f(s, x^k(s), u^k(s)) - f(s, x^o(s), u^o(s)) \Big] \, ds. \tag{2.17}$$

Since f is Lipschitz continuous with a Lipschitz constant K, taking the norm on both sides of equation (2.17) and using triangle inequality, we obtain

$$||x^k(t) - x^o(t)|| \leq \int_0^t K||x^k(s) - x^o(s)||ds. \tag{2.18}$$

Rewriting the expression (2.18) and applying Grönwall's inequality, we have

$$\begin{aligned} ||x^k(t) - x^o(t)|| &\leq \int_0^t K||x^k(s) - x^o(s)||ds \\ &\leq ||x^k(0) - x^o(0)|| + \int_0^t K||x^k(s) - x^o(s)||ds \\ &\leq ||x^k(0) - x^o(0)||e^{Kt} \\ &\leq ||x^k(0) - x^o(0)||e^{Kt_f}. \end{aligned} \tag{2.19}$$

Since $x^k(0) \longrightarrow x^o(0)$ in the norm topology, the right-hand side of expression (2.19) converges to zero with respect to $t \in I$. Hence it follows that

$$\lim_{k \to \infty} \sup ||x^k(t) - x^o(t)|| = 0, \ t \in I. \tag{2.20}$$

Therefore, $x^k \longrightarrow x^o$ as $u^k \longrightarrow u^o$. This shows the continuity of the decision to solution map $u \longrightarrow x(u)$.

Since $\mathcal{U}_{ad}$ is compact, it suffices to show that the map $u \longrightarrow J(u)$ is continuous on $\mathcal{U}_{ad}$. Letting $u^k \longrightarrow u^o$ in $\mathcal{U}_{ad}$, it follows from the above results on the continuity of the map $u \longrightarrow x(u)$ that $x(u^k) \longrightarrow x(u^o)$. By virtue of continuity of ℓ and Φ, it follows that

$$\ell(t, x^k(t), u^k(t)) \longrightarrow \ell(t, x^o(t), u^o(t)) \tag{2.21}$$

$$\Phi(x^k(t_f)) \longrightarrow \Phi(x^o(t_f)) \tag{2.22}$$

Clearly, it follows from (2.21) that

$$\int_{t_0}^{t_f} \ell(t, x^k(t), u^k(t))dt \longrightarrow \int_{t_0}^{t_f} \ell(t, x^o(t), u^o(t))dt \tag{2.23}$$

Summing up expressions (2.22) and (2.23) leads to

$$\int_{t_0}^{t_f} \ell(t, x^k(t), u^k(t))dt + \Phi(x^k(t_f)) \longrightarrow \int_{t_0}^{t_f} \ell(t, x^o(t), u^o(t))dt + \Phi(x^o(t_f)) \tag{2.24}$$

That is

$$J(u^k) \longrightarrow J(u^o) \tag{2.25}$$

This proves that J is continuous on $\mathcal{U}_{ad}$. Since $\mathcal{U}_{ad}$ is compact, it is clear that there exists an optimal AV integration policy $u^o \in \mathcal{U}_{ad}$ at which J attains its minimum. This completes the proof. □

2.4 Solution Method

In this section, we derive necessary conditions of optimality for the optimal control problem formulated above to characterize the mathematical properties of the optimal AV integration policy. Based on the optimality conditions derived, an iterative computational procedure is developed to determine the optimal AV integration policy, i.e., the optimum AV subsidy and investment in AV-specific infrastructure, over any given finite planning horizon.

2.4.1 Necessary Conditions of Optimality

First, we shall introduce the Gâteaux (directional) differential which will be used in the derivation of optimality conditions.

Definition 2. *(Gâteaux differential) Suppose X and Y are Banach spaces and $F : X \longrightarrow Y$. The function F is said to be Gâteaux differential at $x \in X$ in the direction $v \in X$ if the limit*

$$dF(x; v) \coloneqq \frac{d}{d\tau} F(x + \tau v)\bigg|_{\tau=0} = \lim_{\tau \to 0} \frac{F(x + \tau v) - F(x)}{\tau}$$

exists for some fixed v.

Define the Hamiltonian function as follows

$$H(t, x, \psi, u) \coloneqq \langle f(t, x, u), \psi \rangle + \ell(t, x, u),\ (t, x, \psi, u) \in I \times \mathbb{R}^2 \times \mathbb{R}^2 \times \mathbb{R}^2 \tag{2.26}$$

where $\langle \cdot, \cdot \rangle$ represents an inner product and ψ is the adjoint state vector. We denote by ℓ_x, Φ_x, and H_u the gradients of ℓ, Φ with respect to the state vector x, and that of H with respect to the decision vector u, respectively. The notation f_x^* represents the adjoint of the Hessian f_x. We use $AC(I, \mathbb{R}^n)$ to denote the class of absolutely continuous functions defined on I and taking values from $\mathbb{R}^n$. Now we are ready to present the necessary conditions of optimality as follows.

Theorem 2.4.1. *Consider the dynamical system described by equation* (2.9) *with the objective functional given by equation* (2.10). *Let* $u^o(t) \in \mathcal{U}_{ad}$ *be an AV integration policy corresponding to the solution trajectory* $x^o \in AC(I, \mathbb{R}^2)$. *Then, for the pair* $\{x^o, u^o\}$ *to be optimal it is necessary that there exists a function* ψ *satisfying the following necessary conditions:*

$$\int_{t_0}^{t_f} \langle H_u(t, x^o(t), \psi(t), u^o(t)), u(t) - u^o(t) \rangle \, dt \geq 0, \ \forall \ u(t) \in \mathcal{U}_{ad}, \tag{2.27}$$

$$\dot{x}^o(t) = H_\psi = f(t, x^o(t), u^o(t)), \ x^o(t_0) = x_0, \tag{2.28}$$

$$\dot{\psi}(t) = -H_x = -f_x^*(t, x^o(t), u^o(t))\psi(t) - \ell_x(t, x^o(t), u^o(t)), \ \psi(t_f) = \Phi_x(x^o(t_f)). \tag{2.29}$$

Proof. Let $x(t) \in AC(I, \mathbb{R}^2)$ be any solution of the dynamical system (2.9) corresponding to the AV integration policy $u(t) \in \mathcal{U}_{ad}$. Since $u^o(t) \in \mathcal{U}_{ad}$ is optimal with $x^o(t)$ being the associated state trajectory, it follows that

$$J(u^o) \leq J(u). \tag{2.30}$$

Substituting with equation (2.10) yields

$$\int_{t_0}^{t_f} \ell(t, x^o(t), u^o(t))dt + \Phi(x^o(t_f)) \leq \int_{t_0}^{t_f} \ell(t, x(t), u(t))dt + \Phi(x(t_f)), \ \forall \ u(t) \in \mathcal{U}_{ad}. \tag{2.31}$$

Let $u^\epsilon(t) = u^o(t) + \epsilon(u(t) - u^o(t))$ for any $\epsilon \in [0, 1]$. Since U is a closed convex set, $\mathcal{U}_{ad}$ is a closed convex subset of $L_\infty(I, \mathbb{R}^2)$ and hence $u^\epsilon(t) \in \mathcal{U}_{ad}$. Therefore, we have

$$J(u^o) \leq J(u^\epsilon), \ \forall \ \epsilon \in [0, 1] \text{ and } u \in \mathcal{U}_{ad}. \tag{2.32}$$

It follows from the inequality (2.29) that

$$dJ(u^o; u - u^o) \geq 0, \ \forall \ u \in \mathcal{U}_{ad}, \tag{2.33}$$

where $dJ(u^o; u - u^o)$ denotes the Gâteaux differential of the objective functional J at the optimal AV integration policy u^o in the direction $(u - u^o)$.

Let $x^\epsilon(t)$ denote the solution of equation (2.9) corresponding to the AV integration policy $u^\epsilon(t)$ with the same initial condition $x^\epsilon(t_0) = x_0$. Due to regularity of the function f in x and u it follows that

$$\lim_{\epsilon \to 0} u^\epsilon(t) \longrightarrow u^o(t), \quad \lim_{\epsilon \to 0} x^\epsilon(t) \longrightarrow x^o(t).$$

Recall that the state trajectories x^o and x^ϵ satisfy the following differential equations

$$\dot{x}^o(t) = f(t, x^o(t), u^o(t)), \ t \in I, \tag{2.34}$$

$$\dot{x}^\epsilon(t) = f(t, x^\epsilon(t), u^\epsilon(t)), \ t \in I. \tag{2.35}$$

Subtracting equation (2.34) from equation (2.35) leads to

$$\begin{aligned}(d/dt)(x^\epsilon(t) - x^o(t)) = f_x(t, x^o(t), u^o(t))(x^\epsilon(t) - x^o(t)) \\ + f_u(t, x^o(t), u^o(t))(u^\epsilon(t) - u^o(t)) + o(\epsilon)\end{aligned} \tag{2.36}$$

where $o(\epsilon)$ denotes the remaining terms in the approximation. Specifically

$$\lim_{\epsilon \to 0} \{(1/\epsilon) o(\epsilon)\} = 0. \tag{2.37}$$

Let $y(t)$ denote the following limit

$$y(t) = \lim_{\epsilon \to 0} \{(1/\epsilon)(x^\epsilon(t) - x^o(t))\}. \tag{2.38}$$

Dividing both sides of equation (2.36) by ϵ and letting $\epsilon \to 0$, and plugging the expression of $y(t)$, we arrive at the initial value problem

$$\dot{y}(t) = f_x(t, x^o(t), u^o(t)) y(t) + f_u(t, x^o(t), u^o(t))(u(t) - u^o(t)), \ y(0) = 0. \tag{2.39}$$

It follows from expression (2.33) that

$$\begin{aligned}
dJ(u^o; u-u^o) &= \lim_{\epsilon\to 0} \frac{J(u^\epsilon)-J(u^o)}{\epsilon} \\
&= \lim_{\epsilon\to 0} \frac{\int_{t_0}^{t_f} \ell(t,x^\epsilon,u^\epsilon)dt + \Phi(x^\epsilon(t_f)) - \int_{t_0}^{t_f} \ell(t,x^o,u^o)dt - \Phi(x^o(t_f))}{\epsilon} \\
&= \lim_{\epsilon\to 0} \frac{\int_{t_0}^{t_f} \ell(t,x^\epsilon,u^\epsilon)dt - \int_{t_0}^{t_f} \ell(t,x^o,u^o)dt}{\epsilon} + \lim_{\epsilon\to 0} \frac{\Phi(x^\epsilon(t_f)) - \Phi(x^o(t_f))}{\epsilon} \\
&= \lim_{\epsilon\to 0} \frac{\int_{t_0}^{t_f} \left\{\langle \ell_x(t,x^o,u^o), x^\epsilon - x^o\rangle + \langle \ell_u(t,x^o,u^o), u^\epsilon - u^o\rangle\right\} dt}{\epsilon} \\
&\qquad + \lim_{\epsilon\to 0} \frac{\langle \Phi_x(x^o(t_f)), x^\epsilon(t_f) - x^o(t_f)\rangle}{\epsilon} \\
&= \int_{t_0}^{t_f} \left\{\langle \ell_x(t,x^o,u^o), y(t)\rangle + \langle \ell_u(t,x^o,u^o), u-u^o\rangle\right\} dt \\
&\qquad + \langle \Phi_x(x^o(t_f)), y(t_f)\rangle \geq 0. \qquad (2.40)
\end{aligned}$$

This inequality can be rearranged as

$$\begin{aligned}
dJ(u^o; u-u^o) = \int_{t_0}^{t_f} \langle \ell_x(t,x^o,u^o), y(t)\rangle\, dt + \langle \Phi_x(x^o(t_f)), y(t_f)\rangle \\
+ \int_{t_0}^{t_f} \langle \ell_u(t,x^o,u^o), u-u^o\rangle\, dt \geq 0. \qquad (2.41)
\end{aligned}$$

Clearly, the first two terms depend linearly on y and the third term is a linear functional of the integration policy. Note that equation (2.39) is linear in $(u-u^o)$. Since $f_u(t,x^o(t),u^o(t))$ is fixed, it is clear that the map

$$f_u(\cdot,x^o(\cdot),u^o(\cdot))(u(\cdot)-u^o(\cdot)) \longrightarrow y(\cdot) \qquad (2.42)$$

is linear. Since $x^o \in AC(I,\mathbb{R}^2)$ and I is a compact interval, we have $\sup\{\|x^o(t)\|,\ t \in I\} < \infty$. Since the decision constraint set U is compact, it follows that

$$f_u(\cdot,x^o(\cdot),u^o(\cdot))(u(\cdot)-u^o(\cdot)) \in L_1(I,\mathbb{R}^2). \qquad (2.43)$$

According to the theory of differential equations, equation (2.39) has a unique solution $y \in AC(I,\mathbb{R}^2)$. Therefor, we conclude that

$$f_u(\cdot,x^o(\cdot),u^o(\cdot))(u(\cdot)-u^o(\cdot)) \longrightarrow y(\cdot) \qquad (2.44)$$

is a bounded linear map. Let $\Gamma(y)$ represent the sum of first two terms of equation (2.41). That is

$$\Gamma(y) = \int_{t_0}^{t_f} \langle \ell_x(t, x^o, u^o), y(t) \rangle \, dt + \langle \Phi_x(x^o(t_f)), y(t_f) \rangle \, . \tag{2.45}$$

Consequently, the map

$$f_u(\cdot, x^o(\cdot), u^o(\cdot))(u(\cdot) - u^o(\cdot)) \longrightarrow \Gamma(y) \tag{2.46}$$

is a bounded linear map. Thus, by the Riesz representation theorem there exists a $\psi \in L_\infty(I, \mathbb{R}^2)$ such that

$$\begin{aligned} \Gamma(y) &= \int_{t_0}^{t_f} \langle \ell_x(t, x^o, u^o), y(t) \rangle \, dt + \langle \Phi_x(x^o(t_f)), y(t_f) \rangle \\ &= \int_{t_0}^{t_f} \langle f_u(t, x^o(t), u^o(t))(u(t) - u^o(t)), \psi(t) \rangle \, dt \\ &= \int_{t_0}^{t_f} \langle f_u^*(t, x^o(t), u^o(t))\psi(t), u(t) - u^o(t) \rangle \, dt, \end{aligned} \tag{2.47}$$

where f_u^* denotes the transpose of the Hessian f_u as defined before. Using this representation, the equation (2.41) can be rewritten as

$$\begin{aligned} dJ(u^o; u - u^o) &= \int_{t_0}^{t_f} \langle f_u^*(t, x^o(t), u^o(t))\psi(t) + \ell_u(t, x^o(t), u^o(t)), u(t) - u^o(t) \rangle \, dt \\ &= \int_{t_0}^{t_f} \langle H_u(t, x^o(t), \psi(t), u^o(t)), u(t) - u^o(t) \rangle \, dt \geq 0, \ \forall \ u(t) \in \mathcal{U}_{ad}. \end{aligned} \tag{2.48}$$

Hence, we have derived equation (2.27) of the necessary conditions of optimality provided that one can justify that $\psi \in AC(I, \mathbb{R}^2)$. Substituting with equation (2.39) and noting $y(0) = 0$, it follows from equation (2.47) that

$$\begin{aligned} \Gamma(y) &= \int_{t_0}^{t_f} \langle f_u(t, x^o(t), u^o(t))(u(t) - u^o(t)), \psi(t) \rangle \, dt \\ &= \int_{t_0}^{t_f} \langle \dot{y}(t) - f_x(t, x^o(t), u^o(t))y(t), \psi(t) \rangle \, dt \\ &= \int_{t_0}^{t_f} \langle \dot{y}(t), \psi(t) \rangle \, dt + \int_{t_0}^{t_f} \langle y(t), -f_x^*(t, x^o(t), u^o(t))\psi(t) \rangle \, dt \\ &= \langle y(t_f), \psi(t_f) \rangle - \int_{t_0}^{t_f} \left\langle y(t), \dot{\psi}(t) \right\rangle dt + \int_{t_0}^{t_f} \langle y(t), -f_x^*(t, x^o(t), u^o(t))\psi(t) \rangle \, dt \\ &= \langle y(t_f), \psi(t_f) \rangle + \int_{t_0}^{t_f} \left\langle y(t), -\dot{\psi}(t) - f_x^*(t, x^o(t), u^o(t))\psi(t) \right\rangle dt. \end{aligned} \tag{2.49}$$

Based on the observation of equation (2.45), the functional Γ is also given by

$$\Gamma(y) = \langle y(t_f), \Phi_x(x^o(t_f))\rangle + \int_{t_0}^{t_f} \langle y(t), \ell_x(t, x^o(t), u^o(t))\rangle \, dt. \tag{2.50}$$

Since equation (2.49) is equivalent to equation (2.50), clearly it follows that

$$\dot{\psi}(t) = -f_x^*(t, x^o(t), u^o(t))\psi(t) - \ell_x(t, x^o(t), u^o(t)), \ \psi(t_f) = \Phi_x(x^o(t_f)). \tag{2.51}$$

Since f_x^* and ℓ_x are integrable, and equation (2.51) is linear in ψ, it has a unique absolutely continuous solution, hence $\psi \in AC(I, \mathbb{R}^2)$. Therefore, we have derived equation (2.29) of the necessary conditions of optimality. Note that equation (2.28) is simply the state equation along the optimal trajectory. This completes the proof. □

Remark 3. *Following the classical minimum principle [68], we derived the necessary conditions of optimality presented above tailored for characterizing the mathematical properties of the optimal AV integration policy, allowing for the development of an iterative computational procedure presented in the following section. Other tailored versions of the minimum principle are developed also in the literature to address specific problems in transportation engineering, such as the one in [77] for proving that the differential variational inequality solution is a dynamic user equilibrium. Moreover, the proof shown above is well specialized for the optimal integration of AVs by virtue of Property 1 and Assumption 1.*

2.4.2 An Iterative Computational Procedure

In this section, we develop an iterative computational procedure, based on the necessary conditions of optimality presented above, to determine the optimal AV integration policy. This numerical procedure follows a gradient-based method which generates a sequence of AV integration policies $\{u^k\}$ along which the objective functional J converges to its minimum. Let u^k denote the AV integration policy at the k-th iteration. The iterative computation algorithm is presented as follows.

Step 1: Choose any feasible AV integration policy $u^1 = (u_1^1, u_2^1)^T \in \mathcal{U}_{ad}$ and compute the solutions of equation (2.9) giving x^1. At this stage we have the tuple $\{u^1, x^1\}$.

Step 2: Use $\{u^1, x^1\}$ in the adjoint equation (2.29) reproduced below

$$\dot{\psi}(t) = -f_x^*(t, x^1(t), u^1(t))\psi(t) - \ell_x(t, x^1(t), u^1(t)), \ \psi(t_f) = \Phi_x(x^1(t_f)). \tag{2.52}$$

This solves the adjoint equation backward in time, yielding the adjoint vector $\psi^1 := \{\psi^1(t),\ t \in I\}$. At this stage we have the triple $\{u^1, x^1, \psi^1\}$.

Step 3: Use the triple $\{u^1, x^1, \psi^1\}$ in the necessary conditions of optimality to verify if the following inequality holds,

$$\int_{t_0}^{t_f} \left\langle H_u(t, x^1, \psi^1, u^1), u - u^1 \right\rangle dt \geq 0,\ \forall\ u \in \mathcal{U}_{ad}. \tag{2.53}$$

If this holds, then u^1 is the optimal AV integration policy. Otherwise, go to Step 4.

Step 4: Use u^1 to generate the new AV integration policy u^2,

$$u^2 = u^1 - \varepsilon H_u(t, x^1(t), \psi^1(t), u^1(t)) \tag{2.54}$$

for $\varepsilon > 0$ sufficiently small so that $u^2 \in \mathcal{U}_{ad}$. Computing the objective functional $J(u^2)$ at u^2 using equation (2.10), one needs to check if the following stopping criterion

$$|J(u^2) - J(u^1)| > \varpi \tag{2.55}$$

is met for a prescribed small positive number ϖ. If this is satisfied, go to Step 1 with u^2 replacing u^1. For any prescribed $\varpi > 0$, the process is continued while $|J(u^{k+1}) - J(u^k)| > \varpi$ is satisfied within a given maximum number of iterations $N_{\max} \in \mathbb{N}^+$.

Theorem 2.4.2 (Convergence Theorem)**.** *Suppose the necessary conditions of optimality prescribed by Theorem 2.4.1 hold. Then, the algorithm presented above generates a sequence of AV integration policies $\{u^k\}$ along which the objective functional J monotonically converges to its minimum.*

Proof. Starting from any feasible AV integration policy u^1 at the first iteration, it follows from the Lagrange formula that

$$J(u^2) = J(u^1) + dJ(u^1; u^2 - u^1) + o(\varepsilon), \tag{2.56}$$

where $o(\varepsilon)$ denotes the higher order terms and the Gâteaux differential $dJ(u^1; u^2 - u^1)$ is given by

$$dJ(u^1; u^2 - u^1) = \int_{t_0}^{t_f} \left\langle H_u(t, x^1(t), \psi^1(t), u^1(t)), u^2(t) - u^1(t) \right\rangle dt. \tag{2.57}$$

Since $u^2 = u^1 - \varepsilon H_u(t, x^1(t), \psi^1(t), u^1(t))$ as seen in equation (2.54), it follows from equation (2.57) that

$$dJ(u^1; u^2 - u^1) = -\varepsilon \int_{t_0}^{t_f} ||H_u(t, x^1(t), \psi^1(t), u^1(t))||^2 dt < 0, \tag{2.58}$$

which indicates $J(u^1) > J(u^2)$ for a sufficiently small step size $\varepsilon > 0$.

This process is repeated by returning back to Step 1 with u^2 replacing u^1. Hence, following the steps presented in the computational algorithm, one can construct a sequence of AV integration policies $\{u^k\} \in \mathcal{U}_{ad}$ such that $J(u^1) > J(u^2) > \cdots > J(u^k) > \cdots$. This completes the proof. □

2.4.3 Application to Optimal AV Integration

In this section, we are interested to apply the solution method developed above to the AV integration problem formulated in Section 2.3. In fact, that is a standard Bolza problem, whose objective is to reach a desired MPR of AVs at the end of the planning horizon while minimizing the cost associated with AV subsidies and investment in AV-specific infrastructure. This is achieved by solving the Bolza problem defined with the objective functional given by equation (2.14) as reproduced below

$$J(u) = \int_{t_0}^{t_f} (1/2) u^T Q u dt + (1/2) w \left(\phi(t_f) - \tilde{\phi}\right)^2, \tag{2.59}$$

with the corresponding Hamiltonian function given by

$$H(t, x, \psi, u) = \langle f(t, x, u), \psi \rangle + (1/2) u^T Q u. \tag{2.60}$$

Hence, the adjoint equation is written as

$$\dot{\psi} = -H_x = -f_x^*(t, x, u)\psi. \tag{2.61}$$

The gradient H_u is calculated as

$$H_u = \frac{\partial H}{\partial u} = \frac{de^{V_{\text{HV}} + V_{\text{AV}}}}{\left(e^{V_{\text{HV}}} + e^{V_{\text{AV}}}\right)^2} \left(\tilde{\beta}_2(\psi_1 - \psi_2), \tilde{\beta}_3(\psi_2 - \psi_1)\right)^T + Qu. \tag{2.62}$$

2.5 Numerical Results

In this section, we conduct a series of numerical experiments to show the effectiveness and robustness of the proposed approach. All the numerical studies are carried out in MATLAB. The vehicle demand of the market, $d(t)$, could exhibit different functional forms, with logistic functions [78] and Gompertz functions [79] being the most widely used ones. In numerical studies, $d(t)$ is assumed to be a Gompertz function following the work [80]. It is given by

$$d(t) = a \cdot \exp\left(-\exp(b - c(t - t_0))\right), \ t \geq t_0, \tag{2.63}$$

where $a > 0$ is the market saturation since $\lim_{t\to\infty} a \cdot \exp\left(-\exp(b - c(t - t_0))\right) = a$, b determines the displacement along the t-axis, $c > 0$ describes the growth rate, and t_0 is the beginning of the planning period $I := [t_0, t_f]$. Equation (2.63) presents a widely employed functional form of the market demand. However, the theoretical results obtained in this work remain valid regardless of the functional form of $d(t)$.

In view of stochastic demands, one may rewrite equation (2.63) as follows

$$d(t) = a \cdot \exp(-\exp(b - c(t - t_0))) + W(t), \ t \geq t_0, \tag{2.64}$$

where $W \sim \mathcal{N}(0, \sigma^2)$ is a Gaussian random variable with mean 0 and variance σ^2. The larger σ^2 is, the greater uncertainty the demand $d(t)$ exhibits.

It is easy to observe that the theoretical results presented before remain valid. In view of this uncertain demand, a Monte Carlo simulation is to be carried out for computation with the iterative procedure presented in Section 2.4.2. Specifically, in Step 1 of Section 2.4.2 one needs to solve the state equation with multiple sample paths of the stochastic demand. Consequently, the adjoint equation is solved corresponding to each state trajectory in Step 2. The objective value at each iteration is calculated by averaging all the values of J obtained from each sample path of $d(t)$.

For illustrative purposes, we first consider a planning horizon of 60 years, i.e., $I := [0, 60]$. Note that this planning horizon is easily scalable and that it can be determined of the planner's choosing depending on the funding availability. Later we will also present interesting results of different planning horizons. The initial number of HVs is assumed to be $x_{\mathrm{HV}}(0) = 100.4$ million which is the number of registered cars in the

US in 2020 [81], while the number of AVs at $t_0 = 0$ is assumed to be $x_{\text{AV}}(0) = 0$. In other words, the planning is carried out for the years 2020–2060. The planning period can be easily modified if required without introducing any extra complexity in computation. The average price of HVs and AVs is expected to be decreasing with time due to increased technological maturity and reduced cost in mass production [2]. Hence, in numerical studies $r(t)$ and $h(t)$ are assumed to take the functional forms $r(t) = 38 - 0.1t$ and $h(t) = 68 - 0.4t$, $t \in I$, respectively. Consequently, at the beginning of the planning period one has $r(t_0) = 38$ and $h(t_0) = 68$, in thousands. The value of $r(t_0)$ is consistent with the average price of HVs in the US in 2020 [82]. The functional form of the average AV price, $h(t)$, is chosen such that its value is greater than that of $r(t)$, with a larger decreasing rate over the planning period considered. Similarly, the amount of average investment in HV-specific infrastructure, $z(t)$, is assumed to be linearly increasing, specifically, $z(t) = 187 + 0.1t$ in millions. Clearly, $z(t_0) = 187$ million, which is consistent with the value in the US in 2020 [83]. Due to limited information available, these functional forms are chosen in a reasonable way that is consistent with the general understanding in the literature. However, the approach proposed remains valid regardless of the form of these functions. Here these specific functional forms are chosen for the sole purpose of numerical illustrations.

The set of decision variables is defined as $U \coloneqq \{u = (u_1, u_2)^T \in \mathbb{R}^2 : 0 \leq u_1 \leq 1.15r(t_0),\ 0.5z(t_0) \leq u_2 \leq 2z(t_0)\} = \{u \in \mathbb{R}^2 : 0 \leq u_1 \leq 43.7,\ 93.5 \leq u_2 \leq 374\}$, which satisfies the conditions required. The set U can be easily modified depending on the level of funding availability of the government agency. Later in the numerical studies, we shall discuss specifically the impact of the set U on the choice of optimal AV integration policy. The interactive coefficients are chosen as $\gamma_1 = 6 \times 10^{-4}$ and $\gamma_2 = 4 \times 10^{-4}$. For simplicity, the alternative specific constants are chosen as $\{\beta_1 = \tilde{\beta}_1 = 0.1 > 0, \beta_2 = \tilde{\beta}_2 = -0.02 < 0, \beta_3 = \tilde{\beta}_3 = 0.02 > 0\}$. The weight parameters in equations (2.59) are given by $Q = \text{diag}(10^{-4}, 10^{-4})$ and $w = 2 \times 10^4$. These weights are chosen to balance the cost of AV subsidies and infrastructure investment and the penalty on the discrepancy between the desired MPR and the actual MPR achieved. We shall later carry out sensitivity analysis with respect to some important parameters. The step size and stopping criterion are set as $\varepsilon = 0.5$ and $\varpi = 1 \times 10^{-8}$, respectively. The simulation is run for a maximum number of $N_{\max} = 600$ iterations.

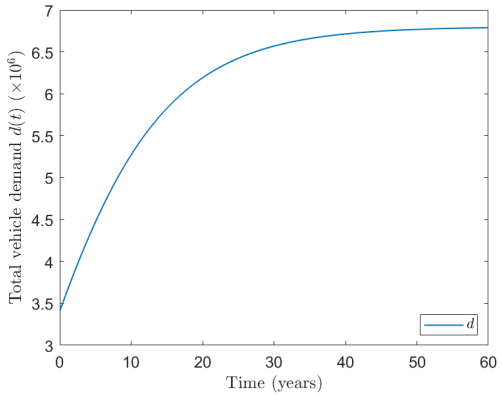

Figure 2.2: An increasing vehicle demand given by the Gompertz function $d(t) = 6.8\exp(-\exp(-0.37-0.1t))$, $t \in I := [0, 60]$.

2.5.1 Numerical Results for Increasing Demand

The market demand $d(t)$ is determined by a number of factors, including economic development, level of industrialization, etc. It has been revealed that the market demand in many developed western countries, such as the UK and Sweden, has halted and is expected to decline [84]. However, for a large number of developing nations, including China and Malaysia, the vehicle demand is projected to increase due to rapid industrialization and urbanization [85]. Hence, it would be interesting to consider both increasing and decreasing functional forms of the demand $d(t)$. We first consider the case with an increasing demand in this section, where $d(t)$ is assumed to be given by the Gompertz function $d(t) = 6.8\exp(-\exp(-0.37-0.1t))$ for the planning horizon $I := [0, 60]$, as illustrated in Fig. 2.2. It is easy to observe that $d(0) = 3.4$ million which is the number of cars sold in the US in 2020 [86]. In what follows, we consider various desired MPRs over the same planning horizon $I := [0, 60]$, with extensive results shown in Fig. 2.3 and Fig. 2.4.

Fig. 2.3a and Fig. 2.3b show the optimal AV subsidy u_1 and the optimal amount of investment in AV-specific infrastructure u_2, respectively. It is observed that for any given $\tilde{\phi}$ both u_1 and u_2 remain relatively low in the first 15 years or so due to a smaller demand $d(t)$ over that time period. With the demand $d(t)$ getting much larger afterwards, u_1 and u_2 take greater values to increase the utility of opting AVs,

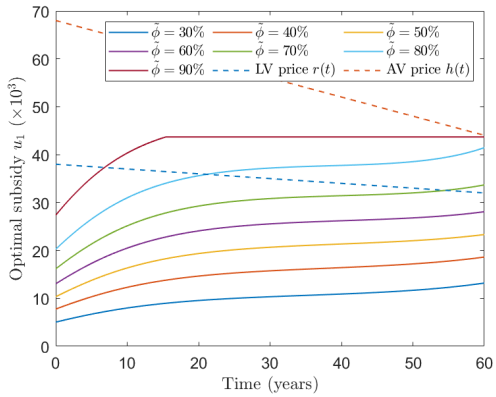

(a) Optimal subsidy for AVs

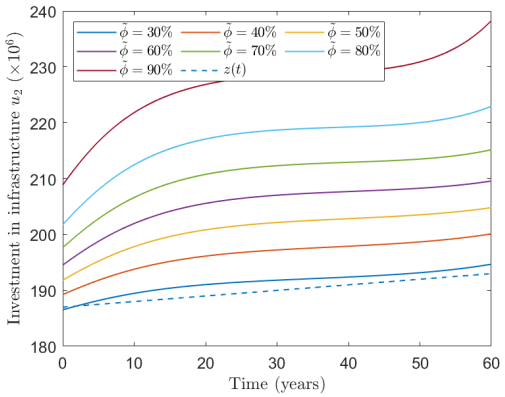

(b) Optimal investment in AV infrastructure

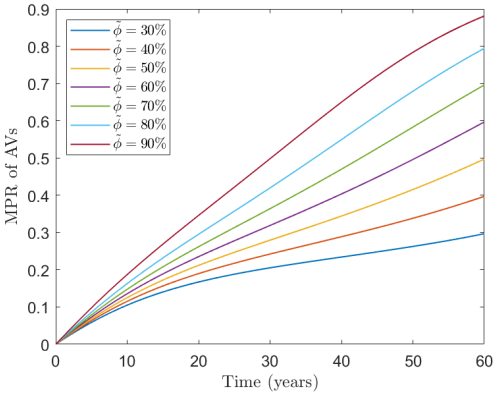

(c) MPR of AVs

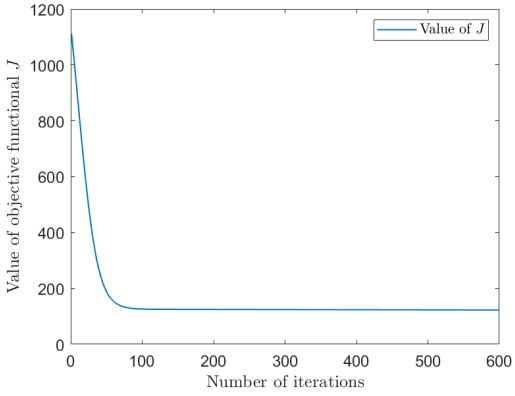

(d) Value of the objective functional J

Figure 2.3: Simulation results corresponding to an increasing demand shown in Fig. 2.2 with various desired MPRs $\tilde{\phi} = 30\%, 40\%, 50\%, 60\%, 70\%, 80\%, 90\%$ over the planning horizon $I := [0, 60]$. (a) Optimal subsidy u_1; (b) Optimal amount of investment in AV-specific infrastructure u_2; (c) Trajectory of the function ϕ representing the MPR; (d) The value of J, corresponding to $\tilde{\phi} = 50\%$, decreases with the increase of the number of iterations, showing the convergence of computation.

resulting in more potential customers being attracted to buy AVs in order to achieve the desired MPR at the end of planning period. In addition, the average investment in HV-specific infrastructure $z(t)$ is assumed to be increasing, contributing to customers choosing HVs. As a result, an increasing trend is observed in u_1 and u_2, as shown in Fig. 2.3a and Fig. 2.3b, respectively. Clearly, within the given period of planning, the

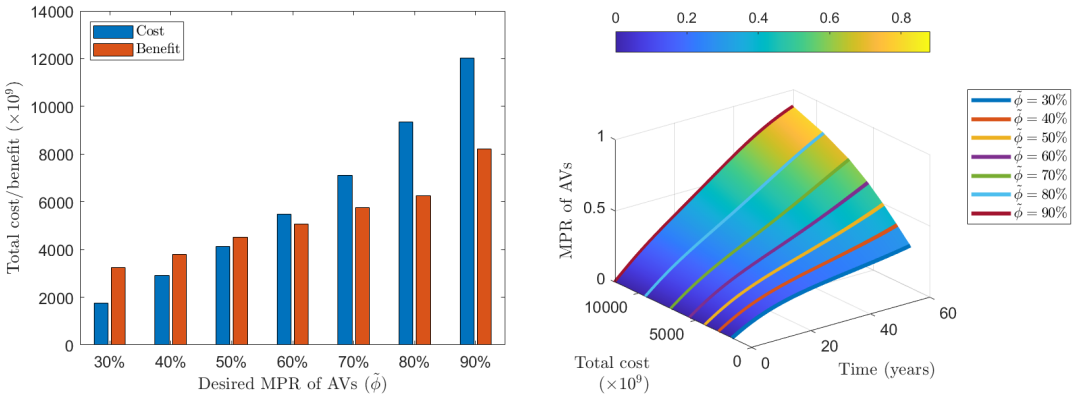

(a) Cost and benefit of AV integration

(b) MPR of AVs with the associated cost of AV integration

Figure 2.4: Simulation results corresponding to an increasing demand shown in Fig. 2.2 with a planning horizon $I := [0, 60]$. (a) Cost and benefit of optimal AV integration over the period I; (b) Illustration of the function ϕ with the associated total cost of AV integration over the period I.

AV subsidy and the investment in AV-specific infrastructure increase with $\tilde{\phi}$. Fig. 2.3c shows the trajectory of the MPR ϕ as a result of application of the optimal integration policy presented in Fig. 2.3a and Fig. 2.3b. It is observed that all the desired MPRs are achieved at the end of the planning period, except for $\tilde{\phi} = 90\%$ due to limited funding for AV subsidies. This is consistent with the fact that the optimal AV subsidy has reached its upper bound for $\tilde{\phi} = 90\%$ as shown in Fig. 2.3a. As a result, much more investment is put in AV-specific infrastructure (the top curve corresponding to $\tilde{\phi} = 90\%$ in Fig. 2.3b) to reduce the discrepancy between the desired MPR and the actual MPR achieved. However, such effort is also limited due to the penalty placed on the cost of investment in infrastructure as seen in equation (2.59). Hence, it is possible that very high MPRs could be achieved within the given period of planning if neglecting the cost of application of the AV integration policy. In other words, only the terminal cost associated with the discrepancy between $\phi(t_f)$ and $\tilde{\phi}$ is considered in the objective functional (2.59). Another alternative could be extending the time horizon I to allow for a longer planning period. In fact, this leaves much room for flexible implementation depending on the funding availability of the government agency. For a specific desired MPR, $\tilde{\phi} = 50\%$, the value of the objective functional J, as a function of the number

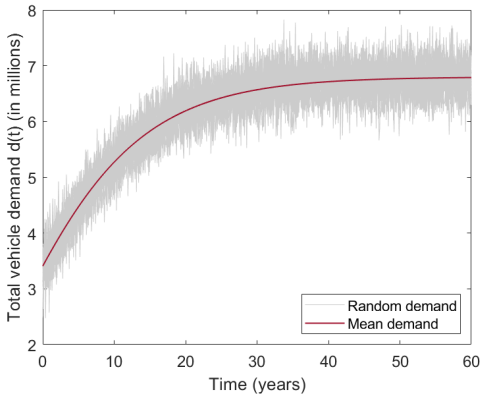

Figure 2.5: A set of 20 realizations of a stochastically increasing demand, with the mean given by the Gompertz function in Fig. 2.2.

of iterations, is shown in Fig. 2.3d. It is observed to decrease with the increase of the number of iterations, which is consistent with the outline of the iterative computational procedure presented in Section 2.4.2.

Clearly, there are costs associated with the implementation of the optimal AV integration policy, namely the amount of AV subsidies and investment in AV-specific infrastructure. However, the adoption of AVs also brings a great deal of benefits, such as crash savings, travel time reduction, fuel efficiency and parking benefits, etc [2]. As revealed in [2], major social AV impacts, in terms of monetary savings, are estimated to be around $\$2,000$ per year per AV, and may eventually approach nearly $\$4,000$. Hence, we are interested to carry out a cost-benefit analysis on AV integration. We consider conservatively the least estimate of $\$2,000$ benefit for each AV per year. The total cost is the sum of the amount of AV subsidies and that of the investment in AV-specific infrastructure over the planning horizon I, while the total benefit is calculated as the monetary savings obtained by all AVs over the same period. Given the period of planning $I \coloneqq [0, 60]$, the total cost and benefit corresponding to various desired MPRs are shown in Fig. 2.4a. It is clearly observed that both the cost and the benefit increase with the increase of the desired MPR. However, the benefit is greater than the cost at relatively low $\tilde{\phi}$, while the cost outweighs the benefit at much higher $\tilde{\phi}$. This is due to the fact that much more AV subsidies and investment in AV-specific infrastructure are required to achieve higher desired MPRs, in the given period of planning. The amount

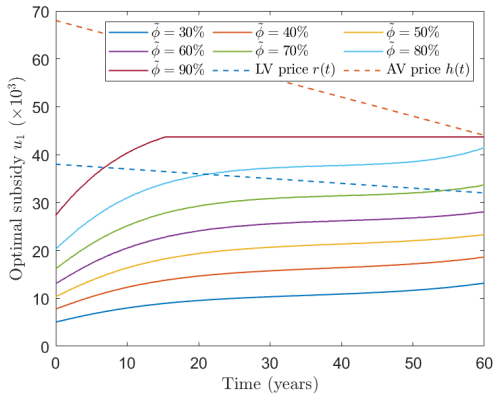

(a) Expected optimal subsidy for AVs

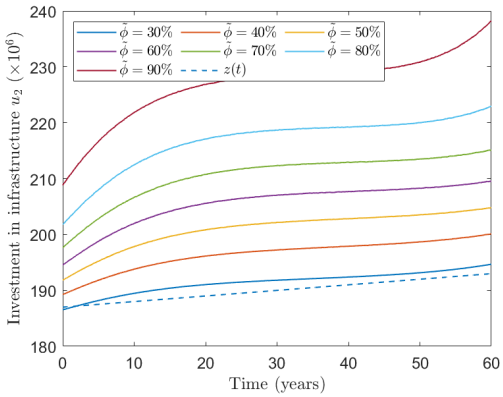

(b) Expected optimal investment in AV infrastructure

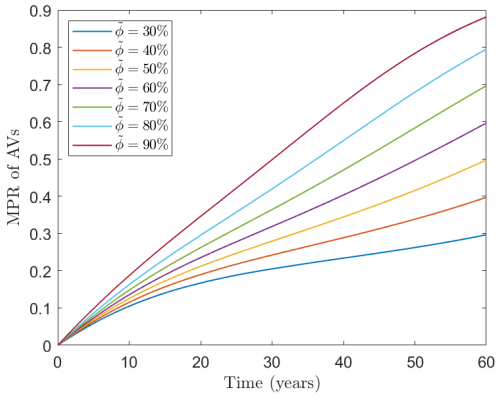

(c) Expected MPR of AVs

Figure 2.6: Simulation results corresponding to a stochastically increasing demand with the mean shown in Fig. 2.2, considering various desired MPRs over the planning horizon $I := [0, 60]$. (a) Expected optimal subsidy u_1; (b) Expected optimal investment in AV-specific infrastructure u_2; (c) Expected trajectory of the function ϕ representing the MPR.

of benefits achieved for very high desired MPRs is not comparable with that of the cost required. For the scenario considered, it might be suggested that the desired MPR, i.e., $\tilde{\phi}$, be set no more than 50% in order to achieve a positive net benefit. This provides significant insights for the government agency into the level of MPR set for a given period of planning based on its funding availability. In addition, the MPR of AVs as a function of time and total cost is shown in Fig. 2.4b. It is clearly observed that the

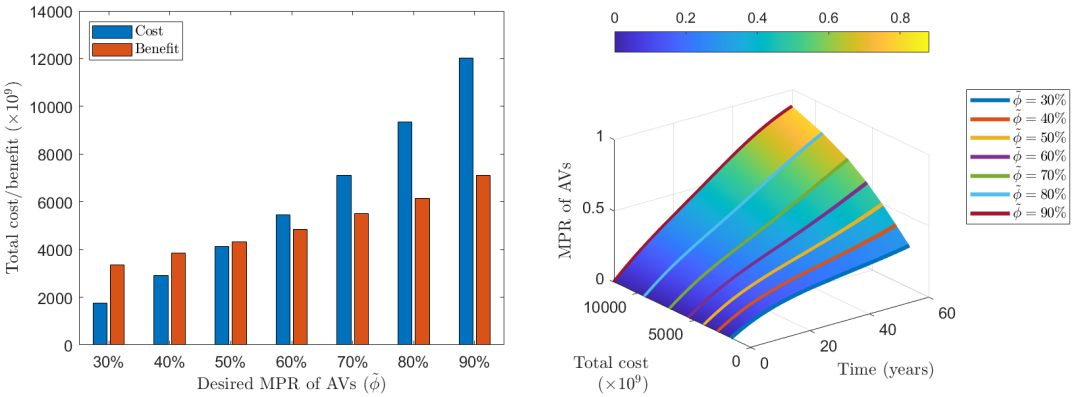

(a) Expected cost and benefit of AV integration

(b) Expected MPR of AVs with the associated cost of AV integration

Figure 2.7: Simulation results corresponding to a stochastically increasing demand with the mean shown in Fig. 2.2, considering various desired MPRs over the planning horizon $I := [0, 60]$. (a) Expected cost and benefit of optimal AV integration over the period I; (b) Expected trajectory of the function ϕ representing the MPR with the corresponding expected cost over the period I.

larger $\tilde{\phi}$ the greater the total cost is, within a given planning period, which is consistent with the results presented in Fig. 2.4a.

We have previously considered a deterministically increasing demand $d(t)$ illustrated in Fig. 2.2. In the following, the demand is assumed to be stochastic as introduced in equation (2.64), where the Gaussian random variable W has a mean 0 and standard deviation $\sigma = 0.3$. A set of 20 realizations of the stochastically increasing demand, with the mean given by the Gompertz function shown in Fig. 2.2, is used for Monte Carlo simulations at each iteration. That is, the state equation and the adjoint equation are solved for each realization $d(t)$ in Step 1 and Step 2 of Section 2.4.2, respectively, for determining the best direction of descent used to update the AV integration policy. The set of results associated with this stochastic demand is shown in Fig. 2.6 and Fig. 2.7. It is clearly observed that the results presented in Fig. 2.6 and Fig. 2.7 for the stochastic demand converge well to those acquired for the deterministic demand shown in Fig. 2.3 and Fig. 2.4, respectively.

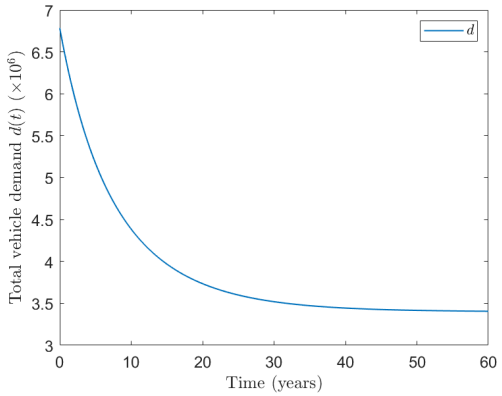

Figure 2.8: A decreasing demand given by $d(t) = 3.4\exp(\exp(-0.37 - 0.1t))$, $t \in I \coloneqq [0, 60]$.

2.5.2 Numerical Results for Decreasing Demand

In Section 2.5.1 we studied the Gompertz function describing an increasing demand, which is projected to be the case for many developing nations [85]. In this section, we consider a decreasing demand $d(t)$ assumed to be given by $d(t) = 6.8\exp(-\exp(-0.37 - 0.1t))$ for the planning period $I \coloneqq [0, 60]$, as illustrated in Fig. 2.8. This is projected to be the case for a number of developed western countries, such as the UK and Sweden [84]. We conducted a series of numerical experiments for various desired MPRs over the period I, with comprehensive results presented in Fig. 2.9 and Fig. 2.10.

Fig. 2.9a and Fig. 2.9b show the optimal AV subsidy u_1 and the optimal investment in AV-specific infrastructure u_2, respectively. It is observed that for any given $\tilde{\phi}$ both u_1 and u_2 remain relatively large in the first 15 years or so. This is because, to achieve the desired MPR, more potential customers need to be attracted to adopt AVs in the presence of a higher demand over that time period. Overall, u_1 and u_2 exhibit a decreasing trend with the decrease of the demand for the sake of less cost resulted from AV subsidies and infrastructure investment. However, an uptick in u_1 and u_2 is also observed due to continued increase of the average investment in HV-specific infrastructure $z(t)$ that contributes to customers choosing HVs. As expected, the amount of AV subsidy and that of the investment in AV-specific infrastructure increase with the increase of the value of $\tilde{\phi}$. Fig. 2.9c shows the trajectory of the MPR ϕ as a result of application of the

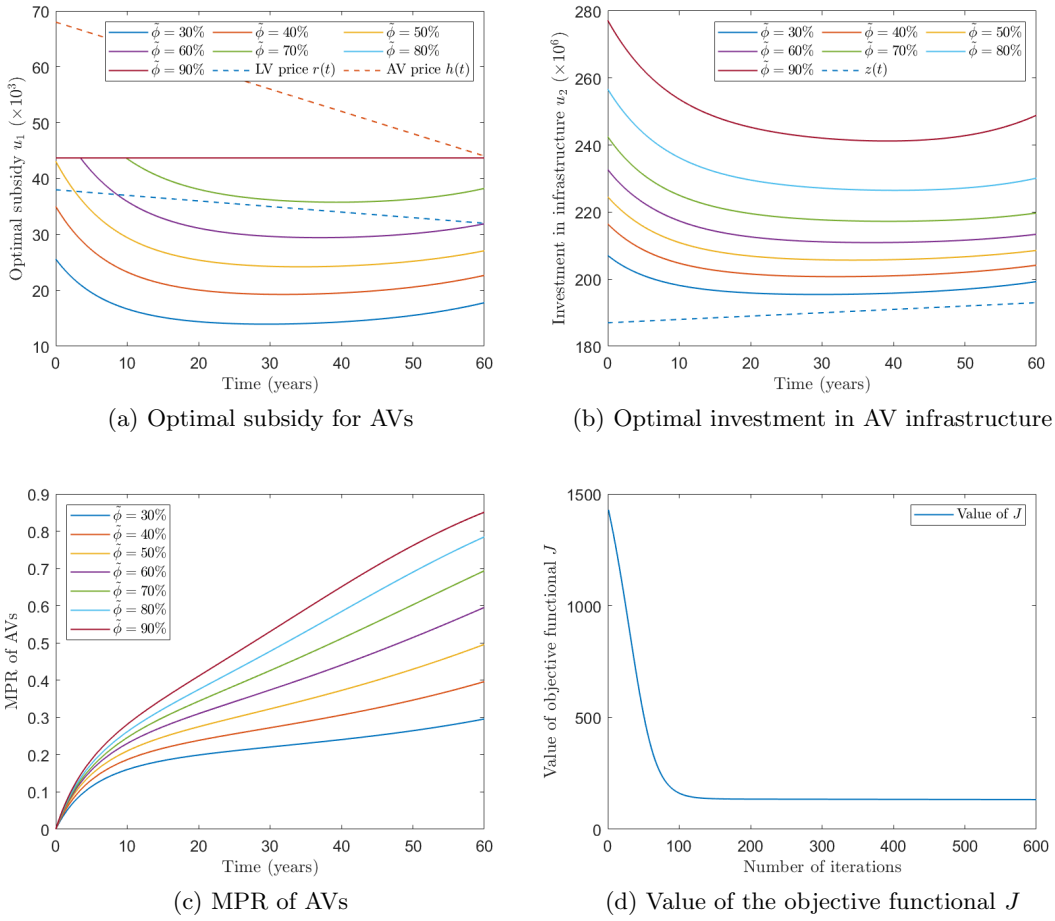

(a) Optimal subsidy for AVs

(b) Optimal investment in AV infrastructure

(c) MPR of AVs

(d) Value of the objective functional J

Figure 2.9: Simulation results corresponding to a decreasing demand shown in Fig. 2.8 with various desired MPRs $\tilde{\phi} = 30\%, 40\%, 50\%, 60\%, 70\%, 80\%, 90\%$ for the planning horizon $I := [0, 60]$. (a) Optimal subsidy u_1; (b) Optimal investment in AV-specific infrastructure u_2; (c) Trajectory of the function ϕ representing the MPR; (d) The value of J for $\tilde{\phi} = 50\%$.

optimal integration policy presented in Fig. 2.9a and Fig. 2.9b. It is observed that all the desired MPRs are achieved at the end of the planning period, except for $\tilde{\phi} = 80\%$ and $\tilde{\phi} = 90\%$ due to limited funding for AV subsidies. This is reflected in the optimal AV subsidy reaching its upper bound for $\tilde{\phi} = 80\%$ and 90% at all times, as shown in Fig. 2.9a. As a result, much more investment is put in AV-specific infrastructure (the top two curves corresponding to $\tilde{\phi} = 80\%$, 90% in Fig. 2.9b) to reduce the discrepancy

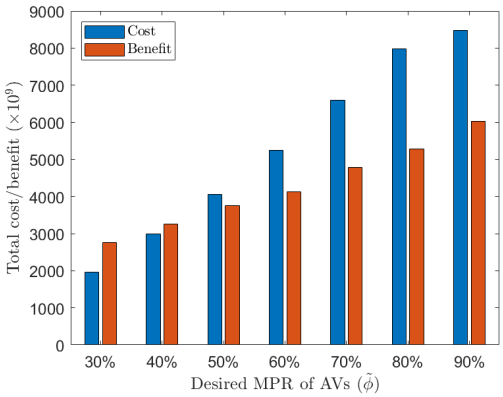

(a) Cost and benefit of AV integration

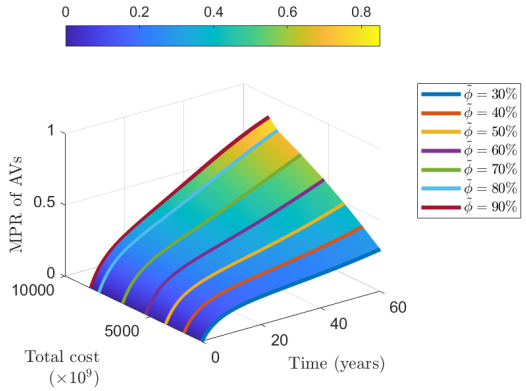

(b) MPR of AVs with the associated cost of AV integration

Figure 2.10: Simulation results corresponding to a decreasing demand shown in Fig. 2.8 with various desired MPRs for the planning horizon $I := [0, 60]$. (a) Cost and benefit of optimal AV integration over the period I; (b) Illustration of the function ϕ with the associated total cost of AV integration over the period I.

between the desired MPR and the actual MPR achieved. However, such effort is also restricted due to the penalty placed on the cost of investment in infrastructure as seen in equation (2.59). Fig. 2.9d shows the value of the objective functional J corresponding to $\tilde{\phi} = 50\%$. It is observed that J decreases with the increase of the number of iterations, indicating convergence of the computation.

Fig. 2.10a shows the the cost and benefit associated with implementing the optimal AV integration policy presented in Fig. 2.9a and Fig. 2.9b. Again, the amount of monetary savings in adopting AVs is conservatively estimated to be $\$2,000$ per year per AV [2]. It is clearly observed that both the cost and the benefit increase with the increase of the desired MPR. However, the benefit is greater than the cost at relatively low desired MPRs, while the cost outweighs the benefit at higher $\tilde{\phi}$. This is due to the fact that much more AV subsidies and investment in infrastructure are required to achieve higher desired MPRs, within the given period of planning. The amount of benefits achieved for very high desired MPRs is not comparable with that of the cost required. Hence, for the scenario considered it is suggested that the desired MPR, i.e., $\tilde{\phi}$, be set at a relatively low level, e.g., no more than 40%, to achieve a positive net benefit over the given period I. Of course, there is a lot of room for modification of $\tilde{\phi}$

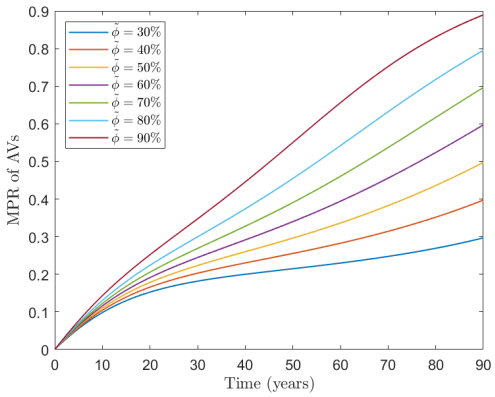

(a) MPR of AVs

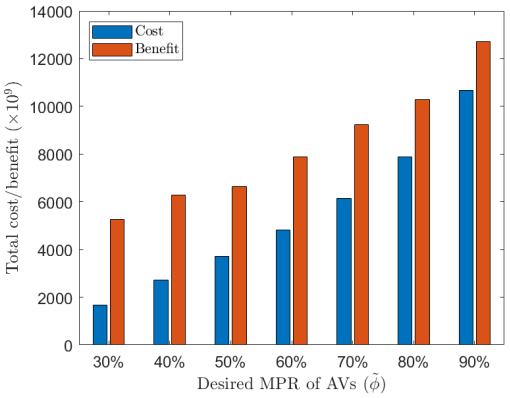

(b) Cost and benefit of AV integration

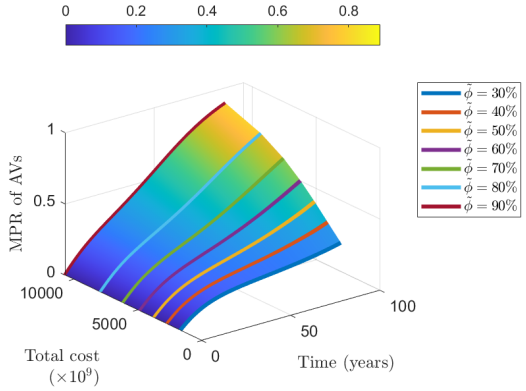

(c) MPR of AVs with the associated cost of AV integration

Figure 2.11: Simulation results corresponding to an increasing demand shown in Fig. 2.2 with various desired MPRs for the planning horizon $I := [0, 90]$. (a) Trajectory of the function ϕ representing the MPR; (b) Cost and benefit of optimal AV integration over the period I; (c) Illustration of the function ϕ with the associated total cost of AV integration over the period I.

depending on the funding availability of the government agency. In addition, the MPR of AVs as a function of time and total cost is shown in Fig. 2.10b. It is easily observed that the larger $\tilde{\phi}$ the greater the total cost is, within the given planning period, which is consistent with the results presented in Fig. 2.10a.

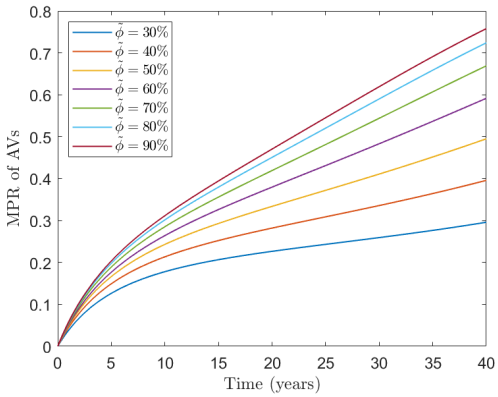

(a) MPR of AVs

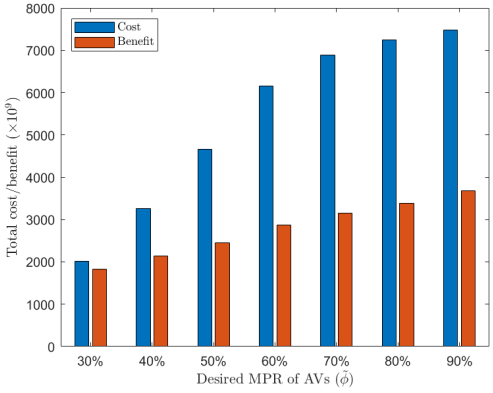

(b) Cost and benefit of AV integration

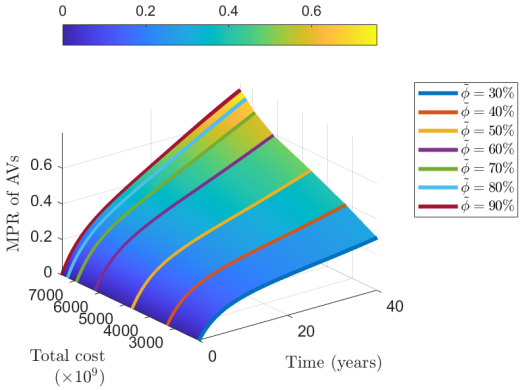

(c) MPR of AVs with the associated cost of AV integration

Figure 2.12: Simulation results corresponding to a decreasing demand shown in Fig. 2.8 with various desired MPRs for the planning horizon $I := [0, 40]$. (a) Trajectory of the function ϕ representing the MPR; (b) Cost and benefit of optimal AV integration over the period I; (c) Illustration of the function ϕ with the associated total cost of AV integration over the period I.

2.5.3 Sensitivity Analysis

In this section, we briefly present interesting results with modification on some parameters. As mentioned before, the planning horizon I can be easily modified by the government agency if necessary depending on funding availability. For example, a longer planning period may be required to reach a desired MPR in case of insufficient resources,

such as AV subsidies and infrastructure investment. Here we consider a longer planning period $I \coloneqq [0, 90]$ and a shorter one $I \coloneqq [0, 40]$ for the increasing and decreasing demand, respectively.

Fig. 2.11 shows the results for a planning horizon $I \coloneqq [0, 90]$, with the increasing demand illustrated in Fig. 2.2. It is observed from Fig. 2.11a that the desired MPR $\tilde{\phi} = 90\%$ is almost attained in 90 years, which was not achieved in 60 years as seen in Fig. 2.3c. More importantly, it is observed from Fig. 2.11b that the benefit obtained from implementing the optimal AV integration policy is greater than the corresponding cost for all desired MPRs considered, given sufficient time for strategic planning, which is consistent with the comparison between Fig. 2.11c and Fig. 2.4b. This is mainly due to the price of AVs having a greater decreasing rate than that of HVs, and the fact that the demand $d(t)$ is increasing with time.

Fig. 2.12 shows the results for a planning horizon $I \coloneqq [0, 40]$, with the decreasing demand illustrated in Fig. 2.8. It is observed from Fig. 2.12a that only $\tilde{\phi} = 30\%$ and $\tilde{\phi} = 40\%$ are well attained in 40 years, whereas the desired MPR of up to 70% could be achieved in 60 years as seen in Fig. 2.9c. Due to a shorter period of planning, much more AV subsidies and infrastructure investment need to be put into place for reaching as close as possible to the desired MPR. Consequently, the cost of implementing the AV integration policy is greater than the corresponding benefit obtained for each desired MPR considered, as observed in Fig. 2.12b. This is also well observed in comparing Fig. 2.12c and Fig. 2.10b, where more AV subsidies and infrastructure investment are required to achieve any desired MPR in 40 years, as opposed to that in 60 years.

In the long run, with the MPR of AVs increasing they are likely to be able to work collaboratively to reduce traffic congestion, increase safety, etc. Hence, in addition to using a constant monetary benefit of $\$2,000$ per AV per year [2] we also consider a scenario where the average amount of monetary benefit for AVs is assumed to increase (linearly) with the increase of MPR. Specifically, the average benefit per AV at time t is given by $k\phi(t)$, with $k = 2\times10^3$ and 6×10^3 considered. With the simulation settings kept the same as in the baseline scenario for Figs. 2.3 and 2.4, the corresponding results on cost and benefit of AV integration in this scenario are shown in Fig. 2.13. It is observed from Fig. 2.13b that the total amount of benefit obtained by AVs is significantly greater than that in Fig. 2.13a at any desired MPR. This is due to the fact that a larger value of

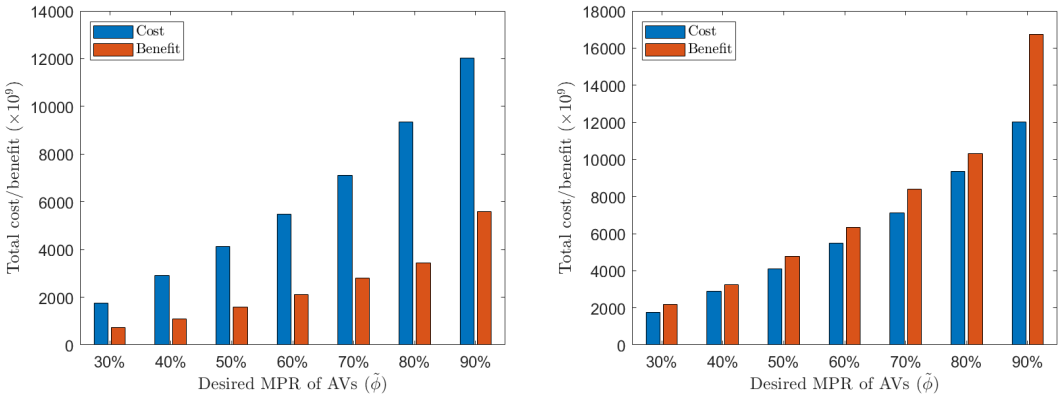

(a) $k = 2000$ (b) $k = 6000$

Figure 2.13: Simulation results corresponding to an increasing demand shown in Fig. 2.2 with a planning horizon $I \coloneqq [0, 60]$. The average amount of monetary benefit for AVs is assumed to be time-variant and increases linearly with the increase of MPR. Specifically, the average benefit per AV at time t is given by $k\phi(t)$, where (a) $k = 2000$ and (b) $k = 6000$.

k leads to a higher amount of average benefit given the same MPR of AVs. As a result, the net benefit corresponding to any desired MPR is negative in Fig. 2.13a due to the choosing of a small k, while it is always positive in Fig. 2.13b because of a sufficiently large k. In addition, compared to Fig. 2.4a the total amount of benefit is observed to be smaller in Fig. 2.13a at any desired MPR. This is because, with $k = 2000$ the average monetary benefit per AV, i.e., $k\phi(t)$, is always less than $\$2,000$ for the MPR considered. These interesting results indicate that more social benefits are expected from the adoption of AVs if AVs are able to work collaboratively for the greater good.

Fig. 2.14 shows the results for a planning horizon $I \coloneqq [0, 60]$, with the decreasing demand illustrated in Fig. 2.8. Unlike previous scenarios where the average AV price $h(t)$ is conservatively assumed to be significantly higher than that of HVs, in this case the price of AVs is considered to be decreasing much faster and becomes the same as the average price of HVs, $r(t)$, after 30 years. The upper bound of AV subsidy, $\overline{u}_1$, is set as the price of AVs at the end of the planning horizon. Despite of similar patterns observed from the comparison between the results shown in Fig. 2.14 and the corresponding ones presented in Fig. 2.9 and Fig. 2.10, several interesting distinctions are worthwhile to

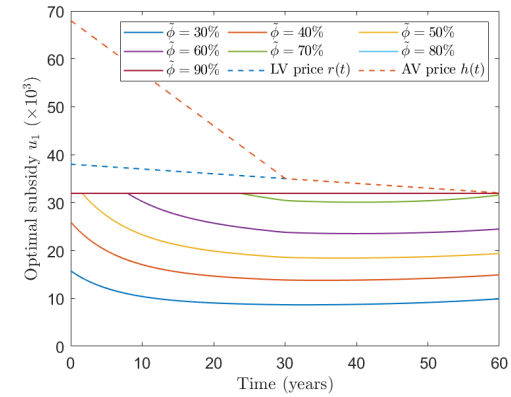

(a) Optimal subsidy for AVs

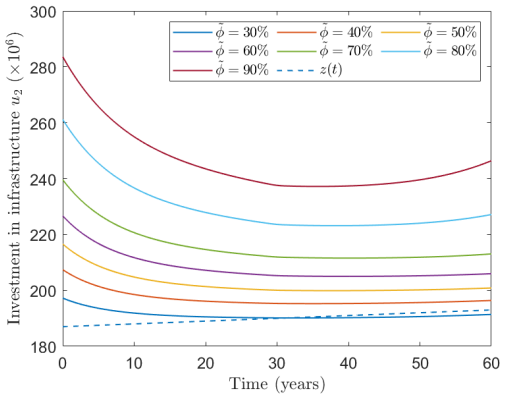

(b) Optimal investment in AV infrastructure

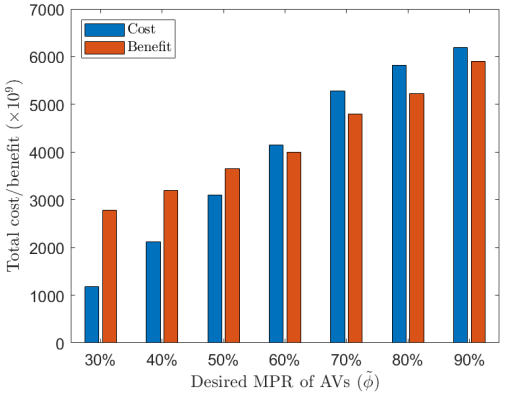

(c) Cost and benefit of AV integration

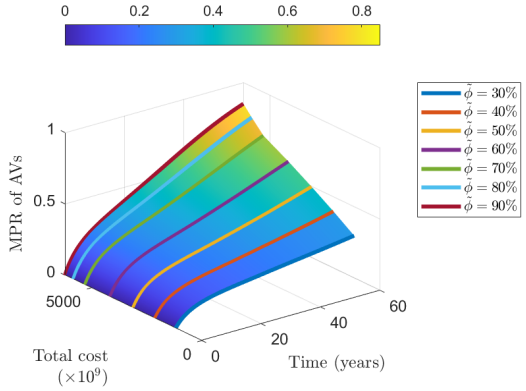

(d) MPR of AVs with the associated cost of AV integration

Figure 2.14: Simulation results corresponding to a decreasing demand shown in Fig. 2.8 with various desired MPRs for the planning horizon $I := [0, 60]$. The average price of AVs, $h(t)$, is assumed to be decreasing much faster than that of previous scenarios, and becomes the same as the average price of HVs, $r(t)$, after 30 years. The upper bound of AV subsidy, $\overline{u}_1$, is set as the price of AVs at the end of the planning horizon. (a) Optimal subsidy u_1; (b) Optimal investment in AV-specific infrastructure u_2; (c) Cost and benefit of optimal AV integration over the period I; (d) Illustration of the function ϕ with the associated total cost of AV integration over the period I.

mention. Comparing Fig. 2.14a to Fig. 2.9a, it is observed that the optimal AV subsidy is considerably less in this case due to much lower prices of AVs. A relatively low level of subsidy is still maintained after 30 years in order to reach the desired MPRs due to

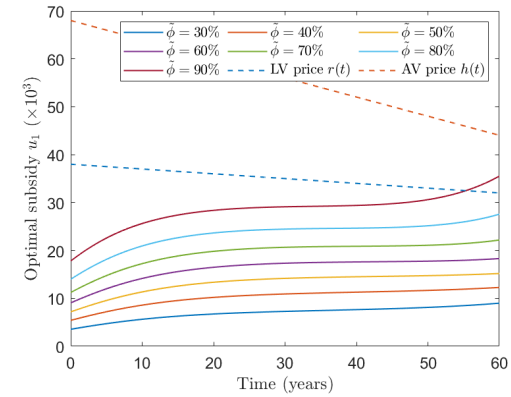

(a) Optimal subsidy for AVs

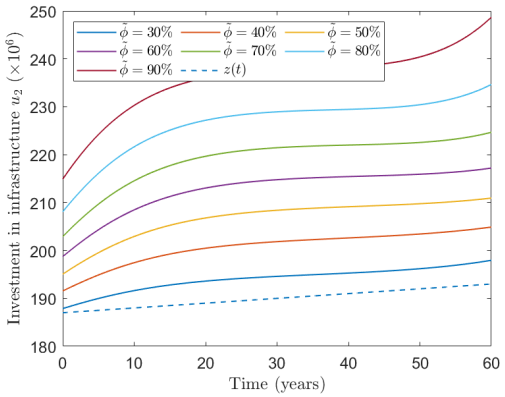

(b) Optimal investment in AV infrastructure

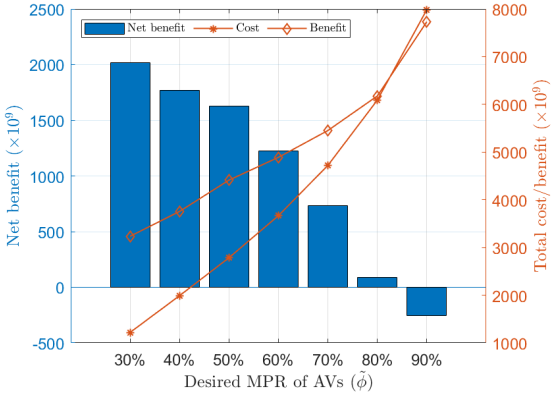

(c) Cost and benefit of AV integration

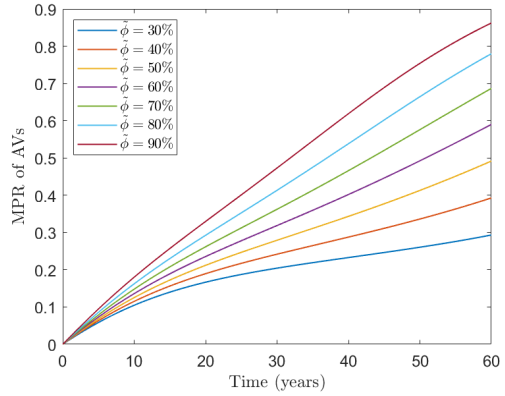

(d) MPR of AVs

Figure 2.15: Simulation results corresponding to an increasing demand shown in Fig. 2.2 with various desired MPRs for the planning horizon $I := [0, 60]$. The weight parameter q_1 associated with AV subsidies u_1 is increased from 10^{-4} to 3×10^{-3}, while all other parameters remain unchanged. (a) Optimal subsidy u_1; (b) Optimal investment in AV-specific infrastructure u_2; (c) Cost and benefit of optimal AV integration over the period I; (d) Trajectory of the function ϕ representing the MPR.

low penetrations in the beginning, i.e., $\phi(0) = 0\%$. A similar observation is also noted for the optimal infrastructure investment from the comparison between Fig. 2.14b and Fig. 2.9b. As a result, the total cost associated with the optimal AV integration policy is much lower in this case, as shown in Fig. 2.14d. Consequently, a positive net benefit is more likely to be attained. For instance, the benefit outweighs the cost for $\tilde{\phi} = 30\%$,

40% and 50%, and a positive net benefit is nearly achieved for $\tilde{\phi} = 60\%$, as observed in Fig. 2.14c. By contrast, in the presence of higher AV prices the cost is observed to have already outweighed the benefit for $\tilde{\phi} = 50\%$, as seen in Fig. 2.10a. Further, an even larger discrepancy between the cost and the corresponding benefit is observed in Fig. 2.10a at larger desired MPRs. However, this is not observed in Fig. 2.14c due to much lower AV prices.

Since the government agency might be interested to balance the cost of implementing the AV integration policy and the discrepancy from achieving the desired MPR, it would be beneficial to study the impact of those weight parameters appearing in equation (2.59), such as $Q = \text{diag}(q_1, q_2)$ and w. Here we are particularly interested in how the weight q_1 associated with AV subsidies would impact the optimal integration policy. To this end, the value of q_1 is increased from 10^{-4} to 3×10^{-3}, while all the other parameters remain unchanged. The simulation results are shown in Fig. 2.15, corresponding to the increasing demand with various desired MPRs for the planning horizon $I := [0, 60]$. It is clearly observed from Fig. 2.15a that the optimal AV subsidy u_1 is much less than that seen in Fig. 2.3a for any desired MPR, due to a much heavier penalty q_1 placed on the cost of subsidizing AV purchases. Consequently, the investment in AV-specific infrastructure u_2 is increased to maintain the competitiveness of AVs in the auto market so that the desired MRPs can be possibly attained, as seen from the comparison between Fig. 2.15b and Fig. 2.3b. Due to much reduced subsidies for AVs, the total cost of implementing the optimal integration policy is significantly lowered, resulting in a positive net benefit for most desired MPRs shown in Fig. 2.15c, as opposed to only $\tilde{\phi} = 30\%$, 40% and 50% observed in Fig. 2.4a. However, this is clearly at the expense of a larger discrepancy between the desired MPR and the actual MPR attained, as observed from comparing Fig. 2.15d with Fig. 2.3c.

2.6 Conclusions

In this chapter, we have developed a continuous-time dynamical model capable of capturing the interactive temporal evolution of the market share of HVs and AVs. A discrete choice model is constructed and incorporated into the dynamical model to describe the likelihood of customers opting HVs or AVs. To achieve the desired temporal

integration of AVs, monetary subsidies and investment in AV-specific infrastructure are considered as decision variables to promote the adoption of AVs. Further, an optimal control problem is formulated with the objective of achieving a desired MPR at the end of the planning horizon, if possible, subject to funding availability, while minimizing the cost associated with AV subsidies and infrastructure investment. A set of optimality conditions is derived to characterize the mathematical properties of the optimal AV integration policy, yielding an iterative computational algorithm for determining the time-variant integration policy. This allows the government agency to optimally subsidize AV purchases and invest in AV-specific infrastructure in an adaptive manner, which is not able to be achieved with agent-based simulations.

The numerical results presented in Section 2.5 are very promising and informative. The proposed approach is shown to be effective in integrating AVs into the auto market subject to funding availability of the government agency. Moreover, the approach is observed to have high degrees of robustness in that it maintains satisfactory performance in the presence of increasing, decreasing, and stochastic demands. It is very interesting to note that the optimal AV subsidies and infrastructure investment are closely related to the time-varying market demand, which offers significant insights into government policy-making for nations observing distinct demand patterns.

The systematic cost-benefit analysis conducted reveals that the desired MPR needs to be appropriately adjusted, depending on the length of the planning horizon and the availability of government funding, in order to achieve a positive net benefit. More importantly, the approach allows the government agency a great degree of flexibility in modifying the desired MPRs over any finite planning horizon. For example, the planning period for AV integration can be set longer in case of a very limited amount of funding available, so that a positive net benefit could be still attained. This might be particularly useful for nations with low government budgets. Due to the generality of the dynamical model, the practicable implementability of the decision variables, and the efficiency of the computation based on the optimality conditions, the procedures presented in this chapter will provide significant managerial insights for government agencies into developing long-term strategic planning policies in the era of AVs.

The present work opens the door to a number of interesting and promising research directions on policy-making in transportation engineering. For example, more different

types of vehicles could be included in modeling purchase decisions with different utility functions. In addition, the future investment in AV-specific infrastructure might come in various forms, such as exclusive AV lanes, roadside units for AV communications, etc. It remains an open question as to which form is preferable for a given city, due to geographical heterogeneity of different cities.

We have not considered shared mobility due to the scope of this work. However, shared AVs are likely to be heavily used thanks to the emerging Mobility-as-a-Service (MaaS) systems, which could impact the travel behavior of customers. In addition, a number of other potential high-level changes could occur to travel patterns that may result from the introduction of AVs, such as longer commutes, work-during-commute, trip chaining, etc. These changes could impact vehicle ownership and use, and will be explicitly considered in future work of developing appropriate subsidizing policies for the integrated transit and MaaS transportation system. Since the optimality conditions derived in the present work are general in prescribing optimal transportation policies, it is feasible to apply the approach to a wide range of policy-making processes in transportation engineering, so as to benefit the customers serviced.

Chapter 3

Optimal Control of Automated Vehicles for Traffic Smoothing

3.1 Introduction

Traffic congestion is a long-standing problem that has gained a significant amount of interests from a wide range of research communities, such as transportation engineering, urban planning, electrical engineering, and computer science, among many others. Over the past few decades, a considerable amount of research has gone into understanding the cause of traffic congestion and developing effective strategies for its mitigation. This trend has been continuing simply because traveling is closely related to the daily life of the general public and it could be impacted significantly by traffic congestion. For example, it is reported that in 2019 congestion cost and travel delay reached a staggering 190 billion dollars and 8.7 billion hours, respectively, in the US [87].

It has been well noted that traffic congestion is not only caused by some noticeable triggers, such as lane changing [88], bottlenecks [89] and merging [90], but could also occur often in the absence of any of these triggers. This is simply due to the nature of unstable traffic flow in which small perturbations amplify and grow into stop-and-go waves traveling upstream in the flow [91]. As a result of the collective behavior of human drivers, unstable traffic has been well observed in real-world experiments [92, 93], resulting in greater traffic congestion and higher fuel consumption and emissions than smooth traffic flow [19, 94, 95].

A number of traffic control strategies have been proposed and implemented to effectively regulate traffic flow, such as traffic signal control [25, 96], ramp metering [34, 97] and variable speed limit (VSL) control [98, 99]. Traffic signal control is widely used at intersections to regulate vehicular movements from various approaches, which requires installation of traffic lights seen in ramp metering as well. The VSL technique is normally implemented through changable message signs with sensors deployed along the roadway. These conventional traffic control techniques heavily rely on infrastructure, such as traffic lights and sensors, at fixed locations, which poses the challenge of limited flexibility due to the high installation cost of fixed infrastructure.

Ground transportation is expected to experience substantial changes with the advent of vehicular sensing and communication technologies. These technological advancements offer promising opportunities for traffic control where smart vehicles act as mobile actuators in the bulk traffic flow. In contrast to the aforementioned traffic control techniques, these new technologies allow vehicles to form dense platoons with small gaps when connected and automated. Hence, a high degree of connectivity among vehicles in the platoon is usually required for implementing those technologies. An important element in designing control laws for vehicle platoons is to ensure string stability [100]. This has been well studied in adaptive cruise control (ACC) [101–104] and cooperative adaptive cruise control (CACC) [105–107]. The control laws of ACC/CACC align with the essence of car-following principles [108]. There have been a number of notable car-following models proposed, such as the Gazis-Herman-Rothery (GHR) model [109], Gipps' model [110], optimal velocity model (OVM) [111], intelligent driver model (IDM) [112], and Newell's car-following model [113], among many others. Notably, IDM and OVM are two widely adopted car-following models capable of reproducing the same type of traffic instabilities observed in phantom traffic jams [16]. A comprehensive overview of car-following models can be found in [114].

Before becoming fully automated, the surface transportation system is expected to include both HVs and AVs, which is optimistically projected to be the case for at least the next thirty years [8]. In a mixed traffic environment where both HVs and AVs are present, it is possible to change the properties of the bulk traffic by controlling a small number of AVs. For example, it has been shown theoretically that the unstable uniform traffic flow can be stabilized with a single [16] or a small number [17] of AVs serving as

mobile actuators. An H-infinity approach is applied to stabilize mixed vehicular platoons with connected automated vehicles [44], where head-to-tail string stability is ensured for each subsystem of the platoon. Recently, a PDE-ODE coupled system has been adopted to represent the impact of controlled AVs on the bulk traffic [115], where the traffic flow is described by a partial differential equation (PDE) while the AV dynamics is given by an ordinary differential equation (ODE). Although this system model is mathematically sound for analysis, it appears to be computationally intractable in certain complex traffic scenarios. A number of simulation-based studies are also conducted using the IDM. Specifically, the impacts of ACC market penetration rate on traffic stability and throughput are studied in [15, 116], where the IDM is applied for both HVs and AVs with different sets of parameter values. Apart from theoretical and simulation studies indicating the possibilities of traffic control via AVs, the seminal field experiments [18] demonstrate that stop-and-go waves can be dampened through intelligent control of a small number of AVs. A comprehensive overview on traffic control using AVs can be found in [117].

While some studies have focused on stabilizing traffic using AVs, ranging from analytical analysis to field experiments as highlighted above, they largely rely on high degrees of connectivity in the sense that the controlled vehicle has to be able to communicate with a number of other vehicles. Furthermore, most prior studies use car-following models linearized at the equilibrium state to design the control law for AVs, which may not guarantee reliable performance due to the nonlinear nature of mixed traffic flow [118]. In this chapter we develop a general mathematical framework to describe mixed traffic in the presence of HVs and AVs. This framework, unlike many prior studies, is not limited to linear traffic dynamics and allows for easy inclusion of different dynamics for HVs and AVs, in the context of traffic smoothing. More importantly, only local information is required for developing the control law of AVs, e.g., relative speed and spacing to the proceeding vehicle, as opposed to the requirement of high degrees of connectivity commonly seen in the literature. Based on the framework developed, we formulate an optimal control problem (called the Bolza problem) with the objective of traffic smoothing and prove the existence of optimal AV controls. The Pontryagin minimum principle (PMP) is applied to address the formulated nonlinear optimal control problem. Further, an iterative computational algorithm is presented to determine the

optimal AV control policy with a proof of its convergence. The mathematical framework developed is further illustrated using the IDM and optimal velocity with relative velocity (OVRV) model (an extension of OVM) for HVs and AVs, respectively. A series of numerical results is presented to show the effectiveness of the proposed approach on traffic smoothing, as well as the improvement on vehicle fuel economy and emissions.

The remainder of this chapter is outlined as follows. In Section 3.2, we develop a general framework for mixed traffic based on car-following principles. In Section 3.3, we formulate an appropriate optimal control problem with the objective of smoothing traffic flow in the presence of stop-and-go waves. The existence of optimal AV controls is also proved in this section. In Section 3.4, we introduce the PMP and present the corresponding necessary conditions of optimality to address the optimization problem formulated in Section 3.3. The proposed approach is further illustrated using the IDM and OVRV model. In Section 3.5, we present a computational algorithm based on the optimality conditions given in Section 3.4 and prove its convergence. A series of numerical results is also presented in Section 3.5 to show the effectiveness of the proposed approach under various scenarios. This chapter is concluded in Section 3.6. The materials presented in this chapter are mostly taken from [45].

3.2 Mathematical Model

In this section, we develop a general framework to model the dynamics of mixed traffic flow in the presence of both HVs and AVs. It is assumed that all vehicles abide by car-following principles, HVs, however, may exhibit different dynamics compared with AVs due to their complex driving behaviors [119].

Let $x_i(t)$ and $v_i(t)$ denote the position and speed of the i-th vehicle at time t, respectively. Following the basic law of physics we have

$$\dot{x}_i(t) = v_i(t), \ \forall \ i \in \mathcal{S}, \tag{3.1}$$

where $\mathcal{S}$ is the set of vehicles present in the mixed traffic. Additionally, the acceleration of HVs is given by the following second order ordinary differential equation

$$\ddot{x}_i(t) = f_{HV}(s_i(t), v_i(t), \Delta v_i(t)), \ \forall \ i \in \mathcal{H}, \tag{3.2}$$

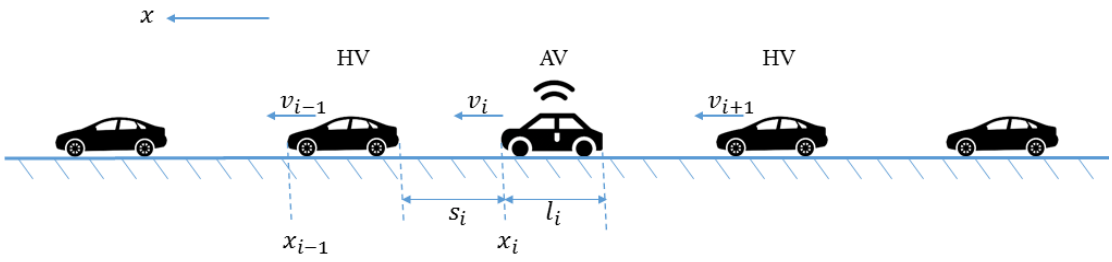

Figure 3.1: A generic car-following setup of mixed traffic consisting of human-driven vehicles (HVs) and automated vehicles (AVs) [45].

where $s_i(t)$ is the inter-vehicle spacing (or inter-vehicle space gap) between the i-th vehicle and its proceeding vehicle at time t, given by $s_i(t) = x_{i-1}(t) - x_i(t) - l_{i-1}$ with l_{i-1} being the length of the $(i-1)$-th vehicle. The term $\Delta v_i(t) = v_i(t) - v_{i-1}(t)$ denotes the relative speed between the $(i-1)$-th vehicle and the i-th vehicle at time t. f_{HV} represents the functional relationship between HV acceleration and the variables s_i, v_i, and Δv_i. $\mathcal{H}$ denotes the set of HVs in the mixed traffic. Similarly, the acceleration of any AV is given by

$$\ddot{x}_j(t) = f_{AV}(s_j(t), v_j(t), \Delta v_j(t), u_j(t)), \ \forall\ j \in \mathcal{A}, \tag{3.3}$$

where $u_j(t)$ is the additive (measurable) acceleration control on the AV apart from following car-following principles. f_{AV} represents the functional relationship between AV acceleration and the variables $s_j, v_j, \Delta v_j$, and u_j. $\mathcal{A}$ denotes the set of AVs. A noticeable merit of this formulation is that it preserves the essence of car-following principles. The interpretations of other variables remain the same as those in equation (3.2). These variables are also illustrated in Fig. 3.1 for the convenience of presentation. Consequently, the dynamics of the mixed traffic can be compactly written as

$$\dot{x}_i(t) = v_i(t), \ \forall\ i \in \mathcal{S}, \tag{3.4}$$

$$\ddot{x}_i(t) = \begin{cases} f_{HV}(s_i(t), v_i(t), \Delta v_i(t)), \ \forall\ i \in \mathcal{H} \\ f_{AV}(s_i(t), v_i(t), \Delta v_i(t), u_i(t)), \ \forall\ i \in \mathcal{A} \end{cases} \tag{3.5}$$

It is easily observed that $\mathcal{S} = \mathcal{H} \cup \mathcal{A}$. The acceleration $\ddot{x}_i(t)$ of the i-th vehicle at time t is essentially a nonlinear function of $s_i(t)$, $v_i(t)$, and $\Delta v_i(t)$ (as well as $u_i(t)$

in the case of AVs). Clearly, the variables appearing in equations (3.4) and (3.5) are time-dependent. For the convenience of notation, we may omit the argument t for the remainder of this chapter whenever appropriate to do so. Note that reaction-time delays are not considered as seen in relevant studies [16–18, 44], in the context of traffic smoothing and stabilization. However, one could describe such delays by incorporating an additional term into equation (3.5) using delay differential equations. That requires a very different mathematical treatment and is out of the scope of this study.

It is easily observed that by having $\ddot{x}_i = 0$ in equation (3.5) we obtain the solution pairs $(v_i^*, \tilde{s}_i^*)$, $\forall\ i \in \mathcal{H}$, and $(v_i^*, \hat{s}_i^*)$, $\forall\ i \in \mathcal{A}$, where $\tilde{s}_i$ and $\hat{s}_i$ represent the spacing between the i-th vehicle, either HV or AV, and its preceding one. For simplicity, we shall denote these tuples at equilibrium by $(v^*, \tilde{s}^*)$ and $(v^*, \hat{s}^*)$ for HVs and AVs, respectively. That is, all vehicles drive at the same speed v^* in a uniform flow solution, where HVs have the same time-independent spacing $\tilde{s}^*$ while it is $\hat{s}^*$ for AVs. Apparently, $\tilde{s}^*$ is not necessarily equal to $\hat{s}^*$. Further, it is expected that $\hat{s}^*$ is very likely to be smaller than $\tilde{s}^*$ due to the fact that AVs have a shorter reaction time. Note that there is no additional control u_i applied to AVs at equilibrium traffic flow since this equilibrium state is maintained by only abiding to car-following principles. However, when stop-and-go waves approach an AV, u_i will take effect on the controlled AV to dampen the undesired traffic waves so that the following vehicles could experience as smooth of a traffic flow as possible. Without loss of generality, we assume that a string of moving vehicles drive at any possible equilibrium speed v^*. Suppose there are $n_1 = \dim(\mathcal{S})$ vehicles present in the mixed traffic with $n_2 = \dim(\mathcal{H}) \in \mathbb{N}^+$ and $n_3 = \dim(\mathcal{A}) \in \mathbb{N}^+$ representing the number of HVs and AVs, respectively. For concise analysis, without loss of generality we assume that the speed perturbation, e.g., vehicle slowdown, occurs to the first vehicle (HV) resulting in stop-and-go waves propagating backwards in the traffic flow.

For the purpose of analysis, we shall write the dynamics of all the vehicles in $\mathcal{S}$ in a

state-space formulation. Let

$$\begin{cases} y_1(t) = x_1(t), \\ y_2(t) = \dot{x}_1(t) = v_1(t), \\ \quad \vdots \\ y_{2i-1}(t) = x_i(t), \\ y_{2i}(t) = \dot{x}_i(t) = v_i(t), \\ \quad \vdots \\ y_{2n_1-1}(t) = x_{n_1}(t), \\ y_{2n_1}(t) = \dot{x}_{n_1}(t) = v_{n_1}(t), \end{cases}$$

and the state vector be

$$y(t) = (y_1(t), y_2(t), \cdots, y_{2n_1-1}(t), y_{2n_1}(t))' \in \mathbb{R}^{2n_1},$$

where the prime symbol $'$ denotes the transpose operator of matrices. Hence, the system dynamics involving all the n_1 vehicles can be written as

$$\dot{y}(t) = \begin{pmatrix} \dot{y}_1(t) \\ \dot{y}_2(t) \\ \vdots \\ \dot{y}_{2i-1}(t) \\ \dot{y}_{2i}(t) \\ \vdots \\ \dot{y}_{2n_1-1}(t) \\ \dot{y}_{2n_1}(t) \end{pmatrix} = \begin{pmatrix} \dot{x}_1(t) \\ \dot{v}_1(t) \\ \vdots \\ \dot{x}_i(t) \\ \dot{v}_i(t) \\ \vdots \\ \dot{x}_{n_1}(t) \\ \dot{v}_{n_1}(t) \end{pmatrix} \in \mathbb{R}^{2n_1}, \ i \in \mathcal{S}, \tag{3.6}$$

where $\dot{x}_i(t)$ and $\dot{v}_i(t)$ are given by equations (3.4) and (3.5), respectively.

For the convenience of notation, we shall write equation (3.6) as a vector differential equation in the following compact form

$$\dot{y}(t) = f(t, y(t), u(t)), \ t \in I, \ y(0) = y_0, \tag{3.7}$$

where $I = [0, T]$ is the time horizon and y_0 is the initial condition. The vector $u(t) = (\cdots, u_j(t), \cdots)' \in \mathbb{R}^{n_3}$ denotes the additive control inputs applied to all AVs. The

nonlinear function f is essentially equivalent to equation (3.6) describing the dynamics of a string of n_1 vehicles. Note that for the i-th vehicle, $\dot{y}_{2i-1}(t) = \dot{x}_i(t)$ and $\dot{y}_{2i}(t) = \ddot{x}_i(t)$ correspond to its speed and acceleration/deceleration, respectively.

3.3 Problem Formulation

Our objective is to minimize stop-and-go waves caused by the collective behavior of all human drivers via optimal control of AVs. Since vehicles are assumed to drive at v^* before perturbations occur, our goal is to minimize the deviation of vehicle speed from v^* after the occurrence of any perturbation. Hence, we formulate an optimal control problem (called the Bolza problem) where the deviation of vehicle speed from its equilibrium is expected to be minimized in the presence of traffic waves. It is expected that the backward traffic waves will be dampened by intelligently controlling AVs. This is because a controlled AV can properly adjust its speed according to the surrounding traffic so that the wave propagation is reduced after passing through the AV, resulting in a smoother traffic for the following vehicles.

Based on the principles introduced above, we introduce the following objective functional for the Bolza problem

$$J(u(t)) \coloneqq \underbrace{\frac{1}{2}\int_I \sum_{i\in\mathcal{A}} w_i \left(y_{2i}(t) - v^*\right)^2 dt}_{\text{running cost}} + \underbrace{\frac{1}{2}\sum_{i\in\mathcal{A}} q_i \left(y_{2i}(T) - v^*\right)^2}_{\text{terminal cost}}, \tag{3.8}$$

representing the cost (penalty) for the speed perturbation of AVs from their equilibrium value due to traffic waves over the time horizon I. The variable v^* is the speed of an AV before any perturbation occurs, and it can be generalized as a function of time if necessary. As detailed above, the backward waves can be reduced if their propagation across AVs is decreased. The positive parameters, $\{w_i\}$ and $\{q_i\}$, denote the weights given to any AV, $\forall\ i \in \mathcal{A}$, corresponding to the running cost and terminal cost, respectively.

Due to practicality, the control u_i is considered to be bounded taking values from the compact set $[\underline{u}_i, \overline{u}_i]$, $\forall\ i \in \mathcal{A}$, where $\underline{u}_i$ and $\overline{u}_i$ are the lower and upper bounds, respectively. Hence, the control constraint set U is defined as follows

$$U \coloneqq \{u \in \mathbb{R}^{n_3} : \underline{u}_i \leq u_i \leq \overline{u}_i,\ \forall\ i \in \mathcal{A}\} \tag{3.9}$$

The optimal control problem is to minimize J shown in equation (3.8) subject to the system dynamics given by equation (3.7) and the control constraint set U. It is expected that every AV can be optimally controlled if the solution to the optimal control problem is implemented.

Remark 4. *Since the objective is to reduce stop-and-go waves traveling backwards, $\underline{u}_i$ in equation* (3.9) *can be chosen as zero. That is, the controller is designed in such a way that AVs would slow down less as opposed to HVs in the presence of traffic waves. Hence, a positive additive (measurable) control input u_i is introduced. Similarly, $\overline{u}_i$ is chosen as a positive number such that the vehicle acceleration remains within its limitations.*

Let $\mathcal{U}_{ad}$ denote the set of admissible controls. For convenience of mathematical analysis, we denote the running cost and terminal cost in equation (3.8) by $\ell(t, y(t))$ and $\Phi(y(T))$, respectively. Note that this is an implicit expression in the sense that the system state y is also a function of the control u which is not explicitly written out. Before addressing the optimal control problem formulated above, we consider the question of existence of optimal AV controls. This is presented in the following theorem.

Theorem 3.3.1. *Consider the dynamical system given by equation* (3.7) *with objective functional shown in equation* (3.8)*. Let $K \geq 0$ be the Lipschitz constant of the Lipschitz continuous function f with respect to the state variable. Let $y(t) = y(u)(t)$, $t \in I$, be the solution to equation* (3.7) *corresponding to the control $u \in \mathcal{U}_{ad}$. Then, there exists an optimal AV control u^o at which J attains its minimum.*

Proof. First of all, we show that the control to solution map $u \longrightarrow y(u)$ from $\mathcal{U}_{ad}$ to $B_\infty(I, \mathbb{R}^{2n_1})$ is continuous. Let $u^k \in \mathcal{U}_{ad}$ be any admissible control. Let $y^k = y(u^k)$ and $y^o = y(u^o)$ denote the solutions of equation (3.7) corresponding to the controls u^k and u^o, respectively. Clearly, y^k and y^o satisfy the following integral equations

$$y^k(t) = y_0 + \int_0^t f(\theta, y^k(\theta))d\theta,\ t \in I, \tag{3.10}$$

$$y^o(t) = y_0 + \int_0^t f(\theta, y^o(\theta))d\theta,\ t \in I, \tag{3.11}$$

where $y^k(t) = y(u^k)(t)$, and $y^o(t) = y(u^o)(t)$, $t \in I$. Subtracting equation (3.11) from equation (3.10) term by term, we obtain the following

$$y^k(t) - y^o(t) = \int_0^t \Big[f(\theta, y^k(\theta)) - f(\theta, y^o(\theta))\Big]\, d\theta. \tag{3.12}$$

Since f is Lipschitz continuous with a Lipschitz constant K, taking norm on both sides of equation (3.12) and using triangle inequality, we obtain

$$||y^k(t) - y^o(t)|| \leq \int_0^t K||y^k(\theta) - y^o(\theta)||d\theta. \tag{3.13}$$

Applying Grönwall's lemma to equation (3.13), it follows that

$$||y^k(t) - y^o(t)|| \leq ||y^k(0) - y^o(0)||e^{KT}. \tag{3.14}$$

Since $y^k(0) \longrightarrow y^o(0)$ in the norm topology, the expression on the right-hand side of equation (3.14) converges to zero with respect to $t \in I$. Hence it follows that

$$\lim_{k\to\infty} \sup ||y^k(t) - y^o(t)|| = 0, \ t \in I = [0, T]. \tag{3.15}$$

Hence, $y^k \longrightarrow y^o$ as $u^k \longrightarrow u^o$. This shows the continuity of the control to solution map $u \longrightarrow y(u)$.

Since $\mathcal{U}_{ad}$ is compact, it suffices to show that the map $u \longrightarrow J(u)$ is continuous on $\mathcal{U}_{ad}$. Letting $u^k \longrightarrow u^o$ in $\mathcal{U}_{ad}$, it follows from the above results on the continuity of the map $u \longrightarrow y(u)$ that $y(u^k) \longrightarrow y(u^o)$. By virtue of continuity of ℓ and Φ, it follows that

$$\ell(t, y^k(t)) \longrightarrow \ell(t, y^o(t)) \tag{3.16}$$

$$\Phi(y^k(T)) \longrightarrow \Phi(y^o(T)) \tag{3.17}$$

Clearly, it follows from equation (3.16) that

$$\int_I \ell(t, y^k(t))dt \longrightarrow \int_I \ell(t, y^o(t))dt \tag{3.18}$$

Summing up equations (3.17) and (3.18) we conclude that $J(u^k) \longrightarrow J(u^o)$. This proves that J is continuous on $\mathcal{U}_{ad}$. Since $\mathcal{U}_{ad}$ is compact, it is clear that there exists an $u^o \in \mathcal{U}_{ad}$ at which J attains its minimum. This completes the proof. □

Remark 5. *The function f appearing in equation* (3.7) *is Lipschitz continuous with respect to the state variable due to the fact that it has bounded first derivatives. Hence, there exists a Lipschitz constant $K \geq 0$ of the function f.*

3.4 Methodology

3.4.1 Pontryagin Minimum Principle (PMP)

Optimal control theory has been widely used in various subjects, ranging from mathematical analysis [120] to management optimization [121] to traffic engineering [122], and many others. The optimal control method, PMP [68], has been successfully applied to optimal eco-driving [123], parking management of AVs [10], and stabilization of building maintenance units [124], among others, to find the optimal control policy so as to drive dynamic systems from one state to another.

Consider a n-dimensional dynamic system given by the following vector differential equation

$$\dot{y} = f(t, y, u),\ t \in I,\ y(0) = y_0, \tag{3.19}$$

where $y(t) \in \mathbb{R}^n$ and $u(t) \in \mathbb{R}^m$ are the state and control vectors, respectively; y_0 is the initial state of the system. Essentially, this is equivalent to equation (3.7). In the case of traffic smoothing, $n = 2n_1, m = n_3$ since the total number of vehicles is n_1 and the number of controlled AVs is n_3. The general objective functional is expressed as follows

$$J(u) = \int_I \ell(t, y(t), u(t))dt + \Phi(y(T)), \tag{3.20}$$

where on the right-hand side, the first and second terms represent the running cost and terminal cost, respectively. This is a generic form of equation (3.8) seen in traffic smoothing. The problem is to find the control policy $u^o(t)$ such that the objective functional $J(u)$ is minimized. To address this problem, the following Hamiltonian function H is introduced

$$H(t, y, \psi, u) \coloneqq \langle f(t, y, u), \psi \rangle + \ell(t, y, u), \tag{3.21}$$

where ψ is the costate vector and $\langle \cdot, \cdot \rangle$ represents the inner product of two vectors. The costate ψ satisfies the following differential equation

$$\dot{\psi} = -H_y = -f_y'(t, y, u)\psi - \ell_y(t, y, u), \tag{3.22}$$

with boundary conditions $\psi(T) = \Phi_y(y(T))$, where f_y is the Jacobian matrix of the vector f and f_y' is its transpose. The costate ψ can be interpreted as marginal costs of the state y due to its small change.

The following theorem presents the necessary conditions of optimality prescribed by PMP.

Theorem 3.4.1. (Necessary conditions of optimality) *See Theorem 6.2.1 of [125].*

Using the above optimality conditions, one can determine the optimal AV control policy for traffic smoothing. A computational algorithm is presented in Section 3.5 following Theorem 3.4.1.

3.4.2 PMP Applied to Traffic Smoothing

The necessary conditions of optimality prescribed by PMP are applied to traffic smoothing via optimal control of AVs, where the speed perturbation due to HVs is expected to be minimized. Rewriting equation (3.8) in the form of equation (3.20), it follows that

$$\ell(t, y, u) = \frac{1}{2} \langle W(z - \tilde{z}), z - \tilde{z} \rangle , \tag{3.23}$$

$$\Phi(y(T)) = \frac{1}{2} \langle Q(z(T) - \tilde{z}(T)), z(T) - \tilde{z}(T) \rangle , \tag{3.24}$$

where $z = (\cdots, y_{2i}, \cdots) \in \mathbb{R}^{n_3}$, $\forall\ i \in \mathcal{A}$, represents the speed of all AVs, while $\tilde{z} = (v^*, \cdots, v^*, \cdots, v^*) \in \mathbb{R}^{n_3}$ denotes the speed vector of AVs before any perturbation occurs. Taking partial derivatives with respect to y leads to

$$\ell_y(t, y, u) = W(z - \tilde{z}),$$

$$\Phi_y(y(T)) = Q(z(T) - \tilde{z}(T)),$$

where the positive semi-definite matrices $W = \text{diag}(\cdots, w_i, \cdots)$ and $Q = \text{diag}(\cdots, q_i, \cdots)$ represent the weights given to the running cost and terminal cost, respectively. Plugging equations (3.6) and (3.23) into equation (3.21) yields

$$H(t, y, u, \psi) = f'(t, y, u)\psi + \ell(t, y, u) = \sum_{i=1}^{2n_1} \dot{y}_i \psi_i + \frac{1}{2} \sum_{j \in \mathcal{A}} w_j (y_{2j} - v^*)^2, \tag{3.25}$$

where $\dot{y}_i$ is given by equation (3.6).

3.4.3 An Illustration Based on IDM and OVRV Model

In this section, we shall present a simple example with IDM and OVRV model under the developed framework, in the absence of lane changing as seen in [16–18, 44]. As noted before, human drivers could exhibit different dynamics compared with AVs in terms of driving behaviors. To better capture the dynamics of HVs, we adopt the well-known IDM [112] which has been extensively used in modeling driver behaviors quantitatively. On the other hand, the controller of commercial AVs is expected to be designed in a way easy for implementation. Indeed, the OVRV model, an extension to the OVM [111], has been widely used to analyze ACC systems [105]. It has been shown that these two car-following models are able to reproduce the same type of instabilities observed in traffic jams [16]. To this end, we adopt IDM for all HVs while using OVRV model for all AVs.

Following IDM, equation (3.2) is explicitly written as

$$\ddot{x}_i(t) = a\left[1 - \left(\frac{v_i(t)}{v_0}\right)^{\delta} - \left(\frac{s^*(v_i(t), \Delta v_i(t))}{s_i(t)}\right)^2\right], \tag{3.26}$$

for $i \in \mathcal{H}$ with

$$s^*(v_i(t), \Delta v_i(t)) = s_0 + v_i(t)T - \frac{v_i(t)\Delta v_i(t)}{2\sqrt{ab}}, \tag{3.27}$$

where the parameters appearing in equations (3.26) and (3.27) are summarized in Table 3.1 [126].

Similarly, following the OVRV model equation (3.3) is written as follows for controlled AVs

$$\begin{aligned}\ddot{x}_j(t) = k_1(x_{j-1}(t) - x_j(t) - l_{j-1} - \eta - \tau v_j(t)) \\ +k_2(v_{j-1}(t) - v_j(t)) + u_j(t),\ \forall\ j \in \mathcal{A},\end{aligned} \tag{3.28}$$

where the relevant parameters are summarized in Table 3.2 [104].

Consider the simplest case where the i-th vehicle is the only AV. Plugging equations (3.26) and (3.28) into equation (3.6) for the mixed traffic dynamics consisting of

Table 3.1: Parameters of IDM

Parameter	**Value**
Desired speed v_0	35.0 m/s
Time gap T	1.0 s
Minimum spacing gap s_0	2.0 m
Acceleration exponent δ	4
Acceleration a	0.5 m/s^2
Deceleration b	2.0 m/s^2

Table 3.2: Parameters of OVRV model

Parameter	**Value**
Gain parameter on the time-gap k_1	0.04
Gain parameter on the relative speed k_2	0.5
Jam distance η	2.0 m
Desired effective time-gap τ	1.0 s
Vehicle length l_i	5.0 m

n_1 vehicles leads to

$$\dot{y} = \begin{pmatrix} y_2 \\ \dot{y}_2 \\ y_4 \\ a\left[1 - \left(\frac{y_4}{v_0}\right)^{\delta} - \left(\frac{s^*(y_4, \Delta y_4)}{s_2}\right)^2\right] \\ \vdots \\ y_{2i} \\ k_1(s_i - \eta - \tau y_{2i}) + k_2(y_{2(i-1)} - y_{2i}) + u_i \\ \vdots \\ y_{2n_1} \\ a\left[1 - \left(\frac{y_{2n_1}}{v_0}\right)^{\delta} - \left(\frac{s^*(y_{2n_1}, \Delta y_{2n_1})}{s_{n_1}}\right)^2\right] \end{pmatrix} \tag{3.29}$$

This yields the Hamiltonian function H given by equation (3.30).

$$
\begin{aligned}
H(t,y,\psi,u_i) = f'(t,y,u_i)\psi + \ell(t,y,u_i) &= \sum_{j=1}^{2n} \dot{y}_j\psi_j + \frac{1}{2}w_i(y_{2i}-v^*)^2 \\
&= y_2\psi_1 + \dot{y}_2\psi_2 + y_4\psi_3 + a\left[1-\left(\frac{y_4}{v_0}\right)^{\delta} - \left(\frac{s^*(y_4,\Delta y_4)}{s_2}\right)^2\right] \\
&\quad + \cdots + y_{2i}\psi_{2i-1} + \left(k_1(s_i-\eta-\tau y_{2i}) + k_2(y_{2(i-1)}-y_{2i}) + u_i\right)\psi_{2i} \\
&\quad + \cdots + y_{2n_1}\psi_{2n_1-1} + a\left[1-\left(\frac{y_{2n_1}}{v_0}\right)^{\delta} - \left(\frac{s^*(y_{2n_1},\Delta y_{2n_1})}{s_{n_1}}\right)^2\right]\psi_{2n_1} \\
&\quad + \frac{1}{2}w_i(y_{2i}-v^*)^2
\end{aligned} \tag{3.30}
$$

Remark 6. *In equation* (3.29)*, $y_2 = v_1$ and $\dot{y}_2 = \dot{v}_1$ denote the speed and acceleration of the lead vehicle, respectively. The speed profile $v_1(t)$ is used along with car-following principles to generate traffic flow for a string of vehicles. However, the control policy obtained for the AV does not require any knowledge of the state of other vehicles except for that of its preceding one. This is also observed mathematically from equation* (3.30) *since $\partial H/\partial u_i = \psi_{2i}$ depends only on the costate of the AV itself.*

3.5 Numerical Algorithm and Simulation Results

In this section, we present a numerical algorithm to determine the optimal AV control policy for traffic smoothing. We prove the convergence of the algorithm and conduct a series of numerical experiments to show the effectiveness of the proposed approach.

3.5.1 Numerical Algorithm

The following algorithm follows the necessary conditions of optimality prescribed by PMP presented in Section 3.4.1. It is based on the gradient method and the main steps are described as follows.

Step 1: Divide the time horizon $I = [0,T]$ into N equal subintervals and assume the control function is piecewise-constant, i.e., $u^\kappa(t) = u^\kappa(t_i)$, for $t \in [t_i, t_{i+1})$, $i = 0,1,\cdots,N-1$, where $u^\kappa(t)$, $t \in I$, is the AV control policy in the κ-th iteration.

Step 2: Integrate the state equations over I with initial state $y(0) = y_0$ and the controls $u^{(\kappa)} \coloneqq u^{\kappa}(t),\ t \in I$, to obtain the state trajectory $y^{(\kappa)}$.

Step 3: Use the tuple $\{y^{(\kappa)}, u^{(\kappa)}\}$ to integrate the costate equations backward in time starting from $\psi^{(\kappa)}(T)$.

Step 4: Use the triple $\{y^{(\kappa)},\ \psi^{(\kappa)},\ u^{(\kappa)}\}$ to compute the gradient $g_\kappa(t) = \frac{\partial H}{\partial u^{(\kappa)}}(y^{(\kappa)},\ \psi^{(\kappa)},\ u^{(\kappa)})$.

Step 5: Compute the cost functional $J^{(\kappa)}(u)$ using equation (3.20).

Step 6: If the L_2-norm square $\int_I \|g_\kappa\|_2^2 dt < \epsilon$, then $u^o = u^{(\kappa)}$ is the optimal control, where $\epsilon > 0$ is a prescribed small positive number; Otherwise, go to Step 7.

Step 7: Construct the control policy for the next iteration: $u^{(\kappa+1)}(t) = u^{(\kappa)}(t) - \varepsilon g_\kappa(t),\ t \in I$, where $\varepsilon > 0$ is the step size used in the gradient method. For the chosen ε, if $u_i^{(\kappa+1)} > \overline{u}_i$, set $u_i^{(\kappa+1)} = \overline{u}_i$; if $u_i^{(\kappa+1)} < \underline{u}_i$, set $u_i^{(\kappa+1)} = \underline{u}_i$.

Step 8: If $\kappa < Z$, where $Z \in \mathbb{N}^+$ is the maximum number of iterations, let $\kappa = \kappa + 1$, go to Step 2; Otherwise, terminate the process.

Remark 7. *The state constraints for car-following are implicitly considered in the framework in a conservative manner to avoid challenges in engineering implementation. Specifically, one needs to choose the control constraint set U with a relatively small range so that a desired minimum following distance is maintained. However, one may be able to improve our results by integrating the objective functional with any state constraints to form an augmented one [125]. Further, a constraint transcription technique [127] can be used to determine the optimal AV control policy.*

Remark 8. *In Step 4 of the algorithm, the gradient g_κ at the κ-th iteration is calculated to determine the best direction of descent used to construct the AV control policy for the next iteration as seen in Step 7. The Hamiltonian function H defined by equation* (3.21) *can be easily written out in an explicit manner as seen in equation* (3.25)*. Specifically, equation* (3.30) *shows the detailed expression of H corresponding to the example given in Section 3.4.3. Taking partial derivatives of H with respect to the control variable $u_i, i \in \mathcal{A}$ for each AV yields elements of the gradient vector g. The L_2 norm in Step 6*

is the most commonly used Euclidean norm and it is calculated as the square root of the sum of the squared vector values.

In what follows, we present some results on the convergence of the algorithm presented above.

Theorem 3.5.1. *Suppose the necessary conditions of optimality given by Theorem 3.4.1 hold. Then, there exists a sequence of control policy* $\{u^\kappa\} \in \mathcal{U}_{ad}$*, generated by the numerical algorithm presented above, along which the objective functional* J *monotonically converges to its minimum.*

Proof. It is easy to observe that $\mathcal{U}_{ad} \subset \mathcal{M}(I,U) \subset L_\infty(I,\mathbb{R}^{n_3})$, where $L_\infty(I,\mathbb{R}^{n_3})$ is a function space with elements being bounded measurable functions, and its subset $\mathcal{M}(I,U)$ denotes the set of measurable functions defined on the interval I and taking values in U. Clearly, $\mathcal{M}(I,U)$ is a Banach space. For convenience of notation, we denote the Banach space $B_\infty(I \times U)$ by Γ and its continuous dual by Γ^*. Now, we define the following duality map for any $\gamma \in \Gamma$

$$D(\gamma) \coloneqq \left\{\nu \in \Gamma^* : \langle \nu, \gamma \rangle = \|\gamma\|_\Gamma^2 = \|\nu\|_{\Gamma^*}^2\right\}. \tag{3.31}$$

Starting from the first iteration, i.e., $\kappa = 1$, we obtain the triple $\{x^{(1)},\ \psi^{(1)},\ u^{(1)}\}$. Define the following function

$$\gamma^1(t,\lambda) \coloneqq \langle \psi^{(1)}, f(t,x^{(1)}(t),\lambda)\rangle + \ell(t,x^{(1)}(t),\lambda) \tag{3.32}$$

which belongs to Γ. Choosing any element $\rho^1 \in D(\gamma^1)$, we obtain $u^{(2)} = u^{(1)} - \varepsilon\rho^1$, where $\varepsilon > 0$ is sufficiently small. Following Lagrange formula, the objective functional in the second iteration is computed as follows

$$\begin{aligned}
J(u^{(2)}) &= J(u^{(1)}) + dJ(u^{(1)}, u^{(2)} - u^{(1)}) + o(\varepsilon) \\
&= J(u^{(1)}) + \langle \gamma^1, u^{(2)} - u^{(1)}\rangle + o(\varepsilon) \\
&= J(u^{(1)}) + \langle \gamma^1, -\varepsilon\rho^1\rangle + o(\varepsilon) \\
&= J(u^{(1)}) - \varepsilon\langle \gamma^1, \rho^1\rangle + o(\varepsilon) \\
&= J(u^{(1)}) - \varepsilon\|\gamma^1\|_\Gamma^2 + o(\varepsilon) \\
&= J(u^{(1)}) - \varepsilon\|\rho^1\|_{\Gamma^*}^2 + o(\varepsilon) \\
&< J(u^{(1)}),
\end{aligned} \tag{3.33}$$

where $dJ(u^{(1)}, u^{(2)} - u^{(1)})$ represents the Gateaux differential of J at $u^{(1)}$ in the direction $(u^{(2)} - u^{(1)})$, and $o(\varepsilon)$ denotes the higher order terms.

Therefore, we have $J(u^{(1)}) > J(u^{(2)})$ for $\varepsilon > 0$ sufficiently small. This process is repeated by returning back to Step 2 with $u^{(2)}$ replacing $u^{(1)}$. Following the steps as presented above, one can construct a sequence of controls $\{u^{(\kappa)}\} \in \mathcal{U}_{ad}$ such that $J(u^{(1)}) > J(u^{(2)}) > \cdots > J(u^{(\kappa)}) > \cdots$. Clearly, this is a monotonically decreasing sequence. Since the cost integrand ℓ and terminal cost Φ are non-negative in equation (3.8), we have $J(u) \geq 0$ for all $u \in \mathcal{U}_{ad}$. Thus, there exists a non-negative real number m_o such that $\lim_{\kappa \to \infty} J(u^{\kappa}) \longrightarrow m_o$. This shows that m_o is the minimum of J in the neighbourhood of any starting point in $\mathcal{U}_{ad}$. This completes the proof. □

3.5.2 Simulation Results

In this section, we conduct a series of numerical experiments to show the effectiveness of the proposed approach, where HVs and AVs are assumed to follow IDM and OVRV model, respectively. Four distinctive scenarios are considered, where the lead vehicle executes various speed profiles and three different penetration rates of AVs are examined. Moreover, vehicle fuel consumption and emissions is studied also using the widely adopted VT-Micro model [128, 129].

Traffic Smoothing

Scenario 1: Without loss of generality, we consider a string of 10 vehicles. In this scenario, all vehicles drive at an equilibrium speed $v^* = 21$ m/s before any perturbation occurs. Starting from $t = 100$ sec, the lead vehicle slows down to 20 m/s with a deceleration rate of -0.05 m/s^2. It accelerates back to v^* after driving at 19.6 m/s for 20 sec. When there is no AV in presence, the speed profiles of all the vehicles are shown in Fig. 3.2a. It is clearly observed that the small perturbation experienced by the lead vehicle amplifies and grows into stop-and-go waves traveling backwards. In fact, the traffic is string unstable. Clearly, the speed deviation experienced by all the following vehicles amplifies due to traffic waves observed in Fig. 3.2a. Note that it is the small perturbation experienced by the lead vehicle that causes the backward waves growing further along the road.

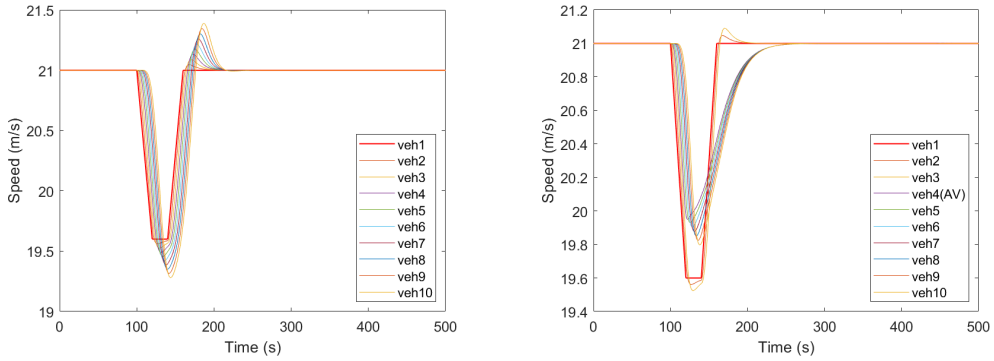

(a) Vehicle speed without AV (b) Vehicle speed with AV

Figure 3.2: Simulation results of Scenario 1, where the lead vehicle slows down at $t = 100$s.

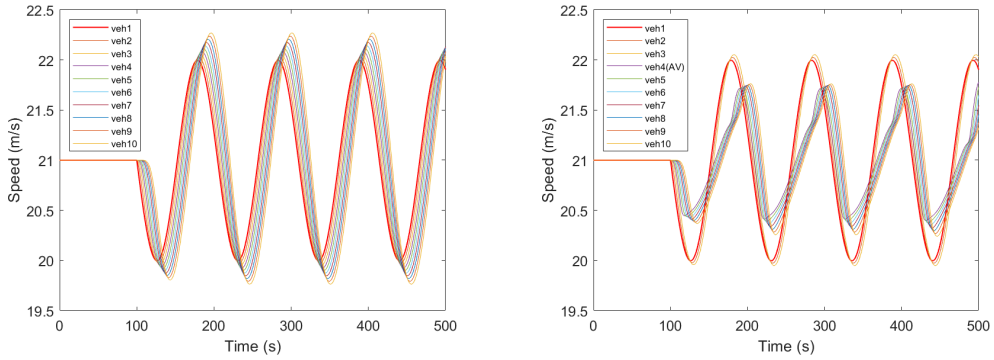

(a) Vehicle speed without AV (b) Vehicle speed with AV

Figure 3.3: Simulation results of Scenario 2, where the lead vehicle executes a sinusoidal speed profile at $\omega = 0.06$ rad/s.

Without loss of generality, it is assumed that the fourth vehicle is an AV while all the others remain to be HVs. Following the approach proposed, the speed profiles obtained for all the vehicles are shown in Fig. 3.2b. Comparing with Fig. 3.2a, it is clearly observed that the phantom jam is reduced starting from the AV. Further, this prevents traffic waves from amplifying as much as that in Fig. 3.2a. More importantly, by intelligently controlling the AV, traffic becomes head-to-tail string stable, which potentially ensures the stability of the bulk traffic on average.

Scenario 2: The experimental setting is the same as that in Scenario 1, except that

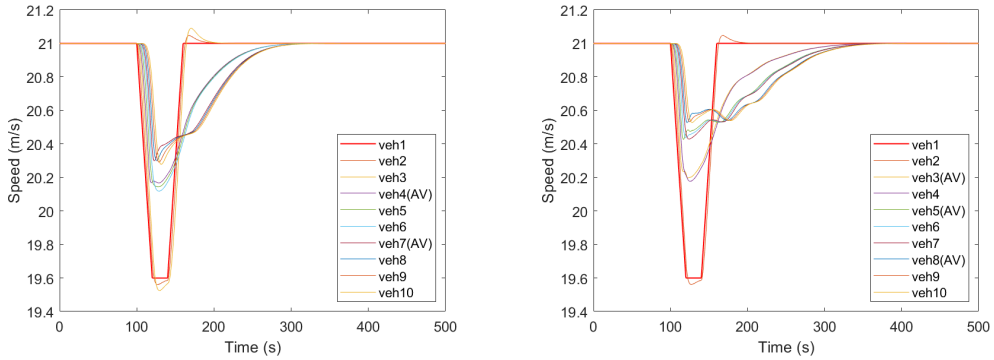

(a) Vehicle speed in the presence of two AVs (b) Vehicle speed in the presence of three AVs

Figure 3.4: Simulation results of Scenario 3 and Scenario 4, in the presence of two and three AVs, respectively.

starting from $t = 100$ sec the lead vehicle begins to execute a sinusoidal speed profile at $\omega = 0.06$ rad/s. The speed profiles are shown in Fig. 3.3a with all vehicles being HVs. It is observed that all the following vehicles continuously experience speed perturbations due to the continued sinusoidal speed of the lead vehicle, resulting in cyclical traffic waves.

As in Scenario 1, we consider the case where the fourth vehicle is an AV while the others are HVs. Using the proposed approach, the vehicle speed profiles obtained are shown in Fig. 3.3b. It is observed that traffic waves are considerably reduced. As a result, all the HVs following the AV experience much smaller perturbations compared with what they have experienced in Fig. 3.3a.

Scenario 3: The experimental setting is the same as that in Scenario 1. Without loss of generality, we consider the case where vehicles 4 and 7 are AVs while the others remain to be HVs. Following the same approach, the speed profiles obtained are shown in Fig. 3.4a. Comparing with Fig. 3.2a, it is observed that traffic waves are significantly reduced due to the collective effect of these two controlled AVs, resulting in a head-to-tail string stable traffic not observed in Fig. 3.2a.

Scenario 4: The experimental setting is the same as that in Scenario 1. In this scenario, it is assumed that there are three AVs, namely vehicles 3, 5, and 8. The speed profiles obtained are shown in Fig. 3.4b using the proposed approach. Comparing with Fig. 3.2a, it is observed that the speed perturbation is significantly reduced due to the

collective effect of three controlled AVs. Consequently, a head-to-tail string stable traffic is achieved.

Note that the collective impact of controlled AVs on the bulk traffic flow depends also on the penetration rate [15]. This is mathematically captured in our model, i.e., the penetration rate can be expressed as $\phi = \frac{\dim(\mathcal{A})}{\dim(\mathcal{H})+\dim(\mathcal{A})} = \frac{n_3}{n_2+n_3} = \frac{n_3}{n_1}$. Hence, it allows for further analytical research to study the explicit impact of ϕ on the overall traffic flow. This is out of the scope of the present study since the focus of this work is to investigate the effectiveness of the proposed distinct AV control strategy on traffic smoothing in the context of a predominantly human-driven traffic flow.

Fuel Consumption and Emissions

In addition to traffic smoothing via optimal control of AVs, we are also interested to study how the proposed AV control strategy could impact traffic performance in terms of fuel consumption and emissions. To this end, we adopt the widely used VT-Micro model [128, 129] to calculate energy consumption and emissions. The VT-Micro model is a regression model that takes the instantaneous vehicle speed and acceleration measurements as input variables. The measure of effectiveness (MOE) is given by

$$\ln(\text{MOE}) = \begin{cases} \sum_{i=0}^{3}\sum_{j=0}^{3}(L_{i,j} \times v^i \times a^j) & \text{for } a \geq 0 \\ \sum_{i=0}^{3}\sum_{j=0}^{3}(M_{i,j} \times v^i \times a^j) & \text{for } a < 0 \end{cases} \tag{3.34}$$

The MOE is the instantaneous fuel consumption rate, in L/s or mg/s. The variables v and a are the instantaneous vehicle speed and acceleration, respectively. $L_{i,j}$ and $M_{i,j}$ are the model regression coefficients for positive and negative acceleration, respectively. A detailed description of equation (3.34) and the VT-Micro model in general can be found in [128, 129].

As previously shown, the controlled AVs are able to dampen traffic waves so that the following HVs would experience less perturbations. As a result, their fuel consumption and emissions could also be impacted by the driving behavior of controlled AVs. For Scenario 1, we compute the total energy consumption and emissions of all HVs following the AV over the period [100, 350] sec when the difference in vehicle speed profiles occurs between the cases without AV (Fig. 3.2a) and with AV (Fig. 3.2b). The results are

Table 3.3: Performance of HVs 5 to 10 over [100, 350] sec in Scenario 1

Setting	**Fuel consumption (ml)**	**HC (mg)**	**CO (mg)**
Without AVs	2450.3	1992.3	31211.6
With AVs	2436.5	1914.1	29670.9
Improvement	0.56%	3.93%	4.94%

Table 3.4: Performance of HVs 5 to 10 over [100, 500] sec in Scenario 2

Setting	**Fuel consumption (ml)**	**HC (mg)**	**CO (mg)**
Without AVs	4007.9	3376.1	54039.9
With AVs	3965.3	3229.8	50855.4
Improvement	1.06%	4.33%	5.9%

Table 3.5: Performance of HVs 5, 6, 8, 9 and 10 over [100, 350] sec in Scenario 3

Setting	**Fuel consumption (ml)**	**HC (mg)**	**CO (mg)**
Without AVs	2042	1660.3	26011.2
With AVs	2028.1	1588.1	24571.1
Improvement	0.68%	4.35%	5.54%

shown in Table 3.3. It is observed that the fuel consumption is reduced by 0.56%, and the emissions, namely HC and CO are reduced by 3.93% and 4.94%, respectively.

Similarly, using the VT-Micro model we calculate the total fuel consumption for vehicles 5 to 10 in Scenario 2 over the period [100, 500] sec when the cyclical perturbation occurs. The corresponding results are summarized in Table 3.4 which shows that the fuel consumption is reduced by 1.06% and the emissions are reduced by 4.33% and 5.9% for HC and CO, respectively. This indicates that more fuel benefits and reduction in emissions could be achieved in the presence of a longer period of perturbations.

In Scenario 3, HVs 5, 6, 8, 9 and 10 are impacted by the collective effect of AVs 4 and 7. The results on fuel consumption over the period [100, 350] sec are given in Table 3.5. It shows a 0.68% reduction in fuel consumption, which is higher than that observed in Scenario 1. In Scenario 4, the fuel consumption is calculated for HVs 4, 6,

Table 3.6: Performance of HVs 4, 6, 7, 9 and 10 over [100, 350] sec in Scenario 4

Setting	**Fuel consumption (ml)**	**HC (mg)**	**CO (mg)**
Without AVs	2041.9	1660.9	26018.8
With AVs	2028.4	1596.9	24730.2
Improvement	0.66%	3.85%	4.95%

7, 9 and 10 following the three controlled AVs, with results summarized in Table 3.6. A 0.66% fuel benefit is observed, which is also higher than that of the baseline Scenario 1.

As observed, the overall head-to-tail string stability appears to increase with the increase of AV penetration rate ϕ, which is consistent with the findings of [15]. However, the fuel benefits for HVs due to the collective impact of controlled AVs may not monotonically increase with the increase of ϕ because of the complexity of the distribution of AVs in the mixed traffic. Since the objective of this chapter is to study the effectiveness of optimal AV controllers on traffic smoothing in a predominantly human-driven traffic flow [16], the variable ϕ is therefore not intended to be set significantly large in the experiments.

3.6 Conclusions

In this chapter, we have developed a general framework capable of simultaneously incorporating the nonlinear dynamics of both HVs and AVs. Under this general framework, an optimal control problem is formulated with the objective of smoothing traffic in the presence of stop-and-go waves due to the collective behavior of human drivers. Further, we prove the existence of an optimal AV control strategy. The optimal control problem is then addressed using PMP. We conduct a series of numerical experiments under various scenarios to show the effectiveness of the proposed approach. The results are promising in the sense that: (1) it is possible to dampen stop-and-go waves via optimal control of AVs, and to achieve head-to-tail string stability; (2) in addition to traffic smoothing, the distinct controller synthesized also brings benefits on vehicle fuel economy and emissions for HVs; and (3) the impact of AV penetration rate on the bulk traffic is demonstrated in a predominantly human-driven traffic flow, and the effect of

controlled AVs is expected to increase with the increase of the MPR.

It is worth noting that, in the present work analytical proofs on stability of mixed traffic, in the presence of controlled AVs, are not derived, and car-following safety is achieved only in a conservative manner. These interesting and challenging questions will be addressed in the following chapter, where a class of additive AV feedback controllers is synthesized for traffic smoothing with performance guarantees using the novel idea of virtual speed tracking.

Chapter 4

Virtual Tracking for Smoothing Nonlinear Mixed Traffic with Performance Guarantees

4.1 Introduction

As introduced in Chapter 3, to properly regulate traffic flow several effective traffic control strategies have been developed and are widely used around the globe, like traffic signal control [25], ramp metering [34], and variable speed limit (VSL) control [98], among others. Apart from these conventional traffic control methods relying on fixed infrastructure, AVs are expected to offer a new paradigm for future traffic control thanks to the potential of serving as mobile actuators in mixed traffic, thereby enabling Lagrangian traffic flow control [39, Chapter 5]. In fact, it has been shown that only a small proportion of AVs is required to stabilize unstable mixed traffic flow [16, 17], with experimental demonstrations shown in [18]. In [44] the classic H-infinity approach is applied to stabilize mixed vehicle platoons with connected automated vehicles. It ensures that speed perturbations do not amplify in each subsystem of the platoon, thereby resulting in head-to-tail string stable flow. Moreover, the controllability and stabilizability of mixed vehicle platoons has been studied using standard rank test techniques for linearized car-following systems, wherein a linear optimal feedback AV controller is

designed for traffic smoothing, with AVs assumed to have access to the global traffic state, i.e., the information of all other HVs [43]. Recently, a machine learning based approach has been proposed to derive AV driving strategies for traffic smoothing [130]. While the approach is shown to be effective in improving vehicle energy efficiency, it requires a significant amount of training data and does not prescribe any analytical form of AV controllers. In addition to control of AVs, certain control strategies have also been proposed for connected vehicles (CVs) to improve traffic efficiency. For example, it is shown that properly controlled CVs can enhance the stability of mixed traffic flow described by the IDM [112], where the vehicle control strategy is developed only for CVs following another CV [131]. In [132], a local cooperative driving strategy is developed to improve traffic efficiency by taking the weighted speed average of the surrounding CVs (within communication ranges) as the desired speed of a subject CV. However, the proposed driving strategy assumes a known relationship between traffic speed and a functional optimization parameter of traffic density, which may not be readily available in a real-world traffic environment. Considering mixed vehicular platoons of CACC, ACC, and HVs, the model parameters of CACC/ACC vehicles can be manually adjusted to balance traffic stability and capacity, without explicitly designing feedback controllers for CACC/ACC vehicles [133]. In addition to optimization-based work on traffic smoothing and stabilization, a number of simulation studies are also conducted on this subject using the IDM. For example, the impacts of MPR of communication-ready vehicles on traffic throughput and stability are studied in [15], with an IDM adopted for HVs. Using real-world data, the impacts of commercially available adaptive cruise control vehicles on highway stability and throughput are investigated in [134].

The aforementioned control techniques applied for traffic smoothing and stabilization largely rely on linearizing car-following models at equilibrium points of traffic flow. In addition, a high degree of vehicle connectivity is normally required for AV controller synthesis. For example, AVs are assumed to be able to access the information of all other HVs [43]. In Chapter 3 (also in [10]), an optimal AV feedback controller is synthesized for smoothing nonlinear mixed traffic without being limited to linearized car-following dynamics. However, analytical proofs on stability of mixed traffic, in the presence of controlled AVs, are not derived, and car-following safety is achieved only in a conservative manner.

In this chapter we develop an effective approach to synthesizing a class of additive AV feedback controllers useful for traffic smoothing with analytical performance guarantees based on the novel idea of virtual speed tracking. The proposed approach is fairly general in the sense that it is applicable to car-following dynamics described by a general functional form, covering a broad class of deterministic car-following models seen in the literature. Moreover, it does not require linearization of nonlinear car-following dynamics, useful for smoothing non-equilibrium mixed traffic. In addition, the approach developed requires only local traffic information without having to rely on high degrees of vehicle connectivity, indicating greater applicability in the near future.

The work presented in this chapter is complementary to the existing studies in the following aspects:

- The idea behind the AV controller synthesis is to closely track a virtual speed profile ahead of the controlled AV, i.e., a subtler version of the disturbance resulting from the immediate preceding vehicle. In doing so, traffic waves can be alleviated when propagating upstream. More importantly, this approach allows for analytical guarantees on convergence of speed tracking, resulting in locally stable traffic, possibly leading to head-to-tail string stability with a sufficient MPR of AVs.

- The approach is developed in the context of a general functional form of car-following dynamics. In other words, it can be implemented for traffic flow described by a broad class of deterministic car-following models. Moreover, it does not require linearization of nonlinear car-folowing dynamics, applicable for smoothing non-equilibrium mixed traffic.

- The additive AV controllers synthesized require only local traffic information, i.e., spacing and relative speed to the preceding vehicle, and do not require vehicle connectivity often assumed in prior studies. This is anticipated to be particularly useful for practical applications since HVs are not expected to have sophisticated communication capabilities in the near future. In fact, the approach is readily implementable for commercially available ACC vehicles thanks to onboard radar sensors monitoring the road ahead.

A brief comparison with vehicle speed harmonization: Speed harmonization is a

method to reduce traffic congestion, which is normally applied at roadway bottlenecks such as lane merging areas and speed reduction zones on a freeway [135, 136]. Mobile traffic sensors are employed to collect and send real-time information at a congested location to a traffic management center, which is then used by a computer to compute optimal speeds for vehicles approaching the congestion. The recommended speeds are sent to CVs or connected AVs on the road via wireless communications. The idea of speed harmonization finds applications in green driving and eco-driving [137–139]. It is noted that speed harmonization, along with its applications such as green driving and eco-driving, normally involves solving an optimization problem for achieving certain objectives like minimizing energy consumption. By contrast, the present study is very much distinct to speed harmonization at various aspects. The essence of this work is to design a virtual speed profile for controlled AVs to follow closely without requiring vehicle connectivity, so as to reduce disturbance to mixed traffic that could be caused even by human driver behavior alone. The proposed approach works well regardless of road locations considered. In fact, it provides an effective method for AVs to dampen stop-and-go waves whenever such traffic waves propagate across AVs. It is also noted that no optimization problem is involved in our framework, which is beneficial for ease of computation. Moreover, the proposed approach ensures analytical guarantees on speed tracking and car-following safety.

The remainder of this chapter is structured as follows. In Section 4.2, we present a general framework to describe mixed traffic in the functional form of car-following dynamics. In Section 4.3, a class of effective additive AV controllers is synthesized based on the concept of tracking a virtual speed profile ahead of the controlled AV. This class of AV controllers are able to not only smooth mixed traffic, but also lead to head-to-tail string stable flow with a sufficient MPR of AVs. In Section 4.4, the general approach is further illustrated with a theoretical IDM and a well-calibrated ACC vehicle model. Extensive numerical results are presented in this section to show the effectiveness and robustness of the new feedback controllers synthesized for AVs on traffic smoothing. We conclude this chapter in Section 4.5 with discussion on some future research directions. The materials presented in this chapter are mostly taken from [51].

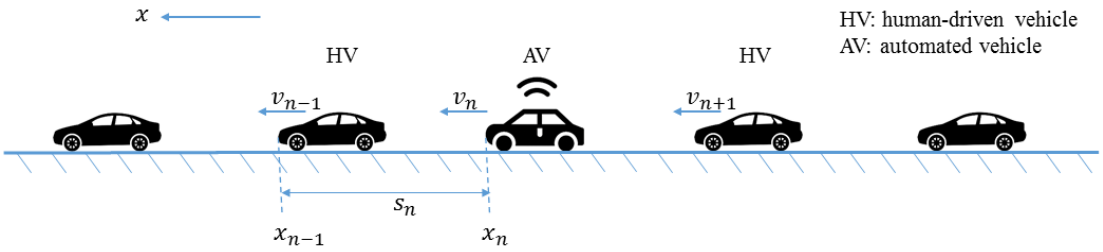

Figure 4.1: Schematic of mixed traffic consisting of human-driven vehicles (HVs) and automated vehicles (AVs). This is for illustration only; there is no specific requirement on the position of AVs in the traffic flow.

4.2 Preliminaries

4.2.1 Car-following Dynamics

We consider general mixed traffic consisting of HVs and AVs, as shown in Fig. 4.1. Without loss of generality, we consider a string of N vehicles denoted by the totally ordered set $\mathcal{N} = \{1, 2, \cdots, N\}$. For any vehicle $n \in \mathcal{N}$, $x_n(t)$ and $v_n(t)$ signify its displacement and speed at time t, respectively. The variable $s_n(t)$ represents the spacing between vehicle n and its immediate preceding vehicle $n-1$ at time t, including the length of the preceding vehicle, specifically $s_n(t) = x_{n-1}(t) - x_n(t)$. In some relevant studies, s_n has been used also to denote the inter-vehicle spacing between vehicle n and its preceding vehicle (e.g., see Fig. 3.1 of Chapter 3), excluding length of the preceding vehicle. However, from the perspective of mathematical analysis there is no fundamental difference at all. For ease of notation, in the present framework we have adopted the widely used notations seen in [114], where the spacing is denoted by $s_n(t) = x_{n-1}(t) - x_n(t)$. In fact, it is the speed of the AV, relative speed to its preceding vehicle, and inter-vehicle spacing (bumper-to-bumper distance) that are needed for implementing the proposed AV controller to be presented in the following section. Such information is readily available thanks to onboard sensors. Lane changing is neglected for convenience of mathematical analysis, as commonly seen in prior studies on smoothing and stabilizing mixed traffic [10, 16–18, 43, 44, 140]. This could be extended to include lane changing and either is appropriate. In the context of traffic smoothing and stabilization, many imperfections,

such as lane changing and driver heterogeneity, are considered as external perturbations to a deterministic single-lane model, based on which mathematical analysis shall be carried out [114].

To better present a complete mathematical framework we first reiterate the car-following dynamics of individual vehicles similar to those seen in Section 3.2. Based on physics, the motion of any vehicle $n \in \mathcal{N}$ is described by the following set of ordinary differential equations [114],

$$\dot{x}_n = v_n, \tag{4.1}$$

$$\dot{v}_n = f(s_n, \Delta v_n, v_n), \tag{4.2}$$

where the dot operator denotes differentiation with respect to time; the nonlinear function f describes the functional relationship between vehicle acceleration/deceleration $\dot{v}_n$ of the n-th vehicle and the variables s_n, Δv_n and v_n; and the relative speed Δv_n with respect to the immediate preceding vehicle is defined as

$$\Delta v_n = \dot{s}_n = v_{n-1} - v_n. \tag{4.3}$$

The above equations (4.1)–(4.2) are the general functional form of car-following dynamics widely adopted in the literature. It is assumed that vehicle speed and acceleration are physically bounded from both above and below. Clearly, the variables involved, such as s_n, v_n, etc. are time-dependent. For brevity of analysis the argument t is omitted.

Let $\mathcal{H}$ and $\mathcal{A}$ denote respectively the totally ordered set of HVs and AVs in the mixed traffic consisting of N vehicles, i.e., $\mathcal{N} = \mathcal{H} \cup \mathcal{A}$. It is assumed that HVs follow the general car-following dynamics described by equations (4.1)–(4.2). For AVs, our goal is to synthesize appropriate additive feedback controllers in a general form, without being limited to any specific car-following model, for smoothing mixed traffic in the presence of perturbations. To this end, the mixed traffic dynamics is written as

$$\dot{x}_n = v_n, \ \forall \ n \in \mathcal{N} \tag{4.4}$$

$$\dot{v}_n = \begin{cases} f(s_n, \Delta v_n, v_n), \ \forall \ n \in \mathcal{H} & \text{(4.5a)} \\ h(s_n, \Delta v_n, v_n) + u_n, \ \forall \ n \in \mathcal{A} & \text{(4.5b)} \end{cases}$$

where u_n is the additive acceleration control on AVs, which preserves the property of abiding by car-following principles [10]. The actual acceleration input applied to AVs

is given by the entirety of equation (4.5b), part of which is the additive term u_n to be characterized. In view of equation (4.5a), it is clear that controlled AVs do not change the way HVs operate since HVs still abide by regular car-following principles. It is also worth noting that the functionals f and h in the above equations do not have to be the same, depending on specific car-following principles followed by HVs and AVs.

As mentioned in Section 3.2, by setting $\dot{v}_n = 0$ in equations (4.5a) and (4.5b) one obtains the solution pairs $(v_n^*, \acute{s}_n^*)$, $\forall\ n \in \mathcal{H}$, and $(v_n^*, \grave{s}_n^*)$, $\forall\ n \in \mathcal{A}$, where $\acute{s}_n^*$ and $\grave{s}_n^*$ represent the spacing between vehicle n, either a HV or an AV, and its immediate preceding vehicle at equilibrium traffic, where all vehicles drive with a uniform speed v^*. For simplicity, we shall denote these tuples corresponding to the equilibrium traffic by $(v^*, \acute{s}^*)$ and $(v^*, \grave{s}^*)$ for HVs and AVs, respectively. In equilibrium traffic flow there is no additional control u_n applied to AVs since the equilibrium state is maintained by adhering to car-following principles only. However, when stop-and-go waves approach a controlled AV, u_n will take effect on the AV to dampen the undesired traffic waves so that vehicles behind could experience smoother traffic flow. To this end, AVs need to be controlled to closely track a subtler version of the disturbance, termed as a virtual speed profile in this study, in order to alleviate the amplification of backward shock waves due to perturbations in unstable mixed traffic. A detailed analytical characterization of the virtual speed profile will be presented in Section 4.3.

4.2.2 String Stability of Equilibrium Flow

In this subsection, we present a brief note on string stability of car-following models linearized at flow equilibrium points. There are two commonly used methods for assessing the string stability of a particular car-following model, namely head-to-tail string stability conditions [17, 44, 141] and λ_2 criteria [15, 114, 134]. The former states that one can relate the speed response of the first vehicle and that of the last vehicle in a platoon using a transfer function G. The platoon is said to be string stable if the head-to-tail transfer function G satisfies

$$|G(\omega)| = \left| \frac{\tilde{V}_N(\omega)}{\tilde{V}_1(\omega)} \right| \leq 1, \tag{4.6}$$

where ω is the root of the characteristic equation, $\tilde{V}_1(\omega)$ and $\tilde{V}_N(\omega)$ are the Laplace transform of the speed perturbation of the first and the last vehicle, respectively. The

condition shown in the above expression (4.6) implies that a disturbance in vehicle speed is not amplified from the first vehicle to the last one in the platoon, and hence the platoon is considered string stable.

String stability of a car-following model can be assessed also at an equilibrium flow using the criteria proposed in [114] given the vehicle dynamics following equation (4.5a) or (4.5b) and abiding by the rational driving constraints (RDC)

$$\beta_1 := \frac{\partial \dot{v}}{\partial s} > 0,\ \beta_2 := \frac{\partial \dot{v}}{\partial \Delta v} > 0,\ \beta_3 := \frac{\partial \dot{v}}{\partial v} < 0. \tag{4.7}$$

The RDC ensures a simple criterion for the existence of car-following models. With the partial derivative of $\dot{v}$ with respect to $(s, \Delta v, v)$ evaluated at the equilibrium flow, the platoon is said to be string stable around the equilibrium state if

$$\lambda_2 := \frac{\beta_1}{\beta_3^3}\left(\frac{\beta_3^2}{2} - \beta_2\beta_3 - \beta_1\right) < 0. \tag{4.8}$$

The two types of criteria presented above work well in assessing the stability of car-following models, and many interesting results have been obtained for traffic smoothing and stabilization based on these criteria, such as [16, 17, 44, 141]. However, it is worth noting that these criteria rely on linearizing nonlinear car-following models at the equilibrium state. Consequently, the approaches developed in the aforementioned studies [16, 17, 44, 141] are better applicable to mixed traffic flow described by linearized car-following models.

The present work is focused on smoothing nonlinear mixed traffic via intelligent control of AVs based on the novel concept of virtual tracking, rather than developing criteria for assessing stability of the traffic flow. Specifically, in what follows, we develop a general approach to smoothing nonlinear mixed traffic with car-following dynamics described by its functional form, without being subject to any specific car-following model. Notably, the new approach allows for analytical proof on convergence in tracking desired speed profiles by AVs. Moreover, the new class of additive AV controllers to be presented are observed to be able to smooth unstable mixed traffic. This is due to the fact that AVs with the synthesized controllers are capable of closely tracking a properly designed virtual speed profile, resulting in reduced perturbations when traffic waves pass the controlled AVs. Consequently, it is possible to achieve head-to-tail string stability for the mixed traffic with a sufficient MPR of AVs due to their collective effect.

4.2.3 Nonlinear Stability Analysis

Due to the highly nonlinear nature of mixed traffic flow, we are particularly interested in designing appropriate AV feedback controllers for traffic smoothing, drawing on nonlinear stability analysis with vehicle motions described by the general functional form in equations (4.4), (4.5a) and (4.5b). Rather than focusing on linear stability analysis of specific linearized car-following models [16–18, 43, 44], we develop a general approach for traffic smoothing via intelligent control of AVs, readily applicable to deterministic car-following models having the general form shown in equations (4.5a)–(4.5b), and satisfying the RDC [114]. To this end, we shall present the well-known Barbalat's Lemma and its corollary.

Lemma 4.2.1 (Barbalat's Lemma [76])**.** *Suppose* $\phi : \mathbb{R}_{\geq 0} \longrightarrow \mathbb{R}$ *is differentiable and has a finite limit, i.e.,* $\lim_{t\to\infty} \phi(t) < \infty$*. If* $\dot{\phi}$ *is uniformly continuous, then*

$$\lim_{t\to\infty} \dot{\phi}(t) = 0. \tag{4.9}$$

Barbalat's Lemma is widely employed in proving stability of dynamical systems. An immediate and useful corollary to Barbalat's Lemma is stated as follows.

Corollary 4.2.2. *[76] If* $\phi : \mathbb{R}_{\geq 0} \longrightarrow \mathbb{R}$ *is twice differentiable and has a finite limit, i.e.,* $\lim_{t\to\infty} \phi(t) < \infty$*, and its second derivative* $\ddot{\phi}$ *is bounded, then*

$$\lim_{t\to\infty} \dot{\phi}(t) = 0. \tag{4.10}$$

4.3 Virtual Tracking for Traffic Smoothing

As introduced before, we consider a generic scenario with a string of N vehicles driving on a single lane. Without loss of generality, it is assumed that the speed perturbation, e.g., vehicle slowdown, occurs to the first vehicle (HV), resulting in stop-and-go waves propagating backward. The controlled AVs are expected to dynamically adjust their speed to closely track a virtual speed profile, i.e., a subtler version of the disturbance resulting from the immediate preceding vehicle, so that undesired traffic waves can be alleviated. Essentially, this is to reduce traffic hysteresis via intelligent control of AVs. For mathematical analysis, we consider any AV, $n \in \mathcal{A}$, with its motion described by equations (4.4) and (4.5b).

4.3.1 Synthesizing a Class of AV Controllers for Virtual Tracking

In view of the mechanism of traffic wave propagation, our objective is to design a class of additive AV controllers so that the controlled AV can closely track a virtual speed profile to effectively smooth traffic flow. That is, when passing a controlled AV the speed perturbation will not amplify as much as it would have in the presence of HVs. Consequently, traffic waves propagating backward will be alleviated, resulting in smoother traffic.

Notably, the virtual profile to be tracked by AVs is designed using only local traffic information readily available, such as spacing and relative speed to the preceding vehicle, which allows for easy implementations. Moreover, the additive feedback controllers of AVs are synthesized with a variable adaptation rate so that fast tracking can be achieved. In addition, the virtual profile to be presented essentially exhibits a subtler version of the disturbance resulting from the immediate preceding vehicle, which ensures that the acceleration of controlled AVs is within realistic bounds given a physically feasible trajectory of the preceding vehicle. Due to the capability of such feedback controllers, it is possible for mixed traffic to achieve head-to-tail string stability with a sufficient MPR of AVs. However, one needs to consider explicit safety requirements in relation to car-following since the virtual speed profile designed for tracking may be overly aggressive. To this end, we also analyze car-following dynamics and derive sufficient conditions for a tunable class of additive AV controllers so that safety is always guaranteed. We present the main results in the following theorems.

Theorem 4.3.1. *Suppose there exists a function* $g : \mathbb{R}_{\geq 0} \times \mathbb{R}_{\geq 0} \times \mathbb{R}_{\geq 0} \longrightarrow \mathbb{R}$ *that satisfies the following conditions*

(i) $g(t, s_n, v_{n-1}) > 0$ *for* $v_{n-1} < v^*$; $g(t, s_n, v_{n-1}) < 0$ *for* $v_{n-1} > v^*$;

(ii) $g(t, s_n, v_{n-1})$ *is twice differentiable in* t *with bounded derivatives, and monotonically increases in* s_n;

(iii) $g(\cdot, \cdot, v^*) = 0$;

(iv) $g(t, s_n, v_{n-1})$ *is bounded from above by a positive real number, say* $\alpha > 0$, *i.e.,* $\sup_{s_n, v_{n-1}} g(t, s_n, v_{n-1}) = \alpha$.

Then, given the additive (measurable) feedback control $u_n = \lambda \left(\Delta v_n + g(s_n, v_{n-1})\right)$ *for any AV* $n \in \mathcal{A}$ *with the positive adaptation rate* λ *relatively large, the surrounding*

traffic of the controlled AV is locally stable in the sense that $\lim_{t\to\infty}(v_n(t)-\tilde{v}_n(t))=0$, *where* $\tilde{v}_n = v_{n-1}+g(s_n, v_{n-1})$.

Proof. Consider the Lyapunov-like function

$$V(t)=\frac{1}{2}\left(v_n-\tilde{v}_n\right)^2,\ t\geq 0. \tag{4.11}$$

Clearly, $V=0$ if and only if $v_n=\tilde{v}_n$; $V>0$ if $v_n\neq\tilde{v}_n$. For lack of better wording, the speed $\tilde{v}_n = v_{n-1}+g(s_n, v_{n-1})$, with $s_n = x_{n-1}-x_n$, is termed as the 'virtual profile' to be tracked by the controlled AV n. The argument t, for brevity, is omitted here and afterward. To be able to reduce traffic waves when propagating backward across controlled AVs, the AV n is expected to track a virtual profile greater than that of its preceding vehicle, v_{n-1}, when $v_{n-1}<v^*$; similarly, the virtual profile $\tilde{v}_n$ is expected to be smaller than the speed of vehicle $n-1$ when $v_{n-1}>v^*$. This is ensured by the condition (i). Moreover, the function g is assumed to monotonically increase in s_n (condition (ii)) for abiding by RDC in car-following [114]; that is, vehicles are more likely to accelerate when the spacing to its preceding vehicle increases. The condition (iii) simply states that the value of the function g vanishes at equilibrium flow. The condition (iv) is introduced to ensure car-following safety. In other words, AVs should be controlled to not track an overly aggressive virtual profile. A sufficient condition characterizing the upper bound of the function g will be derived explicitly later.

Taking the time derivative of equation (4.11) yields

$$\dot{V}=\frac{d}{dt}V=(v_n-\tilde{v}_n)(\dot{v}_n-\dot{\tilde{v}}_n)=(v_n-\tilde{v}_n)\left(h(s_n,\Delta v_n,v_n)+u_n-\dot{\tilde{v}}_n\right), \tag{4.12}$$

with $\dot{\tilde{v}}_n$ given by

$$\dot{\tilde{v}}_n=\dot{v}_{n-1}+\frac{d}{dt}g(s_n,v_{n-1}). \tag{4.13}$$

By virtue of the condition (ii) and the fact that $\dot{v}_{n-1}$ is bounded, it is clear that $\dot{\tilde{v}}_n$ is also bounded. Letting $\varepsilon_n = h(s_n,\Delta v_n,v_n)-\dot{\tilde{v}}_n$, it follows from equation (4.12) that

$$\begin{aligned}
\dot{V} &= (v_n-\tilde{v}_n)(u_n+\varepsilon_n)\\
&= (v_n-\tilde{v}_n)\left(\lambda\left(\Delta v_n+g(s_n,v_{n-1})\right)+\varepsilon_n\right)\\
&= (v_n-\tilde{v}_n)\left(\lambda\left(v_{n-1}-v_n+g(s_n,v_{n-1})\right)+\varepsilon_n\right)\\
&= (v_n-\tilde{v}_n)\left(\lambda(\tilde{v}_n-v_n)+\varepsilon_n\right)\\
&= -\lambda(v_n-\tilde{v}_n)^2+\varepsilon_n(v_n-\tilde{v}_n).
\end{aligned} \tag{4.14}$$

It follows from Young's inequality that

$$\varepsilon_n(v_n - \tilde{v}_n) \leq \frac{1}{2}\varepsilon_n^2 + \frac{1}{2}(v_n - \tilde{v}_n)^2. \tag{4.15}$$

Plugging the inequality (4.15) into equation (4.14) leads to

$$\dot{V} \leq -\lambda(v_n - \tilde{v}_n)^2 + \frac{1}{2}\varepsilon_n^2 + \frac{1}{2}(v_n - \tilde{v}_n)^2 = -(2\lambda - 1)V + \frac{1}{2}\varepsilon_n^2. \tag{4.16}$$

Since $\dot{\tilde{v}}_n$ is bounded, the value of ε_n is also bounded by its definition. Let $\bar{\varepsilon}_n$ denote the upper bound of $|\varepsilon_n|$. Thus

$$\varepsilon_n^2 \leq \bar{\varepsilon}_n^2. \tag{4.17}$$

Hence, the inequality (4.16) can be written as

$$\dot{V} \leq -(2\lambda - 1)V + \frac{1}{2}\varepsilon_n^2 \leq -(2\lambda - 1)V + \frac{1}{2}\bar{\varepsilon}_n^2, \tag{4.18}$$

with $\bar{\varepsilon}_n$ being a constant. Clearly, the function V is bounded and finite given an adaptation rate $\lambda > 1/2$. We now proceed to show that, in fact, $\dot{V}$ converges to zero due to the essence of car-following. Following equation (4.14) and taking the second time derivative of V yields

$$\ddot{V} = -2\lambda(v_n - \tilde{v}_n)(\dot{v}_n - \dot{\tilde{v}}_n) + \dot{\varepsilon}_n(v_n - \tilde{v}_n) + \varepsilon_n(\dot{v}_n - \dot{\tilde{v}}_n). \tag{4.19}$$

By virtue of the condition (ii) and physics of car-following and the fact that addition and multiplication preserve boundedness, it is easy to verify that $\ddot{V}$ is bounded. Note that, given that the lead vehicle immediately ahead reasonably resumes a feasible equilibrium speed after experiencing speed disturbance, the speed of the following controlled AV will approach the same speed in a finite time. In other words, the function V has a finite limit. Since $\ddot{V}$ is bounded as shown above, by virtue of Corollary 4.2.2 it follows that

$$\lim_{t\to\infty} \dot{V}(t) = 0. \tag{4.20}$$

In other words,

$$\lim_{t\to\infty} \left[-\lambda(v_n - \tilde{v}_n)^2 + \varepsilon_n(v_n - \tilde{v}_n)\right] = \lim_{t\to\infty} \left[(v_n - \tilde{v}_n)\left(\varepsilon_n - \lambda(v_n - \tilde{v}_n)\right)\right] = 0. \tag{4.21}$$

Hence, it is easy to verify that $v_n \longrightarrow \tilde{v}_n$ as $t \longrightarrow \infty$, since equation (4.21) holds regardless of the value of the positive adaptation rate λ. Consequently, $v_n \longrightarrow v_{n-1} +$

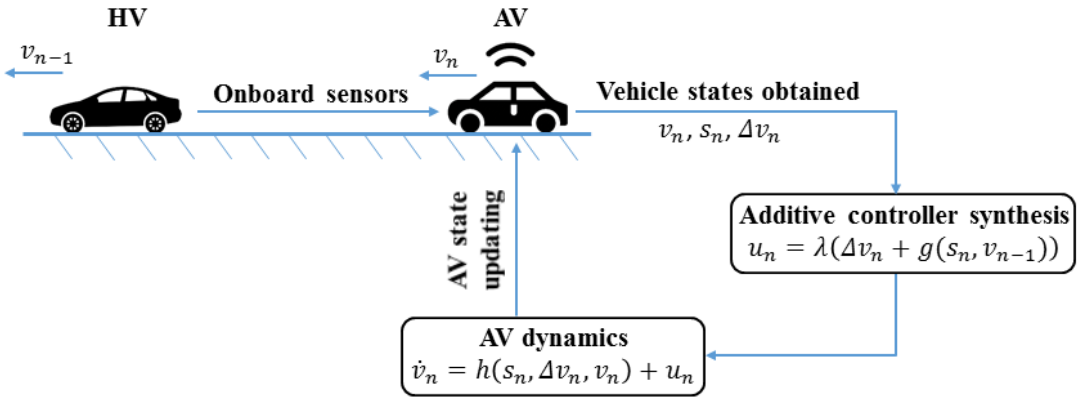

Figure 4.2: Illustration of AV controller synthesis and its implementation. The proposed approach works well regardless of the preceding vehicle type; a HV is shown as the immediately preceding vehicle only for the purpose of illustration [51].

$g(s_n, v_{n-1})$ as $t \longrightarrow \infty$. This indicates that the controlled AV closely tracks the virtual profile $\tilde{v}_n$ as specified, and reaches the equilibrium flow solution, i.e., $v_n \longrightarrow v_{n-1} = v^*$ as $t \longrightarrow \infty$, which is consistent with the condition (iii) of Theorem 4.3.1. This completes the proof. □

In Fig. 4.2 we present a schematic to further illustrate the mechanism of the AV controllers synthesized. As shown in Fig. 4.2, the AV obtains vehicle states like speed (v_n), spacing (s_n) and relative speed (Δv_n) from onboard sensors. Note that obtaining the inter-vehicle spacing (bumper-to-bumper distance), which is practically available, is sufficient for the proposed approach to work effectively, without having to acquire length of the preceding vehicle. As mentioned in Section 4.2, we have adopted the widely used notations of [114], with the spacing denoted by $s_n(t) = x_{n-1}(t) - x_n(t)$, for the purpose of notational consistency. Using these information an additive AV controller u_n is synthesized for the AV to closely track the virtual speed profile $\tilde{v}_n = v_{n-1} + g(s_n, v_{n-1})$. Following the u_n synthesized an acceleration control of the AV is executed according to equation (4.5b). Consequently, the AV state is updated for one time step. This process repeats as the AV moves forward while continuously obtaining local traffic information with respect to the preceding vehicle.

Remark 9. *The reasoning behind the conditions that need to be satisfied by the function g is as follows: (a) to be able to reduce traffic waves when propagating backward across controlled AVs, any AV n is expected to track a virtual speed profile greater than that of its preceding vehicle, v_{n-1}, when $v_{n-1} < v^*$; similarly, the virtual profile $\tilde{v}_n$ is expected to be smaller than the speed of vehicle $n-1$ when $v_{n-1} > v^*$. This is ensured by the condition (i); (b) the rate of change in vehicle speed and acceleration is physically bounded. In addition, vehicles are more likely to accelerate when the spacing to its preceding vehicle increases, which is in line with the RDC. This is reflected by the condition (ii). More importantly, this is consistent with the fact that less effect of the additive control input is anticipated when the spacing s_n is small, while a greater effect is desired when s_n is larger; (c) in equilibrium traffic flow, the virtual profile $\tilde{v}_n$ reduces to v_{n-1}; in other words, $g(s_n, v^*) = 0$. This is satisfied by the condition (iii); and (d) to avoid AVs tracking an overly aggressive virtual profile for safety purposes, the condition (iv) is introduced in alignment with the fact that the virtual profile tracked by the AV needs to be closely related to that of the immediate preceding vehicle. A more detailed analysis will be presented later for deriving sufficient conditions on the upper bound α of the function g. In addition, an implicit condition, $\tilde{v}_n \geq 0$, is applied to the virtual profile. This can be easily achieved via hard constraints, or by selecting a function g that also has a relatively small lower bound. Appropriate explicit forms of g shall be presented later.*

Remark 10. *By setting $g = 0$, the proposed class of additive controllers reduce to $u_n = \lambda \Delta v_n$, with the subtler version of the disturbance becoming $\tilde{v}_n = v_{n-1}$. In other words, the AV is controlled to closely track the speed of its immediate preceding vehicle. This can lead to smoother traffic flow to some extent, but may not be as effective as designing an appropriate function g. In numerical studies, we shall discuss more on the simplest case with $g = 0$, and compare the corresponding results with those obtained using the general additive AV controllers synthesized in Theorem 4.3.1.*

Remark 11. *Theorem 4.3.1 shows that the speed of the AV can be dynamically controlled to closely track a desired virtual profile, leading to smoother traffic. In fact, the impact of the controlled AV on traffic smoothing can be appropriately regulated by modifying the positive adaptation rate λ. By virtue of the expression* (4.18)*, it is observed that the larger λ is, the faster v_n converges to $\tilde{v}_n$. In fact, the tracking rate increases*

exponentially with the increase of the value of λ. Due to the principle in relation to car-following, vehicles behind the controlled AV tend to copy its profile, resulting in smoother traffic.

Remark 12. *In fact, ε_n in inequality* (4.17) *is fairly small by its definition, hence the inequality relaxation seen in inequality* (4.18) *is very loose. In other words, a proper adaptation rate λ can be easily chosen for the controlled AV. We shall further demonstrate this in numerical studies. Moreover, by its definition ε_n tends to decrease (converge in fact) when v_n approaches $\tilde{v}_n$, and eventually arrives at $\varepsilon_n = 0$ in equilibrium flow.*

Remark 13. *Following the virtual speed profile constructed, i.e., a subtler version of the disturbance resulting from the preceding vehicle, allows a controlled AV, as opposed to the case of a HV, to experience less speed reduction when decelerating. In other words, the AV being controlled would keep a tighter gap to its preceding vehicle, compared to the case of a HV, making it less likely for vehicles to cut in in front of the AV. When the AV accelerates back to the equilibrium speed, the proposed smoothing approach tends to reduce the overshoot of its speed. This could leave a larger gap between the controlled AV and its preceding vehicle compared to the case of a HV, inducing possible cut-ins in front of the AV. However, it has been shown in the recent simulation study [142] that AV behavior stabilizing the traffic flow is still beneficial even if it induces additional cut-in maneuvers.*

4.3.2 Sufficient Conditions for Ensuring Car-following Safety

In view of the additive feedback controllers synthesized above, the adaptation rate λ determines the rate of tracking. Specifically, the larger λ is, the faster v_n converges to the desired virtual profile. It is noted that car-following safety may be compromised if the virtual speed profile constructed for tracking is overly aggressive in reducing speed disturbance. Clearly, this is closely related to the upper bound of the function g, i.e., α, which determines the level of mildness of the desired virtual profile. To ensure that any controlled AV keeps a safe distance to its preceding vehicle at all times, we shall present a sufficient condition that analytically characterizes the upper bound α.

Theorem 4.3.2. *Given a control (or operation) horizon $I = [0, T_f]$, car-following safety is guaranteed if the positive upper bound α of the function g, as defined in the condition (iv) of Theorem 4.3.1, is bounded from above by $\frac{s_n(0)-\check{s}}{T_f}$, i.e., $\alpha \leq \frac{s_n(0)-\check{s}}{T_f}$, where $s_n(0) = x_{n-1}(0) - x_n(0)$ is the initial spacing between the controlled AV n and its preceding vehicle $n-1$, and $\check{s}$ denotes the minimum safe spacing.*

Proof. Let $\tilde{s}_n(t)$, $t \in I$, denote the spacing between vehicle $n-1$ and the controlled AV n following the virtual profile $\tilde{v}_n(t)$. Based on kinematics, it follows that

$$\begin{aligned}
\tilde{s}_n(t) &= s_n(0) + \int_0^t \left(v_{n-1}(\theta) - \tilde{v}_n(\theta)\right) d\theta \\
&= s_n(0) + \int_0^t \left(v_{n-1}(\theta) - v_{n-1}(\theta) - g(s_n(\theta), v_{n-1}(\theta))\right) d\theta \\
&= s_n(0) - \int_0^t g(s_n(\theta), v_{n-1}(\theta)) d\theta \\
&= s_n(0) - \sum_i \int_{t_i}^{t_i+\tau_i} g(s_n(\theta), v_{n-1}(\theta)) d\theta,\ 0 \leq t_i < t_i + \tau_i \leq t,\ i = 1, 2, 3, \cdots
\end{aligned} \tag{4.22}$$

where $\{[t_i, t_i + \tau_i], i = 1, 2, 3, \cdots\}$ is the set of disjoint intervals when the immediate preceding vehicle $n-1$ experiences speed perturbations. It is clear that $\sum_i |(t_i + \tau_i) - t_i| = \sum_i \tau_i \leq T_f$. It follows from the condition (iv) of Theorem 4.3.1 that

$$\sup_{s_n, v_{n-1}} g(s_n, v_{n-1}) = \alpha. \tag{4.23}$$

Hence,

$$\sum_i \int_{t_i}^{t_i+\tau_i} g(s_n(\theta), v_{n-1}(\theta)) d\theta < \sum_i \int_{t_i}^{t_i+\tau_i} \alpha d\theta = \alpha \sum_i \tau_i \leq \alpha T_f. \tag{4.24}$$

Therefore, it follows from equation (4.22) that

$$\tilde{s}_n(t) = s_n(0) - \sum_i \int_{t_i}^{t_i+\tau_i} g(s_n(\theta), v_{n-1}(\theta)) d\theta > s_n(0) - \alpha T_f. \tag{4.25}$$

To ensure safety in car-following it is sufficient to have

$$s_n(0) - \alpha T_f \geq \check{s}, \tag{4.26}$$

where $\check{s}$ is the minimum safe spacing. With simple rearrangements of inequality (4.26) it follows that the positive real number α satisfies

$$\alpha \leq \frac{s_n(0) - \check{s}}{T_f}. \tag{4.27}$$

This completes the proof. □

Remark 14. *In case the upper bound α is achievable for the function g, i.e., $g(s_n, v_{n-1}) \leq \alpha$, then the strict inequality '$<$' in the expression* (4.24) *becomes '$\leq$'. However, it is easy to verify that similar steps still hold in the above proof, leading to the same conclusion.*

Remark 15. *In fact, the upper bound on α shown in inequality* (4.27) *is consistent with car-following principles. Specifically, when the initial spacing $s_n(0)$ is large, there is more room for the controlled AV to adjust its speed, resulting in a larger upper bound on α. When the operation horizon T is large there is likely to be more perturbations occurring, thereby leaving less room for constructing the virtual profile, resulting in a smaller upper bound on α.*

Remark 16. *The inequality* (4.24) *is derived in a conservative manner in the sense that it is more likely to expect that $\sum_i \tau_i \ll T_f$ in uniform traffic flow with small perturbations. That is, in view of stop-and-go waves the duration of speed perturbations occurring to a vehicle is hardly comparable to the entire operation horizon. To this end, a much less conservative upper bound for α can be chosen as $[s_n(0) - \check{s}] \,/\, (\sum_i \tau_i)$.*

4.3.3 A Concrete Example of AV Controller Synthesis

Explicit Form of an AV Feedback Controller

Theorem 4.3.1 presents a broad class of additive feedback controllers of AVs, in the general functional form, for smoothing nonlinear mixed traffic. For better illustration, in what follows we present a simple yet useful example considering an explicit form of the function g.

Theorem 4.3.3. *Given the additive (measurable) feedback control $u_n = \lambda\left(\Delta v_n + k \arctan\left[\gamma s_n(v^* - v_{n-1})\right]\right)$, where $\arctan[\cdot]$ denotes the inverse tangent operator, for any AV $n \in \mathcal{A}$ with the positive adaptation rates λ relatively large, e.g.,*

$\lambda > 1/2$, and k relatively small, and a positive scale factor γ, the surrounding traffic of the controlled AV is locally stable in the sense that $\lim_{t\to\infty}(v_n(t) - \tilde{v}_n(t)) = 0$, *where* $\tilde{v}_n = v_{n-1} + k\arctan[\gamma s_n(v^* - v_{n-1})]$.

Proof. Consider the Lyapunov-like function

$$V(t) = \frac{1}{2}(v_n - \tilde{v}_n)^2, \ t \geq 0. \tag{4.28}$$

Clearly, $V = 0$ if and only if $v_n = \tilde{v}_n$; $V > 0$ if $v_n \neq \tilde{v}_n$. Taking the time derivative of equation (4.28) yields

$$\dot{V} = \frac{d}{dt}V = (v_n - \tilde{v}_n)(\dot{v}_n - \dot{\tilde{v}}_n) = (v_n - \tilde{v}_n)\left(h(s_n, \Delta v_n, v_n) + u_n - \dot{\tilde{v}}_n\right), \tag{4.29}$$

with $\dot{\tilde{v}}_n$ given by

$$\begin{aligned}
\dot{\tilde{v}}_n &= \dot{v}_{n-1} + k\Bigg(\dot{v}_{n-1}\frac{\partial}{\partial v_{n-1}}\arctan[\gamma s_n(v^* - v_{n-1})] \\
&\qquad + \dot{x}_{n-1}\frac{\partial}{\partial x_{n-1}}\arctan[\gamma s_n(v^* - v_{n-1})] + \dot{x}_n\frac{\partial}{\partial x_n}\arctan[\gamma s_n(v^* - v_{n-1})]\Bigg) \\
&= \dot{v}_{n-1} + \frac{k\gamma\left[-s_n\dot{v}_{n-1} + (v^* - v_{n-1})\Delta v_n\right]}{1 + [\gamma s_n(v^* - v_{n-1})]^2}.
\end{aligned} \tag{4.30}$$

With a slight abuse of notation let $\varepsilon_n = h(s_n, \Delta v_n, v_n) - \dot{\tilde{v}}_n$. It follows from equation (4.29) that

$$\begin{aligned}
\dot{V} &= (v_n - \tilde{v}_n)(u_n + \varepsilon_n) \\
&= (v_n - \tilde{v}_n)\left(\lambda\left(\Delta v_n + k\arctan[\gamma s_n(v^* - v_{n-1})]\right) + \varepsilon_n\right) \\
&= (v_n - \tilde{v}_n)\left(\lambda(\tilde{v}_n - v_n) + \varepsilon_n\right) \\
&= -\lambda(v_n - \tilde{v}_n)^2 + \varepsilon_n(v_n - \tilde{v}_n).
\end{aligned} \tag{4.31}$$

It follows from Young's inequality that

$$\varepsilon_n(v_n - \tilde{v}_n) \leq \frac{1}{2}\varepsilon_n^2 + \frac{1}{2}(v_n - \tilde{v}_n)^2. \tag{4.32}$$

Plugging the inequality (4.32) into equation (4.31) leads to

$$\dot{V} \leq -\lambda(v_n - \tilde{v}_n)^2 + \frac{1}{2}\varepsilon_n^2 + \frac{1}{2}(v_n - \tilde{v}_n)^2 = -(2\lambda - 1)V + \frac{1}{2}\varepsilon_n^2. \tag{4.33}$$

In view of equation (4.30), it is clear that $\dot{\tilde{v}}_n$ is bounded since each term on the right-hand side is bounded; hence the value of ε_n is also bounded. Let $\bar{\varepsilon}_n$ denote the upper bound of $|\varepsilon_n|$. Thus

$$\varepsilon_n^2 \leq \bar{\varepsilon}_n^2. \tag{4.34}$$

Hence, the inequality (4.33) can be written as

$$\dot{V} \leq -(2\lambda - 1)V + \frac{1}{2}\varepsilon_n^2 \leq -(2\lambda - 1)V + \frac{1}{2}\bar{\varepsilon}_n^2, \tag{4.35}$$

with $\bar{\varepsilon}_n$ being a constant. Clearly, the function V is bounded and finite given an adaptation rate $\lambda > 1/2$. We now proceed to show that, in fact, $\dot{V}$ converges to zero. Following equation (4.31) and taking the second time derivative of V yields

$$\ddot{V} = -2\lambda(v_n - \tilde{v}_n)(\dot{v}_n - \dot{\tilde{v}}_n) + \dot{\varepsilon}_n(v_n - \tilde{v}_n) + \varepsilon_n(\dot{v}_n - \dot{\tilde{v}}_n). \tag{4.36}$$

Since each term in equation (4.36) is bounded and addition and multiplication preserve boundedness, it is clear that $\ddot{V}$ is bounded. Based on similar arguments seen in the proof of Theorem 4.3.1, it follows from Corollary 4.2.2 that

$$\lim_{t\to\infty} \dot{V}(t) = 0. \tag{4.37}$$

That is,

$$\lim_{t\to\infty} \left[-\lambda(v_n - \tilde{v}_n)^2 + \varepsilon_n(v_n - \tilde{v}_n)\right] = \lim_{t\to\infty} \left[(v_n - \tilde{v}_n)\left(\varepsilon_n - \lambda(v_n - \tilde{v}_n)\right)\right] = 0. \tag{4.38}$$

Hence, one has $v_n \longrightarrow \tilde{v}_n$ as $t \longrightarrow \infty$ since equation (4.38) holds regardless of the value of λ; that is $v_n \longrightarrow v_{n-1} + k \arctan\left[\gamma s_n(v^* - v_{n-1})\right]$ as $t \longrightarrow \infty$. This indicates that the controlled AV closely tracks the virtual profile $\tilde{v}_n$ as specified, and reaches the equilibrium flow solution, i.e., $v_n \longrightarrow v_{n-1}$ as $t \longrightarrow \infty$ due to the fact that $v_{n-1} \longrightarrow v^*$ as $t \longrightarrow \infty$. This completes the proof. □

Sufficient Conditions on k for Car-following Safety

In view of the additive AV feedback controllers synthesized above, the adaptation rate k scales the magnitude of the virtual profile, and impacts significantly on car-following safety. To ensure a safe following distance for controlled AVs in tracking the desired speed profile, we present a sufficient condition that analytically characterizes the adaptation rate k as follows.

Theorem 4.3.4. *Given a control (or operation) horizon $I = [0, T_f]$, car-following safety is guaranteed if the non-negative adaptation rate k is bounded from above by $\frac{2[s_n(0)-\check{s}]}{\pi T_f}$, i.e., $k \leq \frac{2[s_n(0)-\check{s}]}{\pi T_f}$, where $s_n(0) = x_{n-1}(0) - x_n(0)$ is the initial spacing between the controlled AV n and its preceding vehicle $n-1$, and $\check{s}$ denotes the minimum safe spacing.*

Proof. Let $\tilde{s}_n(t)$, $t \in I$, denote the spacing between vehicle $n-1$ and the controlled AV n following the virtual profile $\tilde{v}_n(t)$. Based on kinematics, it follows that

$$\begin{aligned}
\tilde{s}_n(t) &= s_n(0) + \int_0^t (v_{n-1}(\theta) - \tilde{v}_n(\theta))\, d\theta \\
&= s_n(0) + \int_0^t (v_{n-1}(\theta) - v_{n-1}(\theta) - k \arctan\left[\gamma s_n(\theta)(v^* - v_{n-1}(\theta))\right])\, d\theta \\
&= s_n(0) - k \int_0^t \arctan\left[\gamma s_n(\theta)(v^* - v_{n-1}(\theta))\right] d\theta \\
&= s_n(0) - k \sum_i \int_{t_i}^{t_i+\tau_i} \arctan\left[\gamma s_n(\theta)(v^* - v_{n-1}(\theta))\right] d\theta, \qquad (4.39)
\end{aligned}$$

with $0 \leq t_i < t_i + \tau_i \leq t$, $i = 1, 2, 3, \cdots$, and $\{[t_i, t_i + \tau_i], i = 1, 2, 3, \cdots\}$ is the set of disjoint intervals when the immediate preceding vehicle $n-1$ experiences speed perturbations. It is clear that $\sum_i |(t_i + \tau_i) - t_i| = \sum_i \tau_i \leq T_f$. By virtue of the range of the inverse tangent function it follows that

$$-\pi/2 < \arctan\left[\gamma s_n(\theta)(v^* - v_{n-1}(\theta))\right] < \pi/2 \qquad (4.40)$$

Hence,

$$\sum_i \int_{t_i}^{t_i+\tau_i} \arctan\left[\gamma s_n(\theta)(v^* - v_{n-1}(\theta))\right] d\theta < \sum_i \int_{t_i}^{t_i+\tau_i} \frac{\pi}{2} d\theta = \frac{\pi}{2} \sum_i \tau_i \leq \frac{\pi T_f}{2}. \qquad (4.41)$$

Therefore, it follows from equation (4.39) that

$$\tilde{s}_n(t) = s_n(0) - k \sum_i \int_{t_i}^{t_i+\tau_i} \arctan\left[\gamma s_n(\theta)(v^* - v_{n-1}(\theta))\right] d\theta > s_n(0) - \pi k T_f/2. \qquad (4.42)$$

To ensure safety in car-following it is sufficient to have

$$s_n(0) - \pi k T_f/2 \geq \check{s}, \qquad (4.43)$$

where $\check{s}$ is the minimum safe spacing. With simple rearrangements of inequality (4.43) it follows that the non-negative adaptation rate k satisfies

$$k \leq \frac{2\left[s_n(0) - \check{s}\right]}{\pi T_f}. \qquad (4.44)$$

This completes the proof. □

Remark 17. *Again, the above upper bound on k is derived in a conservative manner as that seen in inequality* (4.27)*. Similar to what has been stated in Remark 16, in this case a much less conservative upper bound for k can be chosen as* $2\left[s_n(0) - \check{s}\right] / \left(\pi \sum_i \tau_i\right)$.

Remark 18. *The function g given in Theorem 4.3.1 covers a broad class of additive controllers for AVs. The example presented in Theorem 4.3.3 illustrates an explicit form of the function g satisfying all the conditions given in Theorem 4.3.1. In fact, many sigmoid functions satisfy the same set of conditions and can be employed to represent the function g in Theorem 4.3.1, such as the hyperbolic tangent function* $\tanh(\cdot)$*, the Gauss error function $erf(\cdot)$, among others.*

4.4 Numerical Results

In this section we conduct a series of numerical experiments to show the effectiveness and robustness of the additive AV controllers synthesized. We first employ the widely used IDM to describe general car-following dynamics, with the additive controller implemented under various scenarios. Subsequently, the synthesized controller is employed for commercially available ACC vehicles which have been shown to be string unstable for seven vehicle models widely available in the US market [143]. The effects of controlled AVs on traffic smoothing are thoroughly studied in this section.

4.4.1 Illustration with an IDM

In the preceding section we have devised a class of AV feedback controllers in the context of a general functional form of car-following dynamics. The approach proposed is readily applicable to any deterministic car-following model having the general form shown in equations (4.5a)–(4.5b), satisfying the RDC [114]. There have been a number of notable car-following models developed in the literature, such as the Gazis-Herman-Rothery (GHR) model [109], Gipps' model [110], optimal speed model (OVM) [111], IDM [112], and Newell's car-following model [113], among others. Notably, the IDM is widely adopted in the field of transportation engineering due to its capability of reproducing the same type of traffic instabilities observed in phantom jams [16]. It has been

used extensively to model driver behaviors quantitatively for studying traffic flow stability [15–17, 134]. To this end, an IDM is employed for illustrating the general approach proposed. Following IDM, the explicit form of the functional f in equation (4.5a) is given by

$$f(s_n, \Delta v_n, v_n) = a\left[1 - \left(\frac{v_n}{v_0}\right)^{\delta} - \left(\frac{s^*(v_n, \Delta v_n)}{s_n - l_{n-1}}\right)^2\right], \tag{4.45}$$

where

$$s^*(v_n, \Delta v_n) = s_0 + v_n T - \frac{v_n \Delta v_n}{2\sqrt{ab}}. \tag{4.46}$$

For illustrative purposes only, the functional h in equation (4.5b) is taken the same as f. However, other forms of h are also feasible provided that the property of abiding by car-following principles is preserved [10], with the basic RDC satisfied. The parameters appearing in the above equations are summarized in Table 4.1 for numerical studies. Subsequently, we also implement the synthesized additive controller on commercially available ACC vehicles, with the calibrated parameters adopted from [144].

In this study, the IDM is adopted for describing the dynamics of HVs and AVs. It is not only widely used to represent HVs [126, 145], but also heavily employed for AVs in recent studies [15–17, 134]. Notably the IDM is a multi-regime model that can provide a high degree of realism in capturing the dynamics of different congestion levels [146]. Moreover, recent studies have shown that the IDM is capable of accurately capturing ACC (i.e., AVs with Level 1 automation technology) driving behavior when calibrated with the experimental car-following data of commercially available ACC vehicles [144, 147, 148]. Hence, using different model parameter values of the IDM can effectively describe the dynamics of HVs and AVs (or ACC vehicles). Moreover, the proposed approach works well regardless of the deterministic car-following model chosen, as indicated in Theorem 4.3.1 (or Theorem 4.3.3). In the following section, we conduct extensive numerical simulations using the IDM considering both theoretical and calibrated parameter values to show the effectiveness and robustness of the approach developed.

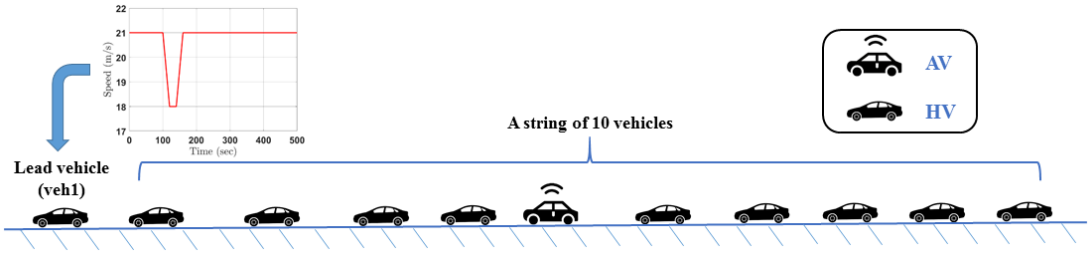

Figure 4.3: Illustration of a string of 10 vehicles following a lead HV that executes a given speed profile. In this illustrative example, vehicle 6 is an AV while the rest are HVs, exhibiting a MPR of 10% [51].

Table 4.1: Parameters of IDM [10]

Parameter	**Value**
Desired speed v_0	35.0 m/s
Time gap T	1.5 s
Minimum spacing gap s_0	2.0 m
Acceleration exponent δ	4
Acceleration a	1.0 m/s^2
Deceleration b	2.5 m/s^2
Vehicle length l_n, $\forall\ n \in \mathcal{N}$	5 m

4.4.2 Simulation Results

In this section, we conduct extensive numerical experiments to show the effectiveness and robustness of the proposed approach, with both theoretical IDM parameters and commercially available ACC vehicle parameters. Without loss of generality, we consider a string of 10 vehicles following a lead HV, that is, 11 vehicles in total. A graphic illustration is shown in Fig. 4.3 with a MPR of 10%. All vehicles are assumed to drive at an equilibrium speed $v^* = 21$ m/s before any speed perturbation occurs. Starting from $t = 100$ sec, the lead HV decelerates, at the rate of 0.15 m/s^2, to a speed of 18 m/s. It accelerates back to v^* after driving at 18 m/s for 20 sec. We implement the synthesized additive controller on AVs for various MPRs, including MPR = 10%, 30%, 50%, 80% and 100%, with AVs assumed to be evenly distributed in the platoon. This assumption on AV distribution is consistent with prior studies on controller design for CVs and AVs in the context of mixed autonomy [141, 149], without considering heterogeneity of parameters. In fact, the performance of our approach is to be evaluated in terms of average speed variation, which is consistent with the approximation of even AV distribution. While assessing system performance in terms of average values, we also present some complementary results on the interaction between neighboring vehicles.

In addition to traffic smoothing, we also study the impacts of controlled AVs on reducing vehicle speed variation quantitatively. To that end, we define the average speed variation (ASV) per vehicle per second, corresponding to any specific MPR over a given period $[t_1, t_2]$, as follows

$$\text{ASV} = \frac{1}{M(t_2 - t_1)} \sum_n \int_{t_1}^{t_2} |v_n(t) - v^*| \, dt, \tag{4.47}$$

where the vehicle index n starts from the first AV in the platoon since vehicles ahead of it do not experience any of its impact on traffic smoothing; M is the total number of upstream vehicles starting from the first AV as well. For example, assuming a MPR of 30% with vehicles 4, 7 and 10 being AVs and the rest being HVs, the ASV is then calculated for vehicles 4–11 with $M = 8$ and the vehicle index n starting from 4 in equation (4.47).

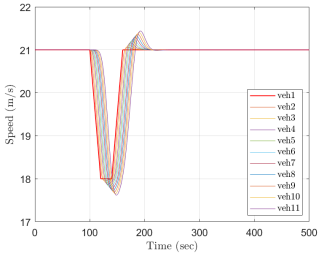

(a) MPR = 0%.

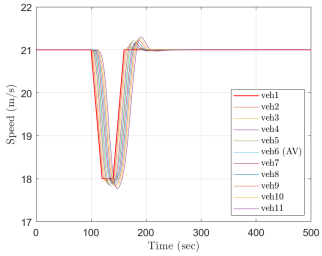

(b) MPR = 10%.

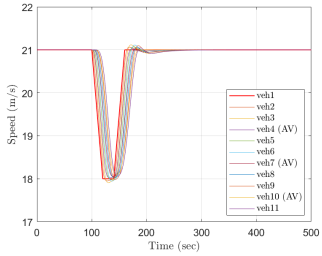

(c) MPR = 30%.

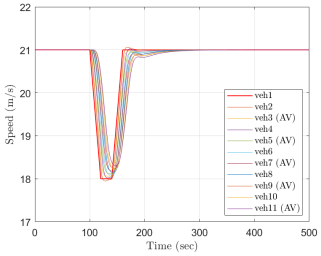

(d) MPR = 50%.

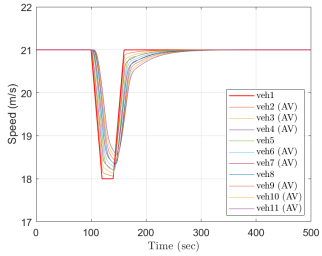

(e) MPR = 80%.

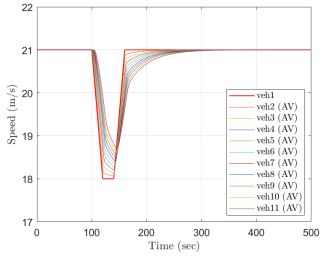

(f) MPR = 100%.

Figure 4.4: Speed profile of all vehicles under different MPRs, where $k = 0.1$, $\gamma = 0.01$ and $\lambda = 1$.

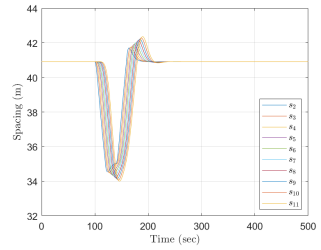

(a) MPR = 0%.

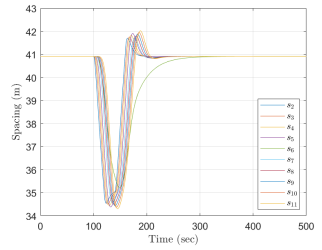

(b) MPR = 10%.

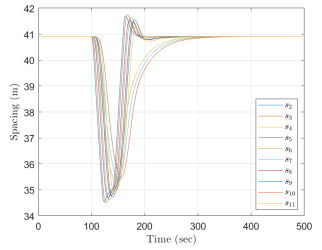

(c) MPR = 30%.

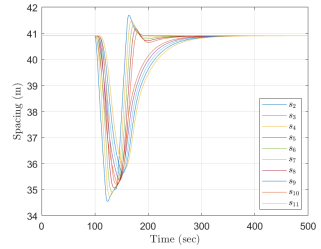

(d) MPR = 50%.

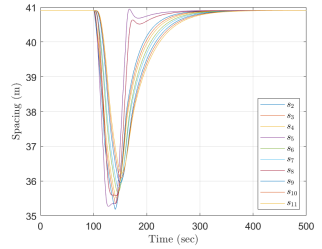

(e) MPR = 80%.

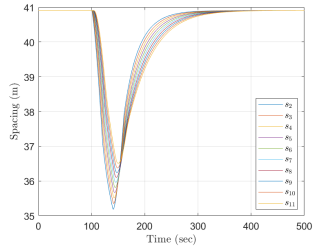

(f) MPR = 100%.

Figure 4.5: Spacing profile of all vehicles under different MPRs, where $k = 0.1$, $\gamma = 0.01$ and $\lambda = 1$.

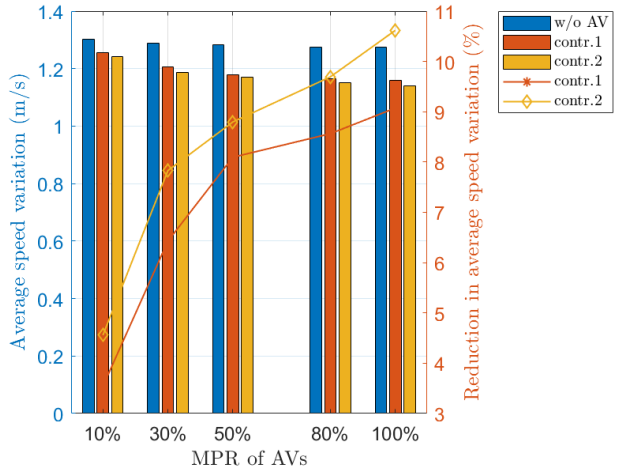

Figure 4.6: Comparison of average speed variation (ASV) between the simple case of a linear additive controller with $g = 0$ (labelled as 'contr.1') and the general nonlinear controller with $g(t, s_n, v_{n-1}) = k \arctan[\gamma s_n(v^* - v_{n-1})]$ (labelled as 'contr.2').

Theoretical IDM Vehicles

In this section theoretical IDM parameters presented in Table 4.1 are employed for all vehicles in numerical experiments. In view of these parameters it is easy to verify that, the initial spacing between a controlled AV n and its preceding vehicle is $s_n(0) = \frac{s_0+v^*T}{\sqrt{1-(v^*/v_0)^\delta}} + l_{n-1} = 40.91$ m, and the minimum safe spacing is given by $\check{s} = s_0 + l_{n-1} = 7$ m. The duration of speed perturbations is slightly overestimated as $\sum_i \tau_i = 150$ sec to ensure the less conservative sufficient condition seen in Remark 17. Consequently, it follows that $k \leq 0.144$. In the subsequent studies we first examine the performance of the additive AV controllers presented in Theorem 4.3.3 with $k = 0.1$, $\lambda = 1$, and $\gamma = 0.01$. Later, we study impacts of these tunable AV control parameters on the performance of traffic smoothing.

Figs. 4.4 and 4.5 show respectively the speed and spacing profiles of all vehicles at various MPRs. In the absence of AVs, the corresponding speed profiles of all the HVs are shown in Fig. 4.4a. It is observed that the small perturbation experienced by the lead HV (veh 1) amplifies and grows into traffic waves traveling upstream along the string of 11 vehicles, resulting in an increased speed variation for all the following vehicles. It is observed from Figs. 4.4b–4.4f that the mixed traffic is better smoothed

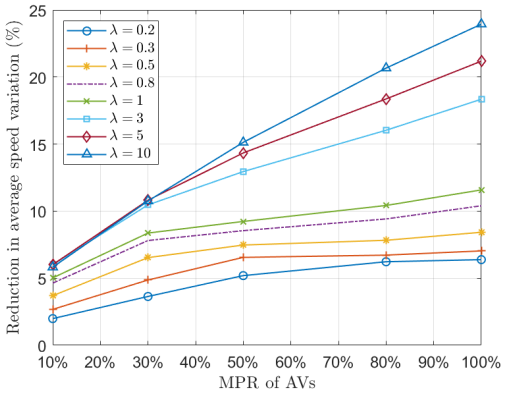

Figure 4.7: Reduction in ASV corresponding to different values of the adaptation rate λ, with $\gamma = 0.02$ and $k = 0.1$.

with controlled AVs, compared to that of Fig. 4.4a. The mixed traffic is observed to be head-to-tail string stable at the MPR = 80% and 100%. Further, the ASV values decrease with the increase of MPR, as shown in Fig. 4.6 (the results corresponding to 'contr.2'). In other words, the improvement in reduction of ASV values is observed to increase with the increase of MPR. That is, a larger presence of AVs is likely to further smooth unstable mixed traffic. Since the value of k used satisfies the sufficient condition given in Remark 17, car-following safety is guaranteed, as observed in Fig. 4.5.

Next, we compare the performance of the general additive AV controllers to that of a linear additive controller $u_n = \lambda \Delta v_n$ [50] in the case of $g = 0$. The corresponding results are presented in Fig. 4.6. In implementing the additive AV controllers, the parameters k, λ and γ remain the same as introduced before. It is observed from Fig. 4.6 that the ASV values of both cases decrease with the increase of MPR. Compared to the case without AVs, the improvement in reduction of ASV increases with the increase of MPR, where the percentage improvements corresponding to the linear additive controller (i.e., in the case of $g = 0$) and the general nonlinear additive controller $u_n = (\lambda \Delta v_n + k \arctan[\gamma s_n (v^* - v_{n-1})])$ (i.e., in the case of $g = k \arctan[\gamma s_n (v^* - v_{n-1})]$) are labelled as 'contr.1' and 'contr.2', respectively. It is noted that a greater reduction in ASV is observed in the general case (using a nonlinear additive controller), indicating smoother traffic flow achieved. The above results suggest that the function g incorporated into the virtual speed profile in the general

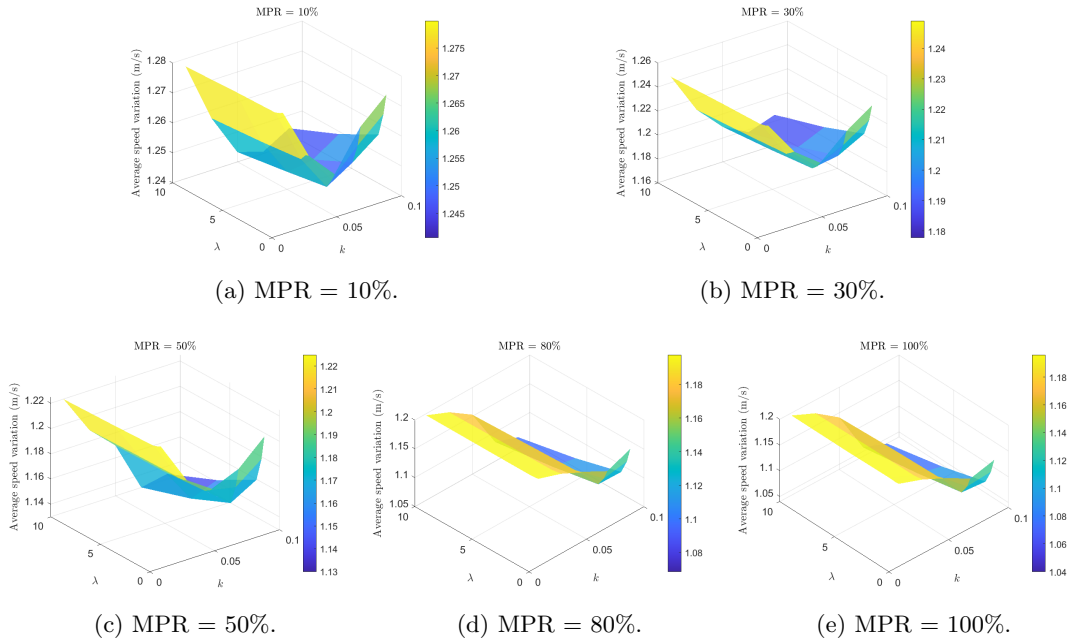

(a) MPR = 10%. (b) MPR = 30%.

(c) MPR = 50%. (d) MPR = 80%. (e) MPR = 100%.

Figure 4.8: ASV in response to the change of k and λ.

case is capable of prescribing a subtler version of the disturbance to be tracked by AVs. However, the general class of controllers require the information of both spacing and relative speed to the preceding vehicle, as opposed to the simple (linear) case where only relative speed is required for controller synthesis. The synthesized nonlinear controllers are expected to work as efficiently as the linear ones in terms of computation time and complexity since only simple algebraic calculation is required for computing u_n without involving any optimization. Fig. 4.6 shows that the general nonlinear controller outperforms the simple linear controller. It is possible to achieve greater improvement by properly tuning the parameters involved in the synthesized controllers, and the level of improvement could vary across different traffic scenarios.

As indicated by the proof of Theorem 4.3.1, the positive adaptation rate λ does not need to be considerably large in order to achieve benefits of reducing vehicle speed perturbations. However, relatively small reductions of ASV may be expected even at high MPRs given a very small value of λ. To this end, we are interested in studying the impact of λ on improving traffic smoothness, i.e., reduction in ASV. The corresponding

results are shown in Fig. 4.7. It is easily observed from Fig. 4.7 that, for any given λ the percentage improvement in reduction of ASV increases with the increase of MPR. This is due to the fact that a greater impact of the controllers implemented is expected with a larger presence of AVs, which is in line with the results presented in Fig 4.6. For some curves corresponding to smaller values of λ, the percentage reduction does not increase significantly with the increase of MPR, compared to that of a larger λ. This is because a relatively large value of λ is required for controlled AVs to effectively track the virtual speed profile synthesized, as indicated in Theorem 4.3.3. In addition to the limited effectiveness due to smaller values of λ (like $\lambda = 0.2, 0.3, 0.5$), the fact that ASV is calculated per vehicle also contributes to insignificant increase in the reduction of ASV even at very high MPRs like 80%$\sim$100%. This is because the value of M in equation (4.47) is larger for a higher MPR. Hence, a 20% increase in MPR (from 80% to 100%), i.e., 2 more AVs in a platoon of 10 vehicles, does not lead to a great increase in ASV reduction for each of the M vehicles. In addition, for any given MPR the reduction in ASV appears to increase with the increase of the value of λ. This is because a larger λ leads to faster tracking of the desired virtual speed profile, thereby resulting in less perturbations and smoother traffic flow. More importantly, the improvement in reducing ASV appears to converge with the increase of the value of λ. This is reasonable since the desired virtual speed profile can be well tracked with a sufficient value of λ. Notably, a larger λ does not compromise physical implementation of the actual acceleration input to AVs with the additive controller being only part of the input, as seen from the resulting vehicle speed profiles shown in Fig. 4.4.

Since the impact of controlled AVs on traffic smoothing is closely related to the values of k and λ, in Fig. 4.8 we present some interesting results on the reduction of ASV in relation to the change of k and λ. Specifically, we study impacts of AVs on reducing ASV, with k and λ ranging in $[0.01, 0.1]$ and $[0.2, 10]$, respectively, where the sufficient condition for car-following safety is guaranteed. For any given MPR considered, it is observed that the reduction of ASV tends to decrease as a result of the increase of k and λ. With respect to both k and λ, the decreasing rate of ASV appears to converge as these two parameters become sufficiently large. Notably, this is consistent with the results shown in Fig. 4.7. Therefore, for implementation moderate values of k and λ can be chosen to achieve satisfactory improvements on ASV, e.g., $k = 0.1$ and $\lambda = 1$.

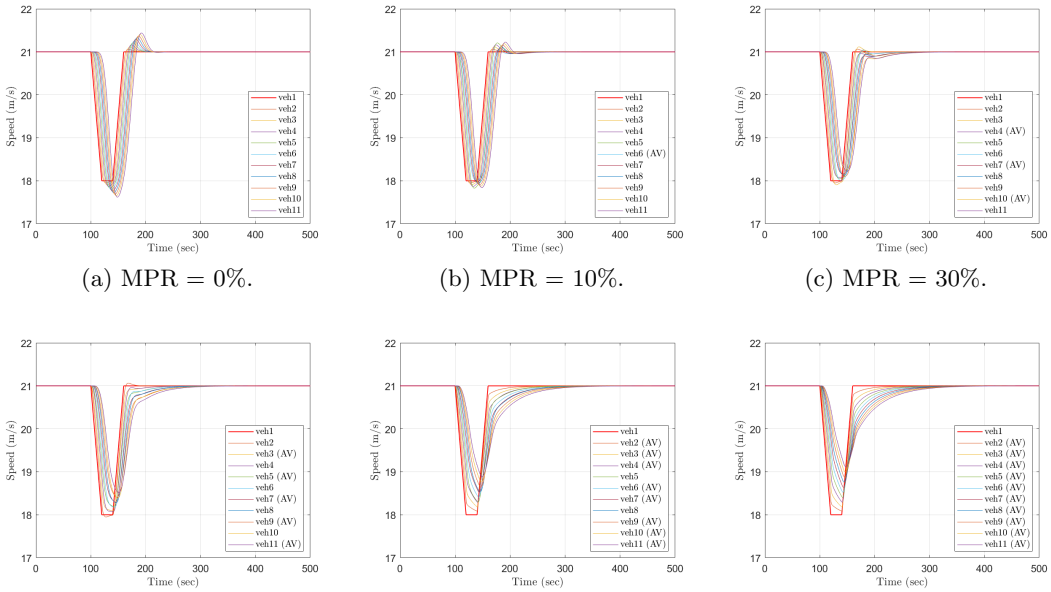

(a) MPR = 0%. (b) MPR = 10%. (c) MPR = 30%.

(d) MPR = 50%. (e) MPR = 80%. (f) MPR = 100%.

Figure 4.9: Speed profile of all vehicles under different MPRs with $k = 0.4$, $\gamma = 0.01$ and $\lambda = 1$.

As mentioned before, the value of k has been properly chosen to satisfy the sufficient condition for car-following safety. Since that is not a necessary condition, it is likely that larger values of k could still ensure safety while achieving better improvement in reducing ASV. To this end, we briefly present a set of results in Figs. 4.9 and 4.10 with a relatively larger value of k, that is, $k = 0.4$ as opposed to $k = 0.1$. It is observed from Fig. 4.9 that the impacts of AVs on vehicle speed profiles are more significant compared to the results shown in Fig. 4.4. It is also interesting to note that a relatively longer period is needed for vehicles behind AVs to resume the equilibrium speed. This indicates that k should not be chosen much larger than the upper bound determined in the sufficient condition for car-following safety. In view of $k = 0.4$, the minimum spacing experienced by AVs, shown in Figs. 4.10b–4.10f, is smaller than their counterpart observed in Figs. 4.5b–4.5f corresponding to the smaller value of $k = 0.1$. However, car-following safety is still maintained in this case, which is consistent with the fact that $k \leq 0.144$ is a sufficient condition for ensuring safety.

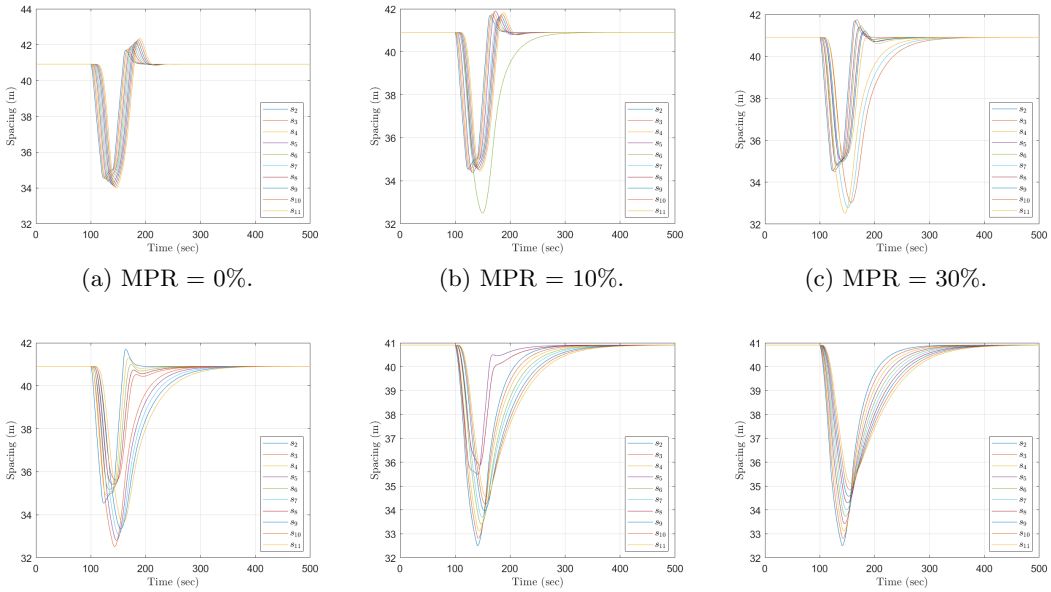

(a) MPR = 0%. (b) MPR = 10%. (c) MPR = 30%.

(d) MPR = 50%. (e) MPR = 80%. (f) MPR = 100%.

Figure 4.10: Spacing profile of all vehicles under different MPRs with $k = 0.4$, $\gamma = 0.01$ and $\lambda = 1$.

Commercially Available ACC Vehicles

In this section, we implement the general additive AV controllers synthesized in Theorem 4.3.3 on commercially available ACC vehicles whose dynamics are characterized by a well calibrated IDM. Recently, it has been revealed that many ACC-equipped vehicles, widely available in the US market, are string unstable, based on analyzing data collected from seven distinct vehicle models with more than 1,900 kilometers of driving in car-following experiments [143]. These data have been used to calibrate the parameters of an IDM capturing the string-unstable behavior of commercially available ACC vehicles [144]. We adopt the calibrated parameters, shown in Table 4.2, to demonstrate the effectiveness of the synthesized controllers on smoothing unstable real-world traffic arising in ACC systems. Specifically, the set of calibrated parameters of an IDM, shown in Table 4.2, are used to characterize commercially available ACC vehicles in simulation. Moreover, this same set of parameters retained from the commercial vehicles are employed also for AVs with the additive controller u_n synthesized in Theorem 4.3.3

Table 4.2: Calibrated parameters of commercially available ACC vehicles [144]

Parameter	**Value**
Desired speed v_0	44.1 m/s
Time gap T	2.2 s
Minimum spacing gap s_0	6.3 m
Acceleration exponent δ	15.5
Acceleration a	0.6 m/s^2
Deceleration b	5.2 m/s^2
Vehicle length l_n, $\forall\ n \in \mathcal{N}$	5.0 m

incorporated into their dynamics. Other than that the simulation settings are largely the same as those of Section 4.4.2.

It is worth noting that the set of parameter values shown in Table 4.2 [144] are obtained based on calibration using experimental data of real-world car-following experiments [143]. Hence, it is expected that these values including the desired speed v_0 could be different from those presented in Table 4.1 for a theoretical IDM. The values associated with vehicle dynamics (like a, b, T, and s_0) are largely consistent with their calibration ranges shown in an excellent study on model calibration for ACC vehicles [148]. In addition to employing an IDM with theoretical parameter values as seen before, in this section we apply the proposed approach to ACC vehicles described by a set of IDM parameter values distinct from the theoretical ones to show its effectiveness and robustness in terms of smoothing mixed traffic. In view of Theorem 4.3.1 (also Theorem 4.3.3), it is noted that the effectiveness of the proposed approach does not depend on the parameter values of the deterministic car-following model adopted; instead, it is closely associated with the parameters involved in the controller synthesis, like λ and k. This is consistent with the knowledge of control design for dynamic systems [76].

Fig. 4.11 shows the speed profile of all vehicles under various MPRs of AVs, where the lead HV executes the same profile as in previous experiments. The non-negative adaptation rate k is chosen as 0.04 to satisfy car-following safety conditions prescribed by Remark 17, while γ and λ remain unchanged as those corresponding to the results of Figs. 4.4 and 4.5. Comparing Fig. 4.11a to Fig. 4.4a, it is easily observed that the

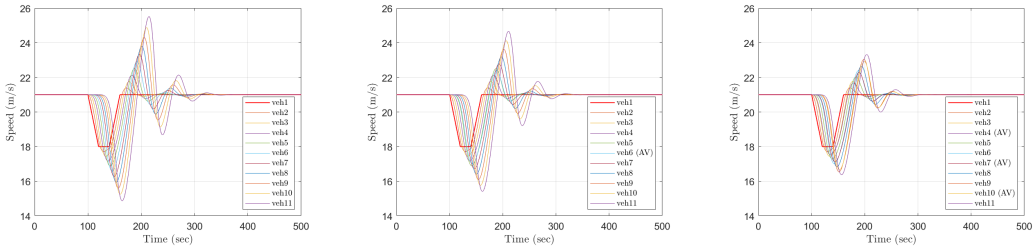

(a) MPR = 0%. (b) MPR = 10%. (c) MPR = 30%.

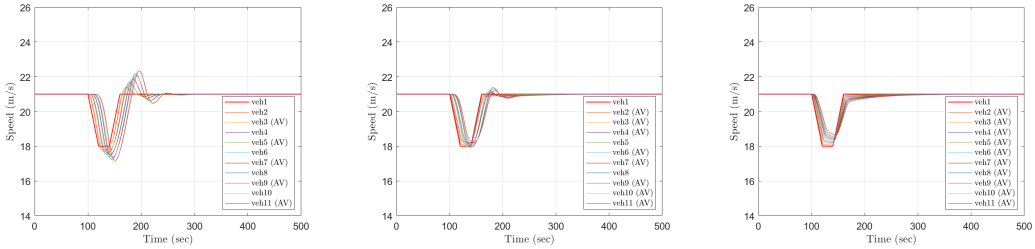

(d) MPR = 50%. (e) MPR = 80%. (f) MPR = 100%.

Figure 4.11: Speed profile of all commercially available ACC vehicles under different MPRs with $k = 0.04$, $\gamma = 0.01$ and $\lambda = 1$.

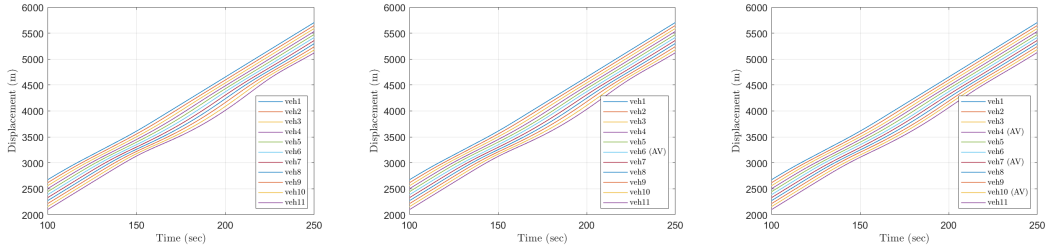

(a) MPR = 0%. (b) MPR = 10%. (c) MPR = 30%.

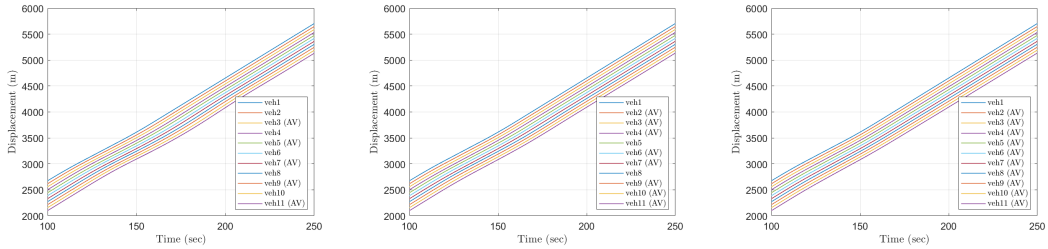

(d) MPR = 50%. (e) MPR = 80%. (f) MPR = 100%.

Figure 4.12: Displacement profile of all commercial ACC vehicles under different MPRs with $k = 0.04$, $\gamma = 0.01$ and $\lambda = 1$.

Table 4.3: Average speed of individual vehicles over the period of $[100, 250]$ sec.

Speed (m/s)	**Veh 2**	**Veh 3**	**Veh 4**	**Veh 5**	**Veh 6**
MPR = 0%	20.206	20.206	20.206	20.206	20.206
MPR = 100%	20.207	20.207	20.207	20.207	20.207
Speed (m/s)	**Veh 7**	**Veh 8**	**Veh 9**	**Veh10**	**Veh 11**
MPR = 0%	20.206	20.206	20.204	20.203	20.202
MPR = 100%	20.208	20.208	20.208	20.209	20.209

same speed perturbations experienced by the lead vehicle amplify and grow much more along the upstream traffic in the ACC flow. With the implementation of the additive AV controllers, the speed perturbations are significantly reduced for the following ACC vehicles, as observed in Fig. 4.11. More importantly, the effect of controlled AVs on smoothing unstable ACC traffic is observed to increase with the increase of MPR. This is also observed from the trajectory of all vehicles shown in Fig. 4.12, with smoother ones achieved at a larger presence of AVs.

Smoother traffic is likely to result in a greater throughput, especially over the period when speed disturbances occur. It is observed from Fig. 4.12a that the shockwaves start to dissipate at around 200 sec when the last vehicle passes the location of 4000 m (approximately). Clearly, it takes roughly 200 sec for all vehicles to traverse the point of 4000 m at 0% penetration of AVs (shown in Fig. 4.12a). Comparing Fig. 4.12b, Fig. 4.12c, Fig. 4.12d, Fig. 4.12e and Fig. 4.12f to Fig. 4.12a, it is observed that it takes less and less time for all vehicles of the platoon to pass the same location as the penetration of AVs increases, indicating an improved throughput. This improvement is closely related to the increased average speed of individual vehicles (shown in Table 4.3 for MPR = 0% and 100%) due to AVs smoothing traffic. These results are consistent with the recent findings of [43].

Fig. 4.13 shows the ASV values of this ACC system setting in the absence of AVs and those corresponding to the application of the general AV controllers. It is observed that the improvement in reducing ASV, due to controlled AVs, increases with the increase of MPR; a significant amount of improvement is easily achieved with a relatively low MPR.

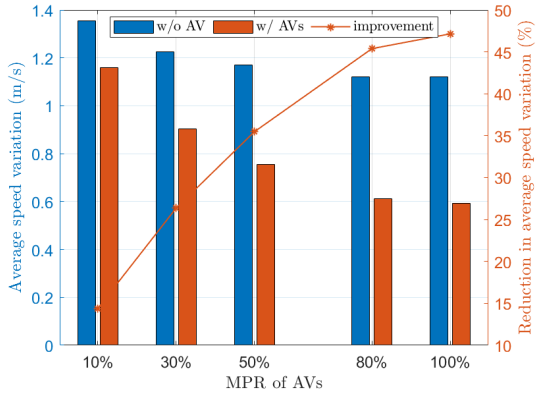

Figure 4.13: Comparison of average speed variation (ASV) with and without using the general additive AV controllers, with $k = 0.04$, $\gamma = 0.01$ and $\lambda = 1$.

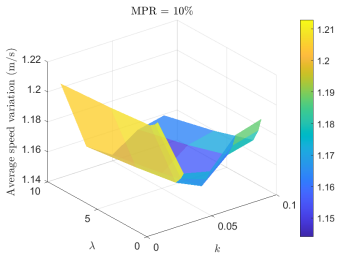

(a) MPR = 10%.

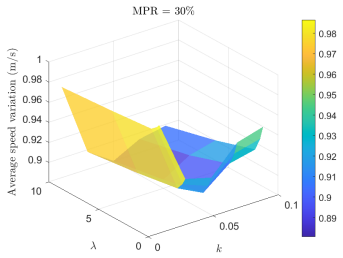

(b) MPR = 30%.

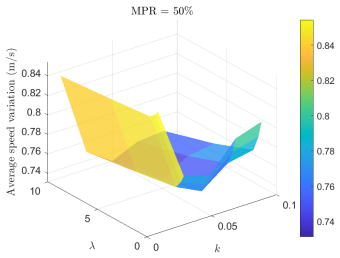

(c) MPR = 50%.

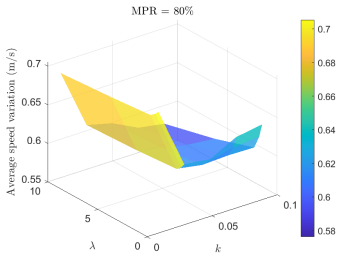

(d) MPR = 80%.

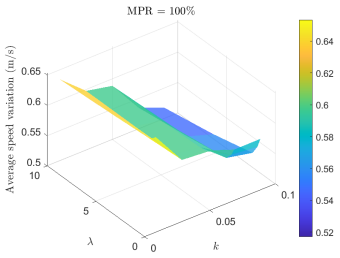

(e) MPR = 100%.

Figure 4.14: ASV in response to the change of k and λ.

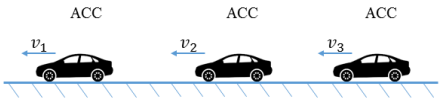

(a) A sequence of ACC-ACC-ACC.

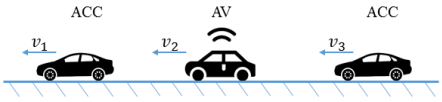

(b) A sequence of ACC-AV-ACC.

(c) A sequence of ACC-AV-AV.

Figure 4.15: Illustration of multiple vehicle sequences considering a platoon of two vehicles following a lead ACC vehicle [51].

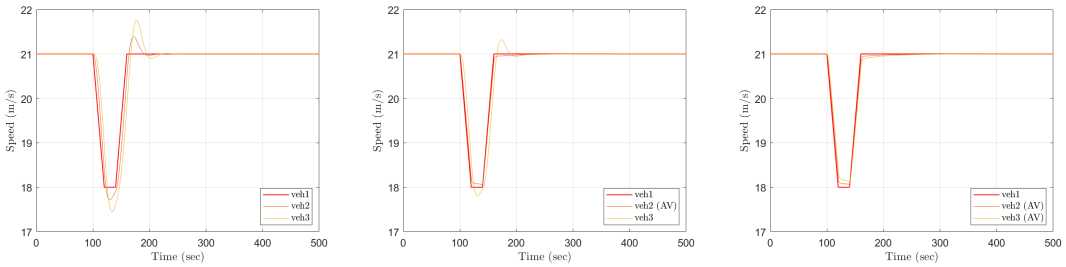

(a) Speed profile corresponding to Fig. 4.15a

(b) Speed profile corresponding to Fig. 4.15b.

(c) Speed profile corresponding to Fig. 4.15c.

Figure 4.16: Speed profile of all three vehicles corresponding to the vehicle sequences shown in Fig. 4.15a, Fig. 4.15b, and Fig. 4.15c.

This is consistent with the results presented in Fig. 4.6. However, more reduction in ASV is observed in Fig. 4.13, compared to that in Fig. 4.6, indicating that the controller synthesized is robust and appears to work very well even in a fairly oscillatory unstable ACC traffic flow. Similar to what has been studied in the preceding subsection, we also present a set of results in Fig. 4.14 to show the impact of the parameters k and λ on reducing ASV. The overall pattern observed is similar to that shown in Fig. 4.8. That is, the impact of k and λ on reducing ASV appears to increase with the increase of their respective values, and the improvement converges as k and λ approach relatively large values.

In addition to the numerical results shown above, we also present some complementary results on the interaction between neighboring vehicles considering different

Table 4.4: The ASV of each individual vehicle over the period of $[100, 200]$ sec corresponding to different sequences shown in Fig. 4.15.

ASV (m/s)	**Vehicle 1**	**Vehicle 2**	**Vehicle 3**
Vehicle sequence of Fig. 4.15a	1.198	1.313	1.434
Vehicle sequence of Fig. 4.15b	1.198	1.185	1.271
Vehicle sequence of Fig. 4.15c	1.198	1.185	1.172

vehicle sequences. Specifically, following previous simulation settings we consider a lead ACC vehicle experiencing the same speed disturbance as before, followed by two ACC vehicles (Fig. 4.15a), an AV and a ACC vehicle (Fig. 4.15b), or two AVs (Fig. 4.15c). A proper comparison among these sequences allows us to better understand the interaction between neighboring vehicles in mixed traffic involving ACC vehicles and AVs. ACC vehicles can be easily replaced by the IDM with parameter values shown in Table 4.1 to study the interaction between HVs and AVs. Since the proposed approach, requiring only local traffic information, works well for AVs regardless of other vehicles' types in the traffic, here for illustration we consider a mixture of ACC vehicles and AVs described by the IDM of Table 4.2 and this IDM with an additive AV controller, respectively. With the simulation parameter values remaining same as those corresponding to the results presented in this section, the speed profile of all the three vehicles is presented in Fig. 4.16 for the sequences considered in Fig. 4.15. In addition, Table 4.4 shows the quantitative ASV experienced by each individual vehicle.

Fig. 4.16a shows that the speed disturbance experienced by the lead vehicle (vehicle 1) is amplified and propagated to the following vehicles (vehicle 2 and vehicle 3). Comparing Fig. 4.16b to Fig. 4.16a, it is observed that the controlled AV (vehicle 2) is able to smooth the speed disturbance passed down by the lead vehicle, experiencing an ASV with a reduction of $(1.313 - 1.185)/1.313 = 9.75\%$. Due to the positive impact of this controlled AV, the following ACC vehicle also experiences less speed disturbance (with 1.434 reduced to 1.271). This is consistent with the findings of [10]. Comparing Fig. 4.16c to Fig. 4.16b, it is observed that the second AV (vehicle 3 in Fig. 4.15c) exhibits less speed disturbance than the third vehicle (ACC) in Fig. 4.15b,

with a $(1.271-1.172)/1.271 = 7.79\%$ reduction of ASV. It is observed from the comparison between the results of Fig. 4.16c and those of Figs. 4.16a and 4.16b that, the second AV (vehicle 3) experiences a smaller reduction of ASV, i.e., 7.79%, than its preceding AV (vehicle 2), i.e., 9.75%. This is because the preceding AV has already smoothed the traffic flow to some extent, leaving less room for improvement for the AV immediately behind. These results validate the fact that the proposed approach works effectively for an AV regardless of the type of its preceding vehicle, since only local traffic information (like relative speed and spacing) is required for controller synthesis. Moreover, AVs adopting the controller synthesized have an positive impact on the vehicles behind in terms of traffic smoothing, which is consistent with a recent finding of [139].

4.5 Conclusions

In this chapter we have synthesized a general class of additive AV controllers that are capable of smoothing nonlinear mixed traffic flow. The controllers are designed in such a way that controlled AVs are able to closely track a virtual speed profile, i.e., a subtler version of the disturbance resulting from the immediate preceding vehicle, with provable guarantees on convergence of tracking. The framework presented is fairly general and the approach proposed allows for AV controller synthesis without having to linearize car-following dynamics at equilibrium points of traffic flow. In other words, the additive AV controllers work in both equilibrium and non-equilibrium traffic, capable of preserving the nonlinear nature of mixed traffic. The controllers synthesized are proven to be able to yield locally stable traffic in the sense of speed tracking which could exhibit head-to-tail string stability with a sufficient MPR of AVs.

Moreover, the approach is developed in the context of a generic functional form of car-following dynamics without being limited to any particular car-following model, allowing for high degrees of applicability. In addition, the additive AV controllers synthesized require only local traffic information, i.e., spacing and relative speed to the immediate preceding vehicle, free from demanding requirements on vehicle connectivity in some existing studies such as vehicle-to-vehicle and vehicle-to-infrastructure communications. This is believed to be particularly useful for practical applications since HVs are not expected to have sophisticated communication capabilities in the near future.

Extensive numerical experiments are carried out to show the effectiveness and robustness of the proposed approach, using a theoretical IDM and a realistic IDM representing real-world ACC vehicles. The results are interesting and promising in that AVs using the additive controllers synthesized are able to effectively smooth nonlinear mixed traffic, leading to stable flow with a sufficient presence of AVs.

Chapter 5

Optimal Feedback Control Law for Automated Vehicles in the Presence of Cyberattacks

5.1 Introduction

As introduced before, the advent of AVs is expected to reshape future transportation systems with a broad range of promising benefits, like reducing energy consumption [8, 139], improving traffic stability [16, 45], optimizing parking space allocation [2, 10], etc. These anticipated potentials of AVs are gradually becoming a reality thanks to the advancement of vehicular sensing, automation, and computing technologies. As an important application of cyber-physical systems (CPS) [150], these AV technologies open a door for malicious actors to compromise vehicle security [151, 152]. In spite of the many aforementioned benefits, the capability of AVs could be compromised by various forms of cyberattacks [153], resulting in unexpected disruption to normal traffic flow causing financial loss or even loss of human lives [154].

There are different forms of attacks that could be introduced to automated or partially automated vehicles like adaptive cruise control (ACC) vehicles without significantly changing vehicle driving behavior [155]. However, even subtle changes to driving behavior may result in widespread disruption to the transportation network, causing

substantial traffic congestion and excessive fuel consumption and emissions [156]. Consequently, cyberattacks on AVs pose a significant risk to the safety, reliability, and efficiency of future transportation systems. For example, it has been shown that even slight attacks on vehicle acceleration can cause stop-and-go traffic waves and even increase the risk of crashes without directly causing vehicles to crash [157]. In addition to such attacks altering AV control commands, i.e., acceleration, AVs are also vulnerable to data injection attacks, where false data is injected into sensor measurements causing a vehicle to execute undesired maneuvers degrading its performance even if it does not directly compromise safety [154]. Although malicious attacks on vehicle control commands and false data injection attacks on sensor measurements are two typical types of cyberattacks on AVs, there are also other forms of attacks, such as spoofing attacks, dedicated denial of service attacks, etc. A detailed introduction of a list of potential cyberattacks on AVs can be found in [158].

Undesired behavior of AVs due to attacks can compromise mixed-autonomy traffic involving both AVs and HVs. Various types of cyberattacks, including the ones mentioned above, have been shown to be able to cause instability to vehicle platoons, and even subtle attacks on a single vehicle can lead to disruptive consequences to the bulk traffic [159], resulting in lower traffic throughput and greater energy consumption [156]. A more detailed discussion about the impacts of cyberattacks on future transportation systems is presented in [154]. In view of these challenges faced by AVs, it is important and necessary to develop effective attack mitigation strategies to enhance the resilience and robustness of automated transportation systems, as AVs gradually become a reality.

Malicious attacks are generally considered to be launched in a stealthy manner. That is, they are assumed to be not known to the system and can not be easily detected based only on measurement data [160]. While such attacks may cause only subtle changes to the driving behavior of attacked vehicles, they could result in disruptive consequences to the traffic flow [159], thereby motivating the development of effective techniques for detecting malicious cyberattacks on AVs. For example, filtering theory is used in [161] to predict and estimate traffic states, whereby the occurrence of an attack is determined if the two state sets, i.e., prediction set and estimation set, intersect. Combining the Kalman filter with convolutional neural networks (CNNs), an anomaly detection approach is developed for detecting and identifying anomalous behavior of

AVs [162]. In addition to CNNs, other machine learning techniques have also been employed recently for real-time detection of cyberattacks, such as Bayesian deep learning with a discrete wavelet transform [163], a generative adversarial network (GAN)-based anomaly detection [164], among others. Moreover, a sandbox framework supporting isolation and evaluation of the data exchanged among connected automated vehicles is developed specifically for detecting false data injection attacks [165].

In addition to developing effective approaches for attack detection, a few studies have touched upon the development of specific mitigation strategies to reduce the impact of attacks on AVs and traffic flow. For example, a distributed neural-network-based adaptive control is proposed for AVs under denial-of-service (DoS) attacks to ensure platooning formation with a desired longitudinal spacing, which requires all vehicles to be wirelessly connected via directed vehicle-to-vehicle (V2V) communication [46]. To correct tracking errors for connected automated vehicles, a flocking control strategy is developed considering false data injection and DoS attacks, where cyberattacks on vehicle tracking errors are assumed to be an unknown constant [47]. For platooning of connected and automated trucks, an improved longitudinal control strategy is proposed to enhance platoon stability in the presence of falsified wireless communication information, where attacks are assumed to be in a given deterministic form [48]. In the event of sensor attacks, it is also possible to increase the resilience of AVs by using multiple sensors to measure the same physical variable, at the cost of creating redundancy [166]. For a comprehensive discussion on the design framework and potential countermeasures against cyberattacks on intelligent vehicles, the reader is referred to [167, 168].

While prior studies mainly focus on studying the impacts of cyberattacks on traffic flow and developing attack detection approaches, few have considered the development of effective mitigation strategies to reduce the impact of attacks on AVs as mentioned above. In addition, previous works normally adopt strong assumptions on the form of attacks (like constant attacks), which may not be readily known in the first place. Moreover, communication (or cooperation) among a group of vehicles is largely required for designing efficient driving strategies of AVs in the presence of attacks. By contrast, in this chapter we focus on developing optimal driving strategies for AVs in the presence of cyberattacks, with an exclusive consideration of stealthy attacks that could significantly

impact the bulk traffic while causing only subtle changes to the driving behavior of individual vehicles being attacked. Unlike many prior works assuming constant attacks or stochastic attacks with a specific probability distribution like the Gaussian distribution, we only assume attacks to have a bounded magnitude (for remaining stealthy) without being subject to any specific probability distribution, which significantly relaxes the assumptions commonly seen in prior studies. From a modeling standpoint, this also appears to be more realistic due to lack of knowledge of malicious attacks. More importantly, we analytically derive a set of necessary conditions of optimality for solving a min-max control problem in a decentralized manner that minimizes the maximum disruption to traffic flow due to AVs being attacked, without requiring vehicle connectivity and much prior knowledge of the attacks. The main contributions of this chapter are summarized as follows.

- We consider two typical types of cyberattacks, namely false data injection attack on sensor measurements and malicious attack on AV control commands, and characterize those attacks as bounded stochastic processes without being subject to any specific probability distribution. This relaxes the assumptions seen in many prior studies where attacks are assumed to be constant or stochastic with a specific probability distribution like the Gaussian distribution.

- We formulate a min-max control problem for minimizing the worst-case potential disruption to traffic flow due to cyberattacks on AVs. This is particularly useful since it does not require prior knowledge of the attacks (including their presence), like functional forms or probability distribution, except for the bounded magnitude. This is complementary to existing studies which are largely focused on studying the impacts of cyberattacks on traffic flow.

- We analytically derive a set of necessary conditions of optimality for solving the nonlinear min-max control problem with mathematical characterization of the maximum disruption possible to traffic flow due to attacks.

- Based on the optimality conditions, we develop an iterative computational algorithm for determining the optimal feedback control law (driving strategy) for AVs in a decentralized manner, without requiring cooperation (communication) among

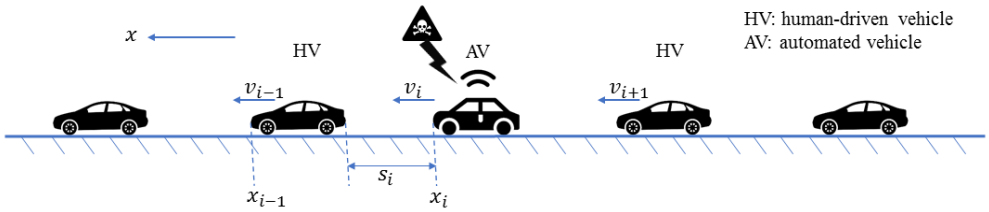

Figure 5.1: Illustration of cyberattacks on automated vehicles in mixed-autonomy traffic involving both automated vehicles and human-driven vehicles [52].

vehicles. A series of numerical results is presented to show the effectiveness of the proposed approach considering different levels of attack severity.

The remainder of this chapter is organized as follows. A generic mathematical framework is presented in Section 5.2 for describing mixed-autonomy traffic flow, with consideration of two typical types of cyberattacks on AVs. Based on the framework presented, in Section 5.3 we formulate a min-max control problem for mixed-autonomy traffic to minimize the maximum disturbance to AVs due to attacks. To solve the min-max problem, we derive a set of necessary conditions of optimality in Section 5.4, based on which an iterative computational algorithm is developed for determining the optimal feedback control law (driving strategy) of AVs. The effectiveness of the proposed approach is demonstrated via numerical simulation in Section 5.5. Finally, we conclude this chapter in Section 5.6 with discussion on future research directions. The materials presented in this chapter are mostly taken from [52].

5.2 Mathematical Modeling of Cyberattacks on AVs in Mixed Traffic

Cyberattacks could be introduced to AVs in various forms [153], among which two typical types, namely false data injection attack on sensor measurements and malicious attack on AV control commands, pose a significant threat to AV systems and are of considerable interest [158, 169]. In this section, we present a generic mathematical framework modeling such attacks on AVs in a mixed-autonomy traffic setting involving both AVs and HVs. The modeling framework is based on car-following dynamics which

allows for incorporating the aforementioned two types of cyberattacks mathematically. Subsequently, we illustrate the framework with specific car-following models commonly used in the literature. While the two types of attacks considered cover a broad range of malicious incidents that could occur to AVs, we are by no means to exhaustively explore all potential forms of attacks in the present study due to complexity of AV systems. This work is expected to inspire further future studies on similar topics involving other types of attacks.

5.2.1 Mixed-autonomy Traffic

In this study we consider mixed-autonomy traffic involving both AVs and HVs, where AVs are vulnerable to cyberattacks as shown in Fig. 5.1. We only consider longitudinal vehicle dynamics as seen in prior works [46, 48, 158], while lateral dynamics could also be studied. Without loss of generality, we consider a string of m vehicles denoted by the totally ordered set $\mathcal{M} = \{1, 2, 3, \cdots, m\}$, with $m \in \mathbb{N}^+$ greater than 1. For any vehicle $i \in \mathcal{M}$, $x_i(t)$ and $v_i(t)$ signify its displacement and speed at time t, respectively. The variable $s_i(t)$ represents the inter-vehicle spacing between vehicle i and its immediate preceding vehicle $i-1$ at time t, specifically $s_i(t) = x_{i-1}(t) - x_i(t) - l_{i-1}$ with l_{i-1} being the length of vehicle $i-1$. These standard notations can be easily found in the literature [114].

Similar to Section 3.2, based on the law of physics the motion of any vehicle $i \in \mathcal{M}$ can be described by the following ordinary differential equations [114]

$$\dot{x}_i(t) = v_i(t), \tag{5.1}$$

$$\dot{v}_i(t) = f(s_i(t), \Delta v_i(t), v_i(t)), \tag{5.2}$$

where the dot operator denotes differentiation with respect to time; the nonlinear operator f characterizes vehicle acceleration $\dot{v}_i$ of the i-th vehicle as a function of the variables s_i, Δv_i and v_i; and the relative speed Δv_i with respect to the immediate preceding vehicle is defined as

$$\Delta v_i(t) = \dot{s}_i(t) = v_{i-1}(t) - v_i(t). \tag{5.3}$$

The above equations (5.1)–(5.3) are the generic functional form of car-following dynamics widely adopted in the literature. Clearly, the variables involved, such as s_i, v_i,

etc. are time-variant. For brevity of mathematical analysis the argument t is omitted whenever appropriate to do so.

Let $\mathcal{H}$ and $\mathcal{A}$ denote respectively the totally ordered set of HVs and AVs in the mixed-autonomy traffic of m vehicles, i.e., $\mathcal{M} = \mathcal{H} \cup \mathcal{A}$. As revealed in the literature, human drivers tend to exhibit different driving behaviors compared to AVs [119, 170]. Hence, we further characterize the functional f shown in equation (5.2) as f_{HV} and f_{AV} for HVs and AVs, respectively. To this end, the mixed-autonomy traffic dynamics is written as

$$\dot{x}_i = v_i, \ \forall \ i \in \mathcal{M} \tag{5.4}$$

$$\dot{v}_i = \begin{cases} f_{\text{HV}}(s_i, \Delta v_i, v_i), \ \forall \ i \in \mathcal{H} & \text{(5.5a)} \\ f_{\text{AV}}(s_i, \Delta v_i, v_i), \ \forall \ i \in \mathcal{A} & \text{(5.5b)} \end{cases}$$

It is noted that the functionals f_{HV} and f_{AV} in the above equations do not need to be the same. Instead, they depend on the specific car-following principles abided by HVs and AVs.

5.2.2 False Data Injection Attack on Sensor Measurements (Type #1 Cyberattack)

Here we introduce the first type of cyberattacks on AVs considered in this study, namely false data injection attacks on sensor measurements (termed Type #1 cyberattack in this study). It is easily observed from equation (5.5b) that the acceleration commands executed by AVs rely on sensor measurements, including inter-vehicle spacing and relative speed appearing in the first and second argument, respectively. These measurements could be corrupted by cyberattacks when used to execute the acceleration commands of AVs [156, 158]. Following [158], for any vehicle $i \in \mathcal{A}$, let $\omega_{1,i}$ and $\omega_{2,i}$ denote the false data injection attacks on spacing and relative speed, respectively. Consequently, due to these attacks the AV acceleration dynamics given by equation (5.5b) becomes

$$\ddot{x}_i = f_{\text{AV}}(s_i + \omega_{1,i}, \Delta v_i + \omega_{2,i}, v_i), \ \forall \ i \in \mathcal{A}. \tag{5.6}$$

In prior studies, cyberattacks on AVs have been assumed to be deterministic or stochastic with a given probability distribution [47, 153, 158, 162, 164]. In this work, attacks like $\omega_{1,i}$ and $\omega_{2,i}$ are also assumed to be stochastic processes, but do not have

to be limited to any specific probability distribution, i.e., distribution-free, which is a significantly milder assumption than those seen in the literature. This also appears to be more reasonable since AVs do not have prior knowledge of the potential attacks. In addition, realistic adversaries generally tend to remain stealthy while being subject to limited resources and energy [171]. Hence, attacks are assumed to be bounded by some known bounds [172], for example, $|\omega_{1,i}| \leq r_1$, $|\omega_{2,i}| \leq r_1$, with $r_1 \in \mathbb{R}^+$ being the upper bound. It is noted that $\omega_{1,i}$ and $\omega_{2,i}$ may not necessarily have the same bound. For simplicity we have used the upper bound r_1 for both since they belong to the same type of attacks.

5.2.3 Malicious Attack on AV Control Commands (Type #2 Cyberattack)

Here we introduce the second type of cyberattacks on AVs commonly seen in the literature, i.e., malicious attacks on AV control commands (termed Type #2 cyberattack in this study), occurring directly to vehicle acceleration [161, 164]. Following [161], let δ_i denote the malicious attack on the acceleration of vehicle i, $i \in \mathcal{A}$. As a result, the AV acceleration dynamics given in equation (5.5b) becomes

$$\ddot{x}_i = f_{\text{AV}}(s_i, \Delta v_i, v_i) + \delta_i, \ \forall \ i \in \mathcal{A}. \tag{5.7}$$

Similarly, the attack signal is assumed to be bounded, i.e., $|\delta_i| \leq r_2$ with $r_2 \in \mathbb{R}^+$ being the upper bound. It is observed that Type #2 cyberattacks may alter AV driving behavior to a greater degree due to direct occurrence to vehicle acceleration, compared to Type #1 attacks. Hence, for attacks to remain stealthy r_2 is likely to be much smaller than r_1. This will be further illustrated in the numerical studies.

5.2.4 Analytical Illustration of Mixed Traffic Under Cyberattacks

Following the generic framework for mixed-autonomy traffic presented in Section 5.2.1, we further illustrate the traffic flow dynamics with concrete car-following models for detailed analytical and numerical analyses. As revealed in the literature, human drivers tend to exhibit different driving behaviors from AVs [119, 170]. In order to capture the dynamics of HVs, a number of car-following models have been proposed, such as Gipps'

model [110], optimal velocity model (OVM) [111], intelligent driver model (IDM) [112], and Newell's car-following model [113], among others. In this study we adopt the IDM for HVs which has been shown to be able to accurately describe car-following dynamics for human drivers [112]. It is also widely used in the traffic engineering community thanks to its favorable performance as shown by [15, 134], among others.

According to the IDM, equation (5.5a) is written as

$$\ddot{x}_i(t) = a\left[1 - \left(\frac{v_i(t)}{v_0}\right)^4 - \left(\frac{s^*(v_i(t), \Delta v_i(t))}{x_{i-1}(t) - x_i(t) - l_{i-1}}\right)^2\right],\ i \in \mathcal{H}, \tag{5.8}$$

with

$$s^*(v_i(t), \Delta v_i(t)) = s_0 + v_i(t)T + \frac{v_i(t)\Delta v_i(t)}{2\sqrt{ab}}, \tag{5.9}$$

where a is the maximum acceleration, b is the comfortable braking deceleration, v_0 is the desired speed, s_0 is the minimum spacing, T is the desired time headway, and l_{i-1} is the length of vehicle $i-1$.

For AVs, the optimal velocity with relative velocity (OVRV) model, an extension to the optimal velocity model [111], is adopted for describing their dynamics. The OVRV model has been widely used for (cooperative) adaptive cruise control (ACC/CACC) systems [104, 105, 173]. It follows a constant time-gap policy in designing vehicle controls, which is consistent with the practical implementation of (semi-)AVs [101, 103]. In addition, it has been shown to fit well to the simulated real trajectories of ACC-equipped vehicles [105, 173].

Following the OVRV model, equation (5.5b) is written as

$$\ddot{x}_i(t) = k_1\left[x_{i-1}(t) - x_i(t) - l_{i-1} - \eta - \tau v_i(t)\right] + k_2\left[v_{i-1}(t) - v_i(t)\right],\ \forall\ i \in \mathcal{A}, \tag{5.10}$$

where η is the jam distance, τ is the desired time gap, k_1 and k_2 are the gains on the effective time gap and relative speed, respectively. As mentioned before, many variables involved in vehicle dynamics are time-variant. For brevity the time argument t may be omitted whenever appropriate to do so.

Consequently, following Section 5.2.2 the AV dynamics under false data injection attacks is given by

$$\ddot{x}_i = k_{1,i}\left[x_{i-1} - x_i - l_{i-1} - \eta - \tau v_i + \omega_{1,i}\right] + k_{2,i}\left[v_{i-1} - v_i + \omega_{2,i}\right],\ \forall\ i \in \mathcal{A}, \tag{5.11}$$

where $k_{1,i}$ and $k_{2,i}$ are the dynamic feedback gains that need to be optimally determined for the vehicle $i \in \mathcal{A}$ to calculate its effective acceleration in the presence of Type #1 cyberattacks. Essentially, determining those dynamic gains leads to the constructing of feedback control laws for AVs, which will be discussed in more detail in the following sections.

Similarly, following Section 5.2.3 the AV dynamics under malicious attacks on vehicle control commands is given by

$$\ddot{x}_i = k_{1,i}\left[x_{i-1} - x_i - l_{i-1} - \eta - \tau v_i\right] + k_{2,i}\left[v_{i-1} - v_i\right] + \delta_i, \ \forall\ i \in \mathcal{A}. \tag{5.12}$$

5.3 Formulation of a Min-max Control Problem for Mixed-autonomy Traffic

Given the stealthy nature of cyberattacks and that AVs do not have prior knowledge of the attacks (like the exact goal of adversaries), to this end, in this section we formulate a min-max control problem that allows for determining the optimal driving strategy of AVs in the presence of cyberattacks introduced before. Specifically, the objective is to find an optimal feedback control law for AVs (essentially an effective acceleration), or equivalently to determine the optimal feedback gains $k_{1,i}$ and $k_{2,i}$, so that a certain cost functional, e.g., vehicle speed disturbance, is minimized, considering the worst-case scenario that could be caused by the attacks. In other words, one aims to minimize the maximum disruption to mixed-autonomy traffic due to cyberattacks in the absence of prior knowledge of the attacks. As discussed in Section 5.2.2, this considerably relaxes the assumptions characterizing cyberattacks in the literature. Following the analytical illustration presented in Section 5.2.4, we will derive state space formulation for mixed-autonomy traffic under cyberattacks and formulate an appropriate min-max control problem in the remainder of this section.

5.3.1 AVs Under Type #1 Cyberattacks

In the presence of Type #1 cyberattacks, the acceleration dynamics of HVs, AVs, and attacked AVs are given by equations (5.5a), (5.10), and (5.11), respectively. Considering the mixed-autonomy traffic with any vehicle i, $i \in \mathcal{A}$, being attacked by Type #1

cyberattacks, we define the state of vehicle i, $i \in \mathcal{M}$, as follows

$$y_{2i-1} = x_i,\ y_{2i} = v_i,\ \forall\ i \in \mathcal{H} \tag{5.13}$$

$$y_{2i-1} = x_i + l_{i-1} + \eta,\ y_{2i} = v_i,\ \forall\ i \in \mathcal{A} \tag{5.14}$$

It follows from Section 5.2 that

$$\dot{y}_{2i-1} = y_{2i},\ \forall\ i \in \mathcal{M} \tag{5.15}$$

$$\dot{y}_{2i} = \begin{cases} \text{equation (5.5a)}, & \text{if } i \in \mathcal{H}, \\ \text{equation (5.10)}, & \text{if } i \in \mathcal{A} \text{ not attacked}, \\ \text{equation (5.11)}, & \text{if } i \in \mathcal{A} \text{ attacked}. \end{cases} \tag{5.16}$$

Let the vector $y = [y_1, y_2, y_3, \cdots, y_{2m-1}, y_{2m}]'$ represent the states of all m vehicles in the presence of Type #1 cyberattacks, with $'$ being the transpose operator of a matrix. For convenience of analytical illustration, we consider a generic scenario where the vehicle $i \in \mathcal{A}$ is attacked while others are not. Then, the evolution of the state vector y is

written as

$$\dot{y} = \begin{bmatrix} \dot{y}_1 \\ \dot{y}_2 \\ \vdots \\ \dot{y}_{2i-1} \\ \dot{y}_{2i} \\ \vdots \\ \dot{y}_{2m-1} \\ \dot{y}_{2m} \end{bmatrix} = \begin{bmatrix} y_2 \\ \dot{y}_2 \\ \vdots \\ y_{2i} \\ k_{1,i}\left[y_{2i-3} - y_{2i-1} - \tau y_{2i} + \omega_{1,i}\right] + k_{2,i}\left[y_{2i-2} - y_{2i} + \omega_{2,i}\right] \\ \vdots \\ y_{2m} \\ \dot{y}_{2m} \end{bmatrix}$$

$$= \begin{bmatrix} y_2 \\ \dot{y}_2 \\ \vdots \\ y_{2i} \\ 0 \\ \vdots \\ y_{2m} \\ \dot{y}_{2m} \end{bmatrix} + \begin{bmatrix} 0 \\ 0 \\ \vdots \\ 0 \\ k_{1,i}\left[y_{2i-3} - y_{2i-1} - \tau y_{2i}\right] + k_{2,i}\left[y_{2i-2} - y_{2i}\right] \\ \vdots \\ 0 \\ 0 \end{bmatrix} + \begin{bmatrix} 0 \\ 0 \\ \vdots \\ 0 \\ k_{1,i}\omega_{1,i} + k_{2,i}\omega_{2,i} \\ \vdots \\ 0 \\ 0 \end{bmatrix}$$

$$= \begin{bmatrix} y_2 \\ \dot{y}_2 \\ \vdots \\ y_{2i} \\ 0 \\ \vdots \\ y_{2m} \\ \dot{y}_{2m} \end{bmatrix} + \begin{bmatrix} \mathbf{0}_{(2i-1)\times 2} \\ k_{1,i} \quad k_{2,i} \\ \mathbf{0}_{2(m-i)\times 2} \end{bmatrix} \begin{bmatrix} \mathbf{0}_{2\times 2(i-2)} & 1 & 0 & -1 & -\tau & \mathbf{0}_{2\times 2(m-i)} \\ & 0 & 1 & 0 & -1 & \end{bmatrix} \begin{bmatrix} y_1 \\ y_2 \\ \vdots \\ y_{2i} \\ y_{2i+1} \\ \vdots \\ y_{2m-1} \\ y_{2m} \end{bmatrix}$$

$$+ \begin{bmatrix} \mathbf{0}_{(2i-1)\times 2} \\ k_{1,i} \quad k_{2,i} \\ \mathbf{0}_{2(m-i)\times 2} \end{bmatrix} \begin{bmatrix} \omega_{1,i} \\ \omega_{2,i} \end{bmatrix}$$

$$= g(y) + KCy + K\omega \tag{5.17}$$

where $\mathbf{0}_{p\times q}$ denotes a zero matrix of dimension $p \times q$; $g(y)$, K, C, and ω are given by

$$g(y) = \begin{bmatrix} y_2 \\ \dot{y}_2 \\ \vdots \\ y_{2i} \\ 0 \\ \vdots \\ y_{2m} \\ \dot{y}_{2m} \end{bmatrix}, \; K = \begin{bmatrix} \mathbf{0}_{(2i-1)\times 2} \\ k_{1,i} \quad k_{2,i} \\ \mathbf{0}_{2(m-i)\times 2} \end{bmatrix},$$

$$C = \begin{bmatrix} \mathbf{0}_{2\times 2(i-2)} & \begin{matrix} 1 & 0 & -1 & -\tau \\ 0 & 1 & 0 & -1 \end{matrix} & \mathbf{0}_{2\times 2(m-i)} \end{bmatrix}, \; \omega = \begin{bmatrix} \omega_{1,i} \\ \omega_{2,i} \end{bmatrix} \tag{5.18}$$

5.3.2 AVs Under Type #2 Cyberattacks

In the presence of Type #2 cyberattacks, the acceleration dynamics of HVs, AVs, and attacked AVs are given by equations (5.5a), (5.10), and (5.12), respectively.

Similarly, with the state of vehicle i, $i \in \mathcal{M}$ defined as in equations (5.13) and (5.14), it follows from Section 5.2 that

$$\dot{y}_{2i-1} = y_{2i}, \; \forall \; i \in \mathcal{M} \tag{5.19}$$

$$\dot{y}_{2i} = \begin{cases} \text{equation (5.5a)}, & \text{if } i \in \mathcal{H}, \\ \text{equation (5.10)}, & \text{if } i \in \mathcal{A} \text{ not attacked}, \\ \text{equation (5.12)}, & \text{if } i \in \mathcal{A} \text{ attacked}. \end{cases} \tag{5.20}$$

Let the vector $\tilde{y} = [y_1, y_2, y_3, \cdots, y_{2m-1}, y_{2m}]'$ represent the states of all m vehicles in the presence of Type #2 cyberattacks. Similarly, for convenience of mathematical analysis, we consider a generic scenario where the vehicle $i \in \mathcal{A}$ is attacked while others

are not. Then, the evolution of the state vector $\tilde{y}$ is written as

$$\dot{\tilde{y}} = \begin{bmatrix} \dot{y}_1 \\ \dot{y}_2 \\ \vdots \\ \dot{y}_{2i-1} \\ \dot{y}_{2i} \\ \vdots \\ \dot{y}_{2m-1} \\ \dot{y}_{2m} \end{bmatrix} = \begin{bmatrix} y_2 \\ \dot{y}_2 \\ \vdots \\ y_{2i} \\ k_{1,i}\left[y_{2i-3} - y_{2i-1} - \tau y_{2i}\right] + k_{2,i}\left[y_{2i-2} - y_{2i}\right] + \delta_i \\ \vdots \\ y_{2m} \\ \dot{y}_{2m} \end{bmatrix}$$

$$= \begin{bmatrix} y_2 \\ \dot{y}_2 \\ \vdots \\ y_{2i} \\ 0 \\ \vdots \\ y_{2m} \\ \dot{y}_{2m} \end{bmatrix} + \begin{bmatrix} 0 \\ 0 \\ \vdots \\ 0 \\ k_{1,i}\left[y_{2i-3} - y_{2i-1} - \tau y_{2i}\right] + k_{2,i}\left[y_{2i-2} - y_{2i}\right] \\ \vdots \\ 0 \\ 0 \end{bmatrix} + \begin{bmatrix} 0 \\ 0 \\ \vdots \\ 0 \\ \delta_i \\ \vdots \\ 0 \\ 0 \end{bmatrix}$$

$$= \begin{bmatrix} y_2 \\ \dot{y}_2 \\ \vdots \\ y_{2i} \\ 0 \\ \vdots \\ y_{2m} \\ \dot{y}_{2m} \end{bmatrix} + \begin{bmatrix} \mathbf{0}_{(2i-1)\times 2} \\ k_{1,i} \quad k_{2,i} \\ \mathbf{0}_{2(m-i)\times 2} \end{bmatrix} \begin{bmatrix} \mathbf{0}_{2\times 2(i-2)} & \begin{matrix} 1 & 0 & -1 & -\tau \\ 0 & 1 & 0 & -1 \end{matrix} & \mathbf{0}_{2\times 2(m-i)} \end{bmatrix} \begin{bmatrix} y_1 \\ y_2 \\ \vdots \\ y_{2i} \\ y_{2i+1} \\ \vdots \\ y_{2m-1} \\ y_{2m} \end{bmatrix}$$

$$+ \begin{bmatrix} \mathbf{0}_{(2i-1)\times 1} \\ \delta_i \\ \mathbf{0}_{2(m-i)\times 1} \end{bmatrix}$$

$$= g(\tilde{y}) + KC\tilde{y} + \delta \tag{5.21}$$

where δ is given by

$$\delta = \begin{bmatrix} \mathbf{0}_{(2i-1)\times 1} \\ \delta_i \\ \mathbf{0}_{2(m-i)\times 1} \end{bmatrix} \tag{5.22}$$

Remark 19. *The state space formulation shown in the above Sections 5.3.1 and 5.3.2 follows a generic car-following dynamics for HVs, which allows for the adoption of any deterministic car-following models including the IDM. The OVRV model was explicitly employed for mathematically incorporating cyberattacks into the state space formulation, which however does not preclude the adoption of other car-following models for AVs with corresponding modifications of the formulation.*

5.3.3 Formulation of a Min-max Control Problem

As mentioned before, AVs generally do not have prior knowledge of the attacks, rendering it difficult for them to adjust the control (driving) strategy dynamically. To address this challenge we formulate a min-max control problem which, once solved, allows AVs to determine the optimal driving strategy in the presence of malicious cyberattacks. The objective is to find an optimal feedback control law for AVs (essentially an effective acceleration), or equivalently to determine the optimal feedback gains $k_{1,i}$ and $k_{2,i}$ dictating the effective acceleration, so that a certain cost functional like vehicle speed disturbance is minimized, considering the worst-case scenario that could be caused by the attacks. In other words, one aims to minimize the maximum disruption to mixed-autonomy traffic due to cyberattacks on AVs.

Considering Type #1 cyberattacks, let Ω denote the space of possible attacks. Hence it follows from the assumption on boundedness that

$$\Omega = \left\{\omega = [\omega_{1,i}, \omega_{2,i}]' : |\omega_{1,i}| \leq r_1, |\omega_{2,i}| \leq r_1, r_1 \in \mathbb{R}^+\right\} \tag{5.23}$$

The AV dynamics given by equation (5.10) follows the rational driving constraints (RDC) [114]

$$\frac{\partial \ddot{x}_i}{\partial s_i} > 0, \ \frac{\partial \ddot{x}_i}{\partial \Delta v_i} > 0, \text{ and } \frac{\partial \ddot{x}_i}{\partial v_i} < 0, \tag{5.24}$$

which ensure a simple criterion for the existence of car-following models and imply that as the inter-vehicle spacing (s_i) or relative speed (Δv_i) increase, the AV i should accelerate. Consequently, the RDC and safety imply that $k_{1,i}$ and $k_{2,i}$ are non-negative [104]. Therefore, the set of admissible feedback gains is given by

$$\mathcal{K} = \{K : k_{1,i}, k_{2,i} \geq 0, \text{ with } K \text{ defined in the expression (5.18)}\} \tag{5.25}$$

In the event of malicious cyberattacks, the goal is to determine an optimal feedback control law for AVs, essentially the operator K or equivalently $k_{1,i}$ and $k_{2,i}$, that minimizes a certain cost (objective) functional, e.g., disruption to the mixed-autonomy traffic, considering the worst-case scenario due to unknown attacks. Hence, one can define a general objective functional as follows

$$J(K, \omega) = \int_{t_0}^{t_f} \ell(t, y(t))dt + \Phi(y(t_f)), \tag{5.26}$$

where ℓ is the integrand of the running cost dependent on dynamic traffic states, Φ is the terminal cost associated with the final traffic states at the end of the time horizon $I = [t_0, t_f]$. This general objective functional can be written out explicitly depending on the specific goal to be achieved. For example, in the context of cyberattacks on AVs a reasonable formulation could be minimizing the speed disturbance experienced by AVs, which can help reduce the propagation of speed perturbation along upstream of the traffic [16, 45]. To this end, an explicit objective functional is given by

$$J(K, \omega) = \frac{w_1}{2} \int_{t_0}^{t_f} \left(y_{2i}(t) - y_{2(i-1)}(t)\right)^2 dt + \frac{w_2}{2} \left(y_{2i}(t_f) - y_{2(i-1)}(t_f)\right)^2, \tag{5.27}$$

where y_{2i} is the speed of AV i and $y_{2(i-1)}$ is the speed of its preceding vehicle, the positive parameters $w_1 \in \mathbb{R}^+$ and $w_2 \in \mathbb{R}^+$ represent the weights placed on the running cost and terminal cost, respectively. Comparing equation (5.26) to equation (5.27), it is easily observed that $\ell(t, y) = (w_1/2)\left(y_{2i} - y_{2(i-1)}\right)^2$ and $\Phi(y(t_f)) = (w_2/2)\left(y_{2i}(t_f) - y_{2(i-1)}(t_f)\right)^2$. It is noted that measurements like speed of the vehicle ahead are correctly obtained without sensor failures, but they are assumed to be under attack when used to execute the acceleration commands of AVs as shown in equation (5.6) [158]. Now the optimal control problem becomes the following min-max problem

$$\min_{K \in \mathcal{K}} \max_{\omega \in \Omega} J(K, \omega), \tag{5.28}$$

where Ω and $\mathcal{K}$ are defined in equations (5.23) and (5.25), respectively. This min-max control problem is solved for each individual AV without requiring cooperation (communication) among vehicles. In the absence of attacks, the controlled AVs will closely track the speed of their immediate preceding vehicles obeying car-following principles. In other words, the methodology developed works effectively for each AV being controlled, regardless of the number of AVs present in the traffic.

Remark 20. *In the presence of Type #2 cyberattacks, the state space formulation of mixed-autonomy traffic flow dynamics is given by equation* (5.21)*. The above min-max control problem shown in equation* (5.28) *becomes*

$$\min_{K \in \mathcal{K}} \max_{\delta_i \in \Delta} J(K, \delta_i), \tag{5.29}$$

with the space of possible attacks given by

$$\Delta = \left\{ \delta_i : |\delta_i| \leq r_2, r_2 \in \mathbb{R}^+ \right\}. \tag{5.30}$$

Remark 21. *It is noted that, for attacks to remain stealthy they are assumed to be launched in a subtle manner (characterized by the values of r_1 and r_2 in this study) as seen in [154–157, 159]. In other words, severe cyberattacks on AVs resulting in direct collisions are not specifically considered here since such attacks may cause noticeably abnormal driving behavior and could be easily detected. While the proposed approach works well regardless of the level of attack severity, it may not necessarily guarantee safety if an extremely severe attack leading to collisions occurs in the first place. However, solving the problem* (5.28) *reduces speed disturbances for AVs, which could result in smoother traffic [45].*

Remark 22. *The formulation of a min-max control problem does not require any prior knowledge, like statistical (probability) distribution, of the cyberattacks, rendering it consistent with their stealthy nature. To the best of our knowledge, this is the first formulation of its kind in the context of cyberattacks on AVs in mixed-autonomy traffic.*

5.4 Optimal Feedback Control Law for Automated Vehicles

To solve the min-max control problem formulated in equation (5.28) subject to mixed-autonomy traffic flow dynamics, in this section we derive a set of necessary conditions of optimality, which allows for the development of an iterative computational procedure to determine the optimal feedback control law (driving strategy) of AVs. In what follows, we consider exclusively Type #1 cyberattacks for the purpose of analytical illustration. A similar mathematical analysis can be carried out for Type #2 cyberattacks with slight modifications.

We introduce a Hamiltonian function as follows

$$H(t, y, \varphi, K) = \langle g(y) + KCy, \varphi \rangle + r_1 \|K'\varphi\| + \ell(t, y), \tag{5.31}$$

where φ is the adjoint state to be characterized, and $\langle A, B \rangle$ denotes the inner product of A and B. Now we are ready to present the main results in the following theorem.

5.4.1 Necessary Conditions of Optimality

Theorem 5.4.1. *Consider the mixed-autonomy traffic flow dynamics in the presence of Type #1 cyberattacks as described by equation* (5.17) *with the objective functional given by equation* (5.27)*. Let K^o be the feedback control law for the AVs under attack, corresponding to the solution state y^o. Then, for the pair $\{y^o, K^o\}$ to be optimal it is necessary that there exists a function φ^o such that the following conditions hold:*

$$H(t, y^o(t), \varphi^o(t), K^o(t)) \leq H(t, y^o(t), \varphi^o(t), K(t)), \tag{5.32}$$

$$\dot{y}^o(t) = H_\varphi(t, y^o, \varphi^o, K^o),\ y^o(t_0) = y_0, \tag{5.33}$$

$$\dot{\varphi}(t) = -H_y(t, y^o, \varphi^o, K^o),\ \varphi^o(t_f) = \Phi_y(y^o(t_f)), \tag{5.34}$$

where y_0 is the initial traffic state, H_φ and H_y are the partial derivatives of H with respect to φ and y, respectively.

Proof. Let $\omega \in \Omega$ be any possible Type #1 cyberattack and consider the cost functional (5.27) reproduced below

$$\begin{aligned} J(K,\omega) &= \frac{w_1}{2}\int_{t_0}^{t_f}\left(y_{2i}-y_{2(i-1)}\right)^2 dt + \frac{w_2}{2}\left(y_{2i}(t_f)-y_{2(i-1)}(t_f)\right)^2 \\ &= \int_{t_0}^{t_f}\ell(t,y(t))dt + \Phi(y(t_f)), \end{aligned} \tag{5.35}$$

with ℓ and Φ defined as

$$\ell(t,y) = (w_1/2)\left(y_{2i}-y_{2(i-1)}\right)^2, \tag{5.36}$$

$$\Phi(y(t_f)) = (w_2/2)\left(y_{2i}(t_f)-y_{2(i-1)}(t_f)\right)^2. \tag{5.37}$$

For any specific $\omega^o \in \Omega$, let $K^o \in \mathcal{K}$ be the optimal feedback control law for AVs under attack, and y^o be the corresponding solution to equation (5.17). Let $K \in \mathcal{K}$ be any other feasible AV control law. Since $\mathcal{K}$ is a convex set, it is easy to verify that $K^\lambda = (1-\lambda)K^o + \lambda K = K^o + \lambda(K-K^o) \in \mathcal{K}$ for any $\lambda \in (0,1]$.

Let y^λ be the solution to equation (5.17) corresponding to the AV control law K^λ. It is clear that $J(K^\lambda,\omega^o) \geq J(K^o,\omega^o)$ due to optimality of K^o. Hence, it follows that

$$\begin{aligned} (1/\lambda)\left[J(K^\lambda,\omega^o)-J(K^o,\omega^o)\right] = \frac{1}{\lambda}\Bigg\{\int_{t_0}^{t_f}\left[\ell(t,y^\lambda(t))-\ell(t,y^o(t))\right] \\ + \left[\Phi(y^\lambda(t_f))-\Phi(y^o(t_f))\right]\Bigg\} \geq 0. \end{aligned} \tag{5.38}$$

Let $dJ(K^o,\omega^o)$ denote the Gâteaux derivative of J at $K=K^o$, then it follows that

$$\begin{aligned} dJ(K^o,\omega^o) &= \lim_{\lambda\to 0}\frac{1}{\lambda}\left[J(K^o+\lambda(K-K^o),\omega^o)-J(K^o,\omega^o)\right] \\ &= \lim_{\lambda\to 0}\frac{1}{\lambda}\left[J(K^\lambda,\omega^o)-J(K^o,\omega^o)\right] \\ &= \lim_{\lambda\to 0}\frac{1}{\lambda}\left\{\left[\int_{t_0}^{t_f}\ell(t,y^\lambda)dt+\Phi(y^\lambda(t_f))\right]-\left[\int_{t_0}^{t_f}\ell(t,y^o)dt+\Phi(y^o(t_f))\right]\right\} \\ &= \lim_{\lambda\to 0}\frac{1}{\lambda}\left[\int_{t_0}^{t_f}\ell(t,y^\lambda)dt-\int_{t_0}^{t_f}\ell(t,y^o)dt\right]+\lim_{\lambda\to 0}\frac{1}{\lambda}\left[\Phi(y^\lambda(t_f))-\Phi(y^o(t_f))\right] \\ &= \lim_{\lambda\to 0}\frac{1}{\lambda}\int_{t_0}^{t_f}\left\langle \ell_y(t,y^o), y^\lambda-y^o\right\rangle dt + \lim_{\lambda\to 0}\frac{1}{\lambda}\left\langle \Phi_y(y^o(t_f)), y^\lambda(t_f)-y^o(t_f)\right\rangle \\ &= \int_{t_0}^{t_f}\left\langle \ell_y(t,y^o), z\right\rangle dt + \left\langle \Phi_y(y^o(t_f)), z(t_f)\right\rangle, \end{aligned} \tag{5.39}$$

where $z(t)$ is defined as

$$z(t) = \lim_{\lambda \to 0} \frac{1}{\lambda} \left[y^{\lambda}(t) - y^{o}(t) \right]. \tag{5.40}$$

Denoting the above Gâteaux derivative given by equation (5.39) as Λ, if follows from the expression (5.38) that

$$\Lambda = \int_{t_0}^{t_f} \langle \ell_y(t, y^o), z \rangle \, dt + \langle \Phi_y(y^o(t_f)), z(t_f) \rangle \geq 0. \tag{5.41}$$

According to the traffic flow dynamics given by equation (5.17), for $K = K^o$ one has

$$\dot{y}^o = g(y^o) + K^o C y^o + K^o \omega^o. \tag{5.42}$$

Similarly, for $K = K^{\lambda}$

$$\dot{y}^{\lambda} = g(y^{\lambda}) + K^{\lambda} C y^{\lambda} + K^{\lambda} \omega^o. \tag{5.43}$$

Subtracting equation (5.42) from equation (5.43) yields

$$(d/dt)(y^{\lambda} - y^o) = \left[g(y^{\lambda}) - g(y^o) \right] + \left(K^{\lambda} C y^{\lambda} - K^o C y^o \right) + (K^{\lambda} - K^o)\omega^o. \tag{5.44}$$

Dividing both sides of equation (5.44) by λ and using Taylor approximations, it follows that when letting $\lambda \to 0$ the function $z(t)$ needs to satisfy the following initial value problem:

$$\dot{z} = g_y(y^o) z + K^o C z + (K - K^o)(C y^o + \omega^o), \;\; z(t_0) = 0. \tag{5.45}$$

Since ω^o is a bounded measurable random process, the driving force $(K - K^o)(Cy^o + \omega^o) \in \mathcal{L}_1(I, \mathbb{R}^{2m})$ is a measurable function, where $I = [t_0, t_f]$ is the time horizon introduced before. Hence, according to the theory of differential equations, the map $(K - K^o)(Cy^o + \omega^o) \longrightarrow y$ is a bounded linear map.

Since ℓ and Φ are bounded and continuously differentiable, it follows that the map

$$y \longrightarrow \int_{t_0}^{t_f} \langle \ell_y(t, y^o), z \rangle \, dt + \langle \Phi_y(y^o(t_f)), z(t_f) \rangle = \Lambda \tag{5.46}$$

is a bounded linear map. Hence, the resulting composition map

$$(K - K^o)(Cy^o + \omega^o) \longrightarrow \int_{t_0}^{t_f} \langle \ell_y(t, y^o), z \rangle \, dt + \langle \Phi_y(y^o(t_f)), z(t_f) \rangle = \Lambda \tag{5.47}$$

is a bounded linear map. Thus, by the Riesz representation theorem there exists a function φ^o such that

$$\begin{aligned}
\Lambda &= \int_{t_0}^{t_f} \langle \ell_y(t, y^o), z\rangle \, dt + \langle \Phi_y(y^o(t_f)), z(t_f)\rangle \\
&= \int_{t_0}^{t_f} \langle (K - K^o)(Cy^o + \omega^o), \varphi^o\rangle \, dt \\
&= \int_{t_0}^{t_f} \left\langle \left(\dot{z} - g_y(y^0)z - K^oCz\right), \varphi^o\right\rangle dt \quad \text{(plugging equation (5.45))} \\
&= \int_{t_0}^{t_f} \langle \dot{z}, \varphi^o\rangle \, dt - \int_{t_0}^{t_f} \left\langle g_y(y^0)z + K^oCz, \varphi^o\right\rangle dt \\
&= \langle z(t_f), \varphi^o(t_f)\rangle - \int_{t_0}^{t_f} \langle z, \dot{\varphi}^o\rangle \, dt - \int_{t_0}^{t_f} \left\langle g_y(y^0)z + K^oCz, \varphi^o\right\rangle dt \\
&= \langle z(t_f), \varphi^o(t_f)\rangle - \int_{t_0}^{t_f} \langle z, \dot{\varphi}^o\rangle \, dt - \int_{t_0}^{t_f} \left\langle z, \left(g_y'(y^0) + C'(K^o)'z\right)\varphi^o\right\rangle dt \\
&= \langle z(t_f), \varphi^o(t_f)\rangle - \int_{t_0}^{t_f} \left\langle z, \dot{\varphi}^o + g_y'(y^0)\varphi^o + C'(K^o)'z\varphi^o\right\rangle dt \qquad (5.48)
\end{aligned}$$

Comparing the above expression (5.48) to equation (5.41) (the definition of Λ) and letting

$$\dot{\varphi}^o + g_y'(y^0)\varphi^o + C'(K^o)'z\varphi^o = -\ell_y(t, y^o(t)), \ \varphi^o(t_f) = \Phi_y(y^o(t_f)), \qquad (5.49)$$

then the adjoint dynamics is given by

$$\dot{\varphi}^o = -g_y'(y^0)\varphi^o - C'(K^o)'z\varphi^o - \ell_y(t, y^o(t)), \ \varphi^o(t_f) = \Phi_y(y^o(t_f)). \qquad (5.50)$$

Based on the expression of $\Lambda = \int_{t_0}^{t_f} \langle (K - K^o)(Cy^o + \omega^o), \varphi^o\rangle \, dt \geq 0$, it follows that

$$\int_{t_0}^{t_f} \left(\langle KCy^o, \varphi^o\rangle + \langle K\omega^o, \varphi^o\rangle\right) dt - \int_{t_0}^{t_f} \left(\langle K^oCy^o, \varphi^o\rangle + \langle K^o\omega^o, \varphi^o\rangle\right) dt \geq 0, \quad (5.51)$$

which is equivalent to

$$\int_{t_0}^{t_f} \left(\langle KCy^o, \varphi^o\rangle + \left\langle \omega^o, K'\varphi^o\right\rangle\right) dt \geq \int_{t_0}^{t_f} \left(\langle K^oCy^o, \varphi^o\rangle + \left\langle \omega^o, (K^o)'\varphi^o\right\rangle\right) dt. \quad (5.52)$$

It is observed that the worst-case scenario due to Type #1 cyberattacks occurs when the attack vector ω^o is *co-directed* with the vector $(K^o)'\varphi^o$ and lies on the boundary of

the set Ω. This is given by $\omega^o = r_1\Theta\left((K^o)'\varphi^o\right)$ where the unit vector Θ is defined as follows

$$\Theta(u) = \begin{cases} \frac{u}{\|u\|}, & \|u\| \neq 0, \\ 0, & \|u\| = 0. \end{cases} \tag{5.53}$$

Since any feasible cyberattack has a bounded magnitude r_1, it easily follows that

$$\left\langle \omega^o, K'\varphi^o \right\rangle \leq r_1\|K'\varphi^o\|, \tag{5.54}$$

$$\left\langle \omega^o, (K^o)'\varphi^o \right\rangle \leq r_1\|(K^o)'\varphi^o\|. \tag{5.55}$$

Hence, it follows from the inequality (5.52) that

$$\int_{t_0}^{t_f} \left(\langle KCy^o, \varphi^o\rangle + r_1\|K'\varphi^o\|\right) dt \geq \int_{t_0}^{t_f} \left(\langle K^oCy^o, \varphi^o\rangle + r_1\|(K^o)'\varphi^o\|\right) dt. \tag{5.56}$$

Consequently, the mixed-autonomy traffic dynamics given by equation (5.17) becomes

$$\dot{y}^o = g(y^o) + K^oCy^o + r_1K^o\Lambda((K^o)'\varphi^o),\ y(t_0) = y_0. \tag{5.57}$$

The pointwise inequality corresponding to the integral inequality (5.56) is given by

$$\langle KCy^o, \varphi^o\rangle + r_1\|K'\varphi^o\| \geq \langle K^oCy^o, \varphi^o\rangle + r_1\|(K^o)'\varphi^o\|. \tag{5.58}$$

Adding the quantity $\langle g(y^o), \varphi^o\rangle + \ell(t, y^o)$ to both sides of the above inequality (5.58) leads to

$$\begin{aligned} &\langle g(y^o) + KCy^o, \varphi^o\rangle + r_1\|K'\varphi^o\| + \ell(t, y^o) \\ &\qquad \geq \langle g(y^o) + K^oCy^o, \varphi^o\rangle + r_1\|(K^o)'\varphi^o\| + \ell(t, y^o). \end{aligned} \tag{5.59}$$

Clearly, this is in fact

$$H(t, y^o(t), \varphi^o(t), K(t)) \geq H(t, y^o(t), \varphi^o(t), K^o(t)), \tag{5.60}$$

which is the first inequality presented in the necessary conditions of optimality in Theorem 5.4.1 with H given by equation (5.31).

It is easy to verify that the partial derivatives of H with respect to the traffic state vector y and the adjoint vector φ, i.e., H_y and H_φ, satisfy the following equations:

$$\dot{y}^o = H_\varphi(t, y^o(t), \varphi^o(t), K^o(t)),\ y^o(t_0) = y_0, \quad \text{(see (5.33))} \tag{5.61}$$

$$\dot{\varphi}^o = -H_y(t, y^o(t), \varphi^o(t), K^o(t)),\ \varphi^o(t_f) = \Phi_y(y^o(t_f)). \quad \text{(see (5.34))} \tag{5.62}$$

This completes the proof of all the necessary conditions of optimality stated in the theorem. □

Remark 23. *The main idea of the above proof is similar to that of [174, Theorem 4.1] which did not consider any car-following dynamics of mixed-autonomy traffic.*

Remark 24. *In the event of Type #2 cyberattacks, the Hamiltonian function given by equation* (5.31) *is replaced with*

$$H(t, \tilde{y}, \tilde{\varphi}, K) = \langle g(\tilde{y}) + KC\tilde{y}, \tilde{\varphi} \rangle + r_2 \|\tilde{\varphi}\| + \ell(t, \tilde{y}), \tag{5.63}$$

where $\tilde{y}$ is the mixed-autonomy traffic state vector in the presence of Type #2 attacks and $\tilde{\varphi}$ is the corresponding adjoint state vector. The set of necessary conditions of optimality along with the proof are similar to those presented above, and are omitted here for brevity.

Remark 25. *In the extreme case when Type #1 and Type #2 cyberattacks occur at the same time, the Hamiltonian function given by equation* (5.31) *is replaced with*

$$H(t, \breve{y}, \breve{\varphi}, K) = \langle g(\breve{y}) + KC\breve{y}, \breve{\varphi} \rangle + r_1 \|K'\breve{\varphi}\| + r_2 \|\breve{\varphi}\| + \ell(t, \breve{y}), \tag{5.64}$$

where $\breve{y}$ signifies the mixed-autonomy traffic state vector in the presence of both types of attacks and $\breve{\varphi}$ is the corresponding adjoint state vector.

5.4.2 An Iterative Computational Algorithm

In this section, we develop an iterative computational procedure, based on the necessary conditions of optimality presented in Theorem 5.4.1, to determine the optimal feedback control law for AVs in the presence of Type #1 cyberattacks (as an illustration). This computational procedure is based on a gradient descent method generating a sequence of feedback control gains $\left\{k^n = \left(k^n_{1,i}, k^n_{2,i}\right)\right\}$ along which the objective functional J converges to its minimum, where $k^n = \left(k^n_{1,i}, k^n_{2,i}\right)$ denotes the AV feedback control gains at the n-th iteration, $n \in \mathbb{Z}^+$. The iterative computational procedure is briefly summarized below.

Step 1: Choose any Type #1 cyberattack $\omega \in \Omega$ and any feasible feedback gain $k^1 = \left(k^1_{1,i}, k^1_{2,i}\right)$ satisfying equation (5.25), and compute the solution of equation (5.17) giving y^1. At this stage we have the tuple $\left\{k^1, y^1\right\}$ after the first iteration $n = 1$.

Step 2: Use $\{k^1, y^1\}$ to solve the adjoint equation (5.34) backward in time, giving the adjoint vector $\varphi^1 = \{\varphi^1(t),\ t \in I\}$. At this stage we have the triple $\{k^1, y^1, \varphi^1\}$.

Step 3: Use the triple $\{k^1, y^1, \varphi^1\}$ to compute the gradient of the Hamiltonian $H_k(t, y^1, \varphi^1, k^1)$ and the integral $\int_{t_0}^{t_f} H_k(t, y^1, \varphi^1, k^1)dt$.

Step 4: If $\int_{t_0}^{t_f} H_k(t, y^1, \varphi^1, k^1)dt < \epsilon$, where $\epsilon \in \mathbb{R}^+$ is a prescribed small positive number used as tolerance, then k^1 is close enough to the optimal feedback gain and used as its approximation. Otherwise, go to Step 5.

Step 5: Use k^1 to generate the new AV feedback gain k^2

$$k^2 = k^1 - \varepsilon H_k(t, x^1, \varphi^1, k^1) \tag{5.65}$$

in the next iteration for $\varepsilon > 0$ sufficiently small so that k^2 is non-negative as specified by equation (5.25). Computing the objective functional J at $K^2 = \left[\mathbf{0}_{(2i-1)\times 2},\ k^2,\ \mathbf{0}_{2(m-i)\times 2}\right]'$ using equation (5.27), one needs to check if

$$|J(K^2) - J(K^1)| > \Xi \tag{5.66}$$

is satisfied for a predefined small positive number $\Xi \in \mathbb{R}^+$. If so, go to Step 1 with k^2 replacing k^1 and repeat the procedure. For the prescribed $\Xi > 0$, the process is continued while $\left|J(K^{n+1}) - J(K^n)\right| > \Xi$ is satisfied within a given maximum number of iterations $N_{\max} \in \mathbb{Z}^+$.

Remark 26. *For any AV feedback gain $k^n = \left(k^n_{1,i}, k^n_{2,i}\right)$ at the n-th iteration, the corresponding feedback matrix is*

$$K^n = \begin{bmatrix} \mathbf{0}_{(2i-1)\times 2} \\ k^n \\ \mathbf{0}_{2(m-i)\times 2} \end{bmatrix}$$

as seen in the expression (5.18)*. Here we have used k^n for ease of interpretation.*

5.5 Numerical Results

In this section, we conduct a series of numerical experiments in MATLAB to illustrate the effectiveness of the approach developed. As introduced in Section 5.2.4, the IDM and OVRV model are employed for HVs and AVs, respectively, with calibrated parameters

Table 5.1: Calibrated parameters of the IDM and OVRV model

Parameter	**Description**	**IDM** [126]	**OVRV** [175]
v_0	desired speed (m/s)	30.0	-
T	time gap (s)	1.5	-
s_0	minimum spacing (m)	2.0	-
a	maximum acceleration (m/s^2)	1.5	-
b	comfortable deceleration (m/s^2)	1.0	-
l_i	vehicle length (m)	5.0	5.0
k_1	gain parameter on the time gap (s^{-2})	-	0.02
k_2	gain parameter on the relative speed (s^{-1})	-	0.13
η	jam distance (m)	-	21.51
τ	desired time gap (s)	-	1.71

summarized in Table 5.1. The IDM parameter values are standard for freeway traffic and have been widely used in the literature [126]. The parameter values of the OVRV model are adopted from [175], which have been calibrated based on field experiments data of commercially available adaptive cruise control vehicles [143]. It is noted that the feedback gains shown in Table 5.1, k_1 and k_2, are taken as the initial values for all AVs. Following the algorithm presented in Section 5.4.2, the optimal feedback gains, $k_{1,i}$ and $k_{2,i}$, will be determined for the vehicle $i \in \mathcal{A}$ resulting in an effective optimal acceleration.

As mentioned before, the proposed approach works in a decentralized manner, i.e., in a car-following scenario involving the controlled AV and its preceding vehicle. While considering an AV under attack that follows a lead vehicle, we are also interested to examine impacts of the attacked AV on traffic flow. Therefore, without loss of generality we consider a general scenario involving a string of 10 vehicles in mixed-autonomy traffic shown in Fig. 5.2, with the second vehicle being an AV under potential cyberattacks. It is noted that the proposed approach does not require vehicle communication and is applied to each individual AV. Hence, the approach does not depend on the market penetration rate of AVs and will work effectively regardless of the number of AVs present in the traffic. Similar to the settings of [46, 48, 158], we only consider longitudinal vehicle dynamics in this study. In the following, we study the impact of cyberattacks (with

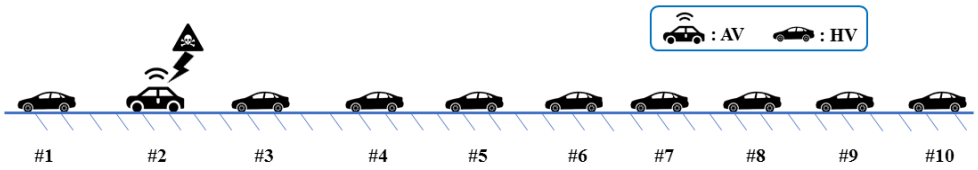

Figure 5.2: An illustrative example of a string of 10 vehicles in mixed-autonomy traffic with the second vehicle being an AV under cyberattacks. It is noted that the methodology developed does not require communication (or cooperation) among vehicles and is directly applied to each individual AV. Hence, the approach does not depend on the market penetration rate of AVs and can work effectively regardless of the number of AVs present in the traffic. As shown in Fig. 5.2, the second vehicle (vehicle # 2) is assumed to be an AV under cyberattacks, for ease of illustrating not only the impacts of attacks on the AV being attacked but also the resulting effects on the following vehicles [52].

various levels of severity characterized by r_1 and r_2) on traffic flow, and examine the effectiveness of the proposed approach in mitigating disruption to mixed-autonomy traffic due to those attacks. Detailed numerical results on AVs under Type #1 cyberattacks are presented in Section 5.5.1, while those corresponding to Type #2 cyberattacks are shown in Section 5.5.2.

5.5.1 AVs Under Type #1 Cyberattacks

In this section, we present a series of numerical results corresponding to AVs under Type #1 cyberattacks. To clearly demonstrate the impacts of attacks on vehicle acceleration and speed, all the vehicles shown in Fig. 5.2 are assumed to be driving at a constant speed of 21 m/s (with zero acceleration) before any attack occurs, over a simulation horizon of $I = [0, 200]$ sec. This setting, similar to the ones in [155, 158], is considered for the purpose of illustration only. The AV (vehicle #2) is under Type #1 attacks during the period of $[60, 80]$ sec. For attacks randomly generated with a bound of $r_1 = 10$, the corresponding results on vehicle acceleration and speed are shown in Fig. 5.3 with the period of attack marked in grey, where the AV follows the OVRV model without employing the optimal feedback control law derived.

It is observed from Fig. 5.3a that the AV experiences fluctuations in acceleration over the period of attack ($[60, 80]$ sec). As a result, its speed is noticeably disturbed even beyond the attacking period, which also causes speed disturbances to the following

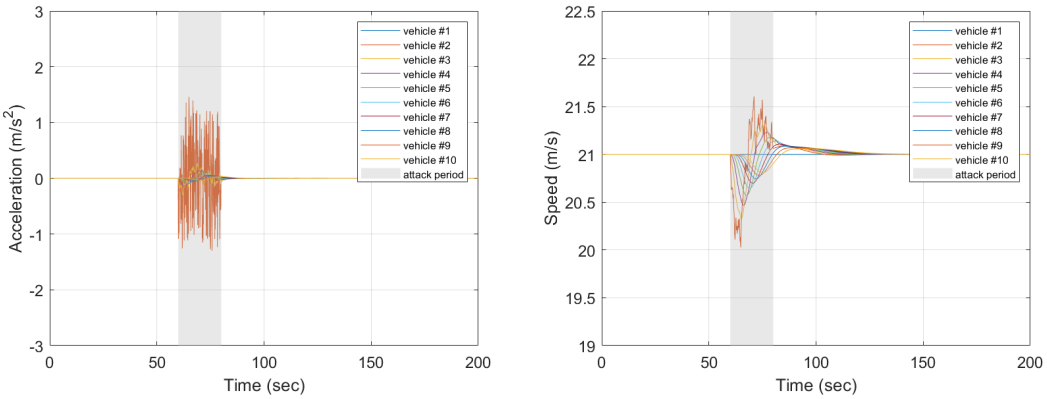

(a) Acceleration (b) Speed

Figure 5.3: Simulation results corresponding to the AV (vehicle #2) under Type #1 cyberattacks with a bound of $r_1 = 10$. The attacks occur during the period of $[60, 80]$ sec (marked in grey) over the simulation horizon $I = [0, 200]$ sec. All the vehicles are assumed to be driving at a constant speed of 21 m/s before the attacks occur. The AV follows the OVRV model without employing the optimal driving strategy developed. (a) acceleration of all vehicles; (b) speed of all vehicles.

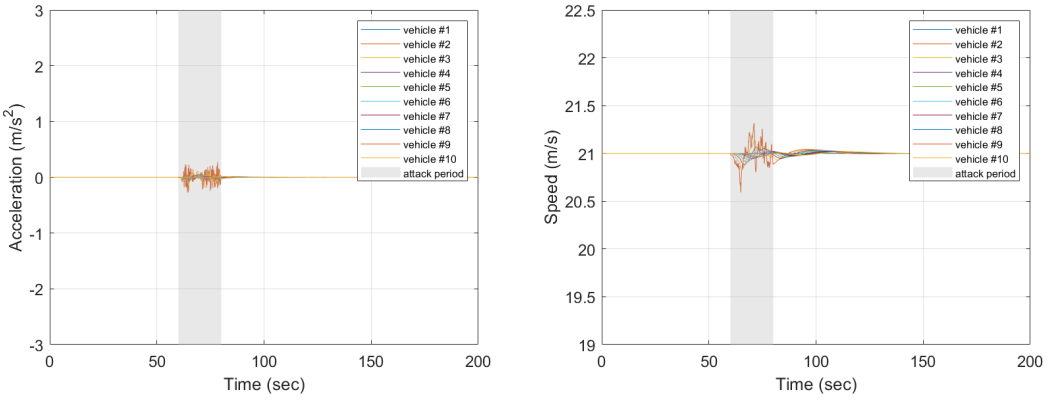

(a) Acceleration (b) Speed

Figure 5.4: Simulation results corresponding to the AV (vehicle #2) under Type #1 cyberattacks with a bound of $r_1 = 10$. The attacks occur during the period of $[60, 80]$ sec (marked in grey) over the simulation horizon $I = [0, 200]$ sec. All the vehicles are assumed to be driving at a constant speed of 21 m/s before the attacks occur. The AV follows the optimal driving strategy proposed. (a) acceleration of all vehicles; (b) speed of all vehicles.

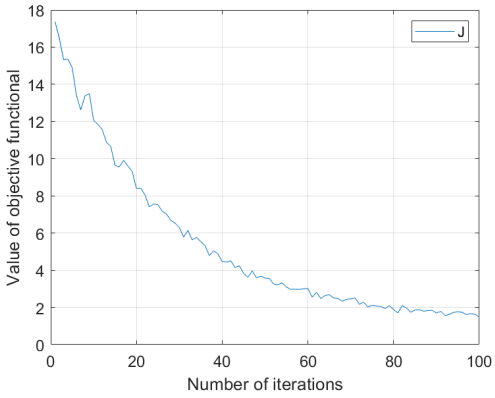

Figure 5.5: Value of the objective functional J corresponding to the AV (vehicle #2) under Type #1 cyberattacks with a bound of $r_1 = 10$. The weights in the objective functional are chosen as $w_1 = w_2 = 1$. Clearly, the value of J tends to decrease and converge as the number of iterations increases, showing convergence of the numerical algorithm.

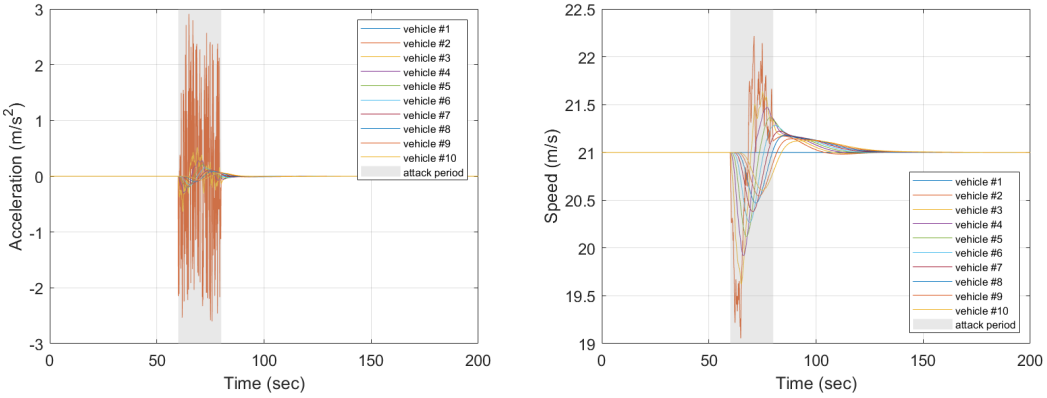

(a) Acceleration (b) Speed

Figure 5.6: Simulation results corresponding to the AV (vehicle #2) under Type #1 cyberattacks with a bound of $r_1 = 20$. The attacks occur during the period of $[60, 80]$ sec (marked in grey). The AV follows the OVRV model without employing the optimal driving strategy developed. (a) acceleration of all vehicles; (b) speed of all vehicles.

vehicles as shown in Fig. 5.3b. With the AV following the proposed optimal driving strategy in the presence of the same attacks, the corresponding results are presented in Fig. 5.4. Comparing Fig. 5.4a to Fig. 5.3a, it is easily observed that the optimally controlled AV exhibits much less disturbances in acceleration. Consequently, speed

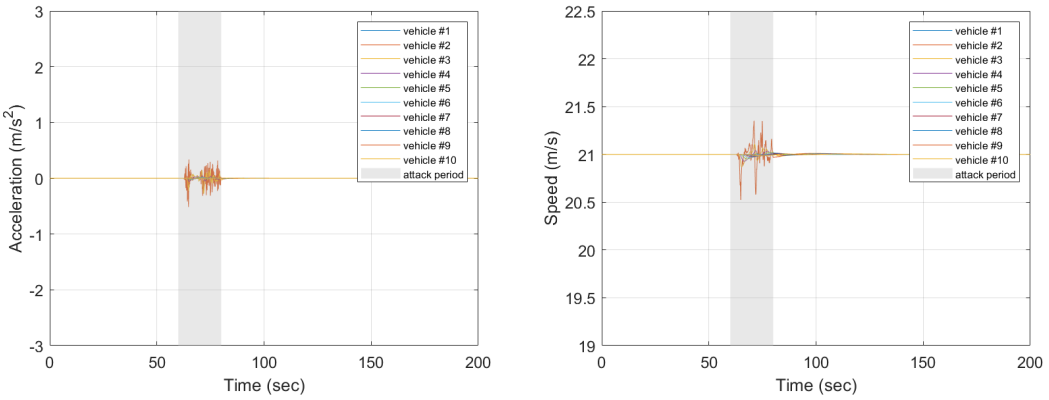

(a) Acceleration (b) Speed

Figure 5.7: Simulation results corresponding to the AV (vehicle #2) under Type #1 cyberattacks with a bound of $r_1 = 20$. The attacks occur during the period of $[60, 80]$ sec (marked in grey). The AV follows the optimal driving strategy proposed. (a) acceleration of all vehicles; (b) speed of all vehicles.

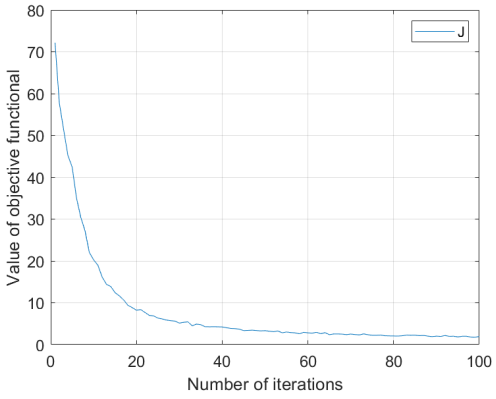

Figure 5.8: Value of the objective functional J corresponding to the AV (vehicle #2) under Type #1 cyberattacks with a bound of $r_1 = 20$. The weights in the objective functional are chosen as $w_1 = w_2 = 1$. Clearly, the value of J tends to decrease and converge with the increase of the number of iterations, showing convergence of the numerical algorithm.

fluctuations experienced by the AV (Fig. 5.4b) are much reduced compared to those shown in Fig. 5.3b. This also results in much less speed disturbances for the following vehicles as observed in Fig. 5.4b. To show convergence of the computational algorithm, the objective functional value is plotted in Fig. 5.5. Clearly, the value of J tends to

decrease and converge as the number of iterations increases, showing convergence of the numerical computation.

Now we increase the severity level of attacks and examine the resulting performance of the proposed approach. Specifically, the bound on attacks, r_1, is increased from 10 to 20. Under the same simulation settings as before, the results on vehicle acceleration and speed are shown in Fig. 5.6, where the AV does not incorporate the optimal driving strategy developed. Clearly, comparing Fig. 5.6a to Fig. 5.3a indicates that the AV suffers from worse fluctuations in acceleration due to more severe attacks. This is also observed from the comparison of Fig. 5.6b with Fig. 5.3b, showing more noticeable speed disturbances in the presence of more severe attacks. With the AV adopting the proposed optimal driving strategy, the corresponding results are presented in Fig. 5.7. Comparing Fig. 5.7a to Fig. 5.6a indicates that the optimally controlled AV experiences much less disturbances in acceleration. Consequently, speed disturbances endured by the AV, shown in Fig. 5.7b, are significantly mitigated compared to the results presented in Fig. 5.6b. This also leads to a considerable reduction in speed perturbation for the following vehicles as observed in Fig. 5.7b. Value of the objective functional J is shown in Fig. 5.8 as a function of number of iterations. Clearly, the value of J tends to decrease and converge as the iteration number increases, showing convergence of the numerical algorithm.

5.5.2 AVs Under Type #2 Cyberattacks

In this section, we present a series of numerical results corresponding to AVs under Type #2 cyberattacks, with simulation settings remaining the same as in Section 5.5.1. For the baseline scenario in which AVs are not employed with the optimal feedback control law derived, we first consider attacks bounded by $r_2 = 1$, which will be increased later to characterize more severe attacks. For illustrative purposes, r_2 is chosen much smaller than r_1 seen in the previous section. This is because Type #2 attacks directly act on vehicle acceleration and have a more easily noticeable impact on AV driving behavior. Hence, r_2 is likely to be relatively small for adversaries to remain stealthy as mentioned in Section 5.2.3. Simulation results of the baseline scenario are shown in Fig. 5.9, where acceleration and speed of the AV (vehicle #2) experience noticeable disturbances due to the attacks, resulting in disruption to the traffic flow as endured by the following

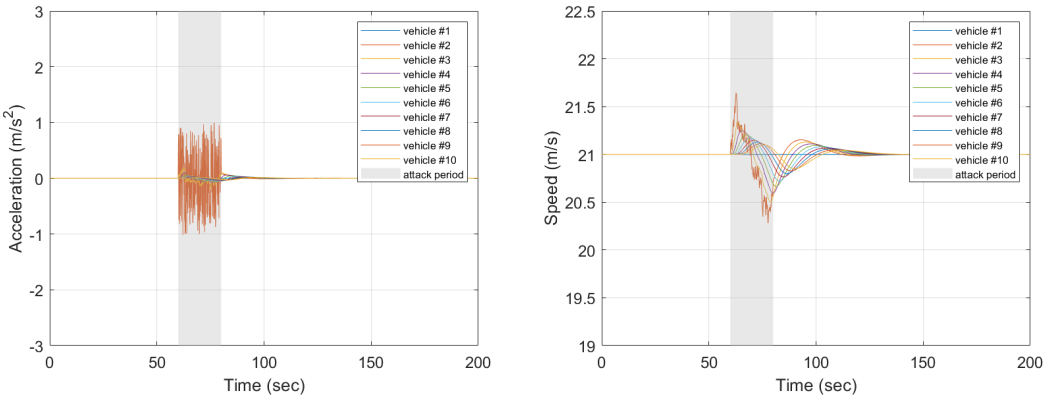

(a) Acceleration (b) Speed

Figure 5.9: Simulation results corresponding to the AV (vehicle #2) under Type #2 cyberattacks with a bound of $r_2 = 1$. The attacks occur during the period of $[60, 80]$ sec (marked in grey). The AV follows the OVRV model without employing the optimal driving strategy developed. (a) acceleration of all vehicles; (b) speed of all vehicles.

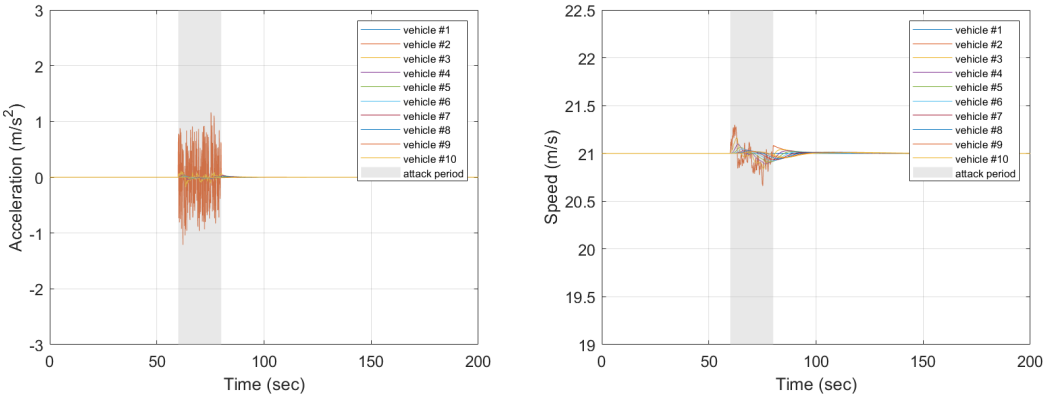

(a) Acceleration (b) Speed

Figure 5.10: Simulation results corresponding to the AV (vehicle #2) under Type #2 cyberattacks with a bound of $r_2 = 1$. The AV follows the optimal driving strategy proposed. (a) acceleration of all vehicles; (b) speed of all vehicles.

vehicles. A set of comparative results is presented in Fig. 5.10, where the AV drives using the optimal strategy derived in the presence of same attacks. Clearly, the results shown in Fig. 5.10 outperform those of Fig. 5.9 in terms of disturbances in vehicle

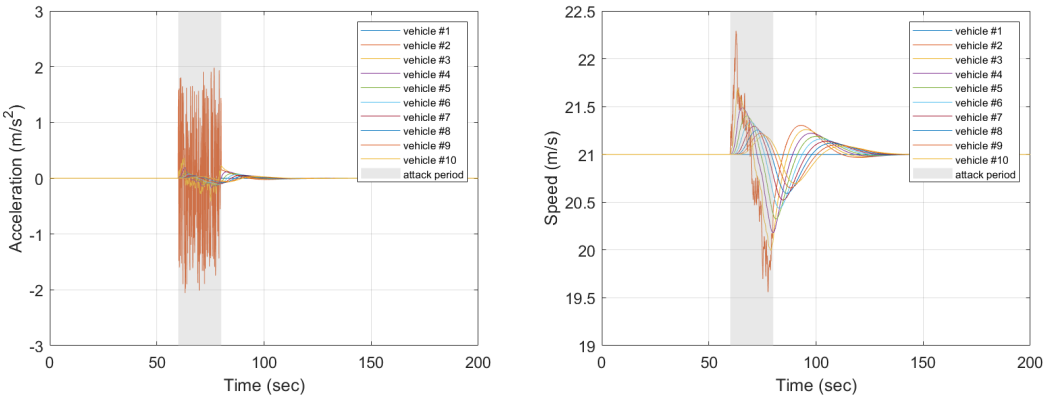

(a) Acceleration (b) Speed

Figure 5.11: Simulation results corresponding to the AV (vehicle #2) under Type #2 cyberattacks with a bound of $r_2 = 2$. The AV follows the OVRV model without using the optimal driving strategy. (a) acceleration of all vehicles; (b) speed of all vehicles.

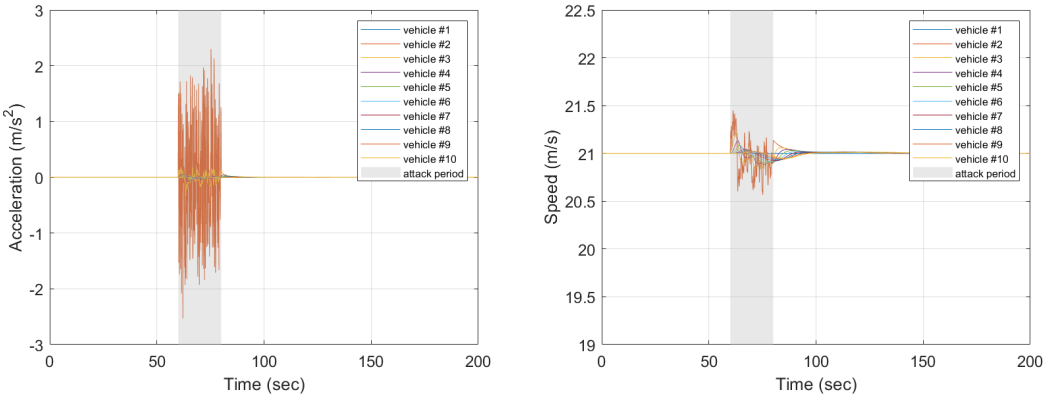

(a) Acceleration (b) Speed

Figure 5.12: Simulation results corresponding to the AV (vehicle #2) under Type #2 cyberattacks with a bound of $r_2 = 2$. The AV follows the optimal driving strategy proposed. (a) acceleration of all vehicles; (b) speed of all vehicles.

acceleration and speed.

Next we increase the severity of Type #2 attacks by doubling the value of r_2 and examine the effectiveness of the proposed optimal AV driving strategy. With the simulation settings kept unchanged, Fig. 5.11 shows vehicle acceleration and speed for the baseline scenario in which the AV does not adopt the optimal driving strategy developed. Comparing Fig. 5.11 to Fig. 5.9, it is observed that the AV (as well as the

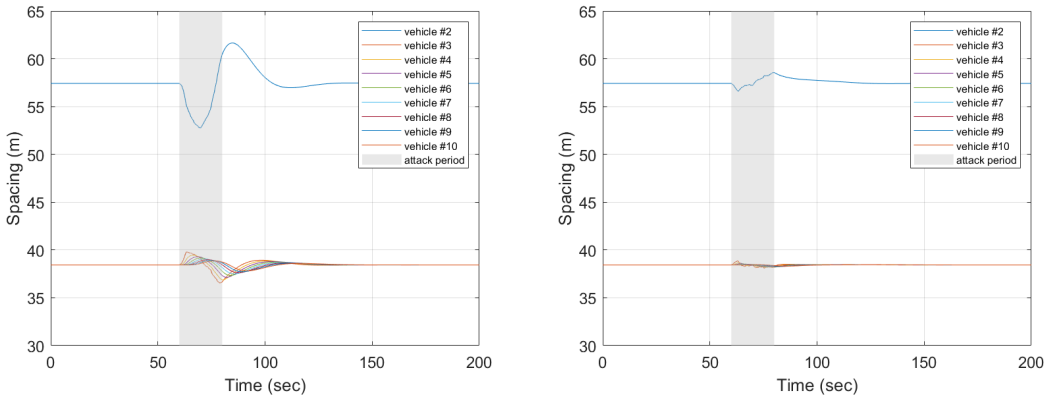

(a) Spacing (b) Spacing

Figure 5.13: Spacing of vehicles #2–#10, with the AV (vehicle #2) under Type #2 cyberattacks with a bound of $r_2 = 2$. The attacks occur during the period of $[60, 80]$ sec (marked in grey). (a) The AV follows the OVRV model without employing the optimal driving strategy developed; (b) The AV follows the optimal driving strategy proposed.

following vehicles) experiences much more disturbances in acceleration and speed due to more severe attacks. With the AV employing the proposed optimal driving strategy, the corresponding results are presented in Fig. 5.12, indicating a significant reduction in speed disturbances with Fig. 5.12b compared to Fig. 5.11b. It is noted that an in-depth comparison on the results of Section 5.5.2 and Section 5.5.1 indicates that mitigating the impacts of Type #2 attacks on vehicle acceleration appears to be more challenging compared to the case of Type #1 attacks. This is consistent with the understanding of the nature of Type #2 attacks directly acting on acceleration.

Following Remark 21 we also present some brief results in Fig. 5.13 to show impacts of the attacked AV on traffic safety in terms of inter-vehicle spacing. Type #2 attacks are considered in this regard since they directly act on vehicle acceleration and have a more easily noticeable impact on AV driving behavior. As introduced in the simulation settings, vehicles are driving at an equilibrium speed of $v^{\mathrm{e}} = 21$ m/s before any attack occurs. Based on the calibrated parameters shown in Table 5.1, the corresponding equilibrium spacing values are calculated as $s^{\mathrm{e}}_{\mathrm{HV}} = (s_0 + v^{\mathrm{e}}T) \Big/ \sqrt{1 - (v^{\mathrm{e}}/v_0)^4} \approx 38.43$ m and $s^{\mathrm{e}}_{\mathrm{AV}} = \eta + \tau v^{\mathrm{e}} = 57.42$ m for HVs and AVs, respectively. Fig. 5.13a shows the spacing values for vehicles #2–#10 with the AV (vehicle #2) following the OVRV model

without employing the optimal driving strategy developed, whereas their counterparts, when the AV follows the optimal driving strategy proposed, are presented in Fig. 5.13b. Comparing Fig. 5.13b to Fig. 5.13a, it is observed that the AV using the optimal driving strategy experiences much less fluctuations in spacing as opposed to the case without adopting the optimal control law developed for AVs. Consequently, vehicles following the AV employing the proposed driving strategy also endure less spacing disturbances.

5.6 Conclusions

In spite of the many benefits promised by AVs, emerging AV technologies open a door for cyberattacks, which could significantly degrade the performance of transportation systems. Hence, developing effective driving strategies for AVs facing attacks is necessary and valuable as AVs gradually become a reality. In this study, we have derived optimal feedback control laws for AVs considering two typical types of cyberattacks, namely false data injection attacks and malicious attacks on vehicle control commands, in a mixed-autonomy traffic setting. The proposed optimal driving strategy can help mitigate the disturbances in acceleration and speed experienced by AVs due to cyberattacks. We characterize the attacks as bounded stochastic processes without being subject to any specific probability distribution, which is not only of theoretical interest but also significantly relaxes the assumptions seen in prior studies. To deal with lack of knowledge of malicious attacks, we formulate a min-max control problem for minimizing the worst-case potential disturbance to traffic flow due to attacks. Based on a generic framework describing mixed traffic, we derive a set of necessary conditions of optimality for the min-max control problem formulated and develop an iterative computational algorithm for determining the optimal control (driving) strategy of AVs in a decentralized manner. The proposed approach is shown to be effective via simulations considering various levels of attack severity.

Chapter 6

Conclusions

6.1 Summary

Enabled by emerging vehicle sensing and communication technologies, AVs are expected to bring a wide range of benefits to future transportation systems, such as improved roadway safety, smoothed traffic flow, and increased urban mobility, among others. In spite of the many benefits promised by AVs, emerging AV technologies open a door for cyberattacks, which could increase the vulnerability of future transportation systems. With this in mind, in this dissertation we have studied multiple aspects of the planning, control, and management of automated transportation systems, particularly in the context of mixed-autonomy traffic involving AVs and HVs, to better prepare a nation for the advent of AVs.

Inspired by the classic Lotka-Volterra equations, in Chapter 2, we develop a continuous-time dynamical model to describe the temporal evolution of the market share of AVs and HVs as HVs are gradually replaced by AVs. To achieve a desired temporal integration of AVs, monetary subsidies and investment in AV-specific transportation infrastructure are considered as decision variables to promote the adoption of AVs. Moreover, we develop an effective approach for determining the optimal time-dependent AV integration policy, allowing a government agency to appropriately subsidize AV purchases and invest in AV infrastructure in an adaptive manner. In addition, a systematic cost-benefit analysis is conducted, along with appropriate sensitivity analysis, to evaluate the desirability of the integration of AVs.

With AVs being integrated into mixed-autonomy traffic flow, they can be employed as mobile actuators to influence the driving behavior of HVs for traffic control and management, known as Lagrangian traffic flow control. In Chapter 3, we develop an optimal control method for AVs to smooth unstable traffic flow, where stop-and-go traffic waves could occur simply due to the collective behavior of human drivers. The well-known Pontryagin's minimum principle is used to determine the optimal driving strategy of AVs to minimize their speed disturbance caused by traffic waves from downstream of the traffic. The resulting traffic exhibits less speed disturbance with vehicles experiencing, on average, less fuel consumption and emissions.

The optimal AV controller designed in Chapter 3 is shown to be effective in smoothing unstable mixed traffic. However, the performance of the synthesized controllers on improving traffic stability is yet to be proven analytically, and car-following safety is ensured in a fairly conservative manner. To address these challenging issues, in Chapter 4, we develop a general approach to synthesizing effective feedback controllers of AVs for smoothing unstable nonlinear mixed traffic flow. Specifically, by leveraging feedback control theory AVs are controlled to closely track a virtual speed profile, i.e., a subtler version of the disturbance resulting from the immediate preceding vehicle. Consequently, traffic waves are reduced when propagating backwards across controlled AVs. Based on the general functional form of car-following dynamics, we derive a class of effective AV controllers that are proven to be able to ensure convergence in speed tracking, leading to smoother traffic. In addition, a set of sufficient conditions is devised for guaranteeing car-following safety. Notably, unlike many existing studies the feedback controllers synthesized for AVs require only local traffic information without having to rely on high degrees of vehicle connectivity, and the rate of smoothing mixed traffic is readily tunable, which is useful for practical implementation.

In spite of the power and benefits promised by AVs, emerging AV technologies open a door for cyberattacks, where a select number of AVs are compromised to drive in an adversarial manner. This could result in network-wide increases in traffic congestion and vehicle fuel consumption, degrading the performance of future transportation systems. In Chapter 5, we derive optimal feedback control law for AVs in the presence of cyberattacks. Notably, attacks are only assumed to have a bounded magnitude (for remaining stealthy) without being subject to any specific probability distribution, which

is not only of theoretical interest but also relaxes the assumptions seen in prior studies. More importantly, to deal with the lack of knowledge of malicious attacks on AVs, we, for the first time, formulate a min-max control problem to minimize the worst-case potential disturbance to traffic flow, considering two types of attacks. Further, an iterative computational algorithm is developed to solve the min-max control problem, giving the optimal driving strategy of AVs in a decentralized manner, which is expected to increase the robustness and resilience of automated transportation systems.

6.2 Future Work

Moving forward, I plan to extend some of the work presented in this dissertation and to study interesting research questions that can arise in future automated transportation systems.

- I plan to conduct field experiments to examine the performance of the vehicle control strategies developed. Real-world traffic environment is much more complex than simulation. Testing the driving strategies developed for AVs using experimental vehicles with low levels of automation, like adaptive cruise control, is expected to motivate the development of more robust and effective vehicle control methods in response to dynamically changing real-world traffic conditions.

- I plan to design provably safe control law for AVs in complex traffic environment with real-time synthesis using control barrier functions (CBFs) [176]. Recent developments in CBFs have opened the door to designing feedback controllers for safety-critical systems. Current approaches to ensuring safety for transportation cyber-physical systems (TCPS) rely on large-scale simulations and field testing, suffering from two fundamental challenges, namely cost and coverage. That is, simulating each and every scenario is costly while field testing is even more so; moreover, certain scenarios outside the operational design domains will inevitably remain uncovered. I plan to leverage CBFs for synthesizing provably safe AV controllers, which can transform the conventional trial-and-error paradigm and improve safety of TCPS, while providing useful coverage at an acceptable cost.

- I plan to tackle important issues arising in large-scale adoption of electric vehicles

(EVs), with a focus on two fundamental questions. The first one is to design social policy to accelerate the adoption of EVs, which will not only bring monetary benefits to travelers, but also have broader impacts on fighting climate change. I will extend the approach proposed in Chapter 2 for incentivizing AV adoption to designing incentive programs like purchase subsidies and strategic deployment of charging stations for EV adoption. This naturally leads to the second question, that is, how to select appropriate locations for the deployment of charging stations while considering smart grids? Travelers having greater access to charging infrastructure are more likely to embrace EVs; in turn, EV owners are likely to travel on routes with easier access to charging stations. Consequently, traffic network equilibrium is affected by the location of charging stations. The problem becomes more challenging when electricity supply is considered, due to limited capacity of power plants and the cost of distributing electricity. I plan to apply network modeling techniques like equilibrium analysis to fully capture the interplay among travelers, charging stations, and smart grids. Based on the analysis of power-traffic equilibrium, classic techniques of operations research, such as linear and integer programming, can be employed to determine the optimal locations for deploying charging infrastructure.

References

[1] S Ilgin Guler, Monica Menendez, and Linus Meier. Using connected vehicle technology to improve the efficiency of intersections. *Transportation Research Part C: Emerging Technologies*, 46:121–131, 2014.

[2] Daniel J Fagnant and Kara Kockelman. Preparing a nation for autonomous vehicles: opportunities, barriers and policy recommendations. *Transportation Research Part A: Policy and Practice*, 77:167–181, 2015.

[3] Yunli Shao and Zongxuan Sun. Energy-efficient connected and automated vehicles: Real-time traffic prediction-enabled co-optimization of vehicle motion and powertrain operation. *IEEE Vehicular Technology Magazine*, 16(3):47–56, 2021.

[4] Jean-François Bonnefon, Azim Shariff, and Iyad Rahwan. The social dilemma of autonomous vehicles. *Science*, 352(6293):1573–1576, 2016.

[5] John Basl and Jeff Behrends. Why everyone has it wrong about the ethics of autonomous vehicles. In *Frontiers of Engineering: Reports on Leading-Edge Engineering from the 2019 Symposium*. National Academies Press, 2020.

[6] Fábio Duarte and Carlo Ratti. The impact of autonomous vehicles on cities: A review. *Journal of Urban Technology*, 25(4):3–18, 2018.

[7] Lanhang Ye and Toshiyuki Yamamoto. Evaluating the impact of connected and autonomous vehicles on traffic safety. *Physica A: Statistical Mechanics and its Applications*, 526:121009, 2019.

[8] Zia Wadud, Don MacKenzie, and Paul Leiby. Help or hindrance? The travel,

energy and carbon impacts of highly automated vehicles. *Transportation Research Part A: Policy and Practice*, 86:1–18, 2016.

[9] Shian Wang, Michael W Levin, and Ryan James Caverly. Optimal parking management of connected autonomous vehicles. In *2021 American Control Conference (ACC)*, pages 1022–1027. IEEE, 2021.

[10] Shian Wang, Michael W Levin, and Ryan James Caverly. Optimal parking management of connected autonomous vehicles: A control-theoretic approach. *Transportation Research Part C: Emerging Technologies*, 124:102924, 2021.

[11] Dimitris Milakis, Bart van Arem, and Bert van Wee. Policy and society related implications of automated driving: A review of literature and directions for future research. *Journal of Intelligent Transportation Systems*, 21(4):324–348, 2017.

[12] Lewis M Clements and Kara M Kockelman. Economic effects of automated vehicles. *Transportation Research Record*, 2606(1):106–114, 2017.

[13] Michael W Levin and Stephen D Boyles. Effects of autonomous vehicle ownership on trip, mode, and route choice. *Transportation Research Record*, 2493(1):29–38, 2015.

[14] Hani S Mahmassani. Autonomous vehicles and connected vehicle systems: Flow and operations considerations. *Transportation Science*, 50(4):1140–1162, 2016.

[15] Alireza Talebpour and Hani S Mahmassani. Influence of connected and autonomous vehicles on traffic flow stability and throughput. *Transportation Research Part C: Emerging Technologies*, 71:143–163, 2016.

[16] Shumo Cui, Benjamin Seibold, Raphael Stern, and Daniel B Work. Stabilizing traffic flow via a single autonomous vehicle: Possibilities and limitations. In *2017 IEEE Intelligent Vehicles Symposium (IV)*, pages 1336–1341. IEEE, 2017.

[17] Cathy Wu, Alexandre M Bayen, and Ankur Mehta. Stabilizing traffic with autonomous vehicles. In *2018 IEEE International Conference on Robotics and Automation (ICRA)*, pages 6012–6018. IEEE, 2018.

[18] Raphael E Stern, Shumo Cui, Maria Laura Delle Monache, Rahul Bhadani, Matt Bunting, Miles Churchill, Nathaniel Hamilton, Hannah Pohlmann, Fangyu Wu, Benedetto Piccoli, et al. Dissipation of stop-and-go waves via control of autonomous vehicles: Field experiments. *Transportation Research Part C: Emerging Technologies*, 89:205–221, 2018.

[19] Fangyu Wu, Raphael E Stern, Shumo Cui, Maria Laura Delle Monache, Rahul Bhadani, Matt Bunting, Miles Churchill, Nathaniel Hamilton, Benedetto Piccoli, Benjamin Seibold, et al. Tracking vehicle trajectories and fuel rates in phantom traffic jams: Methodology and data. *Transportation Research Part C: Emerging Technologies*, 99:82–109, 2019.

[20] Raphael E Stern, Yuche Chen, Miles Churchill, Fangyu Wu, Maria Laura Delle Monache, Benedetto Piccoli, Benjamin Seibold, Jonathan Sprinkle, and Daniel B Work. Quantifying air quality benefits resulting from few autonomous vehicles stabilizing traffic. *Transportation Research Part D: Transport and Environment*, 67:351–365, 2019.

[21] Nasir Uddin Ahmed and Shian Wang. *Optimal control of dynamic systems driven by vector measures: Theory and applications*. Springer, 2021.

[22] Richard E Allsop. SIGSET: a computer program for calculating traffic capacity of signal-controlled road. *Traffic Engineering and Control*, 12:58–60, 1971.

[23] Richard E Allsop. SIGCAP: a computer program for assessing the traffic capacity of signal-controlled road junctions. *Traffic Engineering and Control*, 17(819):338–341, 1976.

[24] Chen Cai, Chi Kwong Wong, and Benjamin G Heydecker. Adaptive traffic signal control using approximate dynamic programming. *Transportation Research Part C: Emerging Technologies*, 17(5):456–474, 2009.

[25] Shian Wang, Nasir Uddin Ahmed, and Tet H Yeap. Optimum management of urban traffic flow based on a stochastic dynamic model. *IEEE Transactions on Intelligent Transportation Systems*, 20(12):4377–4389, 2019.

[26] John D C Little. The synchronization of traffic signals by mixed-integer linear programming. *Operations Research*, 14(4):568–594, 1966.

[27] Dennis I Robertson. "TRANSYT" method for area traffic control. *Traffic Engineering and Control*, 11(6):276–281, 1969.

[28] P B Hunt, D I Robertson, R D Bretherton, and M Cr Royle. The SCOOT on-line traffic signal optimisation technique. *Traffic Engineering and Control*, 23(4):190–192, 1982.

[29] Suvrajeet Sen and K Larry Head. Controlled optimization of phases at an intersection. *Transportation Science*, 31(1):5–17, 1997.

[30] Tichakorn Wongpiromsarn, Tawit Uthaicharoenpong, Yu Wang, Emilio Frazzoli, and Danwei Wang. Distributed traffic signal control for maximum network throughput. In *2012 15th IEEE International Conference on Intelligent Transportation Systems*, pages 588–595. IEEE, 2012.

[31] Pravin Varaiya. Max pressure control of a network of signalized intersections. *Transportation Research Part C: Emerging Technologies*, 36:177–195, 2013.

[32] Yue J Zhang, Andreas A Malikopoulos, and Christos G Cassandras. Optimal control and coordination of connected and automated vehicles at urban traffic intersections. In *2016 American Control Conference (ACC)*, pages 6227–6232. IEEE, 2016.

[33] Shian Wang, Aidan Mahlberg, and Michael W Levin. Optimal control of automated vehicles for autonomous intersection management with design specifications. *Transportation Research Record*, page 03611981221109166, 2022.

[34] Markos Papageorgiou, Habib Hadj-Salem, and Jean-Marc Blosseville. ALINEA: A local feedback control law for on-ramp metering. *Transportation Research Record*, 1320(1):58–67, 1991.

[35] Markos Papageorgiou, Christina Diakaki, Vaya Dinopoulou, Apostolos Kotsialos, and Yibing Wang. Review of road traffic control strategies. *Proceedings of the IEEE*, 91(12):2043–2067, 2003.

[36] Leif Isaksen and Harold J Payne. Suboptimal control of linear systems by augmentation with application to freeway traffic regulation. *IEEE Transactions on Automatic Control*, 18(3):210–219, 1973.

[37] Douglas P Looze, Paul K Houpt, Nils R Sandell, and Michael Athans. On decentralized estimation and control with application to freeway ramp metering. *IEEE Transactions on Automatic Control*, 23(2):268–275, 1978.

[38] N B Goldstein and K S P Kumar. A decentralized control strategy for freeway regulation. *Transportation Research Part B: Methodological*, 16(4):279–290, 1982.

[39] Alexandre Bayen, Maria Laura Delle Monache, Mauro Garavello, Paola Goatin, and Benedetto Piccoli. *Control problems for conservation laws with traffic applications: modeling, analysis, and numerical methods.* Birkhäuser, 2022.

[40] Qi Luo, Romesh Saigal, Zhibin Chen, and Yafeng Yin. Accelerating the adoption of automated vehicles by subsidies: A dynamic games approach. *Transportation Research Part B: Methodological*, 129:226–243, 2019.

[41] Shian Wang, Zhexian Li, and Michael W Levin. Optimal policy for integrating autonomous vehicles into the auto market. *Transportation Research Part C: Emerging Technologies*, 143:103821, 2022.

[42] Shuo Feng, Yi Zhang, Shengbo Eben Li, Zhong Cao, Henry X Liu, and Li Li. String stability for vehicular platoon control: Definitions and analysis methods. *Annual Reviews in Control*, 47:81–97, 2019.

[43] Yang Zheng, Jiawei Wang, and Keqiang Li. Smoothing traffic flow via control of autonomous vehicles. *IEEE Internet of Things Journal*, 7(5):3882–3896, 2020.

[44] Yang Zhou, Soyoung Ahn, Meng Wang, and Serge Hoogendoorn. Stabilizing mixed vehicular platoons with connected automated vehicles: An H-infinity approach. *Transportation Research Part B: Methodological*, 132:152–170, 2020.

[45] Shian Wang, Raphael Stern, and Michael W Levin. Optimal control of autonomous vehicles for traffic smoothing. *IEEE Transactions on Intelligent Transportation Systems*, 23(4):3842–3852, 2022.

[46] Shunyuan Xiao, Xiaohua Ge, Qing-Long Han, and Yijun Zhang. Secure distributed adaptive platooning control of automated vehicles over vehicular ad-hoc networks under denial-of-service attacks. *IEEE Transactions on Cybernetics*, 2021.

[47] Fengchen Wang and Yan Chen. Resilient flocking control for connected and automated vehicles with cyber-attack threats. *ASME Letters in Dynamic Systems and Control*, 1(3):031013, 2021.

[48] Hao Lyu, Ting Wang, Rongjun Cheng, and Hongxia Ge. Improved longitudinal control strategy for connected and automated truck platoon against cyberattacks. *IET Intelligent Transport Systems*, 2022.

[49] Shian Wang and Zhexian Li. Optimal policy for integration of automated vehicles into the auto market: A control-theoretic perspective. In *2021 IEEE International Intelligent Transportation Systems Conference (ITSC)*, pages 3470–3475. IEEE, 2021.

[50] Shian Wang, Mingfeng Shang, Michael W Levin, and Raphael Stern. Smoothing nonlinear mixed traffic with autonomous vehicles: Control design. In *2022 IEEE 25th International Conference on Intelligent Transportation Systems (ITSC)*, pages 661–666. IEEE, 2022.

[51] Shian Wang, Mingfeng Shang, Michael W Levin, and Raphael Stern. A general approach to smoothing nonlinear mixed traffic via control of autonomous vehicles. *Transportation Research Part C: Emerging Technologies*, 146:103967, 2023.

[52] Shian Wang, Michael W Levin, and Raphael Stern. Optimal feedback control law for automated vehicles in the presence of cyberattacks: A min-max approach. *Transportation Research Part C: Emerging Technologies*, in review.

[53] Shian Wang, Michael W Levin, and Raphael Stern. String stable control design for automated vehicles under cyberattacks. *IEEE Transactions on Intelligent Vehicles*, in review.

[54] Toru Seo and Yasuo Asakura. Endogenous market penetration dynamics of automated and connected vehicles: Transport-oriented model and its paradox. *Transportation Research Procedia*, 27:238–245, 2017.

[55] Bart Van Arem, Cornelie JG Van Driel, and Ruben Visser. The impact of cooperative adaptive cruise control on traffic-flow characteristics. *IEEE Transactions on Intelligent Transportation Systems*, 7(4):429–436, 2006.

[56] Daniel J Fagnant and Kara M Kockelman. Dynamic ride-sharing and fleet sizing for a system of shared autonomous vehicles in Austin, Texas. *Transportation*, 45(1):143–158, 2018.

[57] T Donna Chen, Kara M Kockelman, and Josiah P Hanna. Operations of a shared, autonomous, electric vehicle fleet: Implications of vehicle & charging infrastructure decisions. *Transportation Research Part A: Policy and Practice*, 94:243–254, 2016.

[58] Zhibin Chen, Fang He, Lihui Zhang, and Yafeng Yin. Optimal deployment of autonomous vehicle lanes with endogenous market penetration. *Transportation Research Part C: Emerging Technologies*, 72:143–156, 2016.

[59] Zia Wadud. Fully automated vehicles: A cost of ownership analysis to inform early adoption. *Transportation Research Part A: Policy and Practice*, 101:163–176, 2017.

[60] Ramin Shabanpour, Nima Golshani, Ali Shamshiripour, and Abolfazl Kouros Mohammadian. Eliciting preferences for adoption of fully automated vehicles using best-worst analysis. *Transportation Research Part C: Emerging Technologies*, 93:463–478, 2018.

[61] Shukai Chen, Hua Wang, and Qiang Meng. Designing autonomous vehicle incentive program with uncertain vehicle purchase price. *Transportation Research Part C: Emerging Technologies*, 103:226–245, 2019.

[62] Ye Li, Zhibin Chen, Yafeng Yin, and Srinivas Peeta. Deployment of roadside units to overcome connectivity gap in transportation networks with mixed traffic. *Transportation Research Part C: Emerging Technologies*, 111:496–512, 2020.

[63] Alfred J Lotka. Elements of physical biology. *Science Progress in the Twentieth Century (1919-1933)*, 21(82):341–343, 1926.

[64] Vito Volterra. *Variazioni e fluttuazioni del numero d'individui in specie animali conviventi*. Memorie del R. Comitato talassografico italiano, 1927.

[65] Prateek Bansal, Kara M Kockelman, and Amit Singh. Assessing public opinions of and interest in new vehicle technologies: An Austin perspective. *Transportation Research Part C: Emerging Technologies*, 67:1–14, 2016.

[66] Erick Guerra. Planning for cars that drive themselves: Metropolitan planning organizations, regional transportation plans, and autonomous vehicles. *Journal of Planning Education and Research*, 36(2):210–224, 2016.

[67] Ricardo A Daziano, Mauricio Sarrias, and Benjamin Leard. Are consumers willing to pay to let cars drive for them? Analyzing response to autonomous vehicles. *Transportation Research Part C: Emerging Technologies*, 78:150–164, 2017.

[68] Lev Semyonovich Pontryagin, Vladimir Grigorevich Boltyanskii, Revaz Valerianovic Gamkrelidze, and Evgenii Frolovich Mishchenko. *Mathematical theory of optimal processes*. Interscience, 1962.

[69] Pankaj Maheshwari, Pushkin Kachroo, Alexander Paz, and Romesh Khaddar. Development of control models for the planning of sustainable transportation systems. *Transportation Research Part C: Emerging Technologies*, 55:474–485, 2015.

[70] Pankaj Maheshwari, Romesh Khaddar, Pushkin Kachroo, and Alexander Paz. Dynamic modeling of performance indices for planning of sustainable transportation systems. *Networks and Spatial Economics*, 16(1):371–393, 2016.

[71] Everett M Rogers. *Diffusion of innovations*. Simon and Schuster, 2010.

[72] Jurgen Nieuwenhuijsen, Gonçalo Homem de Almeida Correia, Dimitris Milakis, Bart van Arem, and Els van Daalen. Towards a quantitative method to analyze the long-term innovation diffusion of automated vehicles technology using system dynamics. *Transportation Research Part C: Emerging Technologies*, 86:300–327, 2018.

[73] Ramin Shabanpour, Ali Shamshiripour, and Abolfazl Mohammadian. Modeling

adoption timing of autonomous vehicles: innovation diffusion approach. *Transportation*, 45(6):1607–1621, 2018.

[74] Ahmadreza Talebian and Sabyasachee Mishra. Predicting the adoption of connected autonomous vehicles: A new approach based on the theory of diffusion of innovations. *Transportation Research Part C: Emerging Technologies*, 95:363–380, 2018.

[75] Kenneth E Train. *Discrete choice methods with simulation*. Cambridge University Press, 2009.

[76] Hassan K Khalil. *Nonlinear systems*. Prentice Hall, 2002.

[77] Terry L Friesz and Ke Han. The mathematical foundations of dynamic user equilibrium. *Transportation Research Part B: Methodological*, 126:309–328, 2019.

[78] M J H Mogridge. *The car market: a study of the statics and dynamics of supply-demand equilibrium*. Pion Ltd, London, 1983.

[79] Kathleen M C Tjørve and Even Tjørve. The use of Gompertz models in growth analyses, and new Gompertz-model approach: An addition to the Unified-Richards family. *PLOS ONE*, 12(6):e0178691, 2017.

[80] Joyce Dargay and Dermot Gately. Income's effect on car and vehicle ownership, worldwide: 1960–2015. *Transportation Research Part A: Policy and Practice*, 33(2):101–138, 1999.

[81] Hedges & Company. U.S. Vehicle Registration Statistics, 2020. accessed May 17, 2021.

[82] I Wagner. New vehicle average selling price in the United States from 2016 to 2020, 2021. accessed May 17, 2021.

[83] State and Local Finance Initiative. Highway and Road Expenditures, 2021. accessed May 17, 2021.

[84] Adam Millard-Ball and Lee Schipper. Are we reaching peak travel? Trends in passenger transport in eight industrialized countries. *Transport Reviews*, 31(3):357–378, 2011.

[85] Panos D Prevedouros and Ping An. Automobile ownership in Asian countries: historical trends and forecasts. *ITE Journal*, 68(4):24–29, 1998.

[86] I Wagner. Number of cars sold in the U.S. 1951-2020, 2021. accessed May 17, 2021.

[87] David Schrank, Bill Eisele, and Tim Lomax. TTI's 2012 urban mobility report. *Texas A & M Transportation Institute. The Texas A & M University System*, 4, 2012.

[88] Jorge A Laval and Carlos F Daganzo. Lane-changing in traffic streams. *Transportation Research Part B: Methodological*, 40(3):251–264, 2006.

[89] Boris S Kerner. *The physics of traffic: Empirical freeway pattern features, engineering applications, and theory*. Springer, 2012.

[90] Vicente Milanés, Jorge Godoy, Jorge Villagrá, and Joshué Pérez. Automated on-ramp merging system for congested traffic situations. *IEEE Transactions on Intelligent Transportation Systems*, 12(2):500–508, 2010.

[91] Morris R Flynn, Aslan R Kasimov, Jean-Christophe Nave, Rodolfo R Rosales, and Benjamin Seibold. Self-sustained nonlinear waves in traffic flow. *Physical Review E*, 79(5):056113, 2009.

[92] Yuki Sugiyama, Minoru Fukui, Macoto Kikuchi, Katsuya Hasebe, Akihiro Nakayama, Katsuhiro Nishinari, Shin-ichi Tadaki, and Satoshi Yukawa. Traffic jams without bottlenecks–experimental evidence for the physical mechanism of the formation of a jam. *New Journal of Physics*, 10(3):033001, 2008.

[93] Shin-ichi Tadaki, Macoto Kikuchi, Minoru Fukui, Akihiro Nakayama, Katsuhiro Nishinari, Akihiro Shibata, Yuki Sugiyama, Taturu Yosida, and Satoshi Yukawa. Phase transition in traffic jam experiment on a circuit. *New Journal of Physics*, 15(10):103034, 2013.

[94] Michel André and Ulf Hammarström. Driving speeds in Europe for pollutant emissions estimation. *Transportation Research Part D: Transport and Environment*, 5(5):321–335, 2000.

[95] Eva Ericsson, Hanna Larsson, and Karin Brundell-Freij. Optimizing route choice for lowest fuel consumption-potential effects of a new driver support tool. *Transportation Research Part C: Emerging Technologies*, 14(6):369–383, 2006.

[96] Pitu Mirchandani and Larry Head. A real-time traffic signal control system: architecture, algorithms, and analysis. *Transportation Research Part C: Emerging Technologies*, 9(6):415–432, 2001.

[97] Gabriel Gomes and Roberto Horowitz. Optimal freeway ramp metering using the asymmetric cell transmission model. *Transportation Research Part C: Emerging Technologies*, 14(4):244–262, 2006.

[98] Stef Smulders. Control of freeway traffic flow by variable speed signs. *Transportation Research Part B: Methodological*, 24(2):111–132, 1990.

[99] Andreas Hegyi, Bart De Schutter, and Johannes Hellendoorn. Optimal coordination of variable speed limits to suppress shock waves. *IEEE Transactions on Intelligent Transportation Systems*, 6(1):102–112, 2005.

[100] D Swaroop and J Karl Hedrick. String stability of interconnected systems. *IEEE Transactions on Automatic Control*, 41(3):349–357, 1996.

[101] Petros A Ioannou and Cheng-Chih Chien. Autonomous intelligent cruise control. *IEEE Transactions on Vehicular Technology*, 42(4):657–672, 1993.

[102] Swaroop Darbha and K R Rajagopal. Intelligent cruise control systems and traffic flow stability. *Transportation Research Part C: Emerging Technologies*, 7(6):329–352, 1999.

[103] Rajesh Rajamani and Chunyu Zhu. Semi–autonomous adaptive cruise control systems. *IEEE Transactions on Vehicular Technology*, 51(5):1186–1192, 2002.

[104] George Gunter, Caroline Janssen, William Barbour, Raphael E Stern, and Daniel B Work. Model-based string stability of adaptive cruise control systems using field data. *IEEE Transactions on Intelligent Vehicles*, 5(1):90–99, 2019.

[105] Vicente Milanés, Steven E Shladover, John Spring, Christopher Nowakowski, Hiroshi Kawazoe, and Masahide Nakamura. Cooperative adaptive cruise control in

real traffic situations. *IEEE Transactions on Intelligent Transportation Systems*, 15:296–305, 2013.

[106] Meng Wang, Winnie Daamen, Serge P Hoogendoorn, and Bart van Arem. Cooperative car–following control: Distributed algorithm and impact on moving jam features. *IEEE Transactions on Intelligent Transportation Systems*, 17(5):1459–1471, 2015.

[107] Yang Zhou, Meng Wang, and Soyoung Ahn. Distributed model predictive control approach for cooperative car-following with guaranteed local and string stability. *Transportation Research Part B: Methodological*, 128:69–86, 2019.

[108] Louis A Pipes. An operational analysis of traffic dynamics. *Journal of Applied Physics*, 24(3):274–281, 1953.

[109] Denos C Gazis, Robert Herman, and Renfrey B Potts. Car-following theory of steady-state traffic flow. *Operations Research*, 7(4):499–505, 1959.

[110] Peter G Gipps. A behavioural car-following model for computer simulation. *Transportation Research Part B: Methodological*, 15(2):105–111, 1981.

[111] Masako Bando, Katsuya Hasebe, Akihiro Nakayama, Akihiro Shibata, and Yuki Sugiyama. Dynamical model of traffic congestion and numerical simulation. *Physical Review E*, 51(2):1035–1042, 1995.

[112] Martin Treiber, Ansgar Hennecke, and Dirk Helbing. Congested traffic states in empirical observations and microscopic simulations. *Physical Review E*, 62(2):1805–1824, 2000.

[113] Gordon Frank Newell. A simplified car-following theory: A lower order model. *Transportation Research Part B: Methodological*, 36(3):195–205, 2002.

[114] Eddie Wilson and Jonathan A Ward. Car-following models: Fifty years of linear stability analysis–a mathematical perspective. *Transportation Planning and Technology*, 34(1):3–18, 2011.

[115] Thibault Liard, Raphael Stern, and Maria Laura Delle Monache. Optimal driving strategies for traffic control with autonomous vehicles. In *The 21st IFAC World Congress*, volume 53, pages 5322–5329, 2020.

[116] Arne Kesting, Martin Treiber, Martin Schönhof, Florian Kranke, and Dirk Helbing. Jam-avoiding adaptive cruise control (ACC) and its impact on traffic dynamics. In *Traffic and Granular Flow'05*, pages 633–643. Springer, 2007.

[117] Maria Laura Delle Monache, Jonathan Sprinkle, Ram Vasudevan, and Daniel Work. Autonomous vehicles: From vehicular control to traffic control. In *2019 IEEE 58th Conference on Decision and Control (CDC)*, pages 4680–4696. IEEE, 2019.

[118] Wen Xing Zhu and H M Zhang. Analysis of mixed traffic flow with human-driving and autonomous cars based on car-following model. *Physica A: Statistical Mechanics and its Applications*, 496:274–285, 2018.

[119] Wilko Schwarting, Alyssa Pierson, Javier Alonso-Mora, Sertac Karaman, and Daniela Rus. Social behavior for autonomous vehicles. *Proceedings of the National Academy of Sciences*, 116(50):24972–24978, 2019.

[120] Nasir Uddin Ahmed and Shian Wang. Measure-driven nonlinear dynamic systems with applications to optimal impulsive controls. *Journal of Optimization Theory and Applications*, 188(1):26–51, 2021.

[121] Shian Wang and Nasir Uddin Ahmed. Optimum management of the network of city bus routes based on a stochastic dynamic model. *Journal of Industrial and Management Optimization*, 15(2):619–631, 2019.

[122] Shian Wang and Nasir Uddin Ahmed. Dynamic model of urban traffic and optimum management of its flow and congestion. *Dynamic Systems and Applications*, 26(1):575–588, 2017.

[123] Jia Hu, Yunli Shao, Zongxuan Sun, Meng Wang, Joe Bared, and Peter Huang. Integrated optimal eco-driving on rolling terrain for hybrid electric vehicle with vehicle-infrastructure communication. *Transportation Research Part C: Emerging Technologies*, 68:228–244, 2016.

[124] Shian Wang and Nasir Uddin Ahmed. Optimal control and stabilization of building maintenance units based on minimum principle. *Journal of Industrial and Management Optimization*, 17(4):1713–1727, 2021.

[125] Nasir Uddin Ahmed. *Elements of finite dimensional systems and control theory*. John Wiley & Sons, Inc., 1988.

[126] Martin Treiber and Arne Kesting. *Traffic flow dynamics*. Springer, 2013.

[127] Kok Lay Teo, Chuen Jin Goh, and Kar Hung Wong. *A unified computational approach to optimal control problems*. New York: Longman Scientific and Technical, 1991.

[128] Kyoungho Ahn, Hesham Rakha, Antonio Trani, and Michel Van Aerde. Estimating vehicle fuel consumption and emissions based on instantaneous speed and acceleration levels. *Journal of Transportation Engineering*, 128(2):182–190, 2002.

[129] Hesham Rakha, Kyoungho Ahn, and Antonio Trani. Development of VT-micro model for estimating hot stabilized light duty vehicle and truck emissions. *Transportation Research Part D: Transport and Environment*, 9(1):49–74, 2004.

[130] Nathan Lichtlé, Eugene Vinitsky, Matthew Nice, Benjamin Seibold, Dan Work, and Alexandre M Bayen. Deploying traffic smoothing cruise controllers learned from trajectory data. In *2022 International Conference on Robotics and Automation (ICRA)*, pages 2884–2890. IEEE, 2022.

[131] Dong-Fan Xie, Xiao-Mei Zhao, and Zhengbing He. Heterogeneous traffic mixing regular and connected vehicles: Modeling and stabilization. *IEEE Transactions on Intelligent Transportation Systems*, 20(6):2060–2071, 2018.

[132] Dong-Fan Xie, Yong-Qi Wen, Xiao-Mei Zhao, Xin-Gang Li, and Zhengbing He. Cooperative driving strategies of connected vehicles for stabilizing traffic flow. *Transportmetrica B: Transport Dynamics*, 8(1):166–181, 2020.

[133] Yanyan Qin and Hao Wang. Stabilizing mixed cooperative adaptive cruise control traffic flow to balance capacity using car-following model. *Journal of Intelligent Transportation Systems*, 2021.

[134] Mingfeng Shang and Raphael E Stern. Impacts of commercially available adaptive cruise control vehicles on highway stability and throughput. *Transportation Research Part C: Emerging Technologies*, 122:102897, 2021.

[135] Jiaqi Ma, Xiaopeng Li, Steven Shladover, Hesham A Rakha, Xiao-Yun Lu, Ramanujan Jagannathan, and Daniel J Dailey. Freeway speed harmonization. *IEEE Transactions on Intelligent Vehicles*, 1(1):78–89, 2016.

[136] Alireza Talebpour, Hani S Mahmassani, and Samer H Hamdar. Speed harmonization: Evaluation of effectiveness under congested conditions. *Transportation Research Record*, 2391(1):69–79, 2013.

[137] Hao Yang and Wen-Long Jin. A control theoretic formulation of green driving strategies based on inter-vehicle communications. *Transportation Research Part C: Emerging Technologies*, 41:48–60, 2014.

[138] Yuhan Huang, Elvin CY Ng, John L Zhou, Nic C Surawski, Edward FC Chan, and Guang Hong. Eco-driving technology for sustainable road transport: A review. *Renewable and Sustainable Energy Reviews*, 93:596–609, 2018.

[139] Wenbo Sun, Shian Wang, Yunli Shao, Zongxuan Sun, and Michael W Levin. Energy and mobility impacts of connected autonomous vehicles with co-optimization of speed and powertrain on mixed vehicle platoons. *Transportation Research Part C: Emerging Technologies*, 142:103764, 2022.

[140] Vittorio Giammarino, Simone Baldi, Paolo Frasca, and Maria Laura Delle Monache. Traffic flow on a ring with a single autonomous vehicle: An interconnected stability perspective. *IEEE Transactions on Intelligent Transportation Systems*, 22(8):4998–5008, 2021.

[141] I Ge Jin and Gábor Orosz. Dynamics of connected vehicle systems with delayed acceleration feedback. *Transportation Research Part C: Emerging Technologies*, 46:46–64, 2014.

[142] Mingfeng Shang, Florian Hauer, and Raphael Stern. Do cut-ins matter: Assessing the impact of lane changing and string stability on traffic flow. In *2020 IEEE 23rd*

International Conference on Intelligent Transportation Systems (ITSC), pages 1–6. IEEE, 2020.

[143] George Gunter, Derek Gloudemans, Raphael E Stern, Sean McQuade, Rahul Bhadani, Matt Bunting, Maria Laura Delle Monache, Roman Lysecky, Benjamin Seibold, Jonathan Sprinkle, Benedetto Piccoli, and Daniel B Work. Are commercially implemented adaptive cruise control systems string stable? *IEEE Transactions on Intelligent Transportation Systems*, 22(11):6992–7003, 2021.

[144] Felipe de Souza and Raphael Stern. Calibrating microscopic car-following models for adaptive cruise control vehicles: Multiobjective approach. *Journal of Transportation Engineering, Part A: Systems*, 147(1):04020150, 2021.

[145] Arne Kesting and Martin Treiber. Calibrating car-following models by using trajectory data: Methodological study. *Transportation Research Record*, 2088(1):148–156, 2008.

[146] Ankur Sarker, Haiying Shen, Mizanur Rahman, Mashrur Chowdhury, Kakan Dey, Fangjian Li, Yue Wang, and Husnu S Narman. A review of sensing and communication, human factors, and controller aspects for information-aware connected and automated vehicles. *IEEE Transactions on Intelligent Transportation Systems*, 21(1):7–29, 2019.

[147] George Gunter, Raphael Stern, and Daniel B Work. Modeling adaptive cruise control vehicles from experimental data: model comparison. In *2019 IEEE Intelligent Transportation Systems Conference (ITSC)*, pages 3049–3054. IEEE, 2019.

[148] Yinglong He, Marcello Montanino, Konstantinos Mattas, Vincenzo Punzo, and Biagio Ciuffo. Physics-augmented models to simulate commercial adaptive cruise control (ACC) systems. *Transportation Research Part C: Emerging Technologies*, 139:103692, 2022.

[149] Daniel A Lazar, Samuel Coogan, and Ramtin Pedarsani. Capacity modeling and routing for traffic networks with mixed autonomy. In *2017 IEEE 56th Annual Conference on Decision and Control (CDC)*, pages 5678–5683. IEEE, 2017.

[150] Radhakisan Baheti and Helen Gill. Cyber-physical systems. *The Impact of Control Technology*, 12(1):161–166, 2011.

[151] Alexander A Ganin, Avi C Mersky, Andrew S Jin, Maksim Kitsak, Jeffrey M Keisler, and Igor Linkov. Resilience in intelligent transportation systems (ITS). *Transportation Research Part C: Emerging Technologies*, 100:318–329, 2019.

[152] Simon Parkinson, Paul Ward, Kyle Wilson, and Jonathan Miller. Cyber threats facing autonomous and connected vehicles: Future challenges. *IEEE Transactions on Intelligent Transportation Systems*, 18(11):2898–2915, 2017.

[153] Jonathan Petit and Steven E Shladover. Potential cyberattacks on automated vehicles. *IEEE Transactions on Intelligent Transportation Systems*, 16(2):546–556, 2014.

[154] Shah Khalid Khan, Nirajan Shiwakoti, Peter Stasinopoulos, and Yilun Chen. Cyber-attacks in the next-generation cars, mitigation techniques, anticipated readiness and future directions. *Accident Analysis and Prevention*, 148:105837, 2020.

[155] Ye Li, Yu Tu, Qi Fan, Changyin Dong, and Wei Wang. Influence of cyber-attacks on longitudinal safety of connected and automated vehicles. *Accident Analysis and Prevention*, 121:148–156, 2018.

[156] Changyin Dong, Hao Wang, Daiheng Ni, Yongfei Liu, and Quan Chen. Impact evaluation of cyber-attacks on traffic flow of connected and automated vehicles. *IEEE Access*, 8:86824–86835, 2020.

[157] Yue Wang, Esha Sarkar, Wenqing Li, Michail Maniatakos, and Saif Eddin Jabari. Stop-and-go: Exploring backdoor attacks on deep reinforcement learning-based traffic congestion control systems. *IEEE Transactions on Information Forensics and Security*, 16:4772–4787, 2021.

[158] Pengcheng Wang, Xinkai Wu, and Xiaozheng He. Modeling and analyzing cyberattack effects on connected automated vehicular platoons. *Transportation Research Part C: Emerging Technologies*, 115:102625, 2020.

[159] Zulqarnain H Khattak, Brian L Smith, and Michael D Fontaine. Impact of cyberattacks on safety and stability of connected and automated vehicle platoons under lane changes. *Accident Analysis and Prevention*, 150:105861, 2021.

[160] André Teixeira, Iman Shames, Henrik Sandberg, and Karl H Johansson. Revealing stealthy attacks in control systems. In *2012 50th Annual Allerton Conference on Communication, Control, and Computing (Allerton)*, pages 1806–1813. IEEE, 2012.

[161] Eman Mousavinejad, Fuwen Yang, Qing-Long Han, Xiaohua Ge, and Ljubo Vlacic. Distributed cyber attacks detection and recovery mechanism for vehicle platooning. *IEEE Transactions on Intelligent Transportation Systems*, 21(9):3821–3834, 2019.

[162] Franco Van Wyk, Yiyang Wang, Anahita Khojandi, and Neda Masoud. Real-time sensor anomaly detection and identification in automated vehicles. *IEEE Transactions on Intelligent Transportation Systems*, 21(3):1264–1276, 2019.

[163] Elvin Eziama, Faroq Awin, Sabbir Ahmed, et al. Detection and identification of malicious cyber-attacks in connected and automated vehicles' real-time sensors. *Applied Sciences*, 10(21):7833, 2020.

[164] Tianyi Li, Mingfeng Shang, Shian Wang, Matthew Filippelli, and Raphael Stern. Detecting stealthy cyberattacks on automated vehicles via generative adversarial networks. In *2022 IEEE 25th International Conference on Intelligent Transportation Systems (ITSC)*, pages 3632–3637. IEEE, 2022.

[165] Chunheng Zhao, Jasprit Singh Gill, Pierluigi Pisu, and Gurcan Comert. Detection of false data injection attack in connected and automated vehicles via cloud-based sandboxing. *IEEE Transactions on Intelligent Transportation Systems*, 23(7):9078–9088, 2022.

[166] Tianci Yang and Chen Lv. A secure sensor fusion framework for connected and automated vehicles under sensor attacks. *IEEE Internet of Things Journal*, 2021.

[167] Feng Luo and Shuo Hou. Cyberattacks and countermeasures for intelligent and connected vehicles. *SAE International Journal of Passenger Cars-Electronic and Electrical Systems*, 12(1):55–67, 2019.

[168] Dajiang Suo, John Moore, Mathew Boesch, Kyle Post, and Sanjay E Sarma. Location-based schemes for mitigating cyber threats on connected and automated vehicles: A survey and design framework. *IEEE Transactions on Intelligent Transportation Systems*, 23(4):2919–2937, 2022.

[169] Yilin Mo, Emanuele Garone, Alessandro Casavola, and Bruno Sinopoli. False data injection attacks against state estimation in wireless sensor networks. In *49th IEEE Conference on Decision and Control (CDC)*, pages 5967–5972. IEEE, 2010.

[170] Mark Brackstone and Mike McDonald. Car-following: a historical review. *Transportation Research Part F: Traffic Psychology and Behaviour*, 2(4):181–196, 1999.

[171] Zoleikha Abdollahi Biron, Satadru Dey, and Pierluigi Pisu. Real-time detection and estimation of denial of service attack in connected vehicle systems. *IEEE Transactions on Intelligent Transportation Systems*, 19(12):3893–3902, 2018.

[172] Francesca Boem, Alexander J Gallo, Giancarlo Ferrari-Trecate, and Thomas Parisini. A distributed attack detection method for multi-agent systems governed by consensus-based control. In *2017 IEEE 56th Annual Conference on Decision and Control (CDC)*, pages 5961–5966. IEEE, 2017.

[173] Chi-Ying Liang and Huei Peng. Optimal adaptive cruise control with guaranteed string stability. *Vehicle System Dynamics*, 32(4-5):313–330, 1999.

[174] Nasir Uddin Ahmed and Md Suruz Miah. Optimal feedback control law for a class of partially observed uncertain dynamic systems: A min-max problem. *Dynamic Systems and Applications*, 20(1):149–168, 2011.

[175] Felipe de Souza and Raphael Stern. Calibrating microscopic model for commercially available autonomous driving systems: a multi-objective approach. In *Transportation Research Board Annual Meeting*, 2019.

[176] Aaron D Ames, Samuel Coogan, Magnus Egerstedt, Gennaro Notomista, Koushil Sreenath, and Paulo Tabuada. Control barrier functions: Theory and applications. In *2019 18th European Control Conference (ECC)*, pages 3420–3431. IEEE, 2019.